UNIVERSIDAD POLITÉCNICA DE MADRID

ESCUELA TÉCNICA SUPERIOR
DE INGENIEROS DE TELECOMUNICACIÓN

DISTRIBUTED CONTROL STRATEGIES FOR PHOTOVOLTAIC SYSTEMS IN URBAN ENVIRONMENTS

TESIS DOCTORAL

Jorge Solórzano del Moral
Ingeniero de Telecomunicación

2014

Instituto de Energía Solar

Departamento de Electrónica Física

Escuela Técnica Superior de Ingenieros de Telecomunicación

ESTRATEGIAS DE CONTROL DISTRIBUIDO PARA SISTEMAS FOTOVOLTAICOS EN ENTORNOS URBANOS

Autor:

Jorge Solórzano del Moral

Ingeniero de Telecomunicación

Director:

Miguel Ángel Egido Aguilera

Doctor Ingeniero de Telecomunicación

Profesor Titular de Universidad

Madrid, octubre 2014

Tribunal nombrado por el Magnífico y Excelentísimo Sr. Rector de la Universidad Politécnica de Madrid.

PRESIDENTE: José María Ruiz Pérez

VOCALES:

Jorge Aguilera Tejero

Juan Carlos Jimeno Cuesta

Massimo Vitelli

SECRETARIO: Estefanía Caamaño Martín

SUPLENTES:

Juan de la Casa Higueras

Danielle Gallo

Realizado el acto de defensa y lectura de la Tesis en Madrid,
el día de de 2014.

Calificación:

EL PRESIDENTE LOS VOCALES

EL SECRETARIO

AGRADECIMIENTOS

Debo admitir que el convertirme en doctor nunca estuvo dentro de mis planes. Sin embargo, una vez andado el camino me alegro enormemente de haber llegado a este punto; por todo lo aprendido y también por la gente con la que lo he compartido. Además, el haber formado parte del Instituto de Energía Solar ha sido todo un privilegio. Estoy totalmente convencido que el capital humano, la sabiduría y el rigor científico que por aquí circulan no son fáciles de encontrar. Y eso se contagia.

Personalmente, quiero agradecer en primer lugar a Miguel Ángel Egido, por haberme dado la oportunidad de desarrollar esta tesis bajo su dirección y de formar parte del IES. Trabajar a su lado me ha abierto sin duda un nuevo mundo de conocimiento y de oportunidades. Me es inevitable mencionar también su gran calidad humana y sinceridad así como el trato recibido, por lo cual estoy más que agradecido. En una línea paralela, un agradecimiento también para Estefanía Caamaño quien siempre ha estado dispuesta a ayudar o resolver cualquier duda que haya tenido.

Un agradecimiento también al resto de integrantes del IES por hacer tan especial esta institución y al grupo GEDIRCI, Álvaro, Lorenzo, Edu, Manu, Dani. En un título más personal, a Íñigo y Manu por ese año de Máster de incontables anécdotas y la continuación en Olavide. Rodrigo Dartagnan, cuarto integrante y enlace horizontal entre grupos de sistemas; grande. WikiDani, siempre con la respuesta a alguna duda. Almudena, por su eterna sonrisa y sus "soldaduras avanzadas". Alex the guiri, with his contagious laughter. El equipo meteo, Kike, Mario y David; *mens sana in corpore sano*. Alba, organizadora de cañas, qué haríamos sin ti. Marta por prestarme la cámara termográfica numerosas veces. Esther y Elisa: por su paciencia en el despacho. Sin duda a Zamorano por toda la ayuda con temas técnicos y por estar siempre dispuesto a ayudarme con alguna de mis locuras. Y Miguel y Javi, por supuesto, un agradecimiento en la misma línea.

Agradecer también a Begoña Lazpita por ofrecerme la oportunidad de realizar mi estancia en el Institut National de l'Energie Solaire y ayudarme en todo lo posible durante mi estancia allí. También a Pablo con quien pude compartir muy buenos momentos y muchas risas en Chambery. Et aussi a Pierre, on a bien rigolé meeeeeeeec.

A special thanks to Chris Deline from the National Renewable Energy Laboratory and Massimo Vitelli from the University of Napoli for reviewing the document and providing very useful comments for its improvement. Many emails were sent back and forth, especially with Chris, which have helped shape and improve the thesis.

Y por último, agradecer enormemente a mi familia por apoyarme siempre en mis decisiones y dejarme hacer. Aussi a Mélanie pour être la, toujours contente avec ça energie positive.

Abstract

This work is a contribution to photovoltaic (PV) systems with distributed maximum power point tracking (DMPPT), a system topology characterized by performing the MPPT at module level, instead of the more traditional topologies which perform MPPT for a larger number of modules. The two DMPPT technologies available at the moment are known as microinverters and power optimizers, also known as module level power electronics (MLPE), and they provide certain advantages over central MPPT systems like: higher energy production in mismatch situations, monitoring of each individual module, system design flexibility, higher system safety, etc. Although DMPPT is not limited to urban environments, it has been emphasized in the title as it is their natural market, since in large ground-mounted PV plants the extra cost is difficult to justify.

Since 2010 MLPE have increased their market share steadily and continuing to grow steadily. However, there still lacks a profound understanding of how they work, especially in the case of power optimizers, the achievable energy gains with their use and the possibilities in failure diagnosis. The main objective of this thesis is to provide a complete understanding of DMPPT technologies: how they function, their limitations and their advantages. A series of equations used to model PV arrays with power optimizers have been derived and used to point out limitations in solving certain mismatch situation. Because one of the most emphasized benefits of DMPPT is their ability to mitigate shading losses, an extensive study on the effects of shadows on PV systems is presented; both on the *I-V* curve and on MPPT algorithms. Experimental tests have been performed on the MPPT algorithms of central inverters and MLPE, highlighting their inefficiency in *I-V* curves with local maxima. An analysis of the possible mitigation of hot-spots with DMPPT is discussed and experimentally verified. And a theoretical analysis of the possible power and energy gains is presented as well as

experiments in real PV systems. A short economic analysis of the benefits of DMPPT has also been performed.

In order to aide in the previous task, a program which simulates *I-V* curves under shaded conditions has been developed and experimentally verified. This same program has been used to develop a software tool especially designed for PV systems affected by shading, which estimates the losses due to shading and the energy gains obtained with DMPPT.

Finally, a set of algorithms for diagnosing system faults in PV systems with DMPPT has been developed and experimentally verified. The tool can diagnose the following failures: fixed object shading (with distance estimation), localized dirt, generalized dirt, possible hot-spots, module degradation and excessive losses in DC cables. In addition, it alerts the user of the power losses produced by each failure and classifies the failures by their severity and with the advantage that it does not require the use of irradiance or temperature sensors.

Resumen

Este trabajo es una contribución a los sistemas fotovoltaicos (FV) con seguimiento distribuido del punto de máxima potencia (DMPPT), una topología que se caracteriza porque lleva a cabo el MPPT a nivel de módulo, al contrario de las topologías más tradicionales que llevan a cabo el MPPT para un número más elevado de módulos, pudiendo ser hasta cientos de módulos. Las dos tecnologías DMPPT que existen en el mercado son conocidas como microinversores y optimizadores de potencia, y ofrecen ciertas ventajas sobre sistemas de MPPT central como: mayor producción en situaciones de *mismatch*, monitorización individual de cada módulo, flexibilidad de diseño, mayor seguridad del sistema, etc. Aunque los sistemas DMPPT no están limitados a los entornos urbanos, se ha enfatizado en el título ya que es su mercado natural, siendo difícil una justificación de su sobrecoste en grandes huertas solares en suelo.

Desde el año 2010 el mercado de estos sistemas se ha incrementado notablemente y sigue creciendo de una forma continuada. Sin embargo, todavía falta un conocimiento profundo de cómo funcionan estos sistemas, especialmente en el caso de los optimizadores de potencia, de las ganancias energéticas esperables en condiciones de *mismatch* y de las posibilidades avanzadas de diagnóstico de fallos. El principal objetivo de esta tesis es presentar un estudio completo de cómo funcionan los sistemas DMPPT, sus límites y sus ventajas, así como experimentos varios que verifican la teoría y el desarrollo de herramientas para valorar las ventajas de utilizar DMPPT en cada instalación. Las ecuaciones que modelan el funcionamiento de los sistemas FVs con optimizadores de potencia se han desarrollado y utilizado para resaltar los límites de los mismos a la hora de resolver ciertas situaciones de *mismatch*. Se presenta un estudio profundo sobre el efecto de las sombras en los sistemas FVs: en la curva *I-V* y en los algoritmos MPPT. Se han llevado a cabo experimentos sobre el funcionamiento de los algoritmos MPPT en situaciones de sombreado, señalando su ineficiencia en estas

situaciones. Un análisis de la ventaja del uso de DMPPT frente a los puntos calientes es presentado y verificado. También se presenta un análisis sobre las posibles ganancias en potencia y energía con el uso de DMPPT en condiciones de sombreado y este también es verificado experimentalmente, así como un breve estudio de su viabilidad económica.

Para ayudar a llevar a cabo todos los análisis y experimentos descritos previamente se han desarrollado una serie de herramientas software. Una de ellas es un programa en LabView para controlar un simulador solar para el análisis de algoritmos MPPT y que permite almacenar los resultados de las medidas. También se ha desarrollado un programa que simula curvas *I-V* de módulos y generadores FVs afectados por sombras y este se ha verificado experimentalmente. Este mismo programa se ha utilizado para desarrollar un programa todavía más completo que estima las pérdidas anuales y las ganancias obtenidas con DMPPT en instalaciones FVs afectadas por sombras.

Finalmente, se han desarrollado y verificado unos algoritmos para diagnosticar fallos en sistemas FVs con DMPPT. Esta herramienta puede diagnosticar los siguientes fallos: sombras debido a objetos fijos (con estimación de la distancia al objeto), suciedad localizada, suciedad general, posible punto caliente, degradación de módulos y pérdidas en el cableado de DC. Además, alerta al usuario de las pérdidas producidas por cada fallo y con la ventaja de que no requiere del uso de sensores de irradiancia y temperatura.

TABLE OF CONTENTS

List of Figures

List of Tables

List of acronyms

a-Si	amorphous silicon
AM	air mass
BIPV	building integrated photovoltaics
c-Si	crystalline silicon
CMPPT	central maximum power point tracking
CPV	concentrating photovoltaics
DMPPT	distributed maximum power point tracking
FF	fill factor
IEC	International Electrotechnical Commission
IES	Instituto de Energía Solar
IIT-UPC	Instituto de Investigación Tecnológica—Universidad Pontificia de Comillas
INES	Institut National de l'Energie Solaire
LCE	levelised cost of electricity
LMPP	local maximum power point
MLPE	module level power electronics
MMU	maximizer management unit

MPP	maximum power point
MPPT	maximum power point tracking
MPR	maximum power region
MPRT	maximum power region tracking
NOCT	nominal operating cell temperature
NREL	national renewable energy laboratory
O&M	operation and maintenance
PLC	power line communications
PR	performance ratio
PV	photovoltaic
P&O	perturb & observe
SAS	solar array simulator
STC	standard test conditions
UPM	Universidad Politécnica de Madrid

List of symbols

I	current, A
V	voltage, V
P	power, W
I_m, V_m, P_m	current, voltage, power at the MPP; A,V,W
I_w, V_w, P_w	working current, voltage, power; A,V,W
I_i, V_i, P_i	input current, voltage, power; A,V,W
I_o, V_o, P_o	output current, voltage, power; A,V,W
P_{MPPT}	power tracked by the MPPT, W
V_{OC}	open circuit voltage, V
I_{SC}	short circuit current, A
$V_{OC}{}^*$, $I_{SC}{}^*$, $I_m{}^*$, $V_m{}^*$, $P_m{}^*$	… at standard test conditions, V, A, A, V, W
R_p	parallel resistance, Ω
R_s	series resistance, Ω
η	efficiency, %
η_{CE}	European efficiency, %
G	global irradiance, W/m^2
B	direct irradiance, W/m^2

D	diffuse irradiance, W/m^2
B_o	extraterrestial irradiance, W/m^2
D/G	diffuse global ratio, dimensionless
T_C	cell temperature, ^{o}C
T_a	ambient temperature, ^{o}C
β	open circuit voltage temperature coefficient, V/^{o}C
α	short circuit current temperature coefficient, A/^{o}C
V_t	thermal voltage of the p-n junction, V
V_b	breakdown voltage of the diode, V
$M(d)$	conversion ratio, dimensionless
$M(d)_R$	real conversion ratio considering the efficiency, dimensionless
$M(d)_{min}$	minimum conversion ratio, dimensionless
$M(d)_{max}$	maximum conversion ratio, dimensionless
N_T	total number of optimisers in series, dimensionless
N_M	number of mismatched optimisers, dimensionless
N_d	Number of diodes, dimensionless
V_{inv}	inverter voltage, V
P_G	power gain, %
E_G	energy gain, %
E_R	energy recovered, %
S	shaded fraction, %

m	current mismatch, %
θ_s	incidence angle, sexagesimal degrees
θ_{zs}	azimuthal angle, sexagesimal degrees
Z	load, Ω
d	duty cycle, s
T_S	commutation period, s

1 INTRODUCTION

1.1 FRAME OF RESEARCH AND MOTIVATION (INTEGRA FV)

The work presented in this PhD Thesis is mainly the result of the research conducted by the candidate at the Instituto de Energía Solar of the Universidad Politécnica de Madrid (IES-UPM), in Madrid, Spain. During the research period and under the International Doctorate program of the UPM, the candidate worked four months conducting research at the Institut National de l'Energie Solaire (INES), in Chambery, France and some results from this period are also presented.

The fundamental basis of the work presented in this Thesis is the project INTEGRA FV (ENE2008-06763-C02-01) financed by the Spanish Ministry of Science and Technology in which the IES-UPM and Tecnalia, a research centre from the Basque country, have worked together. This project is born at the end of 2008, during a scenario of exponential increase of the photovoltaic (PV) systems in Spain, reaching the world record breaking figure of 2.7GW installed in a year. This increase was mainly based on large ground-mounted PV plants, as the subsidies primed this type of installations. The integration of PV into the urban environment, despite its unquestionable advantages such as producing electricity in the place where it is consumed and competing in price with the user's electricity tariff, still, even to this day, lags behind; although quickly increasing. The main objective of the INTEGRA FV project was to improve the efficiency, feasibility and availability of energy in PV systems, especially in building

integrated photovoltaic (BIPV) systems, thus contributing from a technological point of view to the complete development of PV energy

Several studies [Eclareon, 2013; Parkinson, 2013; Shah, Booream-Phelps et al., 2014] confirm that PV systems have already reached grid parity[1] in several parts of the world. Although this would seem to be reason enough for a large scale deployment of roof-mounted PV systems, this is not the case. There are several reasons for this: political, economic and technical. Although the political ones are evidently out of the scope of this Thesis, it is worth noting that large scale deployment of roof-top PV systems implies the democratization of energy, were now any individual is able to produce its own electricity reducing their dependence on electric utilities. The immense loss of benefit and power of electric utilities is evident and the electric lobbies worldwide are pressuring the governments to avoid this situation. In Spain, this is working extremely well and from 2008 only 2GW have been installed in five years and the government has recently proposed introducing a fee of 0.07€ for each kWh that is produced and instantly consumed; destroying any economic benefit in self-consumption PV systems.

Because distributed PV systems are generally of small size, their price is higher than ground-mounted PV systems, mainly because it is more difficult to apply economies of scale and because of labour costs. While, to this day, ground mounted PV systems are costing around 1€/W_p roof-mounted PV systems of about 3kW are estimated at around 2€/W_p [EPIA, 2012]. In addition, because of their geographic distribution and installation, at usually less accessible places, the O&M costs are also higher. Other technical reasons like the complexity of the installation and the losses due to shading will also incur in a higher price of the final levelised cost of electricity (LCE).

In order to solve some of the problems related with roof-mounted PV installations, increase their efficiency and, therefore, lower the LCE, new system architectures, like that of distributed maximum power point tracking (DMPPT) have been proposed.

[1] Grid parity refers to the moment where the PV levelised cost of electricity (LCE) is less than or equal to the price that the user pays to the utility.

1.2 INTRODUCTION TO DMPPT SYSTEMS

Traditionally, PV systems are composed of a number of PV modules all connected in series or parallel to a central or string inverter who is in charge of the maximum power point tracking (MPPT) and the DC-AC conversion. These new DMPPT systems, also known as module level power electronics (MLPE), have an MPPT algorithm at each PV module or each few modules. The DC-AC conversion can be centralized, as is the case with power optimizers, or distributed (at the same point as the MPPT), as is the case with micro-inverters. Figure 1.1 shows the schema of both of these topologies.

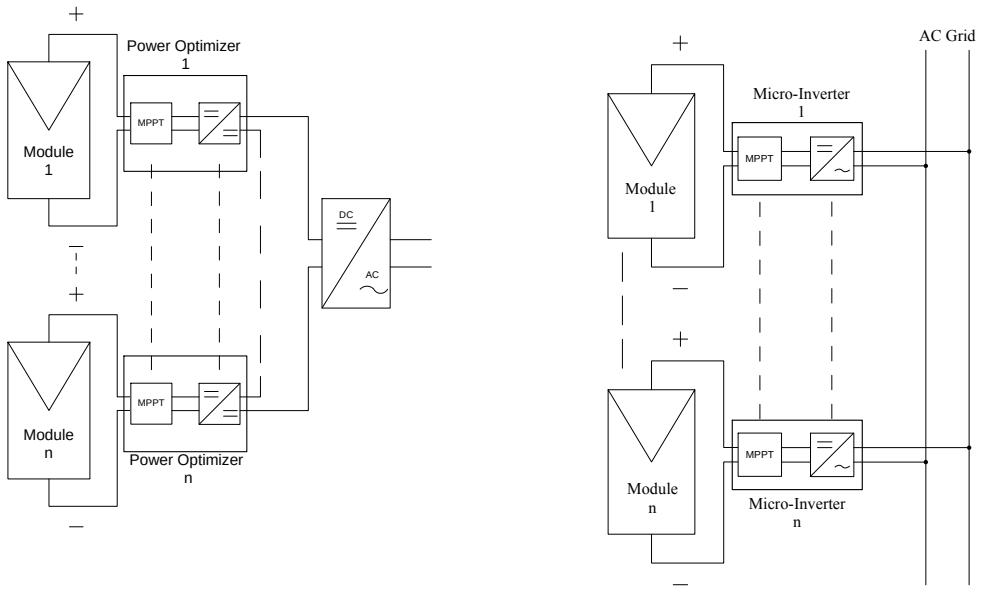

Figure 1.1: Connection diagram of power optimizers (left) and microinverters (right).

Although the idea of using micro-inverters has been present since the early 1990s [Hempel, Kleinkauf et al., 1992] and that of power optimizers since the mid-2000s [Walker and Sernia, 2004], at the beginning of this PhD Thesis, in late 2009, there were only a couple of companies offering these products. In the last few years, DMPPT systems have been introduced in the PV market and their market share is growing steadily: [IMS, 2013; Podewils, 2011; Shiao, 2013]. The common denominator in the claims made by these companies is the extra electricity produced by the use of their products, some claiming "extra power yields up to 30%" and others even claiming "up to 25% extra energy harvests".

Some of the advantages that have been proposed with the use of DMPPT systems are:

- Better optimisation of each module in the system: because each module has its own MPPT, the maximum power of each module can be extracted at all times eliminating the losses due to mismatch.

- Design flexibility: because each module has its own MPPT, this permits connecting together modules of different technology or characteristics. It is also possible to connect together modules installed at different tilt or orientation angles.

- Advanced monitoring systems**:** having an MPPT at each module implies that values of voltage and current of each module are being constantly measured. This provides an immense amount of information that can be used to detect failures easily and rapidly, drastically reducing the O&M work.

- System reliability**:** because of the larger number of units in the system, a single failure will not result in the loss of the entire system's production as would be the case with the central inverter. This would be the case for micro-inverters but not for power optimizers which also have a central inverter.

Even though these advantages seem to be a clear benefit for complex PV installations, like those in the urban environment, there still lacks a profound understanding of the real benefits that can be obtained by using DMPPT. Previous to starting this PhD Thesis at least the following points to be solved could be identified:

- It is known and it has been proven that these systems can provide large power improvements in case of shading but whether this translates to an annual energy improvement is unclear.

- It is also known that there are limitations in the amount of shade that these systems can mitigate and the difference in orientation and tilt angles that can be combined.

- Still no advanced failure diagnosis system has been proposed and the products offered limit themselves to detecting the under-producing modules in the system.

- Is the higher price that must be paid for these systems worth it?

- More electronic parts in system can be translated to a lower reliability of the system.

From what has been exposed it is clear that there is still work to be done in the understanding of the benefits provided by DMPPT. This PhD Thesis aims at solving these issues and to provide a broader understanding on how DMPPT systems function, their real possible benefits, their limitations and their disadvantages. In addition, methods for testing each product are proposed and a model for simulating energy gains as well as an automatic failure diagnosis system have been developed.

1.3 STATE OF THE ART

1.3.1 A BIT OF HISTORY

It has only been in the last few years that the market of DMPPT products has started to pick up its pace, however, research into micro-inverters and real products have been present for over 20 years. The early stages of research and development of DMPPT products were fully focused on micro-inverters having the first references to power optimizers less than 10 years ago [Walker and Sernia, 2004]. The research into microinverters was started by the German *Institut für Solar Energie-versrgungstechnik (ISET)* in the late eighties, publishing their first papers in this area in the early nineties [Hempel, Kleinkauf et al., 1992; Kleinkauf, Sachau et al., 1992]. During this period, research and development into AC module inverters started in parallel in Germany, The Netherlands, Switzerland and the USA [Dunselman, Weiden et al., 1994; Kern and Kern, 2000; Oldenkamp and Jong, 1998a]. From this research in the late eighties and early nineties came the first prototypes and commercial micro-inverters.

The first prototype of a micro-inverter was developed by the *Zentrum für Sonnenenergie und Wasserstoff-Forschung Baden-Württemberg* in Germany and it was presented in 1992. In 1993, Dutch company Mastervolt presents their first grid-tied micro-inverter, the SunMaster 130S, which was designed to mount directly to the back of the panel and to be connected to other micro-inverters and to the power grid (Figure 1.2-left). Some years later, in 2000, this same company replaced their model with the

Soladin 120, designed to connect the PV module directly to a wall socket. During this period, the US company Ascension Technology, had also started working on a micro-inverter and in 1994 they sent an example to Sandia Labs for testing. Later, in 1997, this same company partnered with US module company ASE Americas to produce the 300W SunSine panel (Figure 1.2-right) which was the PV module which included a mounted micro-inverter in the junction box, being it the first plug and play PV Module [Kern and Kern, 2000]. In 1995, another Dutch company, OKE Services, developed a high frequency micro-inverter, the OK4 of 100Watts. This company later developed another improved model, the OK4ALL, which in 2009 was sold to the largest inverter manufacturer, SMA Solar Technology AG (SMA). Other less successful products were also developed, like the MI250 from Advanced Energy Systems, which predicted that in large quantities their inverters could be produced at less than 0.20$/W [Strong, 1999]. Being that the range of prices for today's large-scale inverters, this was a very optimistic prediction. At the time, there was already conscience of the benefits that could be gained by monitoring the production at module level and some models, like the OK4 and the ZSW, included an RS485 communication interface with monitoring facilities. The MI-250 went one step beyond and included communication by a power line communications (PLC) signal.

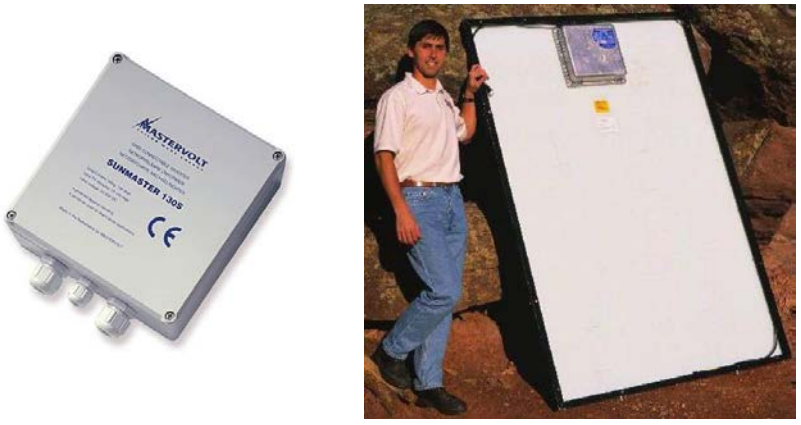

Figure 1.2: Image of one of the first microinverters and the first AC module.

During this period there were also several PV projects that installed AC modules, like the *PV-groei* (PV-growth) in The Netherlands which aimed at installing four AC modules in each of 10,000 roofs [Oldenkamp and Jong, 1998b], a 15kW installation with the SunSine AC module at the Pentagon in 1999 (Figure 1.3) or a 10kW façade with 100W micro-inverters [Knaupp, Schekulin et al., 1996]. And many of the scientific

papers that were being published at the time [Kleinkauf, Sachau et al., 1992; Oldenkamp and Jong, 1998a; Strong, 1999] already mentioned many of the benefits attributed to micro-inverters nowadays, like: higher energy production, advanced monitoring possibilities, safer installations due to small DC voltages, etc. and there were even some studies that estimated energy gains in shaded PV systems with positive results: up to a 7.5% yearly energy gain [Gross, Marttin et al., 1997].

Figure 1.3: 15kW installation with the SunSine AC module at the Pentagon in 1999.

However, as the years passed it became clear that the price of micro-inverters could not compete with that of larger central inverter systems. Because of this and reliability problems like failing micro-inverters, in 2003 they disappeared from the market when the last standing micro-inverter, the OK4, stopped production at the end of a Dutch subsidy program [Katz, 2009]. This was nonetheless only a parenthesis since only five years later, in 2008, micro-inverters, and now also power optimizers, re-entered the market.

1.3.2 THE MODERN PRODUCTS

Of all DMPPT products available today the first one to be commercially available was the micro-inverter from Enphase, which started shipping in late 2008. It was, however, some years before that other companies had started to develop similar products and in May 2009 the first power optimizers were presented at the Intersolar trade fair [Podewils, 2009]. There were three power optimizers presented at the time: SolarMagic

by US semiconductor group National Semiconductors, SolarEdge by the Israeli start-up of the same name and Tigo from the US start-up Tigo Energy. Of these three products, SolarMagic was the one that entered the market with the most force but, curiously, it is also the one that has stopped production; only two years after market introduction. Now they offer an MPPT power production chipset by Texas Instruments rather than an integrated power optimiser unit.

During the following years there was a real invasion of DMPPT products and by the end of 2011 there were over fifteen companies offering power optimizers and at least five offering micro-inverters [Podewils, 2011]. However, many of these companies had a similar future as SolarMagic and have discontinued their production. At this moment, in the world of power optimizers there are only two clear players, SolarEdge and Tigo, coping almost all of the market share with 60% SolarEdge and 40% Tigo [IMS, 2013]. By mid-2013 both of these companies had shipped over 2 million units each.

The success of the SolarEdge products has allowed the company to invest heavily in R&D and since late 2011 they offer a second generation of power optimizers and an improved efficiency of up to 99.5% for the maximum efficiency and 98.8% for the weighted efficiency, as stated by the company. An independent test from Photon International Magazine [Neuenstein and Podewils, 2011] returned lower results: from 97.94 to 99.06%. The company offers either module embedded or module add-on power optimizers. The module embedded option, with Upsolar PV modules, includes all the necessary electronics in the junction box of the PV module, eliminating cabling and the extra housing. In addition, two different types of module add-on versions are offered: one which only works with the SolarEdge inverter or the independent optimizer which can work with any inverter on the market. In the first version, five different models are offered: from 250W_p -600W_p, an input voltage range of 47V-130V and MPPT range from 5-125V depending on each model. All power optimizers from SolarEdge are sold with a 25 year warranty[2] to match PV modules' expected lifetime. They also offer a series of inverters ranging from 2.2kW to 50kW. The SolarEdge system also offers module

[2] Tigo only offers a 10 year warranty and Enphase a 25 year warranty in the US, 20 year warranty in UK, France, Greece, Italy, Luxembourm, Netherlands and Belgium and 10 year warranty in the rest of the world

level monitoring including a monitoring portal, automatic arc detection, automatic DC shutdown for safety issues and automatic alerts.

The Tigo Energy optimizers offer basically the same options as the SolarEdge products but in a more limited range, only offering two module add-on power optimizers from $300W_p$ -$350W_p$ and one module embedded power optimizer (SolarEdge also only offers one). However, in the case of the module embedded option, Tigo has arrived at agreements with six different module companies (while SolarEdge is in partnership with one) to produce their smart modules. For the Tigo system a central management unit, or maximizer management unit (MMU) as they call it, is necessary for the DC safety disconnection, arc detection and monitoring options. However, Tigo is also in a partnership with Kaco who produces an inverter especially for the Tigo system and which includes the MMU. Another feature that differentiates Tigo from SolarEdge is the MPPT function. While SolarEdge utilizes a classic MPPT algorithm applied to each module, Tigo has implemented a centralised approach. The idea is that from the working values of each module a central processing unit calculates the exact *I-V* properties of each module and then each maximizer contains the "impedance matching" components to control the output of each module. This approach could be more cost effective as there is not one MPPT per module. However, their MPPT range, from 16-48V, could cause local maximum power points (MPPs) to not be detected, as is shown in section 4.5 and the necessity of communicating with a central unit for the MPPT function could also result problematic if the communication is lost or if local maxima are present.

In the market for microinverters there are a larger number of players, although the clear leader is Enphase with over 3 million units shipped by July 2013. Even so is their leadership, that, according to the Enphase CEO, the firm boasted a 53.5% market share in the US residential market; that is considering all inverters not only microinverters. However, in the last year or so, many other companies have entered the microinverter market and can jeopardize this leadership, especially some big inverter companies like SMA or PowerOne which have both recently introduced a microinverter to their product portfolio. Other names that are in the game are SolarBridge reaching a different market than Enphase as they are the only AC module producer, Enecsys with over 160,000 microinverters sold and Renesola with a price 15 to 20% lower than Enphase

and delivering 10,000 units per month in the US [Wesoff, 2013a]. Despite the relatively large number of products, there is barely any difference in specifications or in added value. They all offer the standard DC/AC conversion at module level with monitoring possibilities. The power ranges are all very similar as the MPPT range. This second factor is important to consider since almost none of them can track below 22-24V which can seriously affect the efficiency when local MPPs are present, as is shown in section 4.5. Table 1.1 presents the main characteristics of the main microinverters and power optimizers available by July 2014.

1.3.3 THE ACTUAL AND FUTURE MARKET OF DMPPT PRODUCTS

Analysing a market is always a difficult task, especially since the data isn't always available and is sometimes distorted due to economic interests. In the case of the market for DMPPT there are two full analysis available, one by the UK firm IMS research titled "The world market for PV microinverters and power optimizers" [IMS, 2013], recently acquired by IHS, who has published the third yearly version of their report and the other by GTM Research ("The global PV inverter landscape 2013: technologies markets and survivors") [Shiao, 2013] a part of the online media company on renewable energies, Greentech Media. These reports are quite costly, 3000-6000€, and neither of them were purchased to develop this section. All the data presented in this section comes from interviews to IHS members or from articles from Greentech Media or PV-magazine which reference either report.

According to IMS-IHS research the world market in 2013 for microinverters will hit 500MW [Meza, 2013] and that of power optimizers between 600-900MW [Neidlein, 2013]. This sums to a total between 1.1-1.4GW which considering shipments of around 32GW of classic PV inverters corresponds to about 4% of the total inverter market. This is still a low figure, however, it should be considered that this DMPPT technology is still very new and that it is growing fast, 180% in 2011 and 70% in 2012 and that by 2016 it will comprise 10% of the market [Beetz, 2012]. IMS research predicts that power optimizers will grow to a 4GW market by 2016 [Neidlein, 2013] and microinverters to 2.1GW by 2017 [Meza, 2013].

Table 1.1: Characteristics of the main microinverters and power optimizers available by July 2014

Model	Type	Nominal ouptut power	MPPT_range (V)	Efficiency Weighted/Max (%)	
SMA SB240	Microinverter	240W	15/23-32V	95.9/96	
Enphase 250	Microinverter	240W	16/27-39V	96/96.5	
SolarBridge Pantheon II	AC module	238W	18-37	93.2/95.6	
Enecsys	Microinverter	225	23-35	93.5/95	
Power One Aurora	Microinverter	250	12/30-50	95.4/96.5	
Tigo optimizer	Power optimizer: Add-on/module embedded	375 (buck topology)	16-48	98.5/99.5	
SolarEdge (Data shown for OP250)		250W (buck-boost topology)	5-55	(Does not consider the central inverter's efficiency)	
Ampt (Data shown for V40-x)		260W	10-38V	98/99	

Dividing the market by regions, microinverters are inclined towards the US, coping 72% of all the microinverter market in 2012 [Meza, 2013]. Microinverters have reached such high penetration rates in the US that they held a 53.5% market share in the US residential market in 2012 [Wesoff, 2013a], including all inverters. While power optimizers have their market in Europe [Neidlein, 2013], a large growth of the power optimizer market is expected in Asia in the following years and then the Americas.

Despite the different products available, over 25 microinverters and power optimizers, just three — Enphase, SolarEdge and Tigo — accounted for 93% of shipments [Beetz, 2012]. Considering the number exposed in the previous paragraph, it could be 60% power optimizers and 40% microinverters. Inside the power optimizers category it is 60% SolarEdge and 40% Tigo [Neidlein, 2013].

Initially, the DMPPT products were designed for small residential installations affected by shading or with difficult design features like different tilt and orientation angles. Until 2013 it was that way with 91% of these products going to residential systems although a shift is expected having about one third of the products installed in commercial systems by 2017 [Meza, 2013]. Certainly, this shift has already started and many hundred-kilowatt and even megawatt systems have been built with distributed power electronics. For example, SolarEdge has several installations in the hundreds-of-kilowatts range and even a 1.63MW installation in The Netherlands and has announced an 8MW project to be connected in 2014. Tigo has also various installations in the hundreds-of-kilowatts range and a 2.2MW installation with Upsolar-Tigo smart modules in Vermont. This installation was decided to be installed with Upsolar-Tigo modules due to the orography of the terrain, as shown in Figure 1.4. And in August 2013, Enphase announced the construction of a 2MW installation in Canada [Wesoff, 2013b].

Figure 1.4: 2.2MW installation in Vermont with Upsolar-Tigo smart modules

1.4 SCOPE OF THE THESIS

In a broad sense, this Thesis provides a profound understanding of how DMPPT systems work, both power optimizers and micro-inverters, and, therefore, contributes to their development. It also aims at giving the reader the sufficient knowledge and understanding to determine, for any particular PV system, whether the use of DMPPT is positive or not and which of the two technologies, if any, is best to use. This can be divided in the following sections.

In the first place, an analysis is presented of how classic PV systems work, their failures and losses, especially those that are aimed at being mitigated with DMPPT. In this part, a special emphasis is made on the effects of shading over PV modules and PV generators as they are the main effect for which DMPPT were intended in the beginning. Many measurements of *I-V* curves of generators and modules affected by shading are presented and the software that has been developed to simulate *I-V* curves of generators affected by shadows is introduced.

Secondly, a theoretical study of PV systems with power optimizers is presented. In this section only power optimizers are dealt with as they are the ones that present a complex operation in PV arrays. The *I-V* curves of power optimizers are presented and described. Mathematical equations that describe the behaviour of DC/DC converters in

PV arrays have been derived and are presented as the basis to simulate the functioning of power optimizers in PV arrays. And with this set of equations the limitations of power optimizers to mismatch mitigation is highlighted. Also, a theoretical introduction to the power gains obtained with the use of DMPPT in presence of shading is presented.

In a third part, the results from a set of experiments performed on power optimizers and microinverters are presented. Some of these experiments were aimed at verifying what was exposed in the theoretical study, resulting in good agreement. Other experiments were focused on power gains with the use of DMPPT in different shading situations and others in testing the efficiency of the different MLPE. Then a profound study on the effect of incoming shadows on the MPP of the *I-V* curve and how it could affect the MPPT of the different equipment is presented as well as the results from the tests performed on the MPPT algorithms of different equipment: inverters, microinverters and power optimizers. These were aimed at evaluating their efficiency at finding the absolute MPP in *I-V* curves with local maxima. Finally, a standard for testing this ability is proposed.

Chapter 5 presents a model for simulating energy gains with DMPPT. This model is valid for any location worldwide and allows the user to introduce different obstacles that cause shading as well as the I-V curves of different modules to consider module mismatch. Results from energy gain experiments are also presented and a brief economic analysis is performed. This analysis does not aim to be very profound but it does aim to study how the use of DMPPT affects the cost of PV systems.

Finally, the last chapter presents an advanced failure diagnosis procedure that makes use of all the module level data available in DMPPT systems. In this same chapter, the verification of the procedure which was conducted in a real PV system is also presented.

2 BASIC CONCEPTS OF PV SYSTEMS UNDER PARTIALLY SHADED CONDITIONS AND MLPE

This chapter presents a theoretical base of PV systems, especially focused on PV systems under partially shaded conditions, serving as the base to understand the whole document. First of all, the effects of temperature and irradiance changes on PV production are presented as they come into play when shading is present. There is also an introduction to the main MPPT algorithms used and some of the failures and losses that can occur in PV systems are discussed. A special emphasis is made on the effects of shading over PV modules and PV generators, as this is the main failures that DMPPT is focused on mitigating. During this thesis a software tool that simulates *I*-V curves for PV generators under shaded conditions has been developed and its implementation and validation is discussed in this chapter. Many measured and simulated *I*-*V* curves of PV generators with shading are presented and discussed, serving as the basis for the validation of the developed software. Finally, there is a brief description of DC-DC converters as they are the basis of power optimizers and they are the cause of some of the limitations of these systems.

2.1 PV SYSTEMS MODELLING, CONFIGURATION, FAILURES AND LOSSES

2.1.1 IRRADIANCE AND TEMPERATURE DEPENDENCE OF PV MODULES

The characteristics of a PV cell, module or generator are represented by its current-voltage (*I-V)* curve, in which three particular points can be identified:

- The open circuit voltage (V_{oc}), characterized by a zero current in the PV cell, module or generator.
- The short-circuit current (I_{sc}), characterized by a zero voltage.
- The maximum power point (MPP), at which there is an MPP current, I_M, an MPP voltage, V_M, and where the power, defined as $P_M = V_M \cdot I_M$, is maximum.

Figure 2.1 shows a typical *I-V* curve of a sixty cell 240W PV module with the previous points labelled. The same figure also shows the power-voltage curve of the same module.

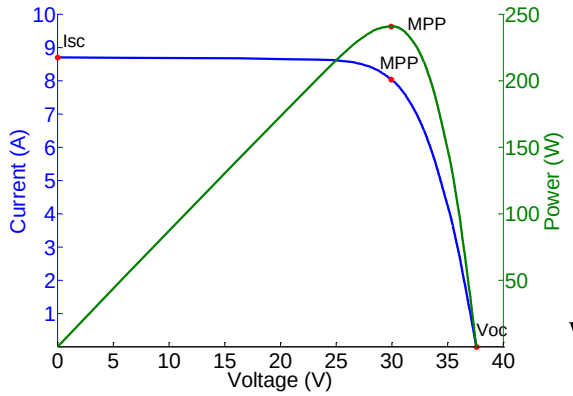

Figure 2.1: *I-V* and *P-V* curves of a 240W PV module with 60 cells in series.

All PV modules are rated at a standard set of conditions known as Standard Test Conditions (STC)[3]. The defined STC are the following:

- G^*: irradiance at STC = 1000W/m^2
- T_c^*: cell temperature at STC = 25ºC

[3] When we want to specify that a point is given at STC an asterisk is added to the parameter: for example P_M^* represents the maximum power at STC.

- Solar spectrum at *AM1*.5:

It is well known that a PV module's *I-V* curve changes its shape depending on the cell's temperature, the incoming irradiance and the solar spectrum. The short-circuit current, I_{sc}, varies mainly and linearly with the incoming irradiance as in equation (2.1).

$$I_{sc}(G) = \frac{I_{sc}^*}{G^*} \cdot G \tag{2.1}$$

However, there is a second-order effect that causes I_{sc} to increase slightly with increasing temperature. This is mainly due to the fact that the band gap of the semiconductor decreases with temperature which causes an increased light absorption. This effect can be modelled by adding a linear term to equation (2.1), obtaining equation (2.2).

$$I_{sc}(G, T_c) = I_{sc}^* \cdot \frac{G}{G^*} \cdot [1 + \alpha \cdot (T_c - T_c^*)] \tag{2.2}$$

Where T_c is the cell temperature and α is the current temperature coefficient which depends on the semiconductor type and is normally given by the manufacturer. Common values are around 0.04-0.05%/K for crystalline silicon cells, meaning that for operating cell temperatures of 70ºC there is approximately a 2% increase in I_{sc}.

The band gap reduction with increasing temperature causes a small effect on I_{sc}, but it is at the same time responsible for a significant reduction of the cell's open circuit voltage, expressed in equation (2.3).

$$V_{oc}(T_c) = V_{oc}^* + \beta \cdot N_s \cdot (T_c - T_c^*) \tag{2.3}$$

Where β is the voltage temperature coefficient which depends on the technology and is typically around -2.1mV/ºC for crystalline silicon cells; being lower (closer to zero) for amorphous silicon solar cells. N_s is the number of cells in series in the module or generator.

Although in a lower factor than the temperature, V_{oc} is also affected by the irradiance, tending it to increase with the illumination level in a logarithmic relation; as shown in equation (2.4).

$$V_{oc}(T_c, G) = V_{oc}^* + \beta \cdot N_s \cdot (T_c - T_c^*) + V_t \cdot N_s \cdot ln\left(\frac{G}{G^*}\right) \quad (2.4)$$

Where V_t is the thermal voltage of the p-n junction and responds to equation (2.5).

$$V_t = mkT/e \quad (2.5)$$

Where m is the ideality factor of the diode, typically between 1 and 1.3 for silicon solar cells, k is boltzmann's constant, T is the operation temperature in Kelvin and e is the electric charge of the electron. V_t can be approximated to 25mV for m = 1 and T = 300K.

It should be noted that, since the influence of the irradiance on V_{oc} is logarithmic, the effect can be considered negligible for irradiances close to 1000W/m². However, it is a very important effect at very high irradiances, for example in concentrating photovoltaic (CPV) applications, and at low irradiances in normal PV applications. For example, for 800W/m², 500W/m² and 100W/m² the effect on V_{oc} is 0.83%, 2.6% and 8.6% respectively. The effects of both, the cell temperature and the irradiance, on the *I-V* curve are presented in Figure 2.2.

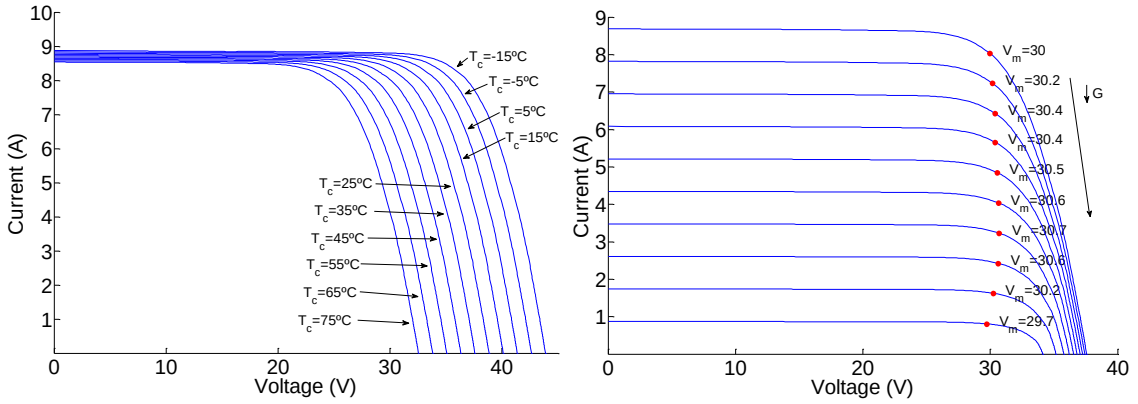

Figure 2.2: Effects of T_c and G on a PV module's electrical characteristics. The plot with changing irradiances shows the corresponding *I-V* curves from 1000W/m² (the one with highest I_{sc}) to 100W/m² (the one with lowest I_{sc}). It has been chosen to display the MPP to show how it changes in voltage with changing irradiance. This is an important point when considering the MPPT efficiency with changing irradiance and the effects are presented in section 4.5.1.

2.1.2 EXTRAPOLATION OF *I-V* CURVES TO DIFFERENT IRRADIANCE AND TEMPERATURE VALUES

The sun's spectrum changes over time and during the same day, due to the changing path of the solar rays through the atmosphere and changes in the actual atmosphere. This affects the response of PV systems due to their spectral response. Spectral losses are typically between 2% and 4% on a yearly basis [Luque and Hegedus, 2002] but can be up to 10% on smaller time scales for a-si [Nann and Emery, 1992]. For this reason, irradiance should be measured with a device of the same spectral response as the device under test and this is also suggested by the International Electrotechnical Committee (IEC) [IEC, 2006]. Others also suggest that it would be better to measure with a pyranometer and apply a spectral mismatch correction.

Considering the exposed effects of temperature and irradiance over the operating conditions, the IEC in their standard IEC-60891 [IEC, 2009] defines the equations for extrapolating the values of voltage and current of an *I-V* curve to new values of voltage and current at different operating conditions. In particular, the standard defines three correction procedures. The first is identical as the one given in the first edition of the standard in 1994, the second is an alternative method of algebraic correction which produces better results in large irradiance corrections (> 20%) and the third is an interpolation procedure which does not require input parameters (G or T_c) but can only be used when a minimum of three *I-V* curves at different operating conditions have been measured. During this thesis, all the extrapolations have been performed using the second procedure, or a small variation, defined by equations (2.6) and (2.7).

$$I_2 = I_1 \cdot [1 + \propto_{rel} \cdot (T_2 - T_1)] \cdot \frac{G_2}{G_1} \tag{2.6}$$

$$V_2 = V_1 + V_{OC1} \cdot \left[\beta_{rel} \cdot (T_2 - T_1) + a \cdot ln\left(\frac{G_2}{G_1}\right)\right] - R'_S \cdot (I_2 - I_1) - k' \cdot I_2 \cdot (T_2 - T_1) \tag{2.7}$$

where:

I_1, V_1 are coordinates of the measured I-V curve;

I_2, V_2 are coordinates of the extrapolated I-V curve;

G_1 is the measured irradiance;

G_2 is the irradiance at which the extrapolation is desired;

T_1 is the measured cell temperature;

T_2 is the cell temperature at which the extrapolation is desired;

V_{OC1} is the open circuit voltage of the measured I-V curve

α_{rel} y β_{rel} are relative temperature coefficients of current (α_{rel}) and voltage (β_{rel}) at 1000W/m^2. They are a function of I_{SC}^* and V_{OC}^*;

a is the correction factor for V_{OC} which is associated to the thermic voltage of the diode and the number of cells in series;

R_S' is the internal series resistance of the device under test;

k' is interpreted as the temperature coefficient of the internal series resistance, R_S'.

In order to be able to apply the extrapolation equation, it is necessary to have values of irradiance and cell temperature of the measured curves or, if extrapolating from STC, to know the value to extrapolate to. As already mentioned, irradiance should be measured with a device of the same spectral response as the device to be extrapolated. If this is not possible, measurements from a pyranometer can be used and a model which considers spectral changes in the incoming radiation can be applied [Martín and Ruiz, 1999].

For the cell temperature, there are three main methods which can be used. The first one is the open-circuit voltage method for which a calibrated sensor with a linear dependence of V_{oc} with respect to the temperature, typically a PV cell or module, is necessary. The procedure uses equation (2.4) to solve for T_c, resulting in equation (2.8), and is also defined by an IEC standard [IEC, 2011].

$$T_c = 25ºC + \frac{1}{\beta \cdot N_s}(V_{oc} - V_{oc}^*) \quad \textbf{(2.8)}$$

If no T_c sensor is available, a thermocouple can be attached to the Tedlar behind the PV module. However, this method is not recommended because the isolation provided by the back sheet of the PV module does not permit obtaining the real T_c.

Finally, if what is desired is to extrapolate to future operating conditions, for example to calculate the presumed production over a whole year, equation (2.9) which relates the operating cell temperature, T_c, the ambient temperature, T_a, and the irradiance can be used.

$$T_c = \frac{NOCT(ºC) - 20}{800W/m^2} \cdot G + T_a \tag{2.9}$$

Where NOCT is the nominal operating cell temperature and is a value given by the manufacturer, typically between 43ºC and 47ºC for glass-tedlar encapsulation.

The parameter a in equation (2.7) is the relative irradiance coefficient of V_{oc} and can be obtained from equation (2.10).

$$a = \frac{V_t \cdot N_s}{V_{oc}^*} \tag{2.10}$$

Obtaining R_s can be done in a number of ways. For example, the IEC-60891 suggests a procedure which measures several *I-V* curves at different irradiances and at constant temperature. Then the curves are extrapolated to STC considering $R_s = 0$, giving different *I-V* curves. R_s is then varied in steps of 10mΩ until there is less than ±0.5% error in P_m. This method proves to be very exact; however, it is very tedious since it requires measurement of different *I-V* curves at different irradiances and constant temperature.

Section 22.10.1 of [Luque and Hegedus, 2002] presents two methods for determining R_S from the main parameter of an *I-V* curve, being the most straightforward one the one presented in equation (2.11).

$$R_s = \frac{V_{oc}^* - V_m^* + m \cdot N_s \cdot V_t \cdot \ln(1 - \frac{I_m^*}{I_{sc}^*})}{I_m^*} \tag{2.11}$$

Finally, obtaining k' should be done, as explained in the IEC-60891, by measuring different *I-V* curves at different temperatures but constant irradiance. Then, these curves are extrapolated and k' is varied from 0mΩ/K in steps of 1mΩ/K until the extrapolated curves match with an error below ±0.5% at P_m. This parameter is not as important as R_s and even if it is kept at 0mΩ/K the error should not be very large.

2.1.3 SHADOWS AND NON-UNIFORM IRRADIANCE

Shadows cast over the PV generator cause a reduction of the incoming radiation and therefore reduce the power generated by the system. If the incoming radiation is reduced by the same amount all over the PV array, the resulting *I-V* curve is evident and can be easily obtained by applying equations (2.6) and (2.7). However, this is normally not the case when there are shadows from nearby objects or dirt patches in certain cells, being the reduction in the incoming radiation non-uniform. This makes the analysis of shading effects a complex exercise. For the purpose of fully understanding the effect of non-uniform irradiance over PV arrays a simulation program in Matlab has been created and it is described and validated in the following sections. This tool will be used throughout the thesis to evaluate the effects of shading over PV arrays.

2.1.3.1 Simulation methodology

Non-uniform irradiance over a PV array causes each cell to have different electrical characteristics and, because they are interconnected, electrical mismatch is present, deforming the shape of the *I-V* curve of the system. When a cell is shaded, the maximum current that it can deliver is diminished in proportion to the shading factor (*SF*). The shading factor is defined in (2.12) as a function of the percentage of shaded area (*S*) and the diffuse/global (D/G) ratio. For example, if 50% of a cell is covered by a shadow at a moment when the D/G ratio is of 20%, *SF* is equal to 40%[4].

$$SF = S * (1 - D/G) \tag{2.12}$$

[4] Note that very large objects could also reduce the diffuse fraction incident on the PV generator. This is considered in the model for simulating energy gains in chapter 5.

If this cell is connected in series with other cells it could[5] start working in negative voltages (where it can deliver more current) in order to match the current of the rest of the cells in series and if the cell works at a negative voltage, this means that there is a power loss. In order to match the current of the normally operating cells, the affected cell works in the second quadrant of its *I-V* curve as can be seen in Figure 2.3.

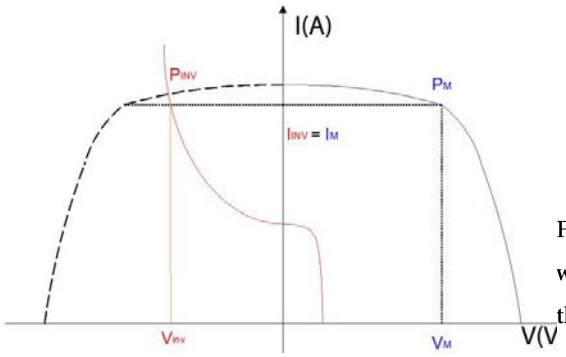

Figure 2.3: Shaded cell's I-V curve (red) and its working point (P_{inv}) at negative bias in order to match the current of the rest of the cells in the module.

A number of factors influence the negative voltage at which the shaded cell, or cells, is working and the amount of power lost. These factors are: the amount of shading over each cell, the number of shaded cells, the specific interconnection of the cells and the modules (series or parallel), the configuration of the by-pass diodes in the modules, and the reverse characteristics of each cell.

Already in 1988 Bishop studied the effect of electrical mismatches in different cell interconnections [Bishop, 1988], while more recently other authors have studied the effect of the diode configuration [Silvestre, Boronat et al., 2009], the effect of having different reverse characteristics of the solar cells [Alonso-García, Ruiz et al., 2006a; Alonso-García, Ruiz et al., 2006b; Meyer and Ernest van Dyk, 2005] and the effects of different array configurations [Woyte, Nijs et al., 2003]. In this section, all these effects are considered to analyse the effects of non-uniform irradiance over PV arrays.

In [Alonso-García and Ruíz, 2006] different models for representing the behaviour of PV cells in reverse bias are reviewed and a new model is proposed and validated, which, in turn, is used in this paper with a slight modification for better adjustment of the curves; the introduction of a linear term, *b (0<b<1)*. The model used responds to equation (2.13):

[5] This depends on the working point of the system, imposed, for example, by the MPPT. In stand-alone systems without an MPPT charge regulator, this point is imposed by the battery.

$$I = \frac{I_{sc} - b \cdot G_p \cdot V + c \cdot V^2}{1 - \exp\left\{B_e \left(1 - \sqrt{\frac{\emptyset_T - V_b}{\emptyset_T - V}}\right)\right\}} \tag{2.13}$$

Where B_e is a non-dimensional cuasi-constant parameter with value ≈ 3, V_b is the breakdown voltage, ϕ_T is the built-in junction voltage (not to be used as an adjustable parameter, using a typical value of ϕ_T = 0.85 for silicon cells of unknown junction structure.), and G_{sh} is the shunt conductance, simply $1/R_{sh}$. The addition of the linear term b and the parabolic term c ($c < 0$) is used in cases where the linear fitting is not sufficient.

R_{sh} is calculated as the slope of the curve from -0.2*N_s*V_{OC} to 0.2*N_s*V_{OC}, or the most negative value obtained in the curve, where N_s is the number of cells in series of the module or generator. And the curve of each cell is simply calculated by dividing each of the current values of the module's *I-V* curve by N_s and the voltage values by the number of parallel cells, N_p, thus considering all cells equal.

Depending on the cell type, its reverse characteristics can be very different. Even for cells of the same type and of the same module there can be a large dispersion in their reverse characteristics [Alonso-García, Ruiz et al., 2006a]. It is therefore necessary to adjust the unknown parameters of equation (2.13) for each cell type. Being B_e a cuasi-constant parameter, its adjustable range is very small, i.e. from 2.5-3.5, so the main adjustable parameters will be c and V_b. The effect of varying these two parameters can be seen in Figure 2.4.

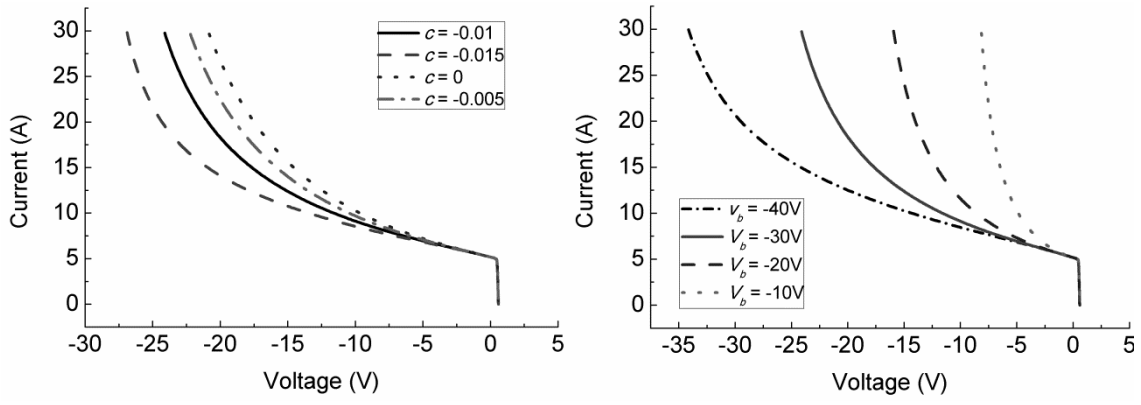

Figure 2.4: Effect of varying *c* (left) and V_b (right) in the reverse characteristics of a solar cell.

Ideally, these parameters would be adjusted for each cell of all the modules used in the simulations. However, this is not practical and the parameters represent the average values of the cells in each module and in section 2.1.3.2 it is shown that this works well

enough. Once the full *I-V* curve (in positive and negative voltages) of a typical cell is obtained, it is possible to simulate a module's or generator's *I-V* curve under shaded conditions.

When shading is present over a module or generator, each cell will have different irradiance values and the *I-V* curve in positive voltages will vary with equations (2.6) and (2.7); while in the negative voltages only I_{sc} of equation (2.13) has been considered to vary. Knowing the incoming irradiance on each cell, its *I-V* curve can be calculated and then added in series or parallel to the rest of the cells in the array. The by-pass diodes have been modeled to have a square curve which conducts at 0.7V, meaning that the by-pass diode will be in forward bias if the cells protected by the same diode add a voltage of -0.7V or lower. Once this occurs, the diode polarizes the group of cells that it protects to -0.7V. In order to validate the model for simulating shaded I-V curves, various PV modules under different shading profiles have been measured with a capacitive charge and compared to the results obtained from the simulation tool. The procedure and results are presented in the following section.

2.1.3.2 Validation of the tool for simulating shaded *I-V* curves

The first step is adjusting the unknown parameters, V_b, and c, without measuring the module's *I-V* curve in the second quadrant. However, it is possible to attain this by partially shading cells from a module and fitting the part of the I-V curve from P_m to where the diode starts working in forward bias (highlighted area of Figure 2.5) which is directly related with the shape of the *I-V* curves in reverse bias of the shaded cells. Doing this, we can estimate the reverse characteristics of the shaded cell(s).

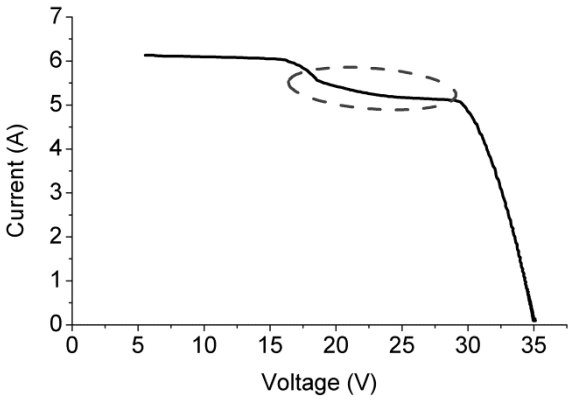

Figure 2.5: *I-V* curve of one of the modules used for the simulations affected by shading over one cell. The highlighted region is the part directly related to the reverse characteristics of the shaded cell.

For each module, all the cells' reverse *I-V* curves are supposed equal and although this simplification could be considered a limitation, especially if there is such a high variability in the reverse characteristics as shown in [Alonso-García, Ruiz et al., 2006a], we will see in that it is not a big problem, especially as the number of shaded cells in a module grows larger.

To avoid errors from the extrapolation of the I-V curve to the specific meteorological conditions, a non-shaded I-V curve of the same module was measured instantly prior to the shaded I-V curve and it was used to simulate the shaded curves with the same method used in the simulations but avoiding the extrapolation.

The first module used is the model M-60 from Bosch, with sixty cells in series and three by-pass diodes. Firstly, the parameters V_b, b, and c were adjusted to match as close as possible shading over different cells. For this, various cells of the same module were shaded and the parameters adjusted until a closest match was obtained, showing two examples in Figure 2.6. The obtained parameters are: V_b = -27V, c = -0.0055 and b = 0.009.

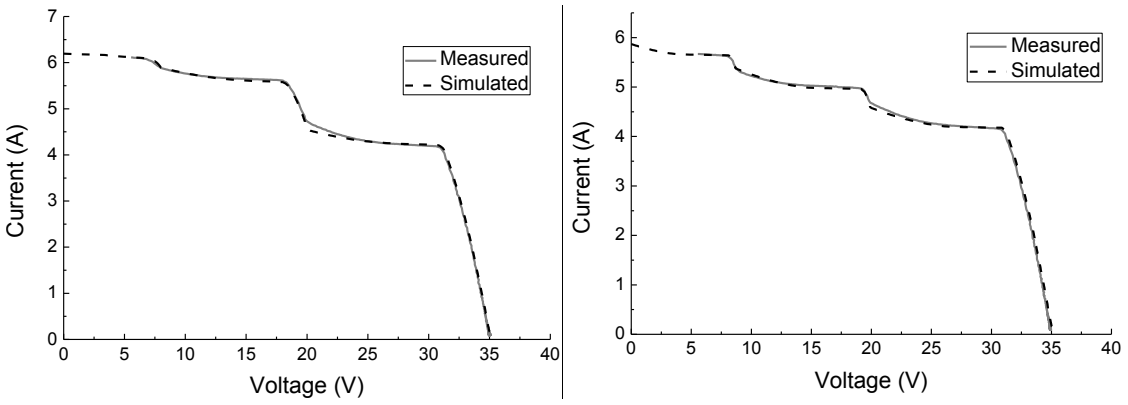

Figure 2.6: Measured and simulated I-V curves with shading on different cells. The two graphs are: shade over 50% of one cell and 12% over another on different by-pass diodes and 50%, 25% and 12% over three different by-pass diodes.

Secondly, the model from PW1400 from Photowatt, with 72 cells in series and four by-pass diodes was used. First of all a cell was shaded at 50% and the same parameters of V_b, c and b of the previous module were used, obtaining the results shown in Figure 2.7-left. It can be clearly seen how the simulated and measured curves do not match. These parameters were varied until a better match was obtained, for V_b = -6.5, c = -0.001 and b = 0.1, obtaining the results of Figure 2.7-right in which a perfect match can be seen.

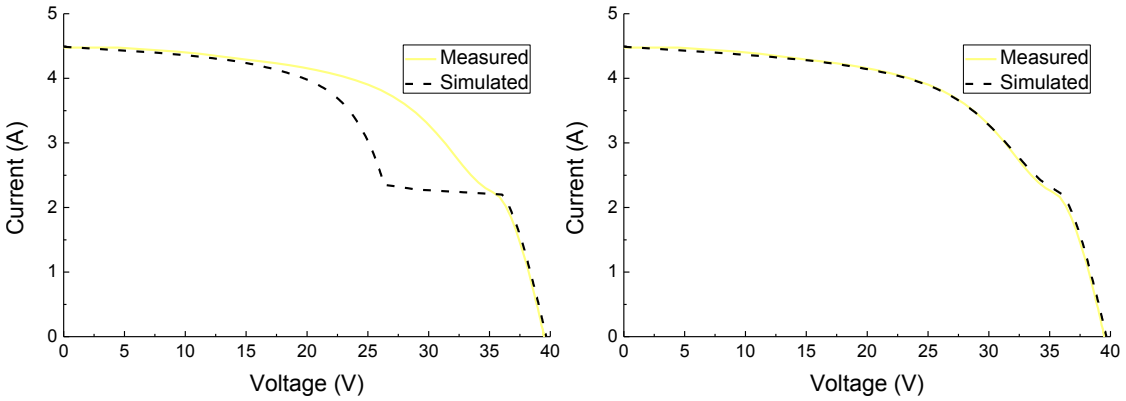

Figure 2.7: Simulated and measured *I-V* curves for the Photowatt PW1400 module and 50% shading over one cell, for the following simulated paremeters: (left)V_b = -27V, c = -0.0055 and b = 0.009 and (right) V_b = -6.5, c = -0.001 and b = 0.1.

Other measurements and simulations were performed to see if the simulation is still precise for other situations. Some more examples are presented in Figure 2.8, in which a perfect match can also be seen.

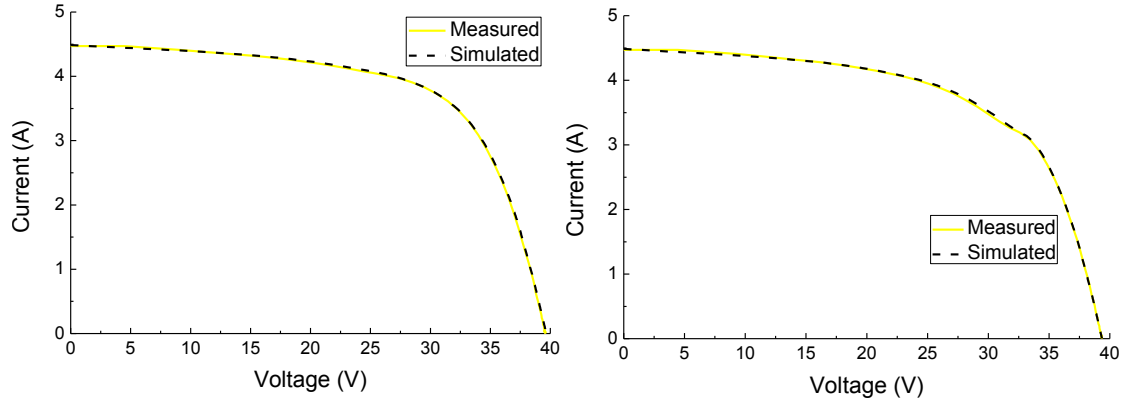

Figure 2.8: Simulated and measured *I-V* curves for the Photowatt PW1400 module and V_b = -6.5, c = -0.001 and b = 0.1, for (left) 10% shade over one cell and (right) 25% shade over one cell.

These experiments show that the simulations match well for when only one cell under the same by-pass diode is shaded, being these also the most difficult to adjust. When only one cell on a module is shaded, a slight difference of the parameters that define the *I*-V curve in reverse bias means a large difference on the curve's shape. However, when many cells are shaded, the negative voltage at which each of them works is much lower and a small difference of these parameters is also a small difference on the curve's shape; see Figure 2.4.

In conclusion, the precision of simulating increases as the number of shaded cells increases. Therefore, the procedure should be to try and match as well as possible the

simulated and real curves of modules with only one shaded cell per by-pass diode knowing that if this is done well any type of shade can be simulated with very little error.

Finally, the validation of a shaded generator is performed. For this purpose, six un-shaded Bosch M-60 PV modules were measured independently. Afterwards, they were connected together and different shading profiles were applied to the full generator and the I-V curves of the shaded generator were measured. In this case an extrapolation was performed in irradiance, however, the difference between maximum and minimum irradiance during all the measurements was only 1.3%. Cell temperature was assumed constant.

Figure 2.9 shows the measured and simulated I-V curves of a whole generator when partial shading is present as well as pictures of the shadows applied. The graph on the left represents an 85% shade on five cells of one module and one by-pass diode and 27% on two cells of another module also in only one by-pass diode. The graph on the right corresponds to 4 fully shaded cells in one module and two by-pass diodes, another 2 cells shaded only 60% in the third by-pass diode and the shadow casted by a large pole in two by-pass diode zones of another module, at different percentages.

In this case module mismatch is also present and is taken into consideration. From the comparison of both curves, it can be observed that the simulation of shaded generators also complies very well with reality.

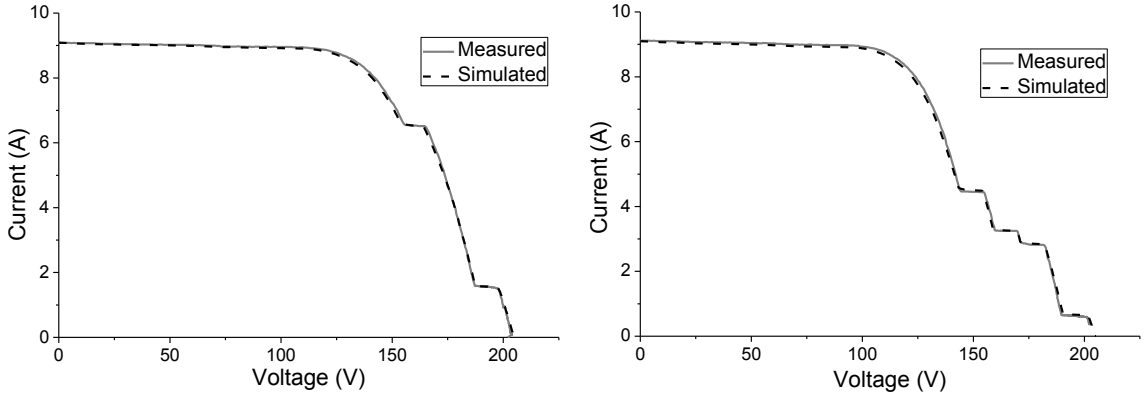

Figure 2.9: Comparison of two measured and simulated I-V curves of a whole generator with different shading on different modules. The graph on the left represents an 85% shade on five cells of one module and one by-pass diode and 27% on two cells of another module also in only one by-pass diode (shadow of the pole of the left picture). The graph on the right corresponds to 4 fully shaded cells in one module and two by-pass diodes, another 2 cells shaded only 60% in the third by-pass diode and the shadow casted by a large pole in two by-pass diode zones of another module, at different percentages (shadow of the pole plus the shadow shown on the right picture).

2.1.3.3 Examples of the effects of shading over PV generators

This section shows various shaded *I-V* curves under different circumstances. Various parameters are varied to see how these affect the shape of the *I-V* curve. For all the examples, the shading percentage corresponds to a proportional loss of I_{SC}, i.e. the diffuse component is considered to be zero.

2.1.3.3.a Effects of shading on the shape of the I-V curve for different values of V_b

For the simulations presented in this section, two values of cell breakdown voltage have been used: V_b=-5V and V_b=-25V. These values are chosen as in one case (V_b=-5V) shading over one cell is not enough to polarize the diode in forward bias while in the other (V_b=-25V), shade over one cell will be enough to polarize the diode in forward bias. In part, these values were also chosen as they match quite well with the values measured in different PV modules used in this thesis. For example, modules Isofoton I-110 and Photowatt PW-1400 have cells with low breakdown voltages (from -5V to -7V) and modules Siliken 60 P6L and Bosch c-Si M 60 have cells with high breakdown voltages (from -15V to -30V). Theoretically, the difference in *Vb* should be attributed to the difference in doping of the less doped side in the p-n junction; normally the base. Curiously, the modules measured with higher V_b correspond to more modern modules

(2012-2014), while the ones with less V_b correspond to older modules (2004-2007), although no explanation has been found for this.

For all examples shown from Figure 2.10 to Figure 2.14 a 238W PV module with 60 cells in series and three by-pass diodes (20 cells per diode) has been used. Figure 2.10 shows the effect of shading over one cell for different degrees of shading and a different V_b of the shaded cell. In all of the examples the shape of the resulting *I-V* curve is different due to the different reverse characteristics of the shaded cell.

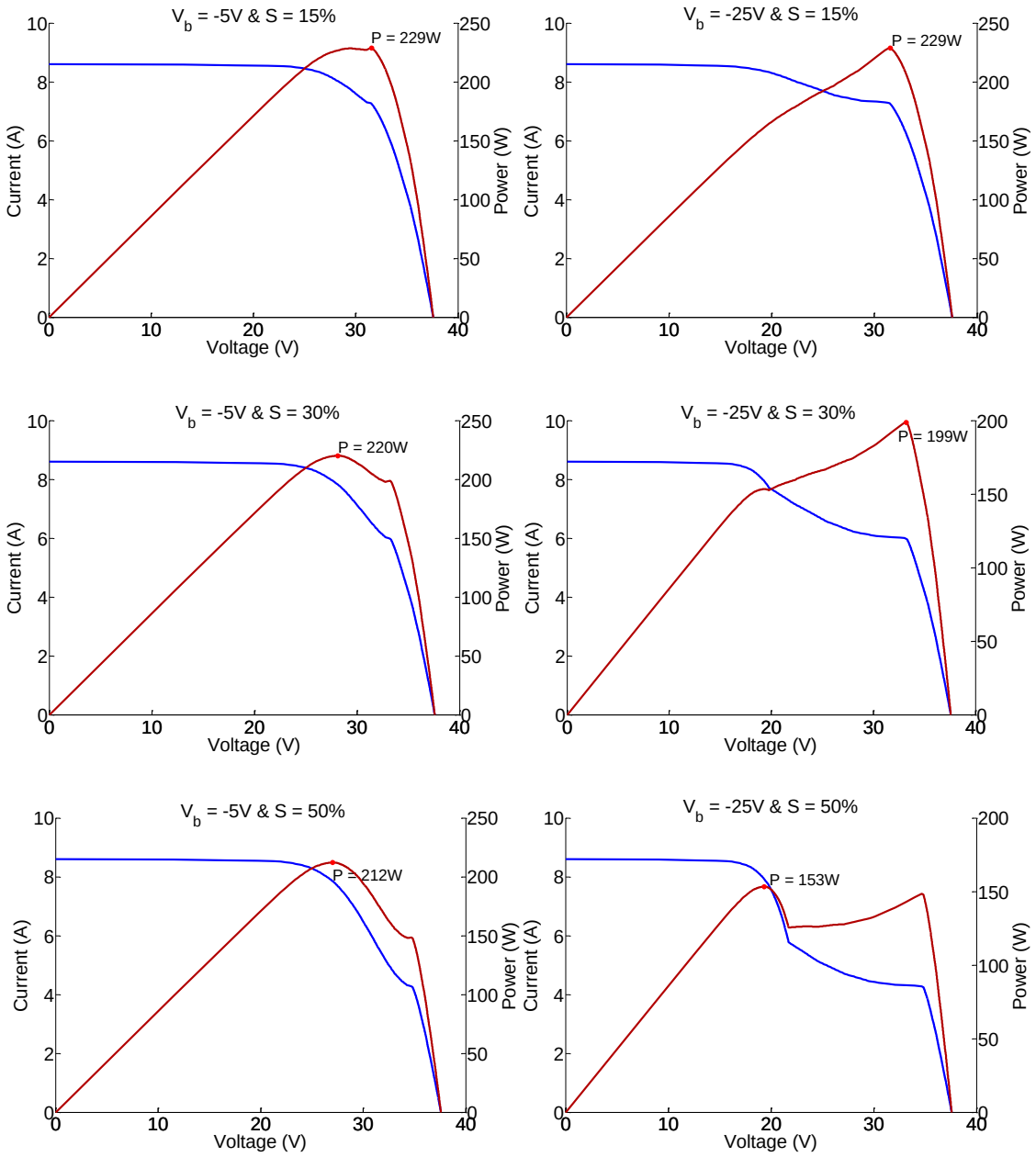

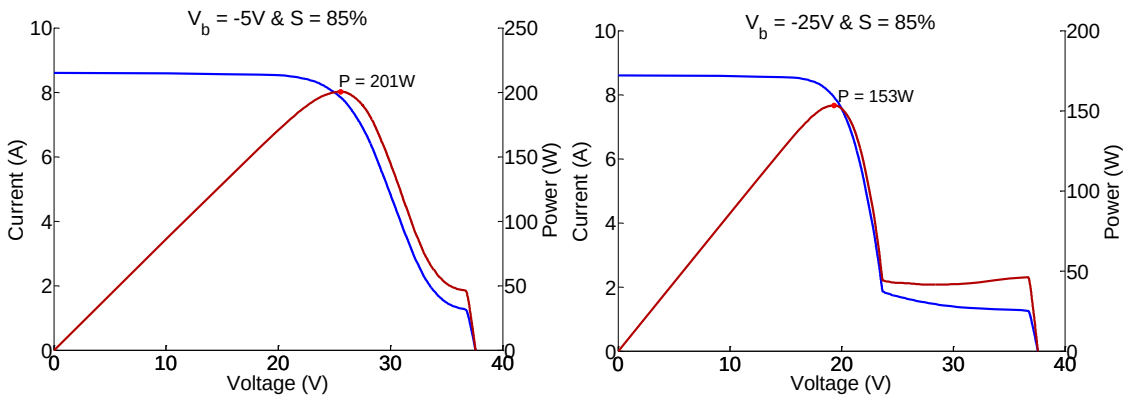

Figure 2.10: 15% (top), 30%(second from top) 50% (third from top) and 85% (bottom) shading over one cell of a 238W (V_{mpp}=30V and I_{mpp}=8.04A) module with 60 cells in series and three by-pass diodes for V_b = -5V (left) and V_b = -25V (right).

At 15% shading, both modules lose the same amount of power because the shaded cell does not work in reverse bias and it is the rest of the cells in series that lower their current to match the shaded cell's current. So the reverse characteristics of the shaded cell have no effect on the MPP, although they do have an effect on the shape of the *I*-V curve, as can be seen. It must be noted that even though there is an irradiance loss of 15% in one cell, the lost power is only 4%. This is because when the module reduces its I_m it is displacing its working point towards V_{oc} and, therefore, increasing its V_m, so the effective power loss is always lower than the reduction in current.

At 30% shade, the shaded cell with a V_b = -5V works in reverse bias, matching the current of the non-shaded cells and lowering the V_m of the module while the cell with V_b = -25V works in forward bias forcing the reduction of current of the rest of the cells. This occurs because if the cell with V_b = -25V worked in reverse bias it would force the by-pass diode in forward bias losing the power of all 20 cells, or one third of the module's power, plus some due to the voltage drop in the diode. Therefore, at this shading percentage, and for this cell, it is still worth reducing the current of the non-shaded cells. For the cell with V_b = -5V the by-pass diode never works in forward bias and losing a maximum of five volts is better than reducing the current of the non-shaded cells. A 10% power difference is also noticed in both cases, being the module with the cell of V_b = -5V the one that loses less power.

In the third case, with 50% shade applied, both cells are working in reverse bias. The module with the cell of V_b = -5V only loses a bit more power than in the previous case,

due to the shaded cell working at a slightly more negative voltage but still at the non-shaded I_m. The module with the V_b = -25V cell has now lost the power from one third of the cells due to the by-pass diode working in forward bias. There is a large power difference between both modules.

Finally, in the case for 85% shading there is no difference with respect to the previous case in the module with the V_b = -25V cell because the by-pass diode is still in forward bias like in the previous case. The module with the V_b = -5V cell has lost more power due to the shaded cell working in slightly more negative voltage.

Figure 2.11 shows shading over the same module as the previous example but this time shading five cells under the same by-pass diode. Because a larger number of cells are shaded, the sum of the negative voltages of the shaded cells is enough to forward bias the diode and, therefore, the power lost is the same in both modules. In this case the only difference is in the shape of the *I-V* curve, which is now much less than in the case with only one shaded cell.

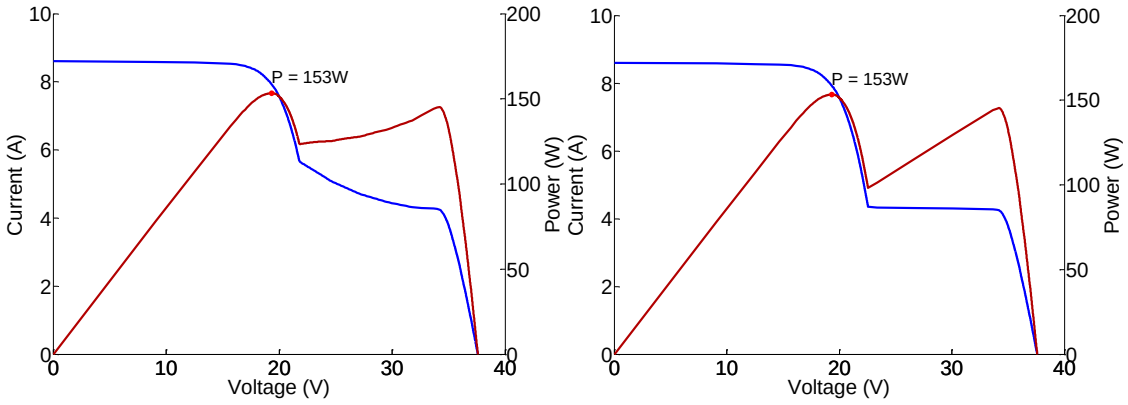

Figure 2.11: 50% shading over five cells of a 238.3W(V_{mpp}=30V and I_{mpp}=8.04A) PV module with 60 cells in series and three by-pass diodes for V_b = -5V (left) and V_b = -25V (right).

In conclusion, when only one, or maybe a few, cells are shaded V_b has a great effect on the shape of the *I-V* curve and on the power loss. For modules with cells that have a low V_b, when only one cell is shaded the by-pass diode does not work at all and it not being there would yield the same result. This also causes that distinct local maxima do not appear, opposite to the case of cells with high V_b, which could affect the efficiency of the MPPT algorithm (section 4.5.2). However, as the number of shaded cells increases the importance of V_b decreases.

2.1.3.3.b *Effects of shading on the I-V curve of PV generators when various sub-modules are shaded*

Figure 2.12 shows two different *I-V* curves were cells of different sub-modules[6] are shaded. Specifically, five cells of one by-pass diode are shaded 85% and one cell of a second by-pass diode is shaded 50%. This is a combination of the examples of Figure 2.10 and Figure 2.11, just to show that the effects can be combined; that is, the shape of the curve in each section in the combined case is very similar to that of the isolated case. However, it must be noted that the activation of the second diode will not occur at the same degree of shade needed to activate the first diode. For example, in Figure 2.12 (right) the MPP is at a point where only one diode is activated while if we were to add the two effects, both diodes should be activated: a 50% shade and an 85% shade both activate their diodes. Now, the activation of the second diode means losing more than 50% of the power left while before it meant only 1/3, meaning that it is more efficient to reduce the current of the non-shaded cells by 50%.

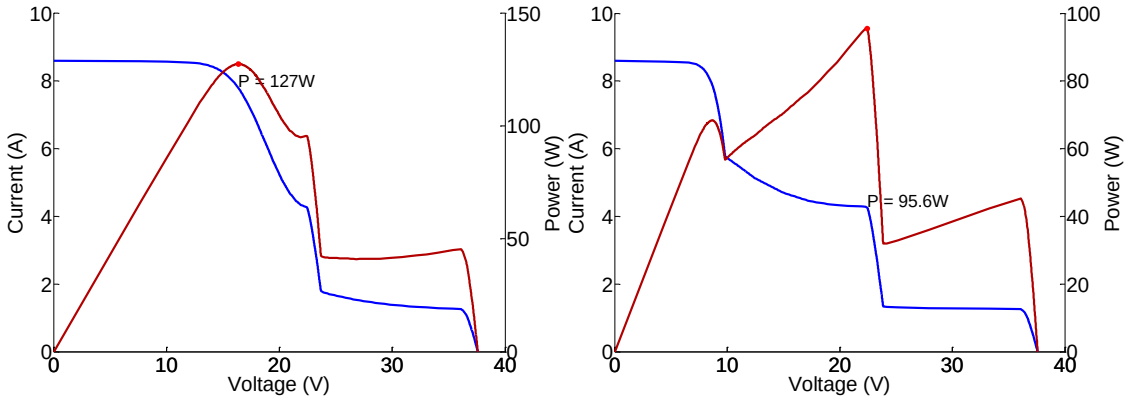

Figure 2.12: 85% shading over five cells of one by-pass diode and 50% over one cell of a second by-pass diode of a 238.3W(V_{mpp}=30V and I_{mpp}=8.04A) module with 60 cells in series and three by-pass diodes for V_b = -5V (left) and V_b = -25V (right).

Similar considerations can be applied to PV generators. Because each sub-module can be considered independent of the rest, a PV generator of 10 modules in series can be considered like 30 sub-modules. However, considering the effect of activation or not of the diode the power loss might not be the same for the same degree of shading. For example, Figure 2.13 shows two examples of shading over an array of 10 PV modules in

[6] A sub-module refers to the group of cells protected by one by-pass diode, i.e. a sixty cell module with three by-pass diodes is made up of three sub-modules.

series with the same shading as the examples in Figure 2.11 (50% shading over five cells) and Figure 2.12 (85% shading over five cells and 50% shading over one cell), only for the cell with V_b = -25V. In the example of the left, the diodes are in forward bias in both the module and the generator and the power lost is the same in both systems: 85W. However, in the example of the right, both diodes are in forward bias in the ten module generator but the module alone only has one of the diodes in forward bias, losing one sub-module. In this case, the power lost in the individual module is less than the power lost in the generator: 142.7W in comparison to 170W. This, we can say, is the basis for power optimization with DMPPT and more examples are seen in section 3.4.

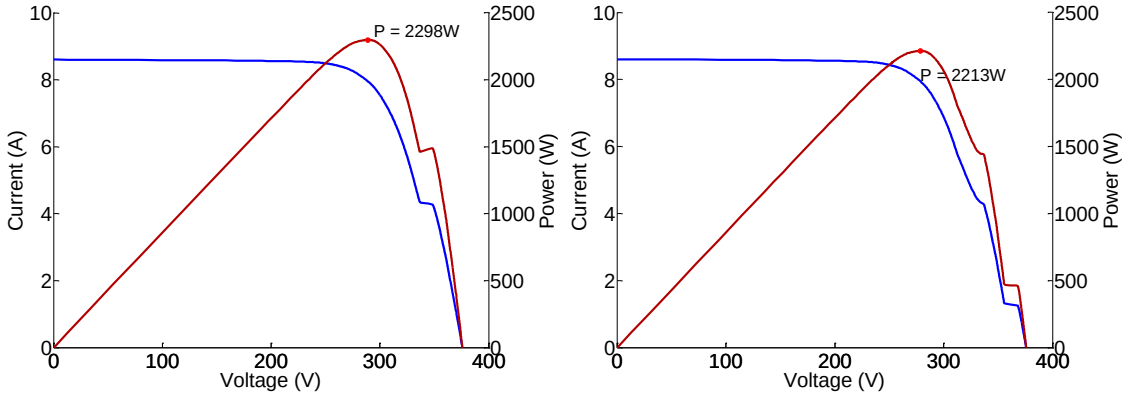

Figure 2.13: *I-V* curves of a ten module generator with the same shading as the examples in left-Figure 2.11 (50% shade over five cells of the same by-pass diode) and right-Figure 2.12 (85% shade over five cells and 50% shade over one cell of two different by-pass diodes). In the left case, because now both by-pass diodes are in forward bias, the power lost is the same as that lost in the single module (85W) while in the right case the power lost in the whole generator is higher (170W with respect to 142.7W). This is the basis for power optimisation with DMPPT.

2.1.3.3.c Effects of shading on the I-V curve of parallel strings

Because the activation of the diode isolates the shaded sub-module very effectively, shading is not much of a problem with respect to current mismatch in series strings; the solution is losing the shaded sub-module. However, when strings are connected in parallel, and because their voltage must be the same, shaded strings can negatively affect the rest of the non-shaded strings in parallel. Figure 2.14 shows two *I*-V curves with the same shading as in Figure 2.13-right but with two parallel strings of five modules each. The shade is applied to two sub-modules of the same string (right) and on sub-modules of different strings (left). If the shade is split up between the strings, V_{mpp} of both strings will be the same and there will be no voltage mismatch, losing the same power as in a

ten module string. However, if all the shading occurs on the same string, there will be a voltage mismatch and the power loss will be higher.

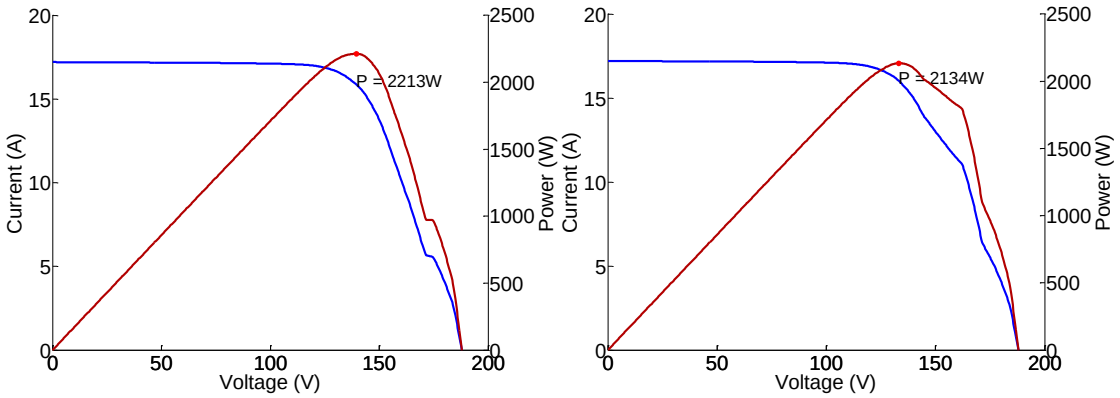

Figure 2.14: *I-V* curves of a PV generator of two parallel strings with five modules each, with the same shade as Figure 2.13-right (85% shade over five cells and 50% shade over one cell of two different by-pass diodes) where the shaded sub-modules belong to different strings (left) and the same string (right). It can be seen how, due to voltage mismatch of the strings, when the shadow affects only one of the strings the power loss is higher than if the shadow is spread over both parallel strings.

Therefore, in parallel strings if the shading is not compensated between strings, the use of DMPPT can prove even more beneficial as the power loss is higher in a CMPPT system but the same in the DMPPT system. If the shading is compensated between strings, the use of DMPPT in a system with parallel strings will not return higher gains than if the same system was one single string. More on this is seen in section 3.4.1. Other options for solving this problem are the use of multi-MPPT inverters, which have a separate MPPT algorithm for each string, eliminating the voltage mismatch between parallel strings and which could result cheaper than DMPPT.

2.1.4 MPPT ALGORITHMS

An MPPT algorithm plays an important role in a PV system since it is in charge of finding the MPP of the module's or generator's *I-V* curve, thus maximizing the energy output of the system. In the previous section, it was assumed that the MPP values from partial shading were achieved by a perfect MPPT algorithm. In reality, some inverters may be operating at a sub-optimal operating point; as will be seen in section 4.5.2.3.

There are numerous references in the literature to MPPT algorithms and reviews of the different methods can be found in the following references [Esram and Chapman, 2007;

Hohm and Ropp, 2003; Reza Reisi, Hassan Moradi et al., 2013; Sanz, 2010]. For example, in [Esram and Chapman, 2007] over 90 different papers and 19 different MPPT algorithms are reviewed. Despite this large number of methods for MPPT the most popular ones and the ones used in commercial inverters are the Perturb and Observe (P&O) and Incremental Conductance (InCond) [Hohm and Ropp, 2003; Sanz, 2010] or small variations of them.

The P&O method is based on the perturbation by means of small changes in the voltage. If an increment of the voltage returns an increment of the power, the algorithm continues to increase the voltage. Otherwise, if it returns a decrement of the power then the algorithm starts to decrease the working voltage. This process is repeated until the MPP is found and then the operating point oscillates around the MPP.

The InCond algorithm is based on the fact that the slope of a *P-V* curve is zero at the MPP, positive on the left of it and negative on the right. By comparing the increment of the power versus the increment of the voltage between two consecutives samples, the change in the MPP voltage can be determined.

In both P&O and InCond schemes, how fast the MPP is reached depends on the size of the increment of the reference voltage.

Both of these techniques have the drawback of oscillation around the MPP. However, if the algorithm is designed well enough, for example with a variable perturbation step [Chao, Dean et al., 2009], this problem can be minimized. Another drawback is that they can lose track of the MPP if the irradiation changes rapidly. For example, when irradiation changes occur, the curve in which the algorithms are based changes continuously, as was seen in Figure 2.2, so the changes in power are not only due to the perturbation of the voltage. As a consequence it is not possible for the algorithms to determine whether the change in the power is due to its own voltage increment or due to the change in the irradiation, possibly causing the MPPT to keep changing the voltage in a direction away from the MPP. There are, however, improved P&O methods that solve this problem [Sera, Kerekes et al., 2006] and there is an international standard [CENELEC, 2010] which proposes a measurement protocol to verify the correct working of MPPTs. More on this is seen in section 4.5.1.

Probably, the biggest issue with MPPT efficiency is not finding local MPPs. Sections 2.1.3 and 4.5.2 show how local MPPs can appear in the I-V curves when shading is present and how the power difference between a local MPP and the global MPP can be quite large. If the MPPT is not capable of finding the absolute MPP and stays at local MPPs, large power losses can occur. Although there are various methods that solve this problem [Alonso, Ibaez et al., 2009; Patel and Agarwal, 2008; Taheri, Salam et al., 2010; Young-Hyok, Doo-Yong et al., 2011] most modern PV inverters, micro-inverters and power optimizers do not include them, as is presented in 4.5, and even today's only standard for measuring MPPT efficiency [CENELEC, 2010] (presented in the following section) does not include an MPPT test when local maxima are present.

2.1.4.1 MPPT efficiency

If the MPPT algorithm does not function properly it will not maximize the power extracted from the PV system, increasing the losses and therefore reducing the performance ratio (PR). The PR is the ratio of AC energy delivered to the grid to the energy production of an ideal, lossless PV plant at 25ºC cell temperature, and is defined in the IEC standard 61724 [IEC, 1998]. It is therefore important to characterize how well an MPPT algorithm works to be aware of the possible losses due to MPPT inefficiency and to improve the algorithm in case necessary. This characterization results in the MPPT efficiency, expressed as equation (2.14) and defined by the European Standard EN 50530:2010 of title: *Overall efficiency of grid connected photovoltaic inverters* [CENELEC, 2010].

$$\eta_{MPPT} = \frac{\int_0^{T_M} P_{MPPT}(t)dt}{\int_0^{T_M} P_M(t)dt} \tag{2.14}$$

Where $P_{MPPT}(t)$ is the power point found by the MPPT algorithm and $P_M(t)$ is the theoretical MPP of the I-V curve, at each time instant.

The Standard also defines two types of efficiencies: static efficiency and dynamic efficiency. The static MPPT efficiency measures the precision of an inverter to operate at the MPP in a static I-V curve of a PV generator; that is with no irradiance or temperature changes. The Standard requires that an I-V curve is set at the I-V simulator, with a constant power, and connected to the inverter. Before measuring, an

initial stabilization time should be waited until the inverter finds the MPP. After the stabilization, the DC power set by the MPPT algorithm should be recorded during 10 minutes[7]. Then, applying equation (2.14) the static MPPT efficiency is obtained. The standard also requires that this test is implemented for powers ranging from 5%-100% of the nominal power and for different shapes of I-V curves, those similar to c-Si modules and thin-film modules.

Because an I-V curve's shape changes with irradiance and temperature, the Standard also defines a dynamic MPPT efficiency. In this test the cell temperature is considered constant and only irradiance changes are taken into account. However, as it was shown in section 2.1.1, not only is the current dependent on the irradiance but also the voltage so the I-V curves' voltage and current will change during the test.

Like in the previous test, the I-V simulator sets a curve and inputs it into the inverter to test. During the test different I-V curves are set depending on a varying irradiance following a pattern similar to Figure 2.15, taken from the Spanish version of the Standard. Specifically, there are two irradiance ranges: from 300W/m^2 to 1000W/m^2 and from 100W/m^2 to 500W/m^2 and the slope of the rising and decreasing ramps are changed: from 0.5W/m^2/s to 100W/m^2/s. The waiting time at high irradiance and low irradiance is 10 seconds.

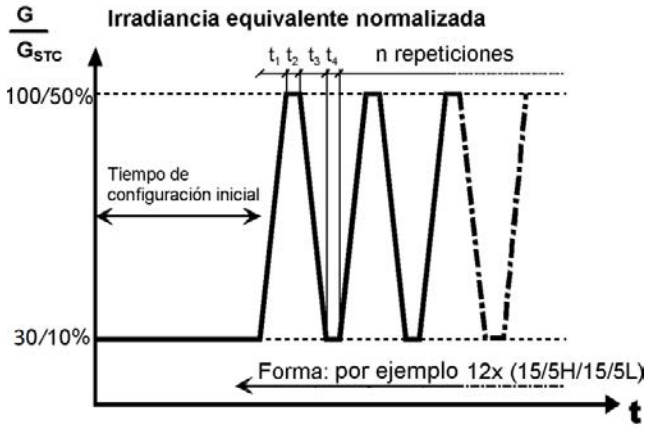

Figure 2.15: General irradiance profile proposed by [CENELEC, 2010] for MPPT efficiency testing

[7] Although the recording frequency is not specified it should be high enough to consider the MPPT fluctuations.

Finally, the dynamic MPPT efficiency is calculated as the average efficiency of each of the applied I-V curves. In total there are 135 different I-V curves with a total test duration of almost 6.5 hours.

Independent authors have also presented different MPPT testing protocols being especially interesting the one presented by [Ropp, Cale et al., 2011] for its short duration; only 11 minutes (Figure 2.16). However, until this PhD Thesis no protocol has been proposed that measures the MPPT efficiency of inverters in cases where local MPPs exist. In section 4.5.3, a protocol for testing the MPPT algorithm's capability of finding the absolute MPP in presence of local maxima is presented.

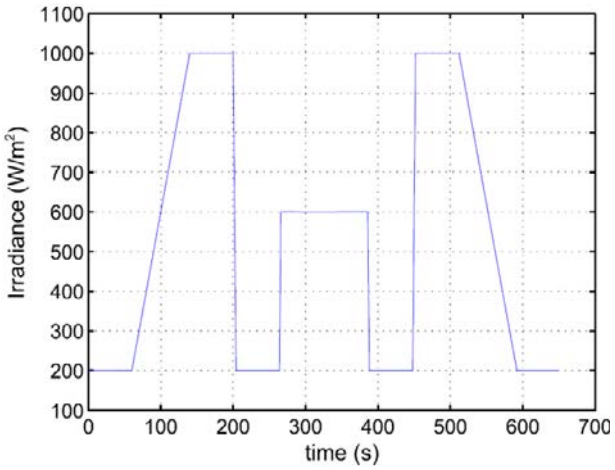

Figure 2.16: Irradiance profile proposed by [Ropp, Cale et al., 2011] for MPPT efficiency testing

2.1.5 HOT-SPOTS

Hot spots are a well-known phenomenon, described as early as 1969 [Blake and Hanson, 1969], still present PV arrays [Lorenzo, Moretón et al., 2013; Muñoz, Lorenzo et al., 2008; Sánchez-Friera, Piliougine et al., 2011; TamizhMani, 2010] and considered a cause of degradation of PV modules [Munoz, Alonso-García et al., 2011; Ndiaye, Charki et al., 2013]. They occur when a cell, or group of cells, operates at reverse-bias, dissipating power instead of delivering it and, therefore, operating at abnormally high temperatures. Typically, hot-spot damage occurs when the cell's power is dissipated in a very small area surrounding a local weak point or shunt. Cells exposed to higher temperatures will degrade at a higher rate than others and, if operation at high temperatures occurs during a prolonged time, it can cause irreparable damage to the solar cell; forcing it to permanently work in reverse bias and rendering useless the rest of

the cells under the same by-pass diode. If the cell's reverse bias is uniformly dissipated over the cell, the temperature rise is moderate, and not likely to cause damage but even if the cell does not result damaged, the exposure to high temperatures will result in a faster degradation of the material used for the module's encapsulation [Oreski and Wallner, 2005; 2009], reducing the radiation that reaches the cell. PV modules should be resistant to hot-spot problems and the international standard IEC-61215 describes the procedure for hot-spot resistance testing [IEC, 2005].

By-pass diodes were introduced in order to limit hot-spot effects to a minimum, however, even with their use, hot-spots can still occur in PV modules due to localized or irregular dirt. In [Lorenzo, Moretón et al., 2013], differences of up to 20ºC between shaded cells and non-shaded cells were observed, caused by irregular dirt over the modules like that of Figure 2.17 (c) and (d), and a study from the TÜV [TamizhMani, 2010] found a 10% failure rate in the hot-spot resistance test of 1220 c-Si modules during the 2007-2009 period. The study also shows an increased trend with respect to previous periods.

This effect is worst when only one cell is partially shaded since it alone has to dissipate the power of the rest of cells protected by the same by-pass diode; the case of localized dirt, bird droppings, leaves, etc. Figure 2.17(a) shows an example of a permanent hot-spot in a real PV system with modules with by-pass diodes. Figure 2.17(b) shows a large bird-dropping with a hot-spot under it (also in modules with by-pass diodes) and Figure 2.17 (c) and d) show other possible causes for hot-spots.

Because hot-spots are related with a cell working in reverse-bias, which in turn is related with the cell being forced to output the same current and the rest of the cells in series and because with DMPPT it is often more power efficient to reduce the current of the non-shaded cells, it seems logical that hot-spots are less probable to occur in DMPPT systems. Section 4.6 presents the theory under this hypothesis and experimental measurements that confirm it.

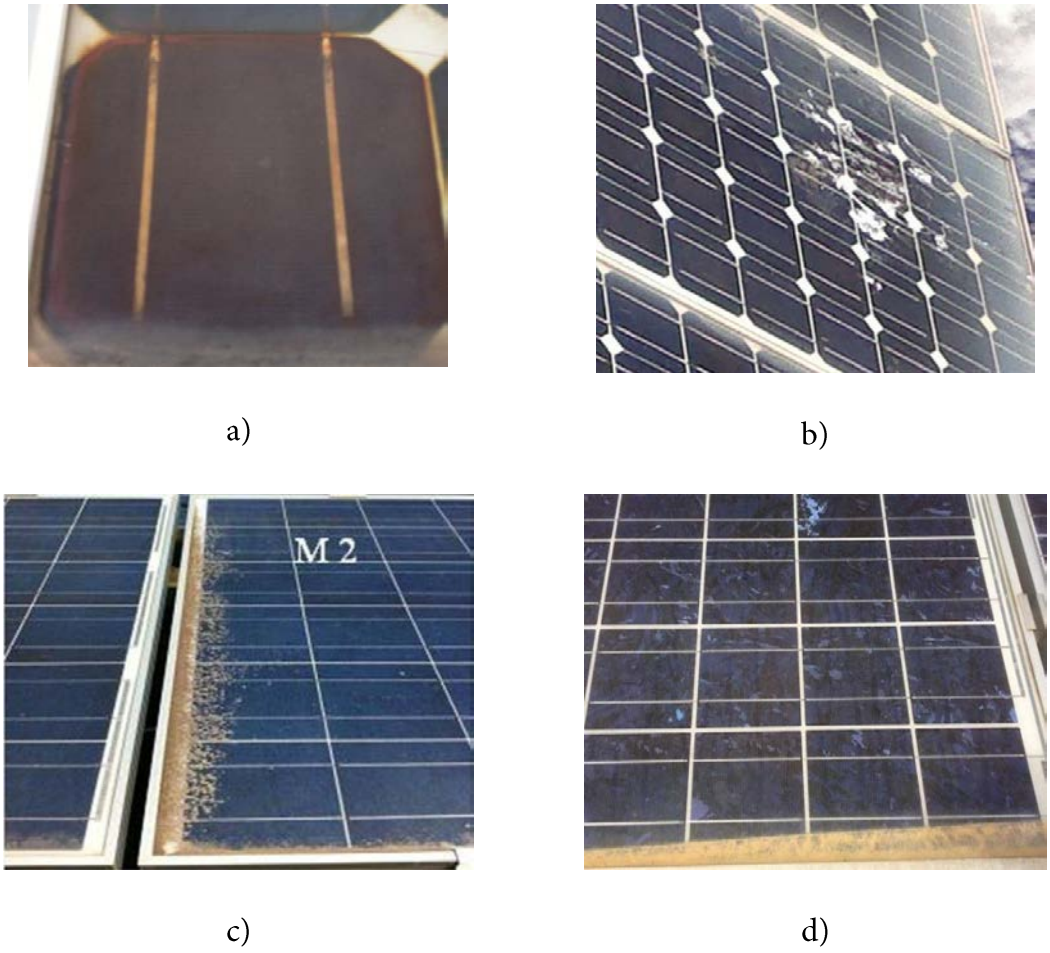

Figure 2.17: Examples of hot-spots and their possible causes. Figure a) shows a permanent hot-spot from a real PV system with by-pass diodes. Figure b) shows a large bird dropping which does not wash away after heavy rain and that has caused a hot-spot. Figures c) and d) show irregular dirt patches which could lead to hot-spots like in[Lorenzo, Moretón et al., 2013].

2.2 APPROACHES TO DMPPT

As it has already been mentioned there are two approaches to DMPPT, microinverters and power optimizers, having each its benefits and disadvantages. This section presents a comparison between both technologies highlighting the advantages of one over the other (throughout the thesis these advantages are tested and verified). In addition the working principles of each technology are briefly described.

2.2.1 COMPARSION BETWEEN MICRO-INVERTERS AND POWER OPTIMIZERS

Microinverters achieve module-level functionality by placing a full DC/AC inverter at each module, making the DC/AC inversion the center of their concept. While power optimizers also allocate power electronics to the module, but conversely keep the DC/AC inversion at the inverter-level. Each technology has its advantages and disadvantages.

- **MPPT voltage range:** Due to the fact that microinverters have to convert the DC voltage to a high AC voltage, the MPPT range of microinverters is lower than that of power optimizers. While SolarEdge's MPPT range goes from 5V-55V, Enphase's only goes from 22V-36V. This will cause MPPT losses when shading is present. Real MPPT efficiency measurements are presented in 4.5.2.3.

- **Reliability:** Warranty periods of both microinverters and power optimizers adapt to the PV standard of 25 years[8]. However, power optimizers have a high switching frequency which allows them to use ceramic capacitors instead of electrolytic capacitors[9], which contain fluids which evaporate causing them to fail more easily. In addition, due to only having the DC/DC conversion, power optimizers require less components, reducing the potential points of failure (Figure 2.18).

- **Conversion efficiency:** As microinverters convert DC to AC at module level, a large voltage boost is required at each conversion, typically from 30V DC to 230V AC, causing higher conversion losses. In terms of conversion efficiency, microinverter systems are behind power optimizers although not by much, around 0.5%-2%.

- **Design flexibility:** Being able to quickly design and install a PV system can contribute to lowering the system price. At this point microinverters might be slightly ahead since they permit connecting systems from 200W while power

[8] Enphase has different warranty periods depending on the location. 25 years for USA, 20 years for Europe and 10 years for Australia and New Zealand.

[9] In fact, the reliability of electronic equipment is strongly dependen ton the number of electrolytic capacitors.

optimizers depend on the lowest compatible PV inverter in the market, ~2kW. In addition, power optimizers have some limitations in irradiation differences between modules due to the conversion limits of DC/DC converters, already mentioned in [Alonso, Roman et al., 2012; Vitelli, 2012]

- **Cost:** Although it would seem that power optimizers should be lower on cost due to having less components, according to the GTM report [Shiao, 2013] costs are very similar for both technologies, being it only a little bit higher for microinverters: 0.59$/W for power optimizers[10] and 0.61$/W for microinverters.

- **Safety:** PV systems with microinverters do not have high DC voltages and both SolarEdge and Tigo permit deactivating the high DC voltages for safer installation, maintenance or firefighting.

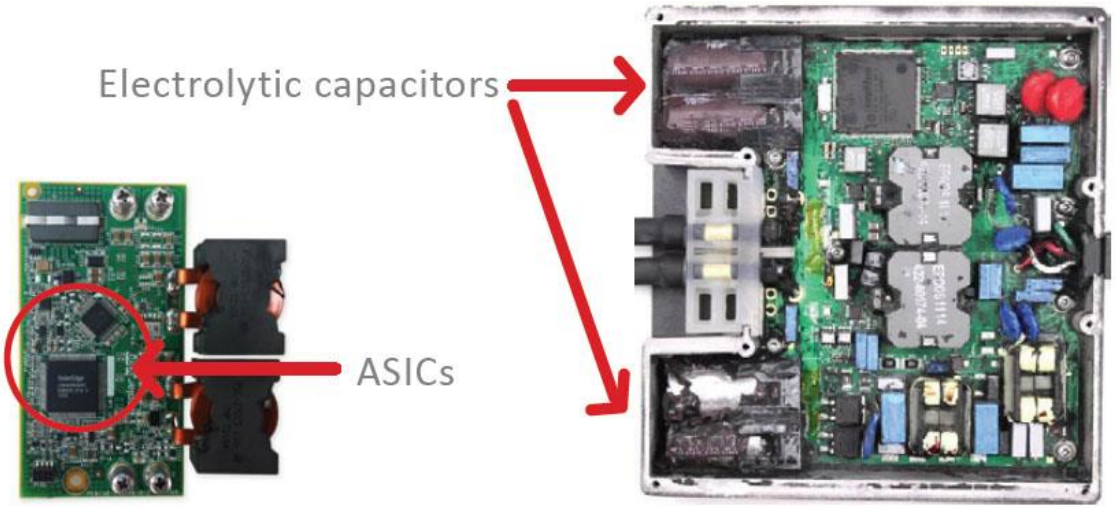

Figure 2.18: PCB of the SolarEdge power box with 186 components (left) and Enphase microinverter with 466 components (right). Figure obtained from the SolarEdge webpage (www.solaredge.com)

Both microinverters and power optimizers have a built in communication interface which allows transmitting the instantaneous values of voltage and current to a central processing unit. With these values, the least producing modules in the system are easily identified, reducing the time and cost of failure detection and diagnosis. In addition, automatic failure diagnosis algorithms can be implemented, like the ones presented in

[10] Including the central inverter.

section 6, which directly return the possible cause of failure, eliminating the need for a technical team in the case of soft failures.

2.2.2 MICRO-INVERTERS

A microinverter has the same working principles as a string PV inverter but with a reduced power rating of its components, in order to match the power of typical PV modules. Microinverters have a power rating from 200-300W and are designed to be connected to one PV module and to the AC grid. In Figure 1.1, a diagram of a PV system with microinverters is shown.

A microinverter is composed of two main modules: the MPPT module and DC/DC module and the DC/AC conversion module. First the MPPT polarizes the PV module at its V_{MPP} by means of its MPPT algorithm. This voltage is then converted to a fixed DC voltage by means of a DC/DC converter, considered inside the MPPT module. Then this fixed DC voltage is converted into AC voltage by means of a series of switches which invert the DC voltage at a given frequency. Then a series of switches, typically an H-bridge of four switches, with PWM chopping converts the DC wave into an AC wave which is fed into the grid.

2.2.3 POWER OPTIMIZERS

A schema of a PV system with power optimizers was shown in Figure 1.1. The system consists of a series of PV modules each connected to a power optimizer[11], having the power optimizers then connected in series or parallel to a central inverter.

In this system topology the central inverter works at a constant voltage and is only in charge of the DC/AC conversion. Some authors have also suggested [Alonso, Roman et al., 2012; Vitelli, 2012] that to have a wider range of shadow mitigation, the inverter should work in a maximum power range tracking (MPRT) mode. This decision depends

[11] Depending on the power of each PV module, more than one module can be connected to each power optimizer.

on the characteristics of the power optimizers used and more about this is discussed section 3.5.

The power optimizers connected to each module incorporate an MPPT algorithm, in charge of finding the module's MPP, and a DC/DC converter in charge of fixing the module's MPP and converting the working values of each PV module to accepted values by the string of power optimizers. Due to the characteristics of the DC/DC converters used, not all working values will be satisfactory converted to acceptable values in the string. Understanding these limitations is not trivial and will be thoroughly discussed in the following sections. But first, the functioning of DC/DC converters will be briefly discussed

2.2.3.1 DC/DC converters for power optimizers

The basic working principle of DC/DC converters is well known in the electronic industry [Erickson, 2001] and their function is to convert a certain input voltage to a certain output voltage losing the minimum possible power; that is decreasing or increasing the current in the same proportion as the voltage is increased or decreased. A short description is presented to fully understand how they work when used as power optimizers in PV arrays.

There are three main types of DC/DC converters: the buck converter, which reduces the output voltage, the boost converter, which elevates the output voltage, and the buck-boost converter which can reduce or elevate the output voltage. All of these converters are digitally controlled by commutation through a transistor, given at a constant frequency, f_s, with a certain duty cycle, d, where $d \in [0,1]$ and is defined in equation (2.15):

$$d = \frac{t_{on}}{T_s} \tag{2.15}$$

where t_{on} is the time for which the switch is closed and T_s is the commutation period, or f_s^{-1}. Figure 2.19 represents the commutation signal.

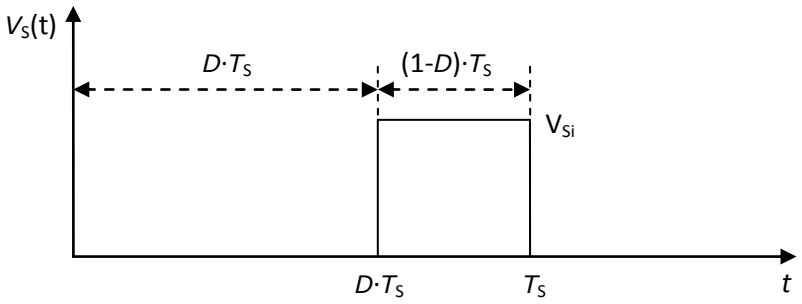

Figure 2.19: Duty cycle image

The conversion ratio, *M(d)*, is a function that depends on the duty cyle, *d*, and the type of converter, and that relates the input and output voltage of DC/DC converters as shown in equation (2.16).

$$M(d) = \frac{V_0}{V_i} \tag{2.16}$$

For buck, boost and buck-boost converters, *M(d)* is related to the duty cycle as in equations (2.17), (2.18) and (2.19) respectively.

$$M(d) = d \tag{2.17}$$

$$M(d) = \frac{1}{1-d} \tag{2.18}$$

$$M(d) = \frac{d}{d-1} \tag{2.19}$$

Therefore, the output voltage and output current can be related to the input voltage and input current through equations (2.20) and (2.21).

$$V_o = M(d) \cdot V_i \tag{2.20}$$

$$I_o = {I_i}/{M(d)} \tag{2.21}$$

In the case of buck converters, *M(d)*, will always be lower than or equal to one. For boost converters, *M(d)* will never be lower than one. And for buck-boost converters *M(d)* can take any value.

Because in some PV systems with power optimizers (like SolarEdge) the inverter's DC voltage is normally fixed, normally at 330V (for 230V grids) to maximize the

DC/AC efficiency, the DC/DC converters in the power optimizers will need to boost or reduce the voltage depending on the string length, needing to work as buck or boost converters. Also when a PV module's I_{MPP} is lower than the rest of the modules in the string, the power optimizer of that module will reduce its voltage and increase its current to match that of the rest of the modules, working as a buck converter. Because of these necessities it seems reasonable that the best DC/DC converters to use with power optimizers are buck-boost converters. Although some authors are not in agreement with this [Roman, Alonso et al., 2006; Vitelli, 2012], this has been the solution adopted by SolarEdge and the benefits and disadvantages are discussed in section 3.6.

3 THEORETICAL ANALYSIS OF PV SYSTEMS WITH DMPPT

3.1 INTRODUCTION

Ideally, DMPPT systems can extract the maximum power of each PV module, therefore potentially reporting higher energy yields than central MPPT systems in module mismatch situations. However, there are certain factors that can reduce the power produced by the DMPPT system, sometimes even below that produced by a central MPPT system. There are essentially three main factors to consider. The first is related with the power conversion efficiency: DMPPT systems will only be able to ensure a higher energy output if the efficiency of the power conversion stages is high enough. Secondly, it is important to also consider the efficiency of the MPPT algorithm, especially when local maxima are present. Finally, there are some limitations due to the series connection of DC/DC converters and their output characteristics that may not allow the working of each PV module in its MPP when the modules are working at different currents. All these issues have been analysed and the results and conclusions obtained are presented in the following sections.

3.2 *I-V* AND *P-V* CHARACTERISTICS OF PV ARRAYS WITH POWER OPTIMIZERS

This section presents a series of *I-V* and *P-V* curves of PV arrays with power optimizers, aiming to provide an understanding of how these systems work. These curves are simulated by taking the MPP as the working point and considering this power to remain constant during the whole voltage range. Measured *I-V* curves of a boost optimizer are presented in section 4.3 to confirm these simulations. It is important to note that, as opposed to *I-V* curves from PV modules, the *I-V* curves of power optimizers are not the only possible working points. The output curve of a power optimizer is with respect to a certain working point, which is designated by the MPPT of the power optimizer and can be the MPP or not. For most of the curves here presented, the MPP is considered as the working point. However, other working points are also considered taking into account that the MPP might not be correctly tracked, as this can certainly be the case as is shown in section 4.5.2.

In pages 152-185 of [Femia, Petrone et al., 2013] a similar study is conducted and can also serve as a good reference. The main drawback of that study is that the maximum voltage and current rating across the converter's switch is used as a limitation, instead of the absolute output ratings, making it a better study for design of power optimizers instead of design of PV systems with power optimizers. Another option is to consider the maximum and minimum conversion ratio of the converters. However, this again is not very practical since the products' data sheets do not give these values. In the study here presented the absolute output rating of the power optimizers are used, making it more realistic and easy to comprehend from a system designer's point of view.

For simplicity, lossless power optimizers have been considered and the same PV module has been used for all curves. The module has sixty cells in series and three by-pass diodes, each covering twenty cells. Its main parameters at STC are: V_{oc}*= 37.5V, V_m*=30V, I_{sc}*=8.69A and I_m*=8.04A.

From Figure 3.1 to Figure 3.3 the ideal *I-V* and *P-V* curves of boost, buck and buck-boost optimizers are shown. It is supposed that there are no output limits and that the input parameters of the optimizers are the MPP of the PV module, whose curve is also

shown in the figures. The *I-V* curves of the optimizers show a constant power hyperbola during the voltage range of each optimizer: above, below, and above and below the MPP for the boost, buck and buck-boost optimizers respectively. This constant power hyperbola of the *I-V* curve is translated into a maximum power region (MPR) in the *P-V* curve.

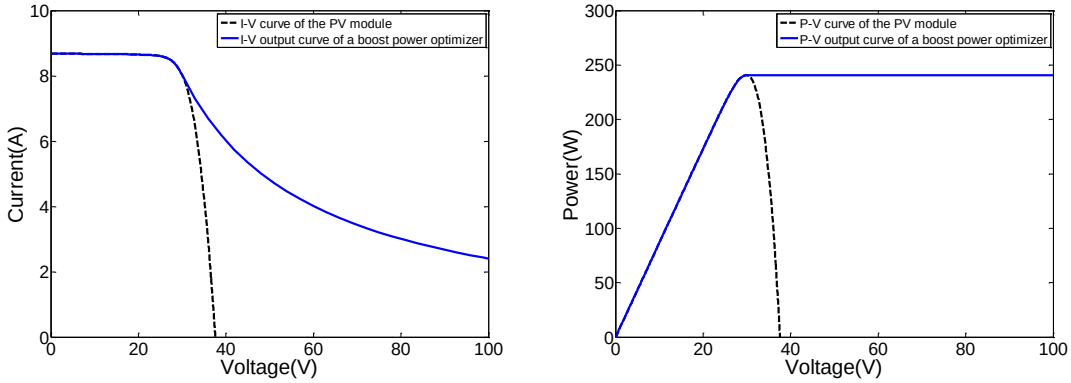

Figure 3.1: *I-V* and *P-V* curves of a boost optimizer with limitless output parameters and conversion ratio.

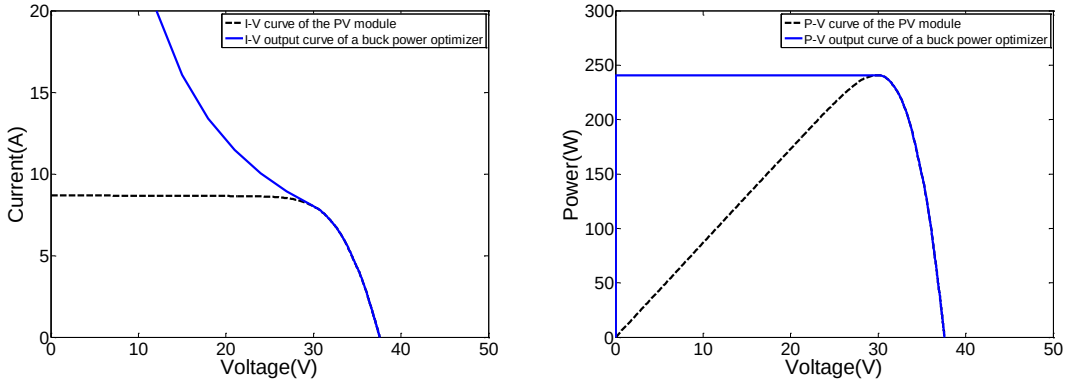

Figure 3.2: *I-V* and *P-V* curves of a buck optimizer with limitless output parameters and conversion ratio.

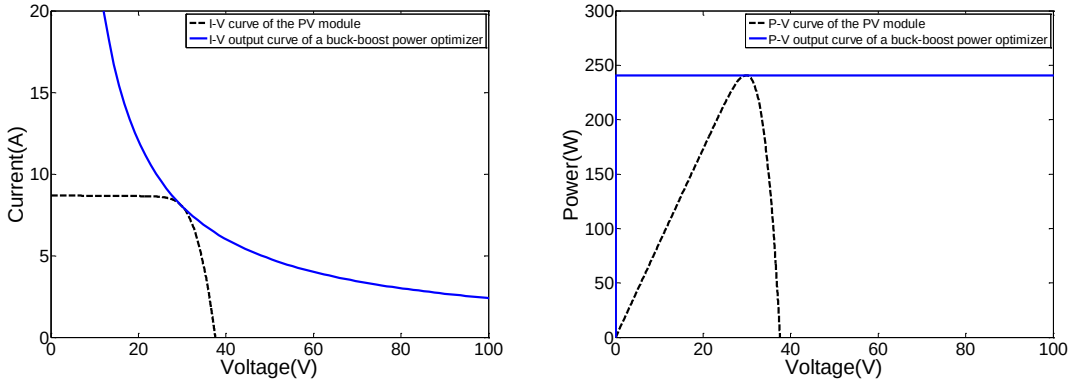

Figure 3.3: *I-V* and *P-V* curves of a buck-boost optimizer with limitless output parameters and conversion ratio.

In reality, due to various factors like the limited switching frequency of the DC/DC converters or the maximum voltage of the output capacitors, the output voltage will be limited. In this case, the constant power hyperbola does not extend across the whole voltage range, being limited by the output parameters. As an example, Figure 3.4 shows the *I-V* and *P-V* curves of the SolarEdge power optimizer (output limits: V_{o_min} = 5V, V_{o_max} = 60V and I_{o_max} = 15A). It can now be seen how the MPR is limited by these output parameters. In this example, the MPR is limited by V_{o_max} and by I_{o_max}. However, if the working current or voltage were to be lower, it could be that V_{o_min} is the limiting factor in the low voltage range, as occurs in the example presented in Figure 3.5-right and also occurs in some real examples presented in section 4.2.2. In the higher voltage range, the limiting factor will always be V_{o_max}.

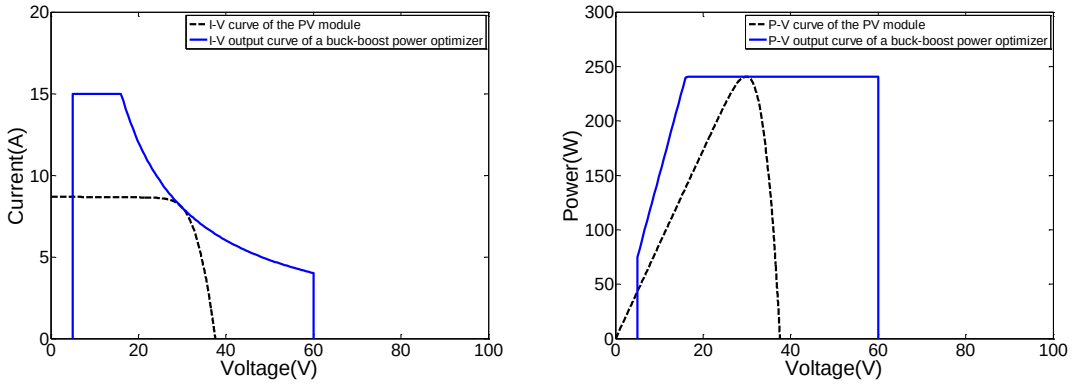

Figure 3.4: *I-V* and *P-V* curves of the SolarEdge power optimizers (buck-boost) with output limits: V_{o_min} = 5V, V_{o_max} = 60V, and I_{o_max} = 15A.

Because the output curve of a power optimizer is directly related to its input, the optimizer's curve will change depending on the working point. For example, Figure 3.5 shows the output curves of a SolarEdge optimizer for two different working points, which correspond to the two local maxima of the module's *I-V* curve. It can be seen how if the working point is that of higher voltage, the maximum output current is around 6A, which could be a restriction when connected to other optimizers in series, as will be seen in the following sections.

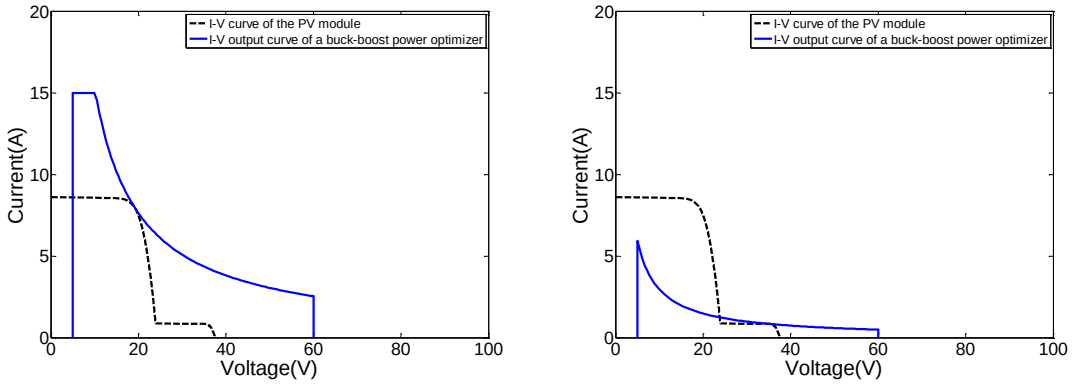

Figure 3.5: Difference in the output *I-V* curve of the SolarEdge power optimizers for an *I-V* curve with local maxima depending on the working point fixed by the MPPT algorithm.

3.3 DC ANALYSIS OF A PV ARRAY WITH POWER OPTIMIZERS

Although the functioning of DC-DC converters is well known [Erickson, 2001], their use in PV arrays introduces some non-trivial constraints that must be taken into consideration when designing a system with power optimizers and when simulating the energy gain obtained. The purpose of this study, which only refers to power optimizers and not micro-inverters, is to present a set of expressions that can be used to model the working state of each power optimizer and to identify the limitations related to the finite output parameters of each power optimizer. In turn, what is here presented should serve as the basis to correctly design a PV system with power optimizers, determine the limitations of the system and to simulate the possible energy gains.

Figure 3.6 shows the block diagram of a PV system with N power optimizers connected in series and its electrical parameters. The following equations can also be used for the case of PV systems with various strings of power optimizers connected in parallel. In this case the inverter's voltage is equal for all strings but the output current of each string can be different.

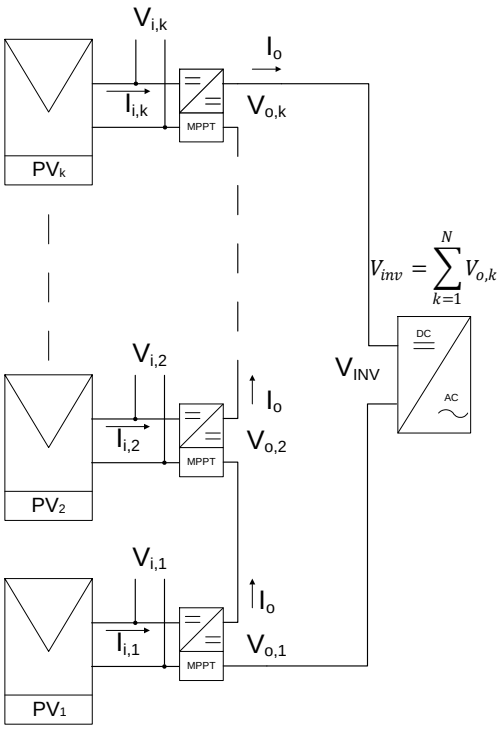

Figure 3.6: Block diagram of a PV system with *N* power optimizers connected in series and its main electrical parameters.

In addition, Table 3.1 presents all the parameters used in this section with a short description of each one.

Table 3.1: Main parameters used to describe and analyse the DC operation of PV systems with power optimizers.

Parameter	**Description**
$V_{i,k}$	Working voltage of each PV module and input voltage to each power optimizer
$I_{i,k}$	Working current of each PV module and input current to each power optimizer
$V_{o,k}$	Output voltage of each power optimizer
I_o	Output current of all power optimizers and input current to the central inverter.
$P_{i,k}$	Working power of each PV module and input power to each power optimizer
$P_{o,k}$	Output power of each power optimizer.
η_k	Efficiency of each power optimizer
$M(d)_k$	Conversion ratio of each power optimizer. Equal to $V_{o,k}/V_{i,k}$.

3.3.1 EQUATIONS USED TO DESCRIBE THE FUNCTIONING OF POWER OPTIMIZERS IN PV ARRAYS

Using Figure 3.6 as a reference, some equations can be directly deduced. Considering lossless cables, it is straightforward that the input voltage of the inverter, V_{inv}, must be equal to the sum of the output voltages of all the power optimizers, represented in equation (3.1), where N_T is the total number of power optimizers in series.

$$V_{inv} = \sum_{k=1}^{N_T} V_{o,k} \tag{3.1}$$

V_{inv} is imposed in the system by the inverter as the operating voltage[12] and, in consequence, each power optimizer is also influenced by this value. V_{inv} can be a constant value or it can change depending on the operating conditions of the system. In a first instance a DMPPT PV system with a constant inverter voltage is considered. If a system with ideal power optimizers (i.e. η = 100%) is supposed, then we can affirm that the output power of each optimizer (represented with the sub-index *k*) is the same as the input power, and the following equations apply:

$$P_{i,k} = P_{o,k} \tag{3.2}$$

$$\sum_{k=1}^{N_T} P_{i,k} = \sum_{k=1}^{N_T} P_{o,k} \tag{3.3}$$

$$I_o = \frac{\sum_{k=1}^{N_T} P_{o,k}}{V_{inv}} \tag{3.4}$$

From equations (3.3) and (3.4), the output current, with respect to the inverter's voltage and the input values of each power optimizer[13], is obtained, as shown in equation (3.5), again considering an efficiency of 100%.

$$I_o = \frac{\sum_{k=1}^{N_T} (V_{i,k} \cdot I_{i,k})}{V_{inv}} \tag{3.5}$$

[12] This can be a constant voltage or the voltage chosen by the MPPT

[13] The input values of each power optimizer are the same as the working values of each PV module.

From equation (3.5) the conversion ratio of each power optimizer, $M(d)_k$, is directly obtained with equation (3.6) as a function of the working values of each PV module and the fixed voltage of the inverter.

$$M(d)_k = \frac{V_{inv} \cdot I_{i,k}}{\sum_{k=1}^{N_T}(V_{i,k} \cdot I_{i,k})} \tag{3.6}$$

The output voltage of each k power optimizer is easily obtained by applying the conversion ratio to the input voltage as in equation (3.7).

$$V_{o,k} = M(d)_k \cdot V_{i,k} \tag{3.7}$$

For simplicity, during the analyses presented in further sections, the efficiency of each power optimizer is not considered. However, especially for low efficiency optimizers it should be considered as it can reduce the *M(d)* limits. For example, the boost optimizer developed by Tecnalia for the Integra project is limited by firmware to an $M(d)_{max}$=2; by limiting the duty cycle to 0.5. Let's consider that there are two modules in the system and that one is mismatched 50%: say the working values are (30V, 4A) and (30V, 8A) and V_{inv} = 90V. For 100% efficiency converters, the non-mismatched module would boost its voltage by two, working at 60V and 4A and being within the system limits. However, if we consider a 90% efficiency (considered in a voltage loss) the converters will have to output 3.6A and 33.3 V and 66.6V respectively. For the first converter it will not be a problem, since its *M(d)* is equal to 1.11, but for the second its *M(d)* should be 2.22, which is out of the limits imposed by the duty cyle. This means that for solving the same mismatch problem, the *M(d)* limits should be less restrictive the lower the efficiency which leads us to define the real conversion ratio, $M_R(d)$, presented in equation (3.8). Because the non-ideal efficiency causes a voltage drop, if V_{inv} is kept constant the converters are forced to boost the input voltage slightly to keep the output voltage the same as in ideal conditions, forcing the current to be lower as expressed by equation (3.9). The output voltage will remain the same as equation (3.7).

$$M_R(d)_k = \frac{V_{inv} \cdot I_{i,k}}{\sum_{k=1}^{N_T}\left[V_{i,k} \cdot I_{i,k} \cdot \eta(P_{i,k})\right]} \tag{3.8}$$

$$I_o = \frac{\sum_{k=1}^{N_T}\left[V_{i,k} \cdot I_{i,k} \cdot \eta(P_{i,k})\right]}{V_{inv}} \tag{3.9}$$

These expressions combined with the characteristics of each power optimizer system, like the $M(d)$ limits, the maximum and minimum output voltages and currents, V_{o_max}, V_{o_min}, I_{o_max} and I_{o_min}, the inverter voltage, V_{inv}, and $\eta(P_i)$, can be used to simulate a DMPPT PV system with power optimizers.

3.3.2 FUNCTIONING OF POWER OPTIMIZERS IN PV ARRAYS

Power optimizers can be divided into two main blocks: the MPPT and the DC/DC converter. The MPPT is in charge of deciding the working point of each PV module, $V_{i,k}$ and $I_{i,k}$, which is also the input to each DC/DC converter. Ideally, this point will be the MPP of the module. However, it could occur that it is not, due to an inefficient MPPT, or due to conversion limits of the DC/DC converter (more on this second point is discussed in section 3.5). This block is directly controlled by a microprocessor embedded into the power optimizer.

On the other hand, the second block, the DC/DC converter, acts solely driven by the voltage imposed by the inverter and the working point of each optimizer. In other words, there is no logic or microprocessor controlling the DC/DC converter and telling it which voltage and current it should output. Considering lossless optimizers, because the inverter's voltage is fixed by the inverter and each optimizer's input power is fixed by the optimizers' MPPT, I_o is also fixed in the system and can be obtained from equation (3.5). In series connections, this I_o is the same for all optimizers, and they will work as a current source. Because each DC/DC converter has fixed input values (designated by the MPPT), the conversion ratio at which the optimizer works can be directly obtained knowing I_o, and is independent from any logic. In addition, when the optimizers are connected in series, it is the input current of each optimizer, $I_{i,k}$, which will have the greatest effect over the conversion ratio of each optimizer.

For a short explanation let's consider a six module PV system with power optimizers where the inverter's voltage is fixed at 200V. Table 3.2 shows the main parameters of all the power optimizers in the system when all the input vales are equal. In this case it is obvious that all conversion ratios and output voltages of each optimizer are also equal.

Table 3.2: Main parameters of a PV system with six power optimizers when all working values are equal and the inverter voltage is fixed at 200V

V_w (V)	I_w (A)	M(d)	V_o (V)	I_o (A)
30	8	1.11	33.3	
30	8	1.11	33.3	
30	8	1.11	33.3	7.2
30	8	1.11	33.3	
30	8	1.11	33.3	
30	8	1.11	33.3	

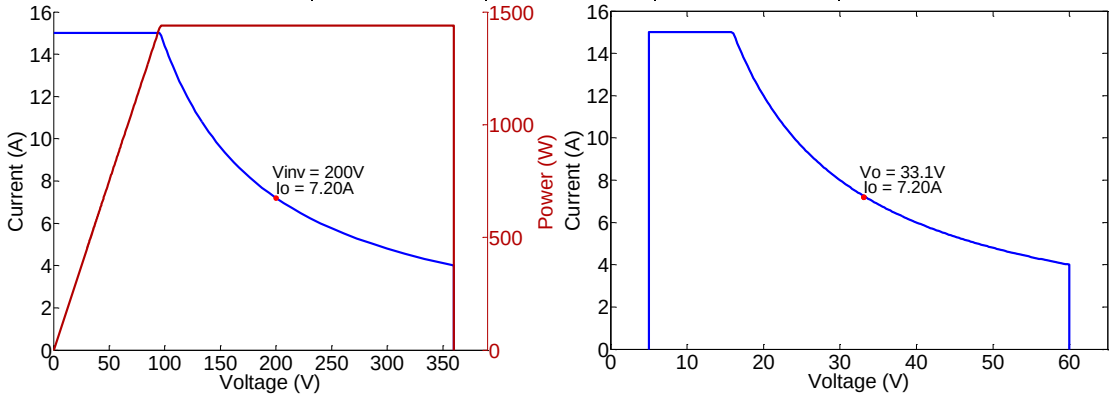

Figure 3.7: (left) *I-V* and *P-V* curves of the output of the six optimizer system with the working parameters of Table 3.2 and (right) output *I-V* curve of each individual optimizer. The working point of the system and of each individual optimizer is also represented.

Now, if one module has a current mismatch, then the parameters of the system change and are no longer equal. From Table 3.3 we can see that the conversion ratio of the mismatched module is lower than the rest, since it is obliged to boost its current in order to match the output current imposed in the system. In turn its output voltage is also lower than the rest of the modules. In this situation, in order to fully solve the mismatch problem it is evident that a buck-boost converter is needed.

It is important to note that also the non-mismatched modules have lowered their current to try to match that of the mismatched module but, since there are a greater number of non-mismatched modules, the drop in current of these modules is less than the rise in current of the mismatched module. This allows the mismatched module to not have such a drastic reduction of its output voltage, staying at 9.52V instead of the

required 8.3 if reaching a current of 7.2A is desired. In turn, this has an effect on the maximum mismatch that is possible to compensate, as seen in section 3.5.

Table 3.3: Main parameters of a PV system with six power optimizers when there is current mismatch in one module and the inverter voltage is fixed at 200V

V_w(V)	I_w(A)	$M(d)$	V_o(V)	I_o(A)
30	8	1.27	38.1	
30	8	1.27	38.1	
30	8	1.27	38.1	
30	8	1.27	38.1	6.3
30	8	1.27	38.1	
30	2	0.32	9.52	

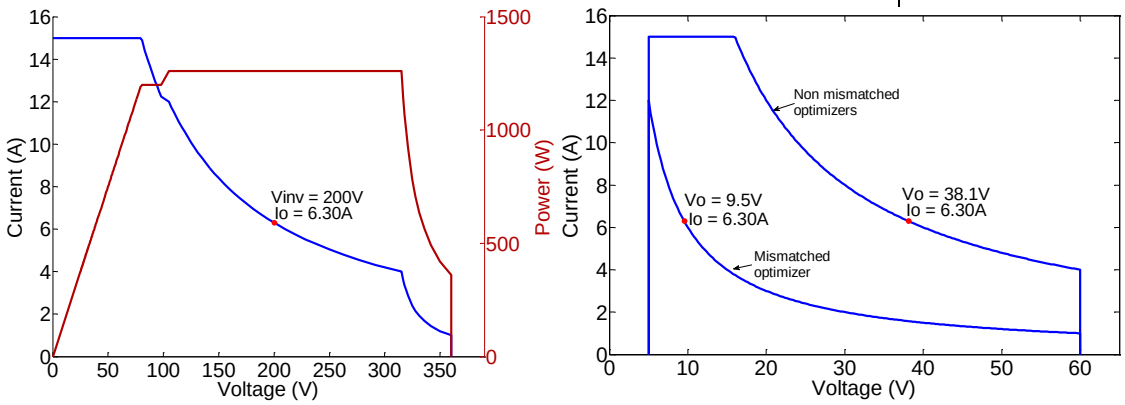

Figure 3.8: (left) *I-V* and *P-V* curves of the output of the six optimizer system with the working parameters of Table 3.3 and (right) output *I-V* curve of the non-mismatched optimizers and also of the mismatched optimizer. The working point of the system and of each optimizer is also represented.

Another case, presented in Table 3.4, where there is a larger number of mismatched modules shows that the current drop of the non-mismatched modules is now higher and the current boost of the mismatched modules is now lower, reducing even more the necessary output voltage drop.

Table 3.4: Main parameters of a PV system with six power optimizers when there is current mismatch in three modules and the inverter voltage is fixed at 200V

V_w (V)	I_w (A)	$M(d)$	V_o (V)	I_o (A)
30	8	1.78	53.3	
30	8	1.78	53.3	
30	8	1.78	53.3	
30	2	0.44	13.3	4.5
30	2	0.44	13.3	
30	2	0.44	13.3	

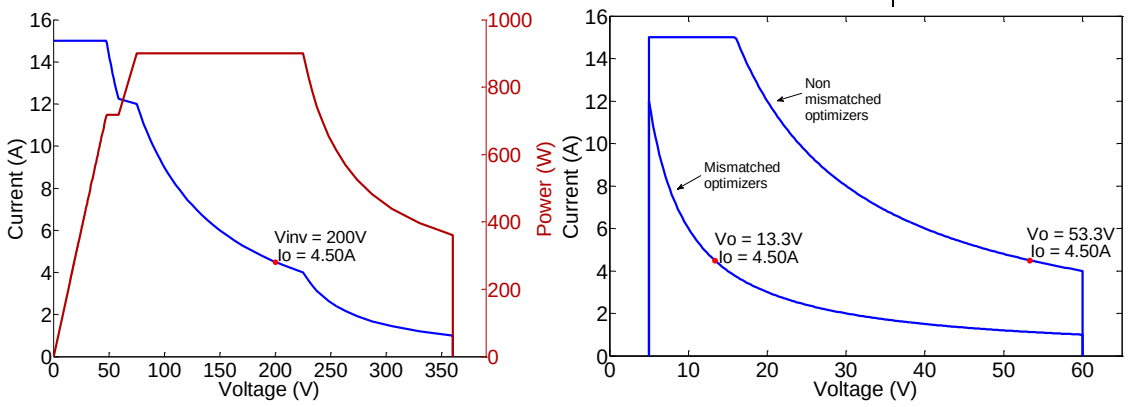

Figure 3.9: (left) *I-V* and *P-V* curves of the output of the six optimizer system with the working parameters of Table 3.4 and (right) output *I-V* curve of the non-mismatched optimizers and also of the mismatched optimizers. The working point of the system and of each optimizer is also represented.

When voltage mismatch is present, as could be the case for a module working with diodes in forward bias or modules of different characteristics and as shown in Table 3.5, the conversion ratio changes equally in all optimizers and, if there is no current mismatch, it is equal for all of them. If the voltage of the mismatched module is lower than the rest, then the average conversion ratio will rise (with respect to the case in Table 3.2) in order to match the voltage of the inverter. Notice that because the power mismatch is the same as in the example of Table 3.3, the output current is also the same, which emphasizes the relation between inverter voltage, power of all optimizers and output current.

Table 3.5: Main parameters of a PV system with six power optimizers when there is voltage mismatch in one module and the inverter voltage is fixed at 200V

V_w (V)	I_w (A)	$M(d)$	V_o (V)	I_o (A)
30	8	1.27	38.1	
30	8	1.27	38.1	
30	8	1.27	38.1	
30	8	1.27	38.1	6.3
30	8	1.27	38.1	
7.5	8	1.27	9.53	

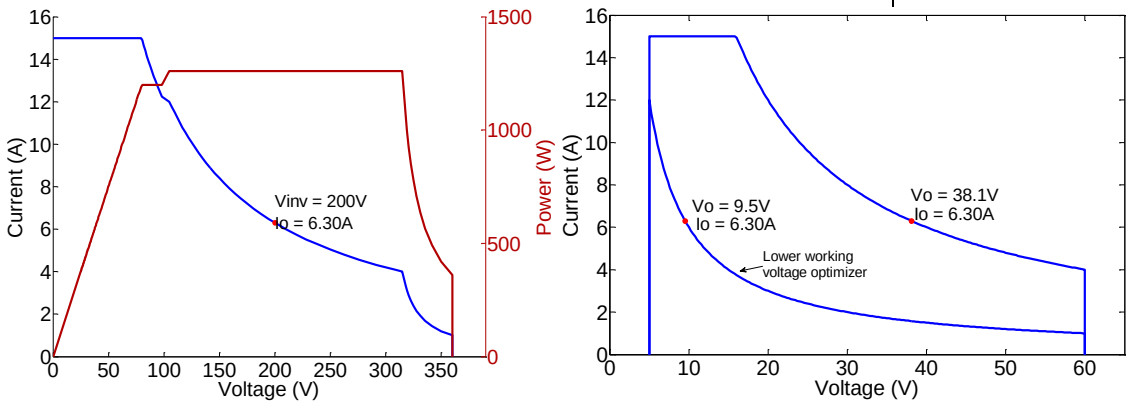

Figure 3.10: *I-V* and *P-V* curves of the output of the six optimizer system with the working parameters of Table 3.5 and (right) output *I-V* curve of the non-mismatched optimizers and also of the mismatched optimizers. The working point of the system and of each optimizer is also represented.

Similar examples in real PV systems with power optimizers are presented in section 4.2 with the idea of validating what has been here presented.

3.4 POTENTIAL FOR COMPENSATION OF MISMATCH LOSSES WITH DMPPT SYSTEMS

Mismatch losses in PV systems can occur mainly due to three reasons: shadows, soiling and dispersion of the modules' electrical parameters. In the following, the potential for energy recovery with the use of DMPPT in these three situations is analysed. It should be noted that the analysis is performed supposing ideal power electronics; that is,

comparing the sum of all modules' MPP and the MPP of the generator and considering an efficiency of 100%.

3.4.1 SHADOWS

3.4.1.1 Theory

The mitigation of the negative effects produced by shading over a PV generator is the most publicized benefit of DMPPT technologies. All manufacturers of DMPPT products highlight this positive effect, going as far as claiming energy gains in shading situations up to 25%. Although power gains in range of 20-30% have been measured in independent studies [Orduz and Egido, 2006; Orduz, Solórzano et al., 2011a; Solórzano, Egido et al., 2010] and in some experiments conducted during this thesis and presented in section 4.4, critical voices suggest that much lower annual energy gains are expected [Rogalla, Burger et al., 2010]. This section only aims at a theoretic introduction and more realistic energy gains are seen in section 5.

Power gains due to shading are possible in situations where some sub-modules are by-passed in central MPPT systems. In these situations, with DMPPT, these sub-modules could be active, providing some power and therefore having the complete system provide more power than before. In situations where the sub-modules are by-passed in both the central MPPT system and the DMPPT system, no power optimisation is possible. For what is exposed, the working point of both the central system and the DMPPT system is considered as the MPP. As shown in section 4.5.2, depending on the MPPT algorithm, this might not be the case and that is also considered in the modelled energy gains in section 5.

For example, let's consider a shadow that progressively enters a PV string shading one sub-module at a time (Figure 3.11-left) and let's consider typical sixty cell modules with three by-pass diodes[14]. There is an initial period in which the current mismatch barely produces any power loss, as while working in the elbow of the *I-V* curve the

[14] These are not the modules from the picture, as these are from 1993, but the typical module commercialized in 2014.

power is almost constant (seen in section 3.4.2) and, therefore, barely any power gain is obtained with DMPPT.

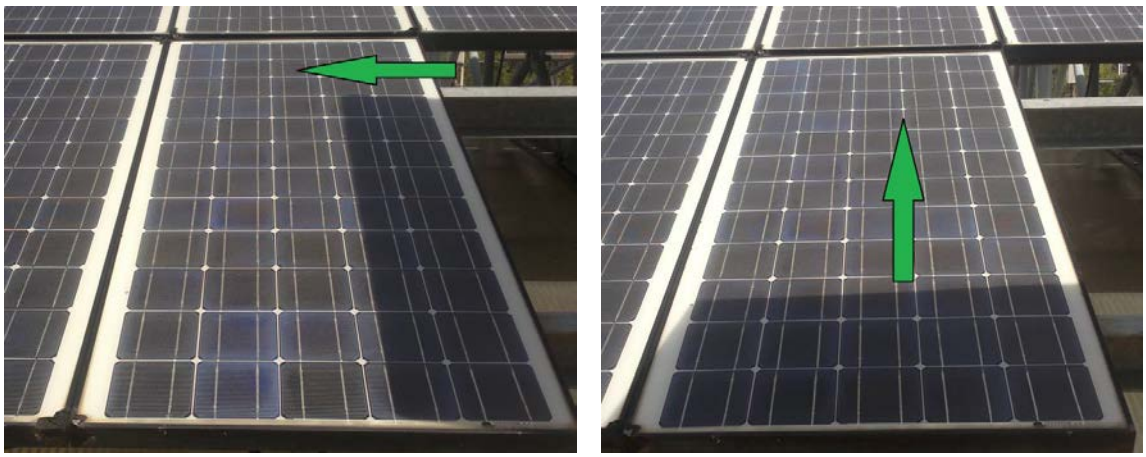

Figure 3.11: (left) Example of a shadow entering a PV module by shading one sub-module at a time and (right) example of a shadow entering a PV module and shading all sub-modules at the same time.

There is a second region in which in a central MPPT system working at the MPP, when a reduction in irradiance of around 8% occurs over one or various cells[15] of one sub-module, the shaded cells start working in reverse bias; causing the diode to work in forward bias and to by-pass all the cells protected by the diode. On the other hand, the MPP of the shaded module in the DMPPT system is localized in a region of lower current, where the shaded cells are not by-passed. At this moment the largest power gains are obtained as the shaded sub-modules can still deliver a lot of power individually (around 85%) but in a CMPPT system they are bypassed. This example is shown in Figure 3.12, where the *I*-V and *P*-V curves for a single PV module and a ten module string are shown, where all cells from one sub-module receive only 70% of the available irradiance. It can be seen how in the single module the MPP is at a region of lower current (i.e. the by-pass diode is not in forward bias) and in the ten module string the MPP is at a point where the shaded sub-module is by-passed (i.e. the diode is working in forward bias). At this point the DMPPT system can produce all the power from nine modules (240.7W each), plus 193W of the shaded module (2359W total), while the CMPPT system can only produce 2321W (loss of one sub-module plus the loss of voltage due to the by-pass diode being in forward bias); resulting in a 1.64% power gain.

[15] This depends on the breakdown voltage of the shaded cells. However, for cells with breakdown voltages < -15V, with only shaded cell it can be enough.

As the shadow progresses the power each individual module can deliver diminishes and so does the power gain, although when the module is fully shaded some power gain is still possible.

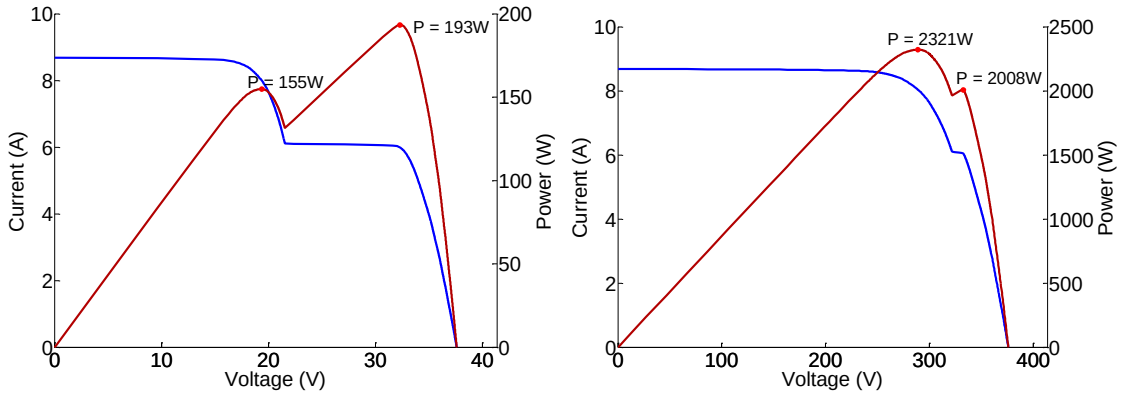

Figure 3.12: ***I-V*** **and** ***P-V*** **curves of the single module (left) and the ten module string (right) when the cells from one sub-module are only receiving 70% of the total irradiance. It can be seen how in the single module the MPP is at a region where all cells work at a lower current, while in the ten module string the MPP is at a region where the shaded sub-module is by-passed. In this situation a power gain is possible when using DMPPT.**

The higher limit of this region depends on the configuration of by-pass diodes of the module. For example, if there are three by-pass diodes in the module, losing one sub-module is losing 33% of the power, so it would seem that if the cells are shaded more than 33% the MPP will change to the region where the cells are by-passed. However, in practice, this percentage is higher: due to the by-pass diode's negative voltage and, more importantly, that as the current is reduced the voltage increases; so the power loss is not directly proportional to the degree of shade. For modules with three by-pass diodes, this higher limit can be estimated at around a 45% irradiance reduction. It is in this region, from a 6%-8% to a 45% irradiance drop, where there is a potential power gain when not all sub-modules are shaded.

The third region is when the cells from both the central MPPT and the DMPPT system are by-passed. In this region there is no potential power gain. The *I-V* and *P-V* curves of the single module and the ten module string can be seen in Figure 3.13. The power of the DMPPT system is now the same as the CMPPT system.

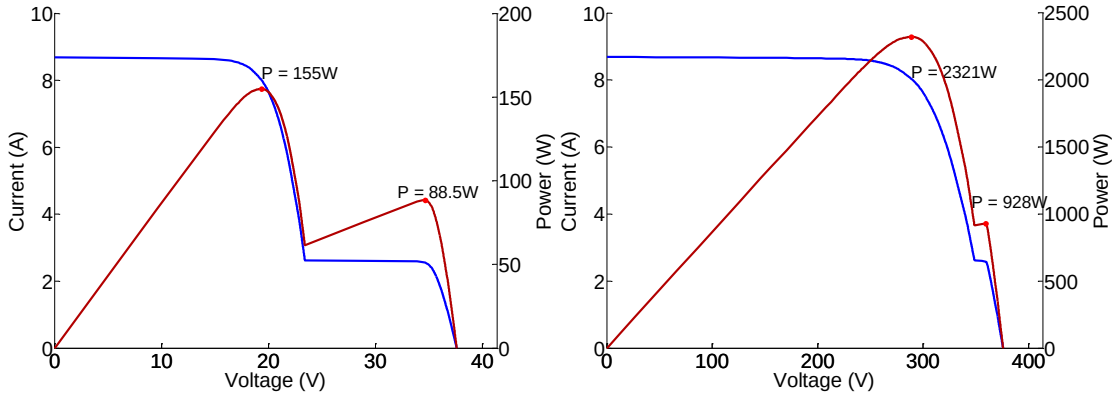

Figure 3.13: *I-V* and *P-V* curves of the single module (left) and the ten module string (right) when the cells from one sub-module are only receiving 30% of the total irradiance. It can be seen how in both cases the MPP is at a region where the shaded sub-module is by-passed. In this case the power produced by a DMPPT system and a CMPPT system is the same.

As the shadow progresses, the second set of ten cells starts to get shaded but since these belong to the same sub-module as the first ten, these new ten cells are already by-passed and the situation does not change.

We must wait until the third set of ten cells starts to get shaded to perceive new power gains. However, because now the relative loss is higher when one sub-module is lost, ~50%, the region where a possible power gain is possible is also higher, up to 60% considering the voltage increase.

Finally, when the third sub-module starts to get shaded (for modules with three by-pass diodes), the region of possible power gains extends to the fully shaded module. When the module is fully shaded (or at least cells from all sub-modules), because now there are no sub-modules producing more current, all cells lower their current to that of the shaded cells. Because in a CMPPT system the whole module (three sub-modules) is by-passed, a constant power gain can be obtained. The module now only receives diffuse irradiance producing a fraction of the power of the non-shaded modules which depends on the D/G fraction. See Figure 3.14, where the power of nine non-shaded modules plus the power of the shaded module add up to 2202W (+2.23%), considering a D/G of 15%.

When the shadow enters the module affecting all sub-modules (Figure 3.11-right), a more constant power gain is obtained as will be seen in the following section.

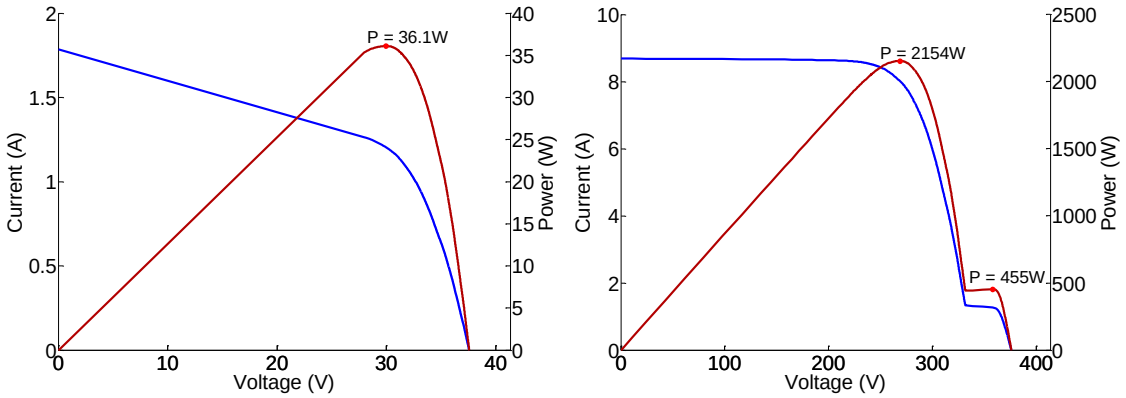

Figure 3.14: *I-V* and *P-V* curves of the single module (left) and the ten module string (right) when one module is fully shaded, receiving only 15% of the total irradiance. It can be seen how at the MPP of the ten module string the whole module is by-passed and its power is lost although 36W are still available.

3.4.1.2 Simulations

In order to better understand the arguments exposed in the previous section, simulations have been performed and the results are exposed in this section. For the simulations, the shading simulation tool that has been presented is section 2.1.3.1 has been used and different D/G ratios have been used in order to study the effects over the potential power gain. During each simulation step, different shading percentages are assigned to each cell as a function of the shadow and the D/G. With the simulation tool the *I-V* curve of each module and the *I-V* curve of the whole generator are both calculated. The MPP of each curve is calculated and the power gain is obtained by dividing the sum of all the individual modules' MPP by the MPP of the generator.

Progressive shadows over the PV generator have been considered; affecting one or various sub-modules at a time. For simplicity in the representation of the results, rectangular shadow profiles, like the one shown in Figure 3.11, are used. The shading percentage refers to the percentage of progression of the shadow. For the examples in Figure 3.11 these would be 35% and 20%, respectively, although for the example of the left this 35% does not correspond with the module's shaded fraction as the top cells are not shaded; it corresponds with the horizontal progression of the shadow. However, as we have seen in section 2.1.3 as long as more than five cells are shaded the effect on the *I-V* curve is the same. For cells with a more negative V_b even with one cell it could be enough. Normally, shadows caused by nearby objects affect more than one cell at a time, so this consideration is realistic.

3.4.1.2.a Effects of the number of serially connected modules and the number of shaded sub-modules on DMPPT power gains

The simulations presented in this section have all considered a D/G ratio of 10%.

Figure 3.15 shows the power gain obtained while a shadow progresses through one module in a ten module string: for (left) a shadow that progresses through the module covering one sub-module at a time and for (right) a shadow that progresses through the module covering all sub-modules from the beginning. These two possibilities are shown in Figure 3.11 (left) and (right) respectively. For the case where the shadow progresses shading one sub-module at a time, the three periods (because there are three by-pass diodes) described in the previous section can be seen[16]. The two periods where no power gain occurs can also be seen, where these correspond to situations where the shaded sub-modules are by-passed at the MPP in both a CMPPT and DMPPT system; situations like the one presented in Figure 3.13.

It can also be seen how the power gain and energy gain are higher for the shadow which progresses shading all sub-modules at a time. Higher power gains are observed because there is a higher proportion of shaded versus non-shaded modules, while higher energy gains are observed because in the CMPPT system the three sub-modules are by-passed from the beginning, while in the DMPPT system they are never by-passed. In this case, because there are ten cells in the vertical position, after 10% shade the first set of cells are completely shaded and the module can only produce what is received in diffuse irradiance. This does not change during the rest of the shadow's progression and, therefore, the power gain remains practically constant after this point.

At the end of the shadow the power gain is the same in both situations.

[16] Because there are three sub-modules, a sub-module is completely shaded at 33% shade.

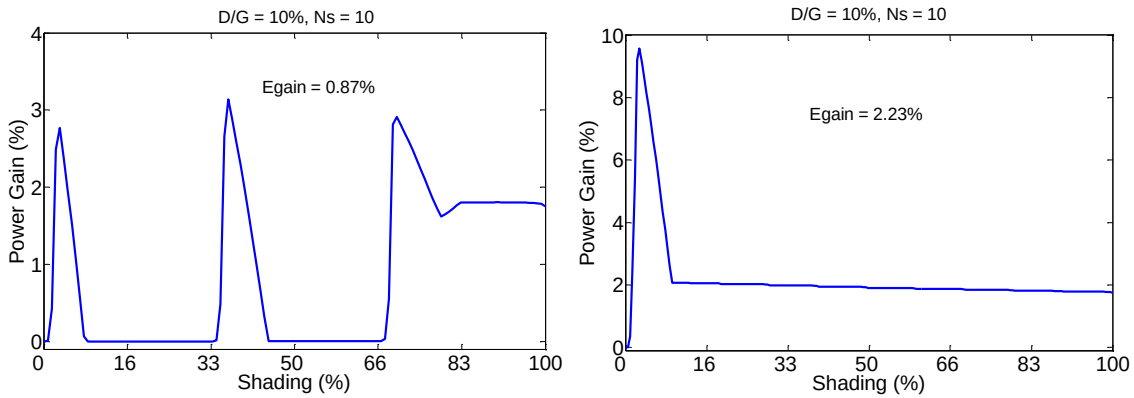

Figure 3.15: Power gain obtained with DMPPT in a ten module string when (left) the shadow progresses shading one sub-module at a time and (right) when the shadow progresses shading the three sub-modules of one module at the same time.

As the shadow affects more modules of the array, the power gains increase because the power gain of the previous shaded modules is always present. For this reason, the power gain increases considerably, up to 18% and up to 30% for both examples, and the final energy gain reaches almost 6% and 8% respectively. This, however, is the energy gain only during the shading period and not during the whole day or year, being the final values considerably lower.

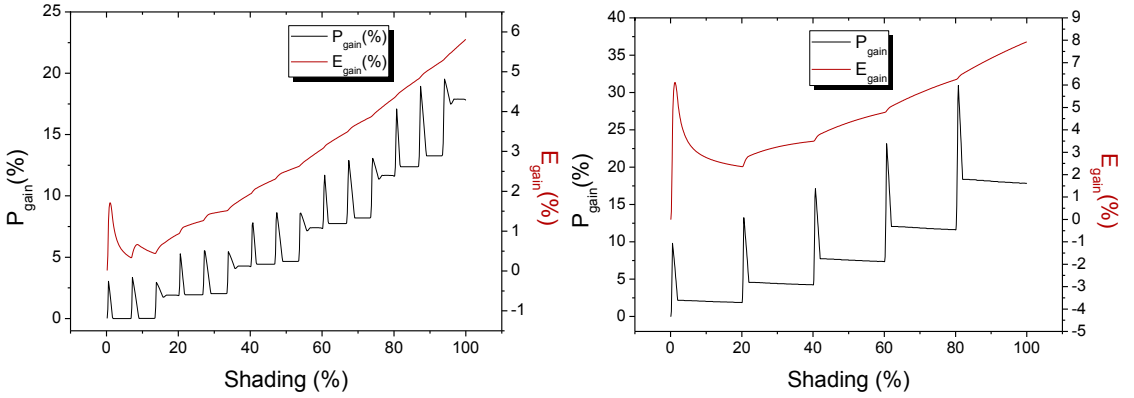

Figure 3.16: Power and energy gains obtainable with DMPPT for a ten module string in which a shadow progresses through five modules of the string while (left) shading one sub-module at a time and (right) shading three sub-modules, or one whole module, at a time.

Finally, if the number of modules in the string is increased, the same shading pattern over one module allows for less power gains, as the proportion of shaded modules to non-shaded modules decreases. However, if the number of modules in the string is double and the same shading occurs over twice the number of modules, then the power gains and the final energy gain is exactly the same as the case with half the number of

modules in series and shade over half the number of modules. This can be seen in Figure 3.17, where the string is increased to 20 modules and the same shading pattern is applied to one module (left) and two modules (right). In the first case, the power gain and energy gain is decreased by two with respect to the ten module string and one shaded module, while in the second case the result is exactly the same.

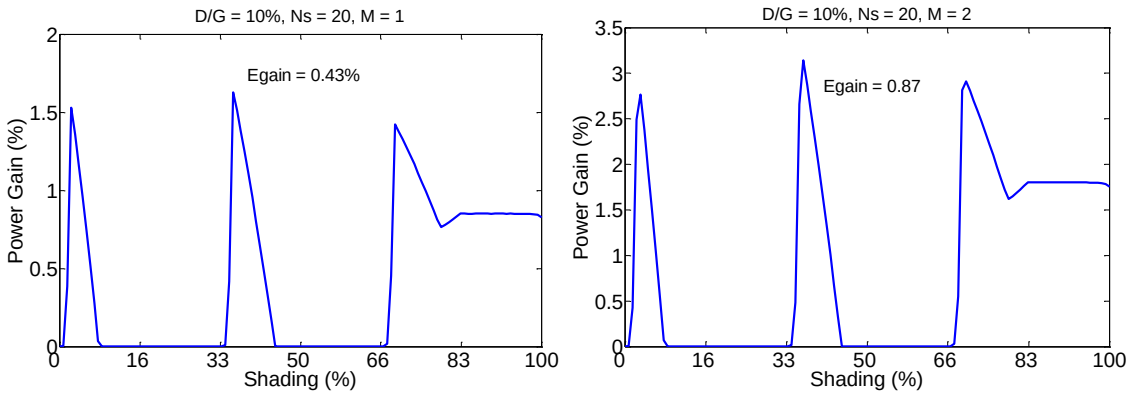

Figure 3.17: Power gain obtained with DMPPT in a twenty module string when the shadow progresses shading one sub-module at a time from (left) one module and (right) two modules.

3.4.1.2.b Effects of the D/G ratio on DMPPT power gains

As has been seen in the previous sections, DMPPT power gains can be obtained at time periods when the shadow does not completely cover the shaded cells of one sub-module and at time periods when the cells are completely covered. At the end of the day, this second period is the one that will add the most to the final energy gain, as when the shadow has finished covering a module this situation remains until the shadow exits the module. It is during this period that the module can only produce what it receives in diffuse irradiance and, therefore, the possible power gain depends directly on how much diffuse irradiance there is. Figure 3.18 shows the power gain obtained with DMPPT for the two shadow progressions presented in the example of Figure 3.15 but now with a D/G ratio of 20%. From the figure it can be seen how for the periods where the cells are not completely shaded (and the sub-module is not by-passed) the maximum power gains are exactly the same as the ones obtained for a D/G ratio of 10% (although they do not occur for the same shaded percentage, as this percentage represents the percentage of module area affected by the shadow, but not the irradiance decrease). Once the cells from all sub-modules are shaded the power gain increases, as during these periods the diffuse component is the only responsible for the power produced by the module. Of

course, at the end, this causes a higher energy gain. For the second shadow profile, the difference in total energy gain is higher, as the time when the module is working with only diffuse irradiance is longer.

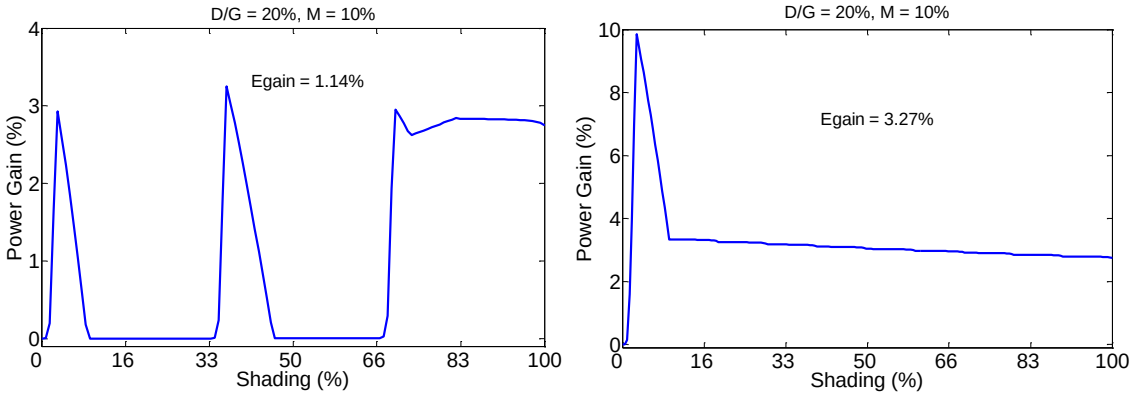

Figure 3.18: Attainably power gain with DMPPT for the same example in Figure 3.15 but now with a D/G ratio of 20%.

However, it should be noted that as the D/G ratio increases a point arrives at which the power gain starts to decrease. For example, as we have seen in the previous examples, before there is an approximately 8% current mismatch there is basically no power gain, as the cells can change their working point while still remaining in the elbow of the *I-V* curve, where there is not an appreciable power loss. This means that for D/G ratios higher than 90% the possible power gain is small.

Figure 3.19 shows the power gain obtained for different D/G ratios as a function of the number of shaded modules in a series string. The shaded modules are considered as completely shaded and only receiving diffuse irradiance. It can be clearly seen how as the number of modules increases the most profitable D/G ratio decreases.

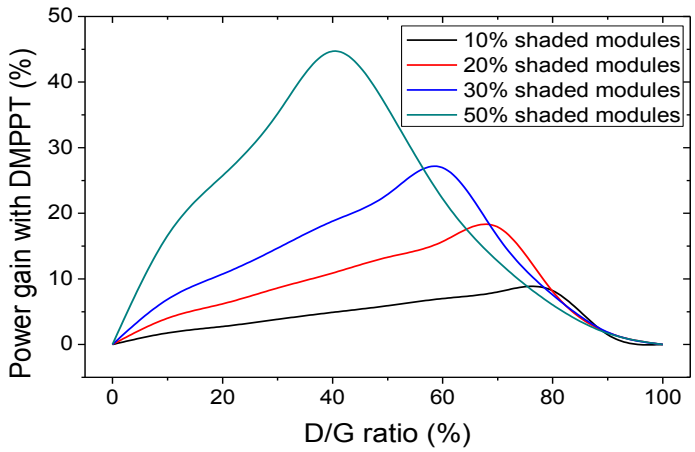

Figure 3.19: Power gain obtained for different D/G ratios as a function of the percentage of shaded modules in a string.

3.4.1.2.c DMPPT power gains in PV generators with parallel strings

In section 2.1.3.3, it was shown that the negative effect of shadows cast over PV generators with parallel strings can be higher than in single string systems. What was exposed was that if the shadow is the same over the same number modules in all the parallel strings, then the negative effect will be the same as if the shadow only occurred in a single string, i.e. there is no voltage mismatch. However, if the shadow is different in each string, there is voltage mismatch and the losses are much higher.

It seems logical to think that a similar effect would occur in power gains obtained with DMPPT; that higher gains will be obtained in parallel strings were the shadows are not distributed across the strings. Figure 3.20 shows the power gains attainable with DMPPT for a two string PV system with ten modules per string. In the example of the left, the shadow progresses past two modules of the same string, while the other string is unshaded. This is the same as the example of Figure 3.17-right, but because now there are two parallel strings of ten modules instead of a single twenty module string, the power gains are higher. However, if the shadow were to be distributed between two modules of different strings, the power and energy gains obtained (Figure 3.20-right) would be exactly the same as the ten module string with one shaded module (Figure 3.15-left) or the twenty module string with two shaded modules (Figure 3.17-right). What is meant to be shown here is that if the system design is done well enough, power gains with DMPPT in PV systems with parallel string should not be considerably higher than in single string PV systems.

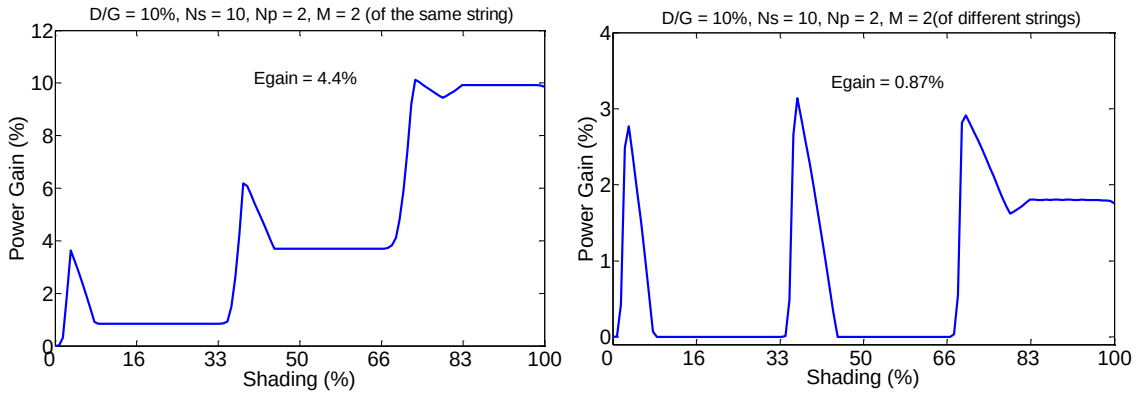

Figure 3.20: Power gain obtained with DMPPT in a PV generator with two parallel strings of ten modules each when the shadow progresses shading one sub-module from two different modules at a time, when the modules are in the same string (left) or when the modules are of different strings (right). When the shadow equally affects a

module from each string, the power gain is the same as if there were only one string. However, if the shadow affects modules from the same string, there is now a voltage mismatch between strings and the power gain is much higher.

3.4.1.3 Conclusions on attainable power gains with DMPPT

The previous examples show attainable power and energy gains for two specific shading situations. It has been shown that in parallel strings higher power gains are possible only if there is a faulty design and the shadow does not affect all strings equally. The examples do not consider other factors that can modify the values. The non-shaded period during the day is not considered and it should definitely be averaged out to calculate the final energy gain. Other factors like the limitation in mismatch compensation due to the output characteristics of DC/DC converters (section 3.5) or the malfunctioning of the MPPT algorithm in presence of local maxima (section 4.5.2) are also not considered. All these effects will influence the final energy gain being a negative influence most of the time. More detailed simulations are presented in chapter 5.

3.4.2 MISMATCH OF ELECTRICAL CHARACTERISTICS

It is well known that there exists certain dispersion in the electrical characteristics of PV modules of a same model. This dispersion can be due to normal manufacturer's tolerances, defects or even field degradation. In series connections, all modules that have a different I_m than the resulting I_m of the generator will show power losses because they are operating away from their MPP and with the use of DMPPT these losses are avoided. This section analyses the effects of this parameter dispersion in series connected PV arrays and the possible gains attainable with DMPPT.

In the literature we can find the following interesting articles which have also addressed this topic [Damm, Heinemann et al., 1995; Herrmann, 2005; MacAlpine, Deline et al., 2012; Massi Pavan, Mellit et al., 2014; Podewils and Levitin, 2011].

[Damm, Heinemann et al., 1995] measured 36 modules of a PV array at irradiances between 600W/m^2 and 1000W/m^2 and combined these modules in different series and parallel configurations. Only one module had a power difference of -8.9% while the rest remained at ±3%. They concluded that losses in parallel configurations were negligible and that the losses increase with decreasing irradiance. They did they study for two

locations of different irradiances obtaining losses between 0.8%-1.4% for different configurations without the worst case module and for the location with the lower irradiation. For the location with the higher irradiation, these losses are between 0%-0.2%. When introducing the worst case module, the losses rise significantly up to 4.5% annually for the location with lower irradiation and up to 2.9% for the location with higher irradiation.

[Herrmann, 2005] used data from a measured poll of 416 modules (three different types) at STC, obtaining tolerances in P_m of up to ±8.7%. Then they simulated their serial connection with different string lengths and considering non-presorted modules and pre-sorted modules with respect to I_m, P_m and I_{sc}. Although the current tolerances obtained for each type of module were of ±6.37%, ±5.31% and ±4.29%, the maximum power mismatch obtained for non-sorted modules was only of 0.56%, which was reduced to 0.34% when sorting with respect to I_m. For the group of thin-film modules, with lower FF, the maximum power mismatch for non-sorted modules in series was only 0.17%. By artificially increasing the tolerance in P_m up to ±20% they obtained a power mismatch of up to 4.6% in the non-sorted case, while if sorting with respect to I_m the power mismatch remained below 0.5%.

A newer study by [MacAlpine, Deline et al., 2012] measured 36 crystalline modules and 38 thin film modules from five arrays. For their worst array, with standard deviations in I_m up to 5.5% they only obtained a power mismatch between 0.2%-0.5%, also concluding that at low irradiances a higher mismatch is present. For the different arrays they obtained an annual simulated energy loss due to mismatch between 0.1%-0.35%, for the normal arrays. In one of the arrays were defective modules were discovered an annual energy loss due to mismatch of 0.70% was calculated.

[Podewils and Levitin, 2011] measured the energy gain obtained with different DMPPT equipment under various situations. One of the situations was for un-shaded conditions and energy gains of 0.9% and 3.2% were obtained for the SolarEdge and Tigo optimizers, respectively. However, the experiments were performed with an artificial light source and the authors acknowledge an uncertainty of ±3% on the uniformity of the light, which could lead to artificial energy gains.

A study a bit different than the rest is that of [Massi Pavan, Mellit et al., 2014] which compared the mismatch effect when using different module classes, i.e. using modules of different power rating of the same model. The authors claim that it is a common practice in large PV plants as many times there such a large number of modules of the same power rating is not available. The authors consider 16 parallel strings of 20 modules in series with different combination of module power ratings in each string. Here, because of the series and parallel connection, both mismatch in voltage and current have an effect. The worst string, in which nine modules of 220W are combined with 11 modules of 235W, returns a power mismatch of 2.75%.

From the first three references it is clear that even large differences in I_m, up to ±6.4%, do not have a significant effect when connecting the modules in series. This seems evident if we take a look at the *P-I* curves of different measured modules, shown in Figure 3.21. The two figures correspond to two modules with different FF: Siliken SLK 60 P6l (left) and Atersa APX90 (right), with FFs of 0.708 and 0.622 respectively. The horizontal line represents a 1% drop in power and in parenthesis the current difference with respect to I_m is shown. For the Siliken module, the current difference is 4.72% and 2.95% depending on if the current is lower or higher than I_m and for the Atersa module these values are 5.76% and 4.54% respectively. In both modules there is a higher current mismatch tolerance from I_m to I_{sc}, although this difference is higher in the Siliken module, which has a higher FF. This is mainly due to the improvement in the series resistance, R_s, of the Siliken module causing a more abrupt fall in the *I-V* curve and, therefore, less current mismatch tolerance. In modules with ideal FFs, the current mismatch tolerance would be equal to the power loss: i.e. a 1% change in current would equal a 1% power loss. In conclusion, the better the FF the higher the losses due to mismatch of electrical characteristics.

Although there are punctual cases, i.e. when there are modules with large power deviations or defects inside the array, it is not very probable that large or even appreciable energy gains will occur with the use of DMPPT produced by the elimination of the mismatch of the modules' electrical characteristics.

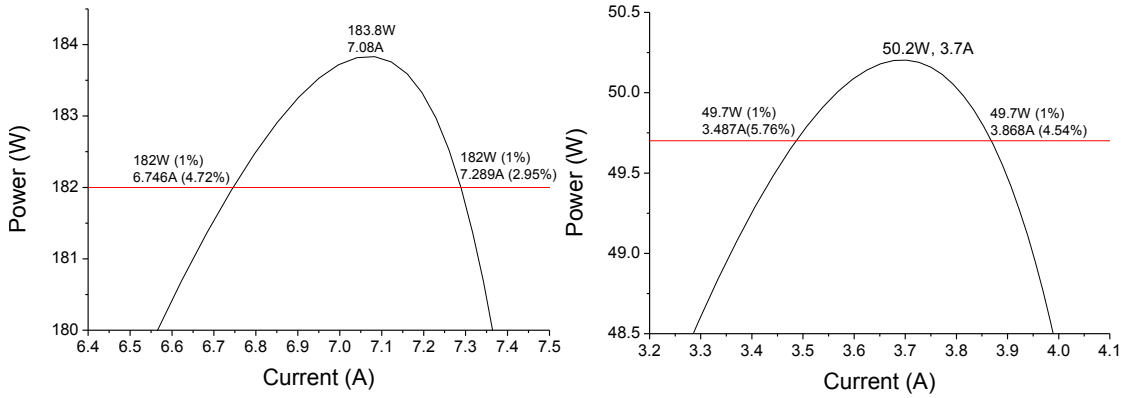

Figure 3.21: P-I curves of two different PV modules were the line for 1% power loss is marked. This line shows that the possible current variation for 1% power drop is up to 5.8% and that it depends on the type of module.

3.5 LIMITATIONS IN THE COMPENSATION OF MISMATCH LOSSES IN PV ARRAYS WITH POWER OPTIMIZERS

Due to the finite voltage output or conversion ratio values of power optimizers and to the constant voltage or limited voltage range of the inverter, situations exist in which even with a DMPPT approach the working of each PV module at its MPP is not possible. This was already pointed out in [Orduz, Solórzano et al., 2011a], in which the author of this thesis participated, and later on other authors [Alonso, Roman et al., 2012; Femia, Petrone et al., 2013; Vitelli, 2012] expanded the study about these limitations and came to the conclusion that for minimizing these losses it is necessary to eliminate the constant voltage at the inverter. [Vitelli, 2012] claims the necessity of both DMPPT and central MPPT as the solution, while [Alonso, Roman et al., 2012] have come up with a new term denoted maximum power range tracking (MPRT) which aims at finding a point in the MPR of the system, allowing for all modules to work at their MPP. However, despite the new MPRT term, the reality is that this algorithm can be implemented in exactly the same way as a normal MPPT algorithm and normal PV inverters can be used and in essence both proposals are the same.

As is shown in sections 2.1.3 and 4.5.2, when there are shadows cast over PV arrays, local maxima can appear in the modules' *I-V* curves and the MPP's voltage and current changes. When the MPP lowers its current due to shading there is an increase in voltage due to having lower losses in R_s. It could also occur that the MPP of the shaded module

has the same I_m than that of the non-shaded modules but a lower V_m due to some by-pass diodes being in forward bias.

Neither of these authors has considered these facts for their analysis and, for the sake of simplicity, it will also not be considered in the following explanation. It also makes sense to not consider it at this moment because, as shown in section 3.3.2, it is the current mismatch that has a greater impact in the conversion parameters. In addition, the potential voltage mismatch that can occur is lower than the potential current mismatch. In modules with three by-pass diodes, the maximum voltage mismatch is approximately 1:3 (cells from only one diode working or from all three) while the current mismatch can be up to 1:10 (only diffuse irradiance or diffuse and direct). However, further on in this Thesis, in section 5, when annual losses due to these limitations are calculated the changes in both current and voltage of shaded *I-V* curves will be considered. For the following examples a hypothetical 240W PV module has been used, with MPP values of: V_m = 30V and I_m = 8A. By considering only changes in current and assuming that the panel works at the MPP, we can define the working point of each panel as expressed in (3.11). Previously, in equation (3.10), a change of variable is introduced to facilitate the development and the following of the equations. While m represents the mismatch in current of each PV module (and m_k the mismatch in the k^{th} module), x represents the percentage of I_m generated by each module.

$$x = (1 - m) \tag{3.10}$$

$$(V_m,\ x_k \cdot I_m), \text{ where } 0 \leq x_k \leq 1 \tag{3.11}$$

As has already been mentioned, the limitations of the mismatch losses compensation can be due to the limited conversion ratio or output values of each power optimizer as well as to the fixed or limited voltage range of the inverter. The output current of each power optimizer depends on the conversion ratio and the working current, and supposing $I_w = I_m$ it can be expressed by equation (3.12):

$$I_{o,k} = \frac{x_k \cdot I_m}{M(d)_k} \tag{3.12}$$

Because all optimizers are connected in series their I_o must be the same. By comparing the output current of each optimizer in the form of equation (3.12), equations (3.13) and (3.14) are obtained; for optimizers *k* and *j*.

$$\frac{x_k \cdot I_m}{M(d)_k} = \frac{x_j \cdot I_m}{M(d)_j} \tag{3.13}$$

$$x_k \cdot M(d)_j = x_j \cdot M(d)_k \tag{3.14}$$

And by considering the worst mismatch situation, which takes place for the most different x_k and x_j (that is when one panel is generating the maximum current, m=0 and x=1, and the other the minimum possible), equation (3.15), which denotes the maximum mismatch that can be compensated with power optimizers, is obtained.

$$m_{max} = 1 - \frac{M(d)_{min}}{M(d)_{max}} \tag{3.15}$$

For example, it is evident that for a system with boost converters with an $M(d)_{max} = 2$, a current mismatch higher than 50% cannot be compensated because the mismatched module cannot boost its current and the non-mismatched modules can only reduce their current.

Because manufacturers provide voltage and current output limits in their datasheets, instead of *M(d)* limits, it is convenient to relate *M(d)* with the output limits and the input values or the working point. This can be done with equations (3.16) and (3.17) although during the rest of the section *M(d)* will be used in order to keep the equations as simple as possible.

$$M(d)_{max} = \frac{V_{o\_max}}{V_w} \tag{3.16}$$

$$M(d)_{min} = max\left\{\frac{I_w}{I_{o\_max}}, \frac{V_{o\_min}}{V_w}\right\} \tag{3.17}$$

In the case of $M(d)_{max}$, because the minimum output current is zero, it will never be a limitation, being the limitation always from V_{o_max}. On the other hand, for $M(d)_{min}$ the limitation could be caused by I_{o_max} or V_{o_min}, as is shown in equation (3.17); this depending on the different products. If we consider a PV string of modules working at

30V and 8A with one mismatched module working at 0.8A (90% mismatch), equation (3.17) for the mismatched module of the SolarEdge system (V_{o_min} = 5V & I_{o_max} = 15A) and the Tigo sytem (V_{o_min} = 0V & I_{o_max} = 9.5A) returns (0.053, 0.167) and (0.084, 0); being the SolarEdge system limited by V_{o_min} and the Tigo system by I_{o_max}. Although there are many possible situations, in most of them the SolarEdge system will be limited by V_{o_min} and the Tigo system by I_{o_max}.

For example, for the SolarEdge optimizers, which have a V_{o_max} of 60V and a V_{o_min} of 5V, and for modules with a V_m of 30V and supposing it equal to V_w, the maximum possible mismatch that can be compensated is of 91.7%. Because diffuse irradiance is usually never lower than 10% of the global irradiance, in shaded conditions it is rare to have a higher mismatch than 90%. So, from this analysis it would seem that the SolarEdge system can solve any mismatch problem.

We can, however, go a step further and relate the maximum possible mismatch with the total number of modules in the system, N_T, the number of mismatched modules, N_M, and the inverter voltage, V_{inv}. First, the limits in number of optimizers in the system must be defined. The limits are imposed by the fact that V_{inv} must be reached without reaching the optimizers' output limits; arriving at equation (3.18) which is imposed as a restriction to the following equations. For example, for a system with a V_{inv} = 330V and with modules of V_m = 30V, the number of modules must be between six and sixty-six. SolarEdge has even more restrictive limits: eight to twenty-five.

$$\frac{V_{inv}}{V_m \cdot M(d)_{max}} \leq N_T \leq \frac{V_{inv}}{V_m \cdot M(d)_{min}} \tag{3.18}$$

Taking equation (3.6) and considering the same working voltage for all optimizers, that all mismatched modules have the same degree of mismatch and using x_k, we arrive at equation (3.19).

$$M(d)_k = \frac{V_{inv} \cdot x_k \cdot I_m}{V_m \cdot [(N_T - N_M) \cdot I_m + N_M \cdot x_k \cdot I_m]} \tag{3.19}$$

And by solving for x_k we arrive at equation (3.20).

$$x_k = \frac{(N_T - N_M) \cdot M(d)_k}{V_{inv}/V_m - N_M \cdot M(d)_k} \tag{3.20}$$

Knowing that the most mismatched module will have the lowest *M(d),* equation (3.21) can be obtained, which represents the maximum possible mismatch in a system with N_T total modules and N_M mismatched modules, and having to meet the restriction imposed by equation (3.18). Now, considering the previous example of a SolarEdge system (V_{inv} = 330V), that there are ten modules and only one mismatched module, the maximum possible mismatch that can be solved is of 86.4%. If the number of modules is increased to 22 (could be a typical 5kW system) the maximum possible mismatch that can be solved drops to 68.2%.

$$m'_{max} = 1 - \frac{(N_T - N_M) \cdot M(d)_{min}}{V_{inv}/V_m - N_M \cdot M(d)_{min}} \tag{3.21}$$

From this equation we can deduce that for a fixed inverter voltage, as the number of modules in the system increases the maximum possible mismatch decreases and that as the number of mismatched modules increases, the maximum possible mismatch also increases. This is shown graphically in Figure 3.22.

However, this only takes into account the limits of the power optimizer with the mismatched module or modules but it is also important to consider the limits of the optimizers with the highest producing modules. As the mismatching increases, the higher producing optimizers will tend towards $M(d)_{max}$ and it is possible that they arrive at this limit. For finding the maximum degree of mismatch that can occur while the maximum producing optimizers are within limits, we can again use equation (3.6) but now for the highest producing optimizers, arriving at equation (3.22).

$$M(d)_k = \frac{V_{inv} \cdot I_m}{V_m \cdot [(N_T - N_M) \cdot I_m + N_M \cdot x_k \cdot I_m]} \tag{3.22}$$

Solving for x_k and by knowing that the highest producing module will have the highest *M(d)* we arrive at equation (3.23), which must also meet the restrictions of equation (3.18).

$$m''_{max} = \frac{N_T \cdot V_m \cdot M(d)_{max} - V_{inv}}{N_M \cdot V_m \cdot M(d)_{max}} \tag{3.23}$$

From this equation we obtain the opposite conclusion as from equation (3.21); as the number of modules in the system increases the maximum possible mismatch also increases and as the number of mismatched modules increases the maximum possible mismatch decreases.

Because there can only be one absolute maximum mismatch in the system, that which keeps the least producing and the most producing optimizer inside its conversion limits, it must be chosen as the minimum of equations (3.21) and (3.23), as shown in equation (3.24).

$$m_{max} = min\{m'_{max}, m''_{max}\} \tag{3.24}$$

If we use the SolarEdge system (V_{inv} = 330V, minimum and maximum number of optimizers equals 8 and 25) as an example and we set the maximum current mismatch to 90% (only diffuse irradiation) we obtain the four figures shown in Figure 3.22 which relate the number of optimizers in the system with the maximum possible mismatch for one, two, four and eight mismatched modules. The figures also show which optimizers are limiting the maximum mismatch: the least producing or the most producing. It can be seen how as the number of optimizers increases the least producing modules permit less mismatch, opposite with the most producing modules and how as the number of mismatched modules increases the opposite occurs.

The figures also reveal how there are not many situations in which it is possible to solve a full mismatch problem. In the examples shown, the only situations when a full mismatch problem can be solved is when two modules are shaded for systems with eight optimizers or when three modules are shaded for systems with ten optimizers or when eight modules are shaded for systems with thirteen or fourteen optimizers. This is a clear drawback for a system which claims the energy gains in mismatch situations as its main benefit. How this is traduced to power loss is seen in some of the examples of section 5.

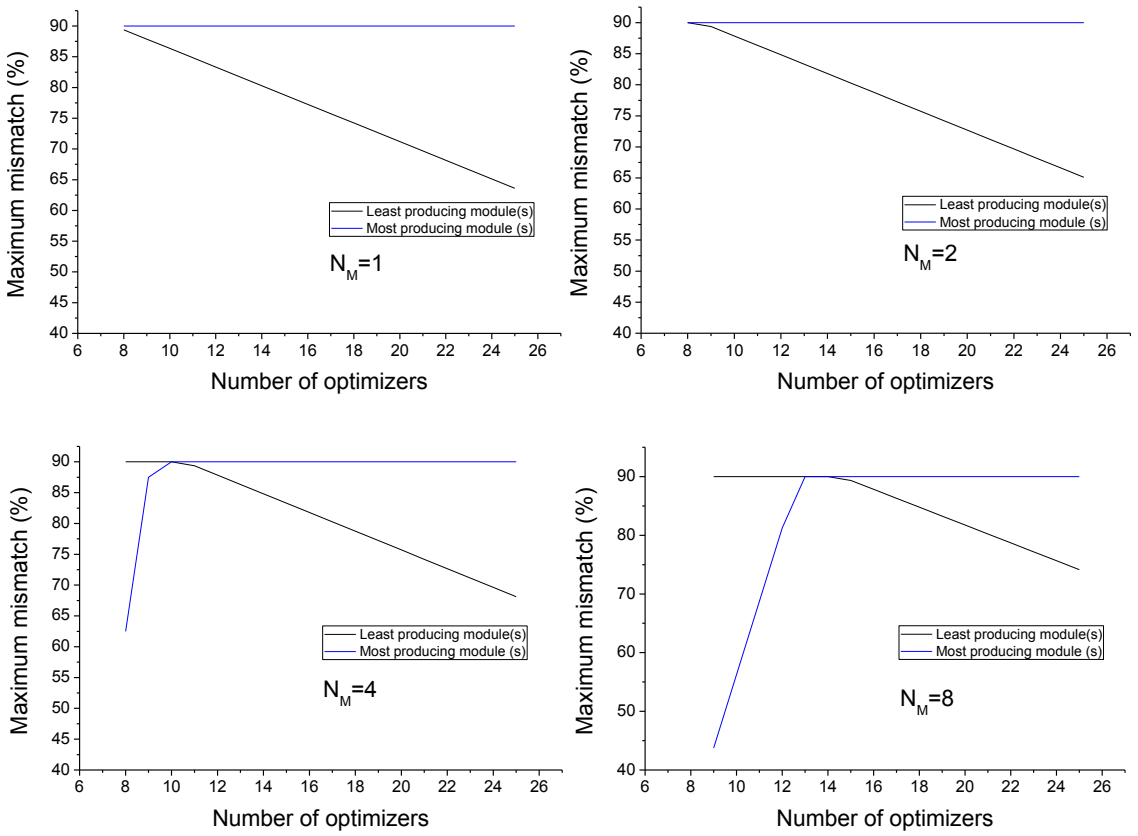

Figure 3.22: Maximum possible mismatch in a SolarEdge system (V_{inv} = 330V) as a function of the number of optimizers in the system and when one-(top-left), two-(top-right), four-(bottom-left) and eight-(bottom-right) modules are mismatched. The figure also shows which optimizers limit the maximum mismatch: the most producing or the least producing.

As an example, Figure 3.23 shows the *I-V* and *P-V* curves of a twenty optimizer system with four mismatched modules. The two graphs show the results for a 70% (left) and 80% (right) mismatch. It can be seen how for the case of 70% mismatch, at an inverter voltage of 330V the working point is inside the MPR, however for the case of 80% mismatch the working point is almost 200W (5%) below the MPR. This is in agreement with the corresponding graph of Figure 3.22, were for N = 20 and M = 4 the maximum mismatch that can be solved is around 75%.

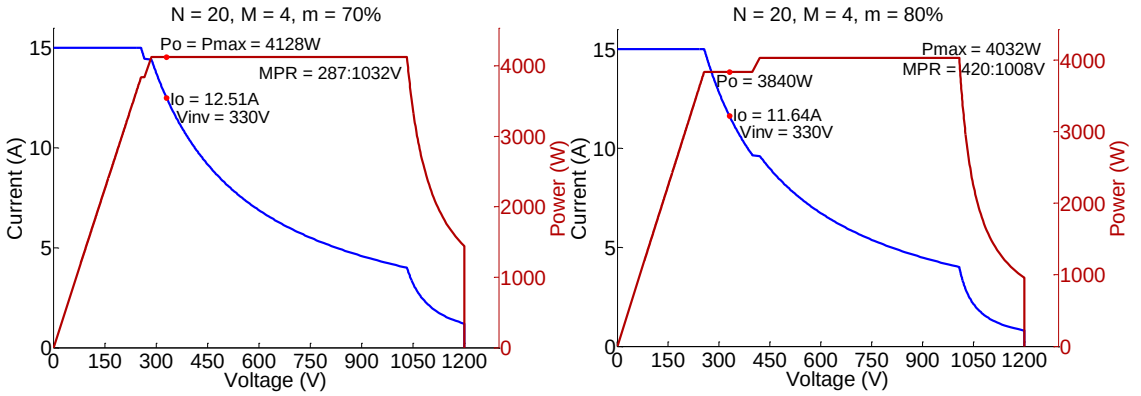

Figure 3.23: *I-V* and *P-V* curves of a twenty optimizer system with four mismatched modules at 70% (left) and 80% (right). It can be seen how for the 70% mismatch case, the working point is inside the MPR while for the 80% case it is 200W or 5% below the MPR.

In order to avoid losses due to conversion limits, two possibilities exist: one is to increase the range of conversion ratio and the other to change the inverter's voltage. The first solution is related to the design of the DC/DC converters and increasing the range of the conversion ratio can be costly and DC/DC conversions with a very high or very low *M(d)* are less efficient. The second solution is more straightforward. For minimizing losses due to conversion limits of power optimizers by changing the inverter's voltage, two options exist: changing the voltage of the inverter as a function of the number of optimizers connected in series and keeping this voltage constant or using an inverter with an MPPT algorithm.

It seems logical that as the number of optimizers in a string increases the fixed voltage at the inverter should also increase. This is represented in Figure 3.24-left, where the maximum possible mismatch for one module is represented as a function of the inverter voltage and where it can be seen that the inverter voltage for having a maximum mismatch of 90% increases as the number of modules in the string increase. However, that only represents the case for one mismatched module in the string and as the number of mismatched modules increases, the inverter voltage necessary for solving all the mismatch decreases. As can be seen in Figure 3.24-right, which shows the case for a ten module SolarEdge system, the inverter's optimum voltage varies from approximately 150-550V when eight modules or only one module are mismatched.

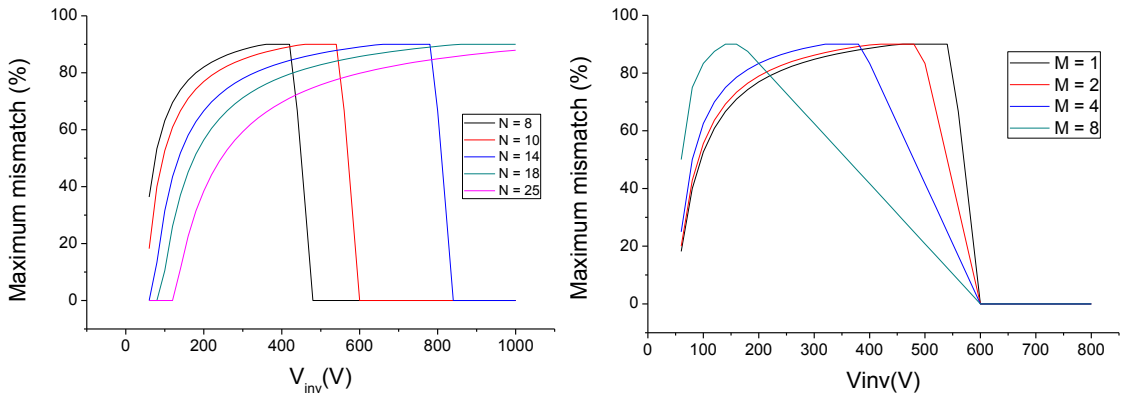

Figure 3.24: Maximum possible mismatch as a function of the inverter's voltage in a SolarEdge system for (left) a different number of optimizers in series and one mismatched module, $M = 1$, and (right) a different number of mismatched modules in a ten optimizer system, $N = 10$.

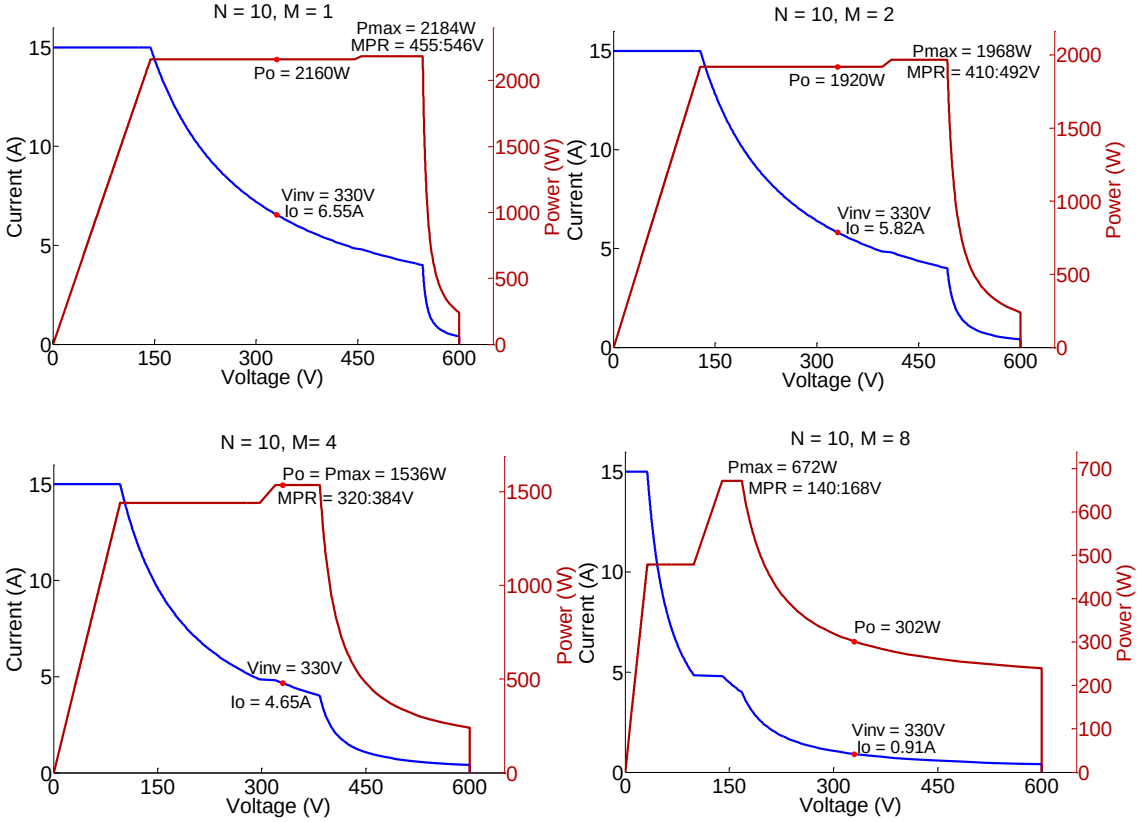

Figure 3.25: *I-V* and *P-V* curves of a ten optimizer PV system, N=10, with a different number of mismatched modules, M, being the mismatch considered at 90%. The working point of a system with V_{inv} = 330V is marked as well as its output power, the maximum possible power and the MPR. These four curves correspond to the four cases of Figure 3.25-right and it can be seen how the MPR corresponds to the range of 90% mismatch. Again with this figure the need for a variable inverter is reinforced.

It is therefore clear that the best option is to not have a fixed inverter voltage but an inverter voltage range. As was already presented in [Orduz, Solórzano et al., 2011a] and later on by [Alonso, Roman et al., 2012],the inverter voltage for which all optimizers are

within conversion limits can be represented by equations (3.25) and (3.26). Specifically, equation (3.25) represents the minimum inverter voltage for which none of the least producing optimizers will reach conversion limits and equation (3.26) represents the maximum inverter voltage for which the most producing modules will not reach conversion limits.

$$V'_{inv} = V_m \cdot M(d)_{min} \cdot \left[N_M + \frac{(N_T - N_M)}{(1 - m_{max})}\right] \tag{3.25}$$

$$V''_{inv} = V_m \cdot M(d)_{max} \cdot [N_T - m_{max} \cdot N_M] \tag{3.26}$$

However, these equations are only valid for one specific situation of mismatch, especially in relation to the ratio between mismatched modules and total number of modules, *M*:*N*. If the absolute inverter's voltage range wants to be calculated it is necessary to consider all the possible ratios of mismatched modules vs total number of modules, being this from $M = 1$ to $M = N\text{-}1$. If we also consider the maximum possible mismatch to be 90% ($m_{max} = 0.9$) we arrive at equations (3.27), (3.28) and (3.29) which indicate the necessary inverter voltage range so that none of the optimizers reach conversion limits[17].

$$V_{inv\_min} = V_m \cdot M(d)_{max} \cdot \left[{}^{N_T}/_{10} + 0.9\right] \tag{3.27}$$

$$V_{inv\_max} = V_m \cdot M(d)_{min} \cdot [10 \cdot N_T - 9] \tag{3.28}$$

$$V_{inv\_range} = \left[V_{inv\_min}, V_{inv\_max}\right] \tag{3.29}$$

[17] Note that for arriving at these equations, $M = 1$ is used in equation (3.26) and $M = N\text{-}1$ in equation (3.25) since the worst situation for the most producing modules is when there are N-1 mismatched modules and in this case the necessary V_{inv} for not reaching conversion limits is minimum and opposite for the other case.

3.6 CHOOSING THE MOST CONVENIENT DC/DC CONVERTER TOPOLOGY FOR POWER OPTIMIZERS

The two main factors to consider when deciding which DC/DC converter topology to use for designing power optimizers are: the electronics (cost, design and efficiency) for implementing the DC/DC converter and the possibilities of shadow mitigation considering the conversion limits explained in section 3.5. The various products in the market include all of these topologies, i.e.: SolarEdge (buck-boost), Tigo Energy (buck) and STMicroelectronics (boost).

[Erickson, 2001] states that buck-boost converters are characterized by lower efficiencies and higher costs because of enhanced component stresses, being the most expensive topology. For example, for the same output voltage than buck and boost converters, the buck-boost converters must have switches that can handle double the voltage and current and previous authors have always considered the boost topology to be the best suited [Femia, Lisi et al., 2008; Roman, Alonso et al., 2006]. In addition the frequency of the switches is also higher, causing lower efficiencies and higher stress (which could reduce the reliability). Buck and boost are very similar electronically and much simpler than buck-boost converters. Electronically wise it can be concluded that the buck-boost converter is the worst option, making the boost and buck converters equally acceptable. This, added to the fact that in short strings boosting the voltage can be helpful in reaching the optimum inverter voltage, has caused previous authors to consider the boost topology as the most convenient topology [Roman, Alonso et al., 2006; Vitelli, 2012], although this should be reconsidered.

When considering the mismatch compensation possibilities the situation changes. For example, in a ten module PV generator with boost converters and considering V_m to be 30V, if one module is shaded at 1/3, this means that the rest of the modules must boost their output voltage by three, arriving at an output voltage of 840V for the system. If this same module is shaded by 90% then the output voltage must 2730V which is not an acceptable voltage as the DC voltage of PV systems is limited; up to 1000V and down to 600V in some places like the US. For compensating mismatches of 90%, the maximum number of optimizers that can handle a system while staying below 1000V is only four. If we consider that the MPPT range of inverters is usually lower than 800V,

then this number is even lower. Only considering this fact, it is clear that boost converters are not a good option for power optimizers connected in series. An option for using boost converters would be to have a parallel connection, although this would increase the current and force having larger diameter cables.

Buck converters are a good option if the number of modules in the system is not very low. For example, let's consider a PV array of 4.8 kW made up of twenty 240W modules with V_m = 30V, with Tigo buck converters (V_{o_min} = 0V) and connected to an inverter with voltage range from 180-550V. With no shade the array will be working at 550V with a conversion ratio just below one. And the maximum possible mismatch that can be compensated is when fifteen modules are shaded, while the inverter works at 180V. This seems like a pretty fair situation. If there are less modules, say ten, the highest mismatch situation that can be compensated is four out of ten modules at 90% mismatch.

With buck-boost converters, the situation is more flexible. However, for the SolarEdge system, which has buck-boost converters with V_{o_min} = 5V and V_{o_max} = 60V, with the same previous inverter we can compensate the losses for shading over 1-7 for the ten module generator but only from 11-18 modules for the twenty module generator. The reason is that the V_{o_min} = 5V is very limiting. If we had V_{o_min} = 0V like in the Tigo system, we could compensate any mismatch losses in both, the ten and twenty module arrays.

In conclusion, we could say that if we are sure that we will use arrays with a large number of modules buck converters are the best option. However, for arrays with less modules, buck-boost converters should be used, despite their higher cost, or do not use power optimizers at all because the mismatch compensation will be limited. Despite what previous authors have mentioned, boost converters are probably the worst option.

4 EXPERIMENTAL ANALYSIS OF PV SYSTEMS WITH DMPPT

While the previous chapter presents the theoretical concepts of PV systems with DMPPT, this present chapter presents a series of experiments that were conducted with the aim of verifying the theoretical concepts previously exposed and gaining a higher understanding of how DMPPT systems behave in PV arrays. Just like in the previous chapter, more focus is placed on power optimizers than in micro-inverters because of their higher complexity. In this chapter, the results of the following measurements are presented: the behaviour of power optimizers in PV arrays under different working conditions (how the conversion ratio of each optimizer changes with the working conditions, what occurs when conversion limits are reached and the efficiency of the different components), measurements of the output curve of a boost power optimizer, the efficiency of the MPPT of different equipment (including central inverters) especially focused on finding the absolute MPP in presence of local maxima and, finally, results showing the power gain obtained with a prototype power optimizer for different shading situations.

The obtained results agree very well with the theory presented in chapter 3. With all this theoretical understanding and with the experimental results that back up the theory, an advanced model for simulating energy gains with DMPPT systems is presented in

chapter 5, accompanied of simulations for different shading profiles, as well as a verification of the simulations with a real PV system.

4.1 THE SOLAR ARRAY SIMULATOR: SAS E4360

In a large part of the experiments performed and presented in this chapter a solar array simulator (SAS) has been used. It's characteristics, functioning and the software control that has been developed is described in this section.

The SAS used during this thesis is the model SAS E4360 from Agilent Technologies. The E4360 is a DC current source with very low output capacitance that simulates the output characteristics of a solar array. It is capable of simulating the *I-V* curve of a solar array under different conditions such as temperature, irradiation, degradation, or shading and it has three operating modes:

- Fixed mode: the output has the rectangular characteristics of a standard power supply and is of no use for simulating *I-V* curves.
- SAS mode: the output has an *I-V* characteristic that follows an exponential model of a solar array. The model is specified using the four main parameters of an *I-V* curve: V_{OC}, I_{SC}, V_M and I_M. This mode can be used for a single curve, where the user defines these four parameters and the curve is simulated by the SAS, or in list mode, where the user defines a list of these four parameters and a time step and the SAS changes the *I-V* as a function of the time step and the new parameters. This mode can be used for simulating a pattern of *I-V* curves at different irradiance or temperature. However, it cannot be used for simulating *I-V* curves with local maxima.
- Table mode: the output is defined by a table of *I-V* points specified by the user. The tables are stored in non-volatile memory, which may contain up to 30 tables with a maximum of 4,000 *I-V* points per table. This mode allows *I-V* curves with local maxima to be simulated and is the mode that has been used for performing the measurements presented in this section. The only restriction in the *I-V* curves is that it should not have a $\frac{\Delta V}{\Delta I}$ smaller than 1 Ohm at any time.

The E4360 allows choosing the *I-V* curve resolution from 256 or 4000 points depending on the curve generation time desired, being it 30ms or 250ms respectively. In addition, the SAS can record the voltage and current operating points every 100ms. The SAS is composed of two output modules, each of 600W, 5.1A and 120V. These outputs can be connected in parallel to double the current or in series to double the voltage.

Perhaps the main drawback of the SAS for testing the MPPT of PV inverters is its low voltage output, which even with both output modules connected in series only reaches 240V while the MPPT range of inverters is usually between 180-600V. An *I*-V curve with a V_{OC} of 240V will typically have a V_M of 200V or less and each diode that is in forward bias (one shaded sub-module) reduces the V_M by about 10V, thus giving very little range of measurement.

The SAS allows controlling it locally or remotely. The local control is only useful for setting individual curves and the remote control provided by Agilent is not very intuitive and does not allow fully using the SAS, especially in Table Mode. For this reason, a control software has been developed in LabView. This software allows using all the functions of the SAS, recording the working values for further analysis and viewing the working point on top of the *I-V* and *P-V* curves. In Table Mode, the software allows inserting two different *I-V* curves and adding them together in series to simulate two modules in series or increasing the voltage. Another interesting addition of this developed software is that, in List Mode, it allows inserting a list of irradiance and temperature values (instead of V_{OC}, I_{SC}, V_M and I_M) and it calculates the corresponding *I-V* curve for each condition, using equations (2.6) and (2.7). Two screenshot of the developed software can be seen in Figure 4.1.

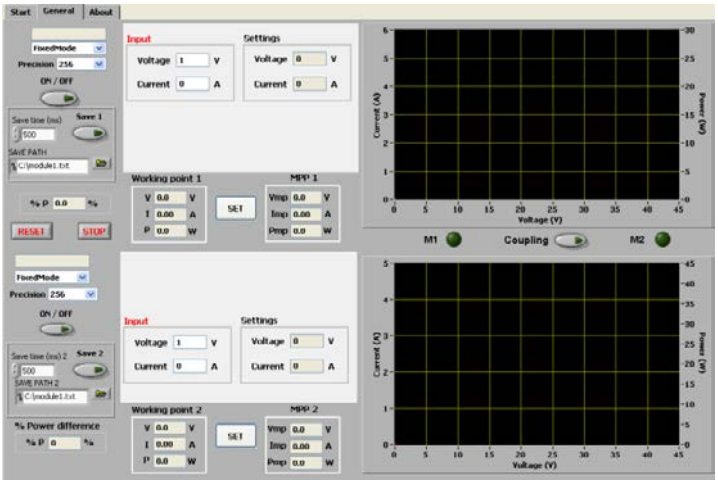

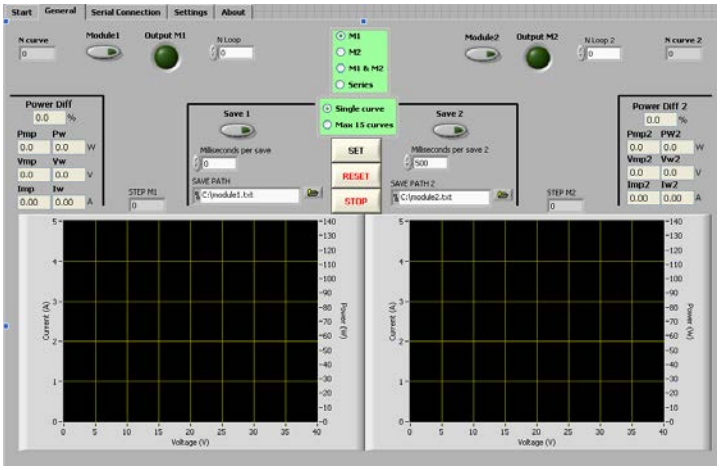

Figure 4.1: Screenshots of the developed LabView software for controlling the SAS E4360 and recording the results.

4.2 MAIN WORKING PARAMETERS OF POWER OPTIMIZERS AT DIFFERENT CONDITIONS

This section presents the results obtained from testing the main working parameters of the SolarEdge system under different conditions: normal operation, shade over one module, shade over many modules, cloudy days and out of range conversion parameters. The experiments performed are aimed at verifying the equations that describe the functioning of power optimizers in PV arrays presented in section 3.3.1 and also the limitations due to the limited conversion parameters presented in section 3.5. The efficiency of the power optimizers is also measured with the idea of using it in the model for simulating energy gains presented in section 5.

The experiments have been performed with a SolarEdge system and a PV generator which forms part of MagicBox: a solar house presented in the Solar Decathlon 2005 and now installed at the Instituto de Energía Solar in Madrid for research purposes. The generator is made up of Isofoton I-110/12 PV modules, with a V_M of 17.4V and I_M of 6.32A. In order to better match the voltage range of the power optimizers, the modules were grouped in serially connected pairs each connected to a power optimizer and all optimizers were connected in series to the SolarEdge inverter. Magic Box and the measurement setup can both be seen in Figure 4.2. At the set-up there are eleven PV module pairs (two Isofoton I-110 modules in series) available which can be all

connected in series to a string inverter, or to the SolarEdge or Tigo optimizers. However, not in all experiments are the eleven modules used, sometimes only using ten. Because the Tigo system was only installed for ten optimizers, the experiments conducted with SolarEdge after the Tigo system arrived are with ten modules, while those previous to the Tigo system arriving are done with eleven optimizers.

Although the SolarEdge monitoring portal provides data of the voltage and current values every 15 minutes, for the purpose of having more frequent and reliable data another measuring system has been built. All optimizers' V_i, I_i and V_o as well as the system's I_o were measured with an Agilent 34970A data-logger; in total measuring 34 different values. The voltage was measured directly by the data-logger and the current was measured by incorporating a shunt resistance in series at the input of each power optimizer and measuring the voltage drop at the shunt resistance. The data-logger has a 0.004%dcV measuring accuracy and the shunt resistances are calibrated at less than 1%.

Figure 4.2: A picture of Magic Box, an experimental PV home used in various experiments of this PhD Thesis, and the measurement for testing the SolarEdge and Tigo power optimizers. At the set-up there are eleven PV module pairs (two Isofoton I-110 modules in series) available which can be all connected in series to a string inverter, or to the SolarEdge or Tigo optimizers.

4.2.1 MODULES AT NORMAL OPERATION

Normal operation is considered when there are no shadows over the PV generator. This, however, does not mean that optimizers will have the same I_i as there can be some mismatch of the modules' electrical parameters and also the MPPT algorithm is constantly moving around the MPP and might not be working at the same current at the same time. This can be seen in Figure 4.3, where all modules' currents are within ±2% of the average current, which is within normal current mismatch limits, as seen in section

3.4.2, and that the current varies rapidly, due to the MPPT. It can also be seen how there is a homogeneous current increase in all the modules; a total of 15% during the measurement, which corresponds to an increase in irradiance. It is also clear how the *M(d)* is not related with this current increase; because all the modules are increasing their current in the same proportion the *M(d)* does not have to change. It is true that there is a slight increase in the *M(d)* of all the modules, about 2%, but it corresponds to the slight decrease in V_m of the modules due to the increase in cell temperature, caused by the increasing irradiance and ambiance temperature. Because the inverter's voltage remains constant and the input voltage of each optimizer decreases, the *M(d)* must increase.

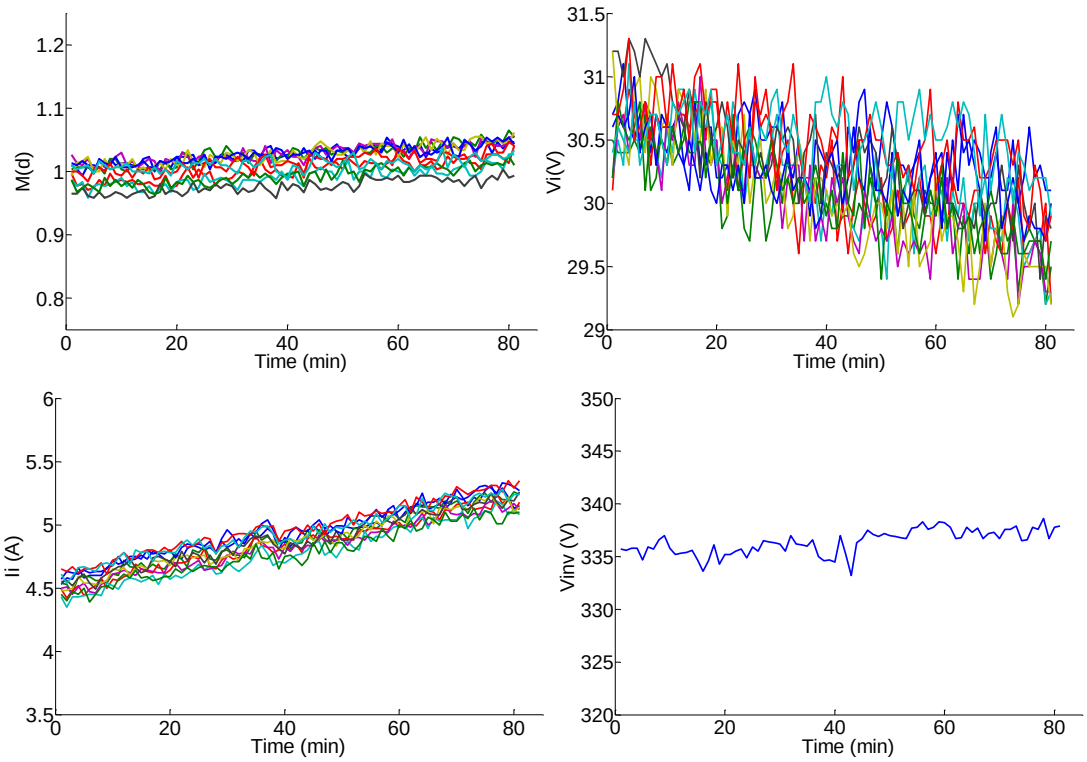

Figure 4.3: Working parameters of the SolarEdge system under unshaded conditions.

4.2.2 DECREASING IRRADIANCE OVER ONE MODULE (REACHING V_{O_MIN})

As the irradiance over a module decreases, its current decreases proportionally. As shown by the equations and examples presented in section 3.3 this causes the mismatched module to reduce its voltage and boost its current in order to try and match that of the non-mismatched modules. In turn, the non-mismatched modules reduce

their current to try and match that of the mismatched modules. The non-mismatched modules, because they are more, will reduce their current less than the mismatched module will boost its current or reduce its voltage.

Figure 4.4 shows the input current and output voltage of the ten optimizers in the system with respect to time and while one of the modules reduces its current progressively. It can be seen how there is a clear correlation between the output voltage and the input current of the shaded module. As the input current decreases the output voltage decreases proportionally until the minimum output voltage is reached, which in this case is 5V. Once the minimum output voltage is reached the optimizer of the shaded module is bypassed, being its output voltage of -0.7V. At this state, the module is at V_{oc} and the optimizer periodically conducts a search on the module's *I-V* curve, as can be seen by the spikes after minute 14, to see if there is enough current to turn it on again.

With respect to the non-shaded modules it can be seen how their output voltage increases as the shaded module's current decreases. It can also be seen how the increase in V_o of each non-shaded module is not as large as the decrease in voltage of the shaded module and how the voltage of all the non-shaded modules increases by the same amount. It can also be seen how when the shaded module is by-passed there is a sudden voltage drop in this module and also a sudden voltage rise in the non-shaded modules. All of this is in agreement with what was exposed in the theory of section 3.3.

Another interesting example, similar to the one exposed, is when the reduction in current is due to a shadow over one sub-module. This means that in the *I-V* curve of the module there are still points were I_w could be the same as that of the non-affected modules[18]. If the MPPT does not find these points and V_{o_min} is reached, it could occur that the optimizer disconnects itself, although it is not necessary. However, the tests exposed in section 4.5.2.3.b show that for SolarEdge this is not the case and once V_{o_min} is reached the MPPT searches the whole *I-V* curve in order to find other working points with higher currents.

[18] Points were the by-pass diode of the shaded cells is in forward bias

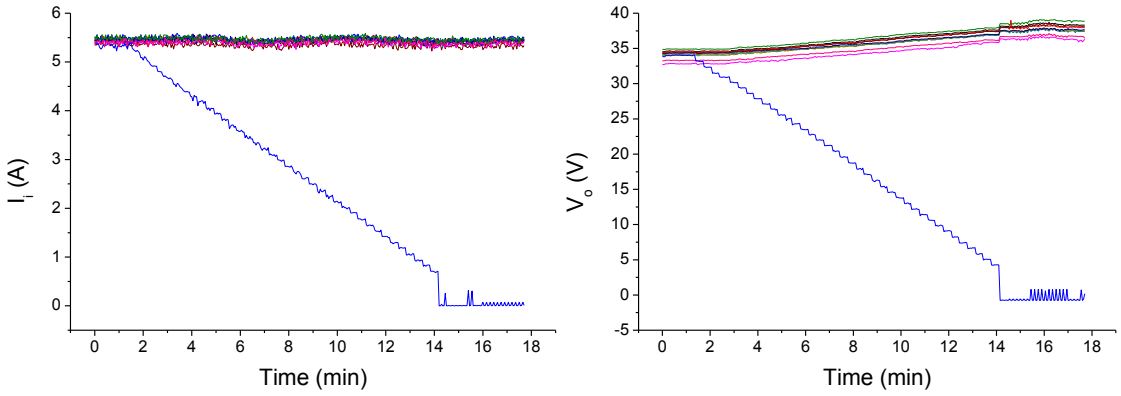

Figure 4.4: Input current (left) and output voltage (right) of each power optimizer with respect to time, while one module has its input current diminished progressively, simulated with the SAS E4360. It can be seen how the decrease in V_o is directly proportional to the decrease in I_i.

4.2.3 INCREASING IRRADIANCE OVER ONE MODULE (REACHING V_{O_MAX})

Although this situation can, at first glance, seem uncommon, there could be the case were one or more modules are facing east and one or more modules are facing west. In this case, as the sun's relative position changes along the day, the irradiance that the western facing modules receive increases while the irradiance of the others decreases. Opposite to the example presented in the previous section, V_o of the optimizer with the module under test will now tend towards V_{o_max}.

This situation has been simulated with the SAS-E4360 from Agilent and described in section 4.1. What is meant from this experiment is to see what happens when an optimizer reaches its V_{o_max}. Figure 4.5 shows I_i and V_o of the ten optimizers in the system as well as the MPP of the module with increasing current. It can be clearly seen how the relation between I_i and V_o also holds in this case; as I_i increases V_o increases. Again, like in the previous example the non-affected modules also change their V_o. Even though in this example I_i does vary slightly due to a decreasing irradiance during the measurement period, during the first 2.5 minutes I_i is constant and V_o decreases.

But what is most interesting to see in this example is what occurs when V_{o_max} is reached. In the previous example, when V_{o_min} was reached, the optimizer disconnected itself by turning on its by-pass diode. However, in this example in order to stay within the optimizer's output limits, the MPPT of the optimizer limits the I_w of the module, as can be seen in Figure 4.5-left which shows the MPP of the module and I_i of the

optimizer which is equal to I_w of the module. The moment when this limitation starts is the same as when V_{o_max} (60V) is reached. A slight reduction in the I_w is also appreciated, which is because the other modules are also slightly reducing their I_w due to decreasing irradiance.

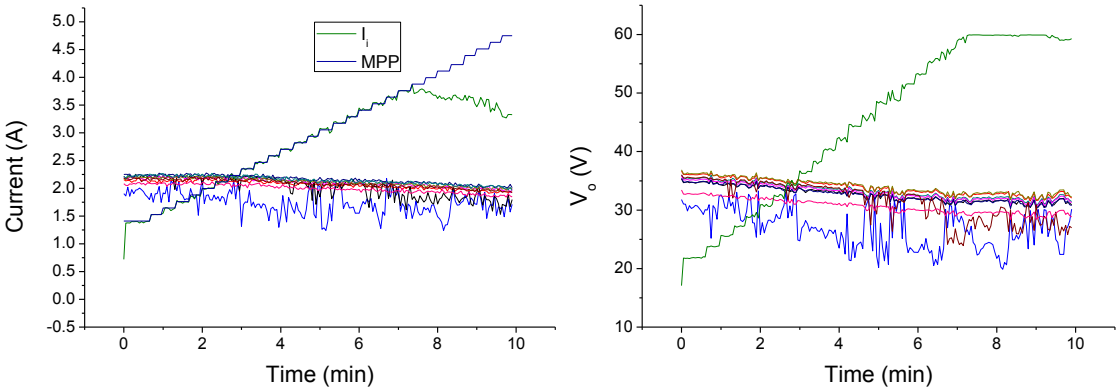

Figure 4.5: I_i and V_o of the optimizers in a ten module system in a situation where one the optimizer's V_o increases progressively until V_{o_max} is reached. The MPP of the module with increasing current is also shown and it can be seen how when V_{o_max} is reached the optimizer reduces the module's I_w so as to respect its output limits.

4.3 *I-V* AND *P-V* CURVES, AND EFFICIENCY OF POWER OPTIMIZERS

4.3.1 *I-V* AND *P-V* CURVES

To measure the *I-V* curve of a power optimizer a capacitive load developed at the IES-UPM has been used, which works as a variable resistance, using the same method as to measure a normal *I-V* curve. However, the problem is that the time it takes to sweep a normal *I-V* curve is very low (milliseconds) and it is not enough for the MPPT algorithm of the optimizer to find the MPP. Therefore a higher capacitor, 300mF, has been added and the curve has been swept very slowly; taking various seconds. Previous work [Orduz and Egido, 2006] estimated the time for the optimizer to find the MPP at around 1000ms and that a capacitance of 300mF is enough to correctly trace the *I-V* curve of an MPPT module. It is important to take samples spaced out more than 100ms to not get incorrect readings. The obtained *I-V* and *P-V* curves for a PV module with and without a power optimizer are shown in Figure 4.6.

The used optimizer is a prototype developed by Tecnalia for the Integra-FV Spanish national project. It uses a boost DC/DC converter topology with a maximum $M(d) = 2$. In the figure it can be observed how the obtained curve has a similar form to the theoretical curve of a boost optimizer presented in section 3.2. However, it is not exactly the same and it can be seen how the MPP of the PV module is higher than the maximum power obtained with the power optimizer. This is due to the efficiency of the optimizer, which is not ideal and in this case is 95% for an $M(d) = 1$ and 89.4% for $M(d) = 2$. There is quite a high efficiency drop with an increasing $M(d)$ and although other authors [Roman, 2006] have also found a decreasing efficiency with $M(d)$ it has not been so high as the one here presented. The reason for such a high drop can also be due to the MPPT algorithm moving slightly from the MPP during the measurement which is totally possible. In order to precisely measure the efficiency with respect to $M(d)$ these tests should be conducted in a more controlled manner, like those exposed in section 4.3.2.

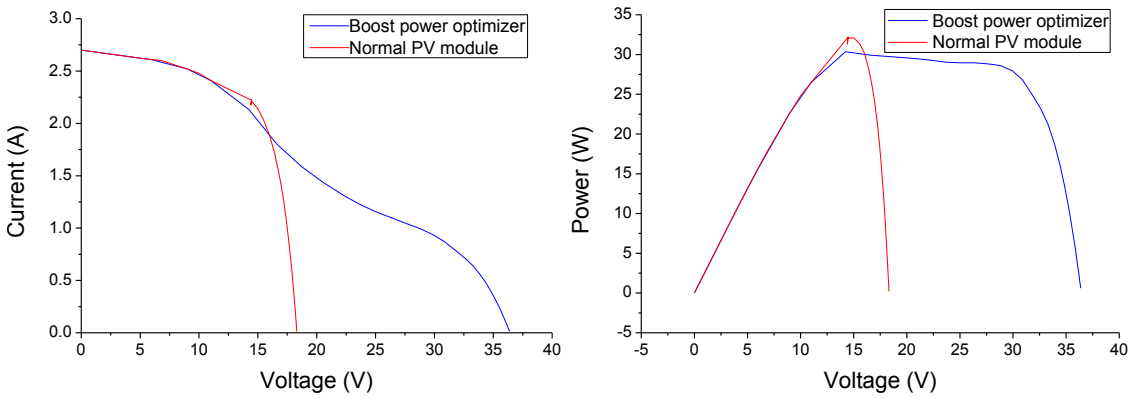

Figure 4.6: Measured *I-V* and *P-V* curves of a boost power optimizer.

4.3.2 EFFICIENCY MEASUREMENTS

4.3.2.1 Efficiency of a prototype optimizer at different voltages

Measuring the conversion efficiency of a power conditioning device is as easy as measuring the input power and the output power. For equipment like inverters, this can be done throughout the day as the power will change with the irradiance and a large range of powers will be obtained. However, this method is very time consuming and has the drawback of a changing input voltage and working temperature, which affects the

efficiency. A faster approach is to connect a variable DC source at the input and vary the input power throughout the power range of the inverter. It is important to only vary the current, as the efficiency is voltage dependent. An efficiency curve should be taken for a constant voltage, which is another reason for not measuring the inverter's efficiency while the PV system is working, as the input voltage will vary along the day.

For the case of power optimizers it is also important to keep the conversion ratio constant, as previous studies [Roman, 2006] have already shown that the efficiency of a power optimizer depends on the input voltage and the conversion ratio, *M(d)*. Because the optimizer is not connected to the grid, a load must be connected to its output to drain the power. The load, which should be a variable resistor, as a function of the input voltage and conversion ratio can be obtained from solving equation (4.1) and knowing that $M(d) = V_o/V_i$, arriving at equation (4.2).

$$P_o \equiv {V_o^2}/{Z} = V_i \cdot I_i \equiv P_i \tag{4.1}$$

$$Z = M(D)^2 \cdot \frac{V_i}{I_i} \tag{4.2}$$

Where *Z* is the load connected at the optimizer's output port.

For the prototype converter, measurements have been performed for three different input voltages: 15V, 25V y 35V, with an $M(d) = 1.2$. During each measurement V_i and *M(d)* are kept constant while varying I_i in order to vary the input power. At the same time, *Z*, should be varied according to equation (4.2) so *M(d)* and V_i are kept constant. At the same time, the input and output power are measured and the efficiency is directly obtained by their division.

Figure 4.7 shows a maximum efficiency of 95.9% between 140 y 160W. The European efficiency calculated with equation (4.3) is 93.2%.

$$\eta_{CE} = 0{,}2 \cdot \eta_{10\%} + 0{,}6 \cdot \eta_{50\%} + 0{,}2 \cdot \eta_{100\%} \tag{4.3}$$

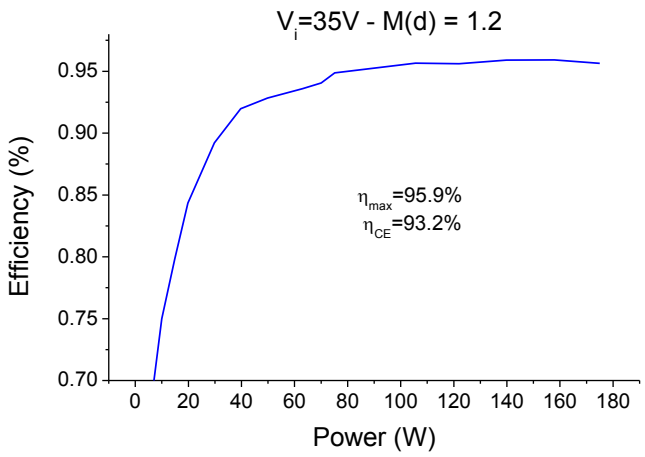

Figure 4.7: Prototype converter's efficiency at 35V and $M(D) = 1.2$

Figure 4.8 shows a maximum efficiency of 95.6% at 120 W and is above 95% between 100W and 130W. The european efficiency is of 93.1%.

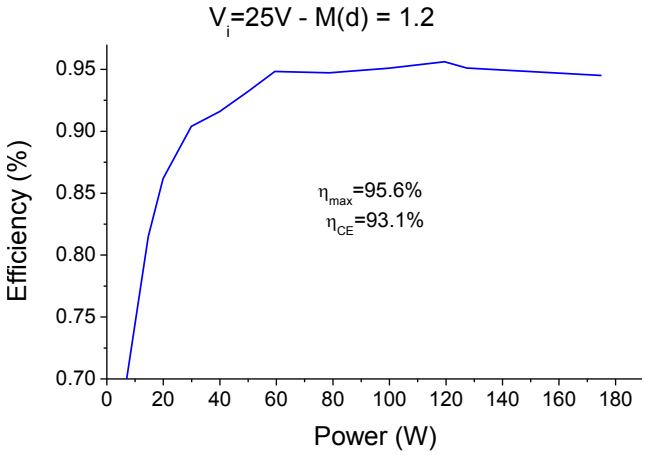

Figure 4.8: Prototype converter's efficiency at 25V and $M(D) = 1.2$

Figure 4.9 shows a maximum efficiency of 93.5% at 140 W and a European efficiency of 91.6%.

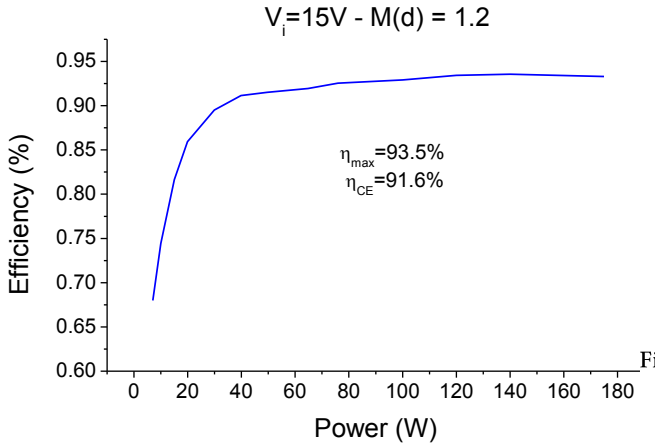

Figure 4.9: Prototype converter's efficiency at 15V and $M(D) = 1.2$

For the measurements at 15V, the highest value that was measured is at 75W due to the DC source which limits the input current to 5.1A. The rest of the values are interpolated following the same shape as the curves for 25V and 35V.

From the measurements it can be clearly seen how the efficiency drops as the voltage drops. In part, this is because for working at lower voltages higher currents must be used for the same power, increasing the resistive losses in the converter.

4.3.2.2 Efficiency of the SolarEdge optimizer

Because the SolarEdge optimizer has a security function which sets its output voltage at 1V if it is not connected to the SolarEdge inverter, it is not possible to apply the method presented in the previous section for measuring the conversion efficiency. For measuring the efficiency of the SolarEdge optimizer the only possibility is to do it under normal operation. The setup used for the measurements is the same as that of Figure 4.13, where V_i, I_i, V_o and I_o are measured with an Agilent 34970A datalogger. This time, however, only the values of one optimizer are recorded. It is important to only record the values of one optimizer or to record all four values in adjacent channels. Otherwise, because there is a time lapse between each recorded channel, it could occur that, because the input values and output current are constantly changing, due to the MPPT searching for the MPP, the output values recorded do not coincide with the real input values, giving erroneous efficiency measurements. Even when measuring only four channels this occurs as can be seen from Figure 4.10-left. For this reason the values have been averaged for each power point, resulting in Figure 4.10-right.

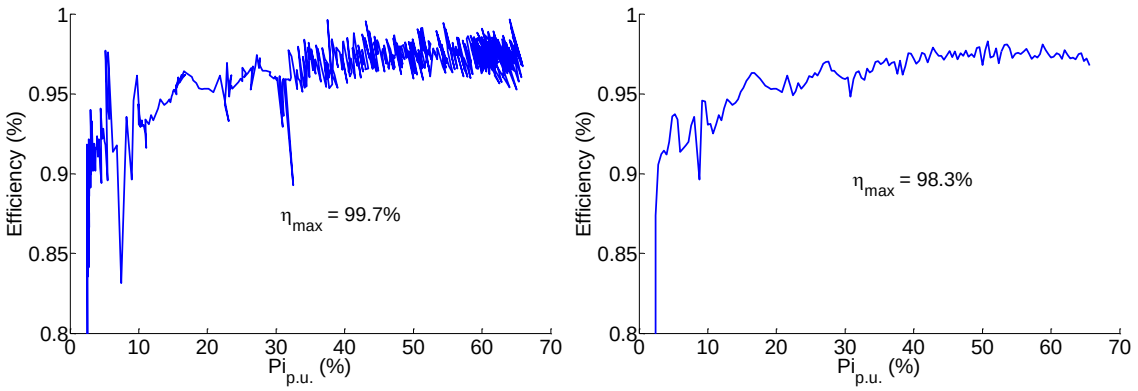

Figure 4.10: Efficiency measurements of the SolarEdge power optimizer.

The maximum efficiency obtained is of 98.3% which is very close to the one given by the manufacturer of 98.6%. It should be noted that the new power box by SolarEdge has a maximum efficiency of 99.5%. It is also worth noting that at 5% of nominal power, the power box already has an efficiency over 90% and at 10% of nominal power it is already at 93%. Because of the used modules, during the measurement the input power does not reach 100% of nominal power (250W), therefore it is estimated at 1% below maximum efficiency, that is 97.3%.

4.4 POWER GAINS UNDER SHADED CONDITIONS

In the literature, there exists various measurements of power gains with the use of DMPPT in real PV systems: we can find the following [Deline, Meydbray et al., 2012; Neuenstein and Podewils, 2009; 2011; Orduz, Solórzano et al., 2011a; Podewils and Levitin, 2011; Sanz, Vidaurrazaga et al., 2011; Solórzano, Egido et al., 2010]. Although the methods used for the experiments vary considerably, all of these references have concluded that depending on the shadows applied the power gain observed varies greatly. In the following paragraphs a brief review of the methods used and the results obtained are presented.

Probably, the laboratory that has conducted the most experiments of power gains with DMPPT is the Photon Lab, from the Photon International magazine and presented in [Neuenstein and Podewils, 2009; 2011; Podewils and Levitin, 2011]. They have mainly tested the SolarEdge, SolarMagic and Tigo optimizers, but also tested the Xandex Sunmizer and the EHW Smart power box and obtained real power gains in AC. Except for in [Neuenstein and Podewils, 2009], in which the SolarMagic optimizer was tested outdoors, the experiments conducted were indoors with a solar simulator. For all the experiments different conditions were reproduced (unshaded, horizontal shading, dormer windows and poles) on two generators: one with DMPPT and the other with central MPPT. Both generators were calibrated and the power difference eliminated. In the first experiments [Neuenstein and Podewils, 2009] the authors obtained the highest

power gains, up to 300%, for dormer windows[19]. They do, however, claim low measurement accuracy and in the following set of experiments, [Neuenstein and Podewils, 2011; Podewils and Levitin, 2011], the highest power gains were observed for horizontal shading (~32%) in a one string configuration and in poles (~14%) in a two string configuration. For the one string configuration, the gains observed with poles were also high (~18.5%). In these experiments, dormer windows did not return large power gains (~1.5%). For unshaded conditions, up to 3.2% power gain is obtained with the Tigo power box and 0.9% with SolarEdge. The authors do however claim an uncertainty of ±3% on the uniformity of light, which could be the cause for this power gain. In the outdoor experiments losses of ~5% were obtained for unshaded conditions. Apart from the uncertainty on the uniformity of light, another drawback from the indoor experiments performed is the lack of diffuse irradiance. Because the obstacles are placed so close to the modules, as can be seen in Figure 4.11, the shaded cells do not receive any diffuse radiation. From this we learn that if possible it is better to conduct the experiments under real sun.

Figure 4.11: Picture taken from [Podewils and Levitin, 2011] which shows the dormer window and horizontal shadows applied to measure power gains. Such close proximity of the obstacle to the modules eliminates any diffuse radiation from the shaded cells, altering the results and obtaining lower energy gains than what is really possible.

[19] This could possibly be a measurement error or problems with the inverter MPPT.

[Deline, Meydbray et al., 2012] and [Sanz, Vidaurrazaga et al., 2011] conducted outdoor measurements were two generators, one with DMPPT and one with central MPPT, were shaded and the power gain observed. Both of them also took into account the power difference between both strings, but not the possible module mismatch, although as we have seen in section 3.4.2 this is normally below 0.5%. [Deline, Meydbray et al., 2012] reproduces the shadows by using a black, 50% open vinyl/polyester fabric, with an average transmittance of 37% and the Enphase microinverters for the DMPPT system, taking all measurement in AC. Using a fabric with such a high transmittance can return artificially high power gains since the shaded modules will have quite a lot of irradiance in comparison with real shaded systems and this is a particularly beneficial D/G[20] ratio as shown in Figure 3.19. With this method they obtained power gains of up to 30% with heavy shading and 0.5% for non-shaded conditions; this second one being attributed to the 0.5% higher efficiency of the Enphase microinverter.

[Sanz, Vidaurrazaga et al., 2011] conducted power gain measurements with a power optimizer prototype and observing power gains up to 204%, which are strangely high. The paper is not very elaborated so it is hard to understand why such high power gains are obtained. They also point out that they observed higher power gains in days with passing clouds which is something interesting to look into.

The measurements by [Orduz, 2009] and the ones here presented differ from the rest in that they do not use two generators but the same exact generator and quickly (in less than a minute) change from central MPPT to DMPPT. Being this change so fast and done in clear days, the change in shading and irradiance can be considered negligible. The advantage is that any possible mismatch or power difference between generators is out of the equation but there is the disadvantage of not being able to test whole days or

[20] Appendix A shows an analysis of the annual D/G ratio for Madrid and Santander. The results show that only 10% of the irradiation occurs for D/G ration between 20% and 80% for Madrid on an optimally tilted surface, being most of over 70% for D/G ratios below 15%. For Santander, a cloudier location, 35% of the irradiation occurs between 20% and 80% D/G ratios.

many different conditions. If possible it would be better to use the method of two parallel generators. [Orduz, 2009] concluded that the highest power gains, over 10%, are obtained when there is shading over one or various sub-modules between 25% to 60%. This goes in the line with what was exposed in the theory of section 3.4.1 and is also validated in [Solórzano, Egido et al., 2010] and in the following experiments. It is also somewhat validated by the experiments of the Photon Lab with the high power gains obtained with pole shading.

In what follows a description of the experiments and the results obtained are presented.

4.4.1 DESCRIPTION OF THE SYSTEM UNDER TEST

The PV generator used for these experiments is located at the rooftop of the IES-UPM in Madrid. It is made up of a total of 13 modules: twelve Isofoton I-47 modules and one I-94. Because the I-94 model is the same as the I-47 but with two strings of cells in parallel, the twelve I-47 modules are connected in parallel in order to match the characteristics of the last module. In the end there are seven modules with the following characteristics:

- V_{oc}^{*}= 19,8V
- V_{m}^{*} = 16V
- I_{sc}^{*} = 6.54A
- I_{m}^{*} = 5,88A
- N_{C_s} = 33
- N_{C_p} = 2

Figure 4.12 shows a picture of the PV generator used for the power gain experiments, with the modules numbered from 1-7.

Figure 4.12: The generator used for the power gain experiments.

Prior to the experiments all modules' *I-V* curves were measured and extrapolated to STC, obtained the values presented in Table 4.1. With the obtained mismatch in I_m and what was exposed in section 3.4.2, no power gain in unshaded conditions is expected.

Table 4.1: Main values at STC of the measured *I-V* curves of the seven modules used for the power gain experiments.

Module	V_{OC}* (V)	I_{SC}* (A)	V_M* (V)	I_M* (A)	P_M* (W)	$\Delta(P_M/P_{M\_max})$ (%)	$\Delta(I_M/I_{M\_max})$ (%)
1	16.1	6,28	11,7	5,36	62,6	-5,58	-2,01
2	16,3	6,37	11,9	5,22	61,6	-7,09	-4,57
3	16,2	6,50	11,8	5,44	64,1	-3,32	-0,55
4	16,2	6,20	11,9	5,28	62,7	-5,43	-3,47
5	16,2	6,42	11,8	5,31	62,9	-5,13	-2,93
6	16,2	6,32	11,9	5,39	63,9	-3,62	-1,46
7	16,7	6,52	12,1	5,47	66,3	0	0

A prototype power optimizer developed by Tecnalia-Robotiker for the Spanish national I+D INTEGRA-FV project has been used. Each module was connected to one optimizer in the DMPPT system and an SMA SB-700 inverter at fixed voltage was used. For the central MPPT system the inverter was set to a fixed voltage. Because of the low efficiency of the prototype and in order to evaluate the possible gains with DMPPT, the production was measured at the optimizers' input. For the measurements, an Agilent 34970A datalogger was used which records V_i and I_i of all optimizers, I_o and V_{inv}.

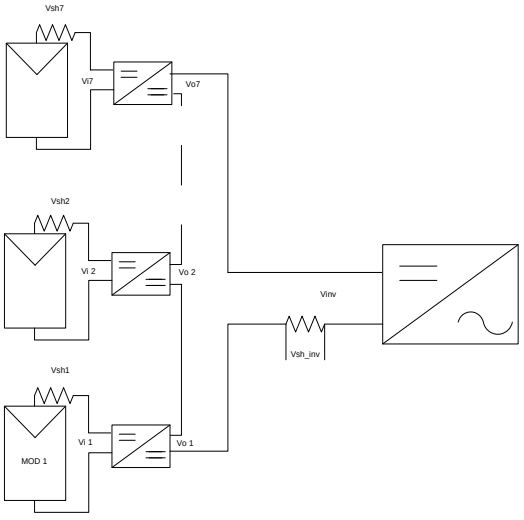

Figure 4.13: Schema of the system used for power gain measurements with the shunt resistances and showing all values that were measured.

4.4.2 PERFORMED EXPERIMENTS WITH APPLIED SHADOWS

The first experiments were conducted while shading only module seven. Figure 4.14 shows the four shadows applied. The three shadows from the pole correspond to the real shadow at different times of the day, simulating the progression of the shadow across the module.

Figure 4.15 shows the *I-V* curves of the generator for the four shadows shown in Figure 4.14. With the *I-V* curves and the working voltage of the system it is possible to see whether the inverter is working at the MPP or not, which, as can be seen in Table 4.2, does not always happen. The purpose of having the measured *I-V* curves is to see whether the working voltage of the CMPPT system corresponds with the MPP voltage on the *I-V* curve, although the power of the *I-V* curve might not correspond with the measured power, as these were taken at different times and different irradiance and temperature values.

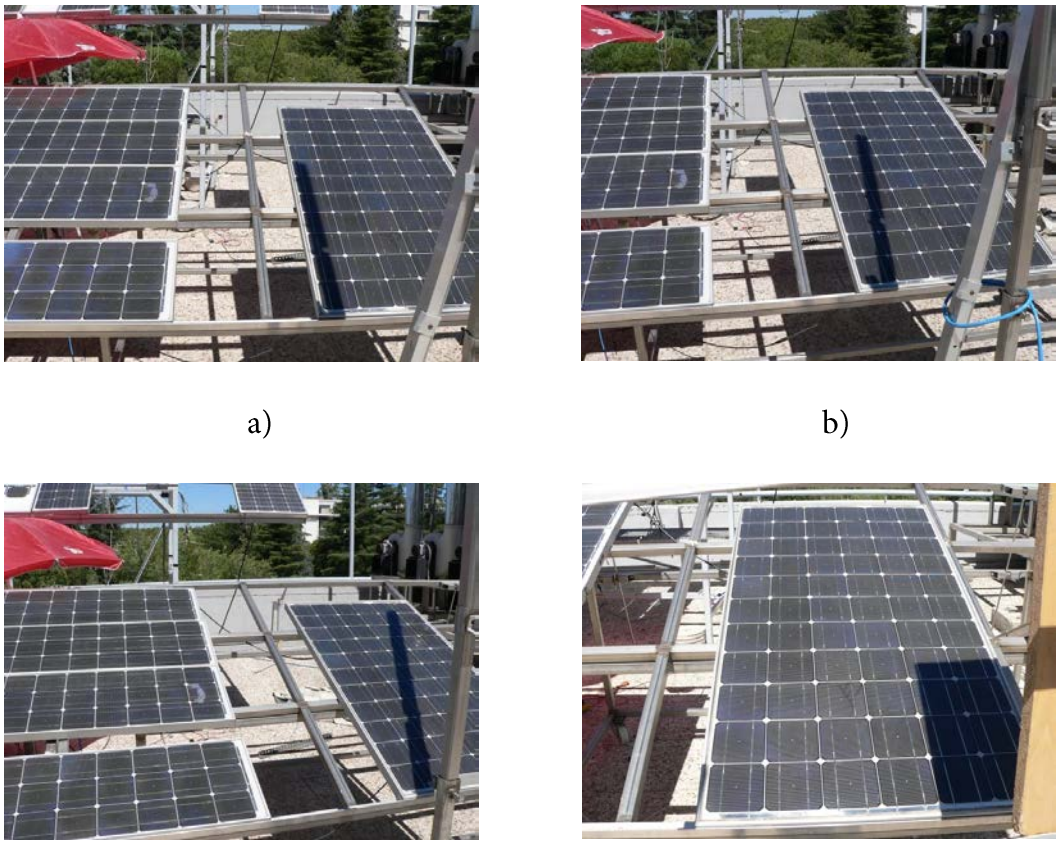

a) b)

c) d)

Figure 4.14: Shadows applied to one module of the seven module generator used for measuring power gains with DMPPT.

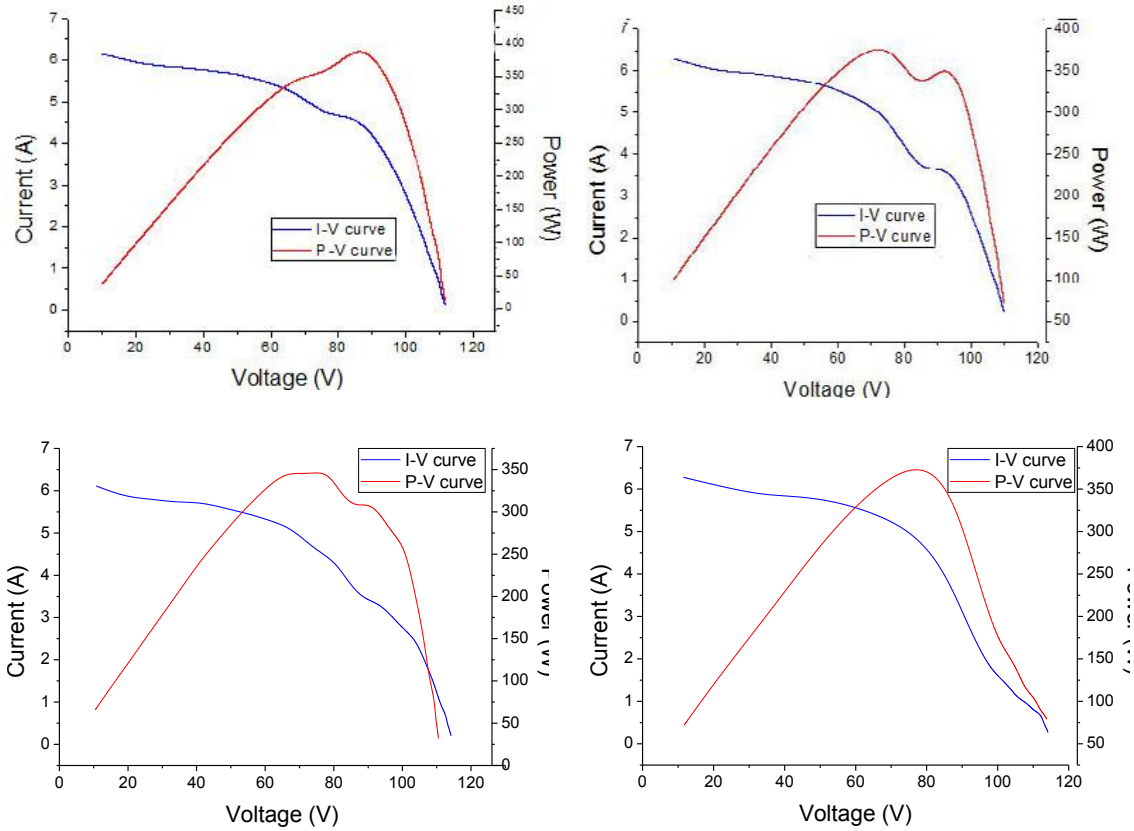

Figure 4.15: a)-d) *I-V* curves at G = 1000W/m² of the generator for the four shadow patterns presented in Figure 4.14.

From the results it is clear that the biggest improvement is obtained for the shadows cast by the pole. This agrees with the theory presented in section 3.4.1 which predicts that the most improvement is obtained for shadows which cover less than entire cells. It can be seen that the highest improvement is obtained from shadow b), gaining over 20% with DMPPT. However, this high power gain is in large part due to the fact that the inverter in the MPPT system is not finding the absolute MPP and is working at a local MPP. This by itself is already a loss of approximately 11% (380W/345W @ STC), and if the absolute MPP was found the gain (P_{gain_real}) would be similar to that of shadow a), as is logical since the same number of sub-modules are shaded and with the most shaded cell being shaded by the same percentage. If this was the case then the shadow of Figure 4.14c), which covers cells from all sub-modules, would be the one that returns the highest power gains with the use of DMPPT.

Table 4.2: Power gains and working values obtained with DMPPT in presence of the shadows presented in Figure 4.14.

Shadow	G (W/m²)	Working voltage (V)	P_o^* (W)	η(%)	P_{gain_real} (%)	P_{gain_ideal} (%)
a) CMPPT	1027	89,4	437		-2,52	8,43
a) DMPPT	1032		426	89,9		
b) CMPPT	1034	95,3	380		8,68	20,9
b) DMPPT	1032		413	89,9		
c) CMPPT	1037	77,9	404		0,99	12,3
c) DMPPT	1040		408	89,9		
d) CMPPT	1032	78,6	413			
d) DMPPT	1031		383	90,2	-7,26	2,81

Where P_{gain_real} and P_{gain_ideal} are defined in equations (4.4) and (4.5).

$$P_{gain\_real} = \frac{P_{DMPPT}}{P_{CMPPT}} - 1 \tag{4.4}$$

$$P_{gain\_ideal} = \frac{P_{DMPPT}}{\eta \cdot P_{CMPPT}} - 1 \tag{4.5}$$

4.4.3 Conclusions on power gains

The performed experiments have shown that higher power improvements are obtained as a larger number of sub-modules are shaded. They have also shown that larger improvements can be obtained from shadows that do not cover entire cells, because in this case, with DMPPT the shaded module can provide more power than if entire cells are shaded. We could therefore think that DMPPT has more potential in presence of shadows from thin objects like poles or antennas. However, these objects will probably cause shade over less sub-modules so this assertion is not entirely clear. More on this will be seen in chapter 5.

Another important point that is found from these experiments is the importance of the MPPT efficiency in the final power yield and power gains. It has been seen that in the case where the MPPT of the central inverter does not find the absolute MPP, important power gains are obtained. Also if the MPP is out of the inverter's MPPT range, larger power gains are obtained. The following section presents the experiments performed on the MPPT efficiency of various inverters, micro-inverters and power

optimizers, especially focused in situations where local maxima exist and in the capability of the MPPT algorithm in finding the absolute MPP.

4.5 MPPT EFFICIENCY

The MPPT efficiency represents the amount of energy extracted from a PV module or generator in relation to the maximum possible energy, that at the MPP. It is given as a percentage and is usually calculated for a prolonged period of time where the *I*-V curve of the system is changing. At the time of writing this Thesis only the European Standard EN 50530:2010 of title: *Overall efficiency of grid connected photovoltaic inverters* [CENELEC, 2010] contains a test protocol for testing the MPPT efficiency of inverters, which is described in section 2.1.4.1.

This Standard, however, presents some drawbacks. The first and main drawback is that neither of the two methods for testing MPPT efficiency (static and dynamic) considers local maxima appearing in the *I-V* curve; situation which is common when irregular irradiance, due to shadows, clouds or localized dirt, is present in the PV array. Secondly, the Standard is only thought for PV inverters, not considering MPPT charge regulators, power optimizers or micro-inverters. Although this is a minor point when testing static and dynamic MPPT efficiency, it can be important when testing MPPT efficiency in presence of local maxima.

During this section, the static and dynamic efficiency of micro-inverters and power optimizers are tested, an addition to the CENELEC standard is proposed for measuring MPPT efficiency in *I*-V curves with local maxima and the same equipment, as well as central inverters, is measured considering this new standard. Although this PhD thesis is mainly focused on PV systems with DMPPT, the results of measuring central inverters' MPPT efficiency in presence of local maxima are presented as the results are important for modelling energy gains with DMPPT, the focus of section 5.

4.5.1 MPPT STATIC AND DYNAMIC EFFICIENCY OF MLPE

These tests were performed with the irradiance sequence proposed in [Ropp, Cale et al., 2011], which can be seen in Figure 2.16. The main reason for using this sequence instead of the one proposed by the CENELEC standard [CENELEC, 2010] is that the lowest irradiance used is of 200W/m^2 while in the CENELEC standard it is of 100/m^2. In the case of the SolarEdge optimizers at 100W/m^2 the optimizer under test reaches V_{o_min} causing it to disconnect from the system and, therefore, to not follow the MPP. Although this should be considered as an inefficiency of the system, it should not be considered for the dynamic efficiency of the MPPT algorithm. Especially since when there are fast irradiance changes these will affect a large part of the generator, causing a current drop in many modules, being it less likely that they reach V_{o_min}; as is shown in section 3.3.2. Another reason for using this sequence is the short duration, 10 minutes, in comparison with the duration of the CENELEC procedure, 6.5 hours.

The response of the MPPT algorithm of the three main brands of MLPE (SolarEdge, Enphase and Tigo) to the measurement protocol proposed in [Ropp, Cale et al., 2011] is shown in Figure 4.16. It can be seen how both the SolarEdge optimizer and Enphase microinverter follow the pattern almost perfectly with a total efficiency of 98.3% and 99.1% respectively. However, the Tigo optimizer does not follow the irradiance changes fast enough, remaining at a lower current point. The speculative reason for this occurring is that the Tigo MPPT is controlled by a central unit, the MMU, which decides the I_M of each panel with a "complex algorithm" as stated by Tigo, instead of using a P&O or variant method. Tigo also claims that their algorithm must undergo a learning process. From the measurements here presented and also those presented in section 4.5.2 it seems that this MPPT method presented by Tigo is still not fully functional.

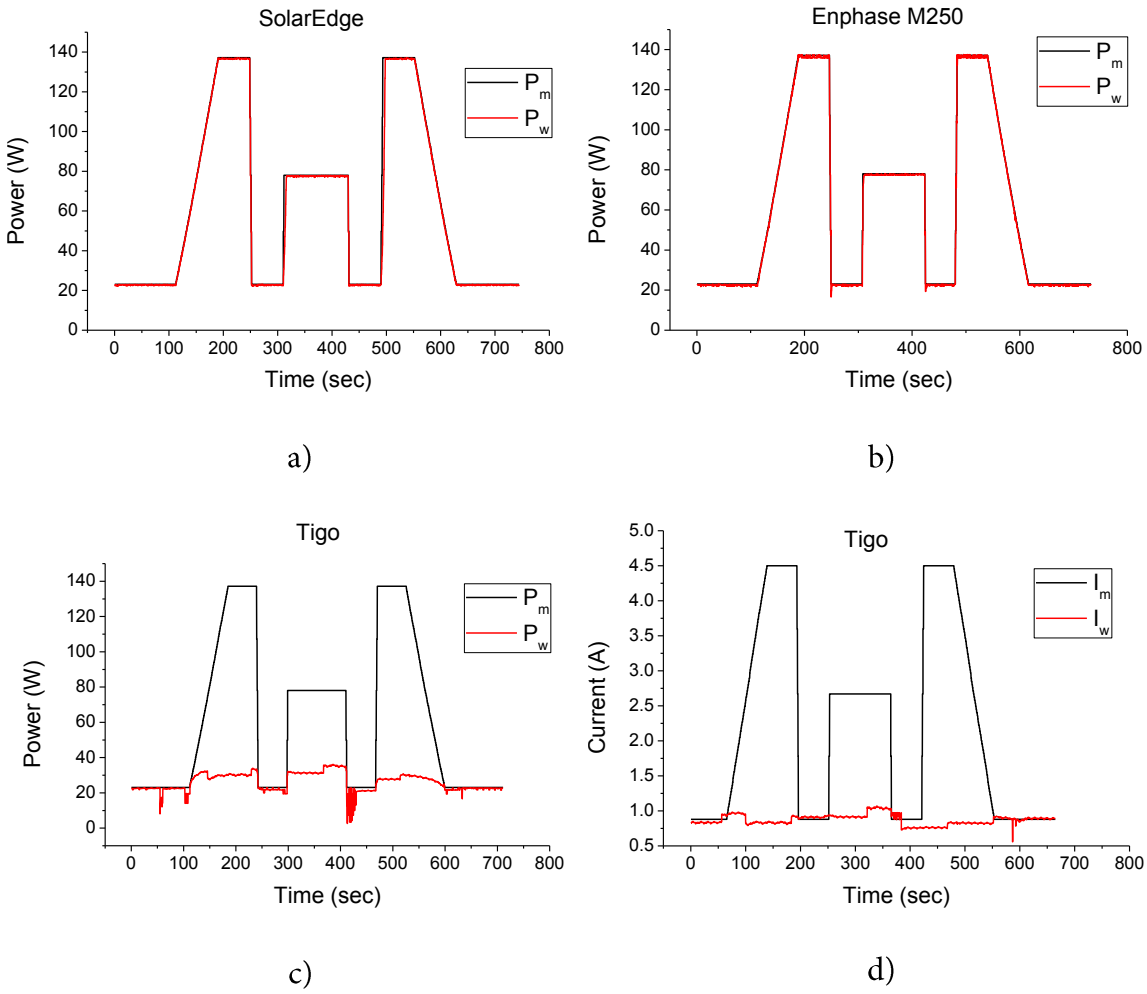

Figure 4.16: Response of the SolarEdge (a), Enphase (b) and Tigo MPPT (c) algorithms to the test protocol proposed in [Ropp, Cale et al., 2011] and the working current with respect to I_M of the Tigo optimizer (d).

4.5.2 MPPT EFFICIENCY IN PRESENCE OF LOCAL MAXIMA

It is well known that standard P&O MPPT algorithms are not capable of finding local maxima and although there are many published algorithms that claim that they can find the absolute MPP in presence of local maxima [Alonso, Ibaez et al., 2009; Patel and Agarwal, 2008; Taheri, Salam et al., 2010; Young-Hyok, Doo-Yong et al., 2011] not all modern PV inverters include them, as is shown in this section. This negative effect can be responsible for a large, and easily prevented, energy loss. A year round estimation of these losses for different shadow profiles is presented in section 5.

The following sections present a profound study and experimental results of local maxima in PV arrays and the effects on the MPPT algorithm of inverters and MLPE. A summary of the main findings is presented hereafter:

- There are still modern PV inverters which fail in finding the global MPP in presence of local maxima. Some PV inverters incorporate an algorithm that periodically searches the *I-V* curve for the global MPP. However, this option is deactivated by default and must be enabled by the user.

- All of the MPPT algorithms of MLPE that have been tested have failed in finding the global MPP in presence of local maxima. This is worrying since this technology has been purposely developed for mitigating the losses in situations of partial shadows and not finding the global MPP reduces this effect.

- It has been shown that as the number of serially connected modules increases the apparition of distinct local maxima in the *I-V* curve in shading situations is less common. This means that MPPT algorithms of MLPE are more prone to working inefficiently in presence of local maxima. Again emphasizing the importance of these algorithms in finding the absolute MPP.

- Incoming shadows into PV arrays tend to cast a different amount of shade in various cells of the generator. This causes a smoother deformation of the *I-V* curve, not causing distinct local maxima in the initial periods of the shadow. This allows an MPPT algorithm that is normally not capable of finding the absolute MPP to gradually shift towards a lower working voltage. When the shadow has deeply covered the generator, distinct local maxima appear but the working point is already at a lower voltage and working at the global MPP. So, in this case, inefficient MPPT algorithms tend to always work at the absolute MPP. This has also been shown experimentally.

- This effect is amplified if the modules are composed of cells with a low V_b.

- On the other hand, if the inverter starts when the generator is shaded, the start-up *I-V* curve has very distinct local maxima and it is very probable that the MPPT algorithm starts working at the local MPP. An inefficient MPPT

algorithm this situation will be prolonged until the shadow is almost fully out of the PV generator causing large energy losses. Again this is also shown experimentally.

- Although there is a standard that defines the testing of the MPPT efficiency of inverters [CENELEC, 2010], it does not consider the presence of local maxima in the tests. For this reason a test protocol has been proposed that should be incorporated into the standard so that installers can be aware of the behaviour of the inverter they are to install.

4.5.2.1 Theoretical analysis of local maxima in PV arrays

Local maxima appear in *I-V* curves when irregular irradiance is present over the PV generator. Causes of this could be due to shadows of nearby objects, clouds or irregular or localized dirt patches. Occasionally, local maxima can also appear due to defects in certain cells inside a module or due to severe hot-spots. In order to perform a series of measurements the most realistic possible, it is important to first understand the effect of each of these "defects" over the PV generator's *I-V* curve.

Although section 2.1.3 already presents the effects of shadows and irregular irradiance over *I-V* curves, what is presented hereafter is more specific of the effects that these changes over the *I-V* curve have on MPPT testing in presence of local maxima. We can identify four points that are of special importance to consider when simulating the *I-V* curves to be used in these tests:

a) The reverse characteristics of the shaded cells

b) The number of cells and sub-modules shaded simultaneously

c) The number of modules connected in series and in parallel

d) The nature of the passing shadow

All of these points are important in determining whether or not the MPPT algorithm will find the absolute MPP or not and many situations can occur where the absolute MPP is found even when the MPPT algorithm is normally not capable of finding it. In

the following paragraphs each of these effects is analysed accompanied by figures. If nothing is said the *I-V* and *P-V* curves are presented at an irradiance 1000W/m^2.

Depending on the reverse characteristics of the shaded cells, it can occur that, for the same shadow, local maxima are present or not. Figure 4.17 shows two *I-V* and *P*-V curves of the module[21] each with a cell shaded 90%[22] but with the shaded cell having different breakdown voltages in each case (V_b = -5V and V_b = -25V for the left and right curve respectively). It is clear that the left curve presents no local maxima, as the power is always increasing from V_{OC} until V_M, while the right curve does have a local maximum point. This occurs because the negative operating voltage of the cell in the left case is not negative enough to forward bias the by-pass diode.

In the left case the MPPT would have no problem in operating at the MPP, while in the right case it is probable that the operating point of the curve is the local maximum at only 19.9% of maximum power (46.5W vs 156.7W).

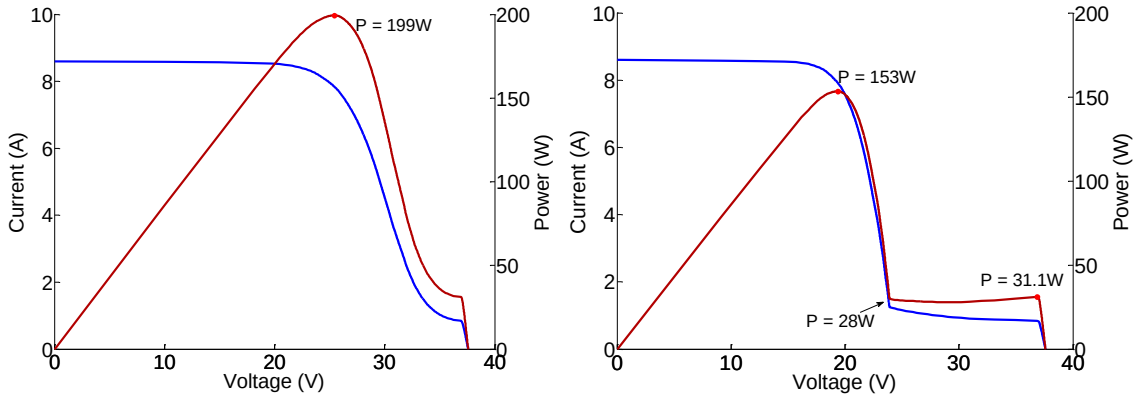

Figure 4.17: *I-V* and *P-V* curves of a PV module with 90% shade over one cell of one by-pass diode for Vb = -5V (left) and Vb = -25V (right).

This effect of not having local maxima for cells with low breakdown voltages does not occur when many cells under the same by-pass diode are shaded. For example, Figure 4.18 shows the same example as that of Figure 4.17 but now the twenty cells under the same by-pass diode are shaded. As can be seen, the shape of the curve and the position

[21] PV module with 60 cells in series and three by-pass diodes

[22] 90% shade or 10% radiation is a typical in a clear day at midday for a PV module shaded by a nearby object; that is, only receiving diffuse radiation.

of the two maxima are almost exactly[23] the same in both cases; for V_b=-5V and V_b=-25V. This was already shown in section 2.1.3 and it reaffirms the fact that as the number of shaded cells increases the reverse characteristics of the shaded cells play a less important role.

In this case, if absolute maxima are not found by the MPPT algorithm, both operating points will be at the local maximum, at only 18.2% of maximum power.

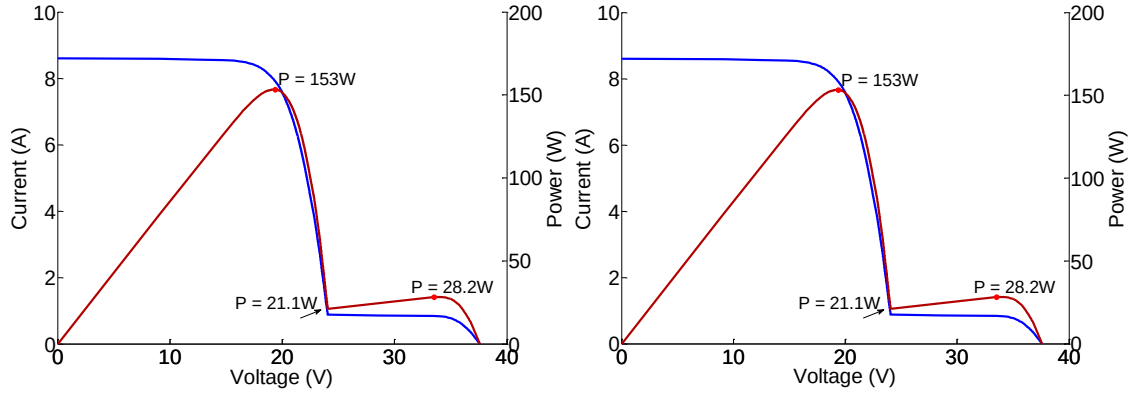

Figure 4.18: ***I-V*** **and** ***P-V*** **curves of a PV module with 90% shade over the 20 cells of one by-pass diode for Vb = -5V (left) and Vb = -25V (right).**

Again, this situation changes as the number of modules connected in series increases. During the following examples, unless specified, all twenty cells of each sub-module are shaded. For example, Figure 4.19 shows the *I-V* and *P-V* curves of a PV generator with ten modules of the previous examples in series having the twenty cells of one by-pass diode shaded at 90% and the zoomed in region where a local maximum could appear. It can be seen that even though the shaded module has a distinct local maximum, when it is connected in series with ten other modules this local maximum disappears.

[23] There is a tiny difference due to the difference in reverse characteristics of the shaded cells.

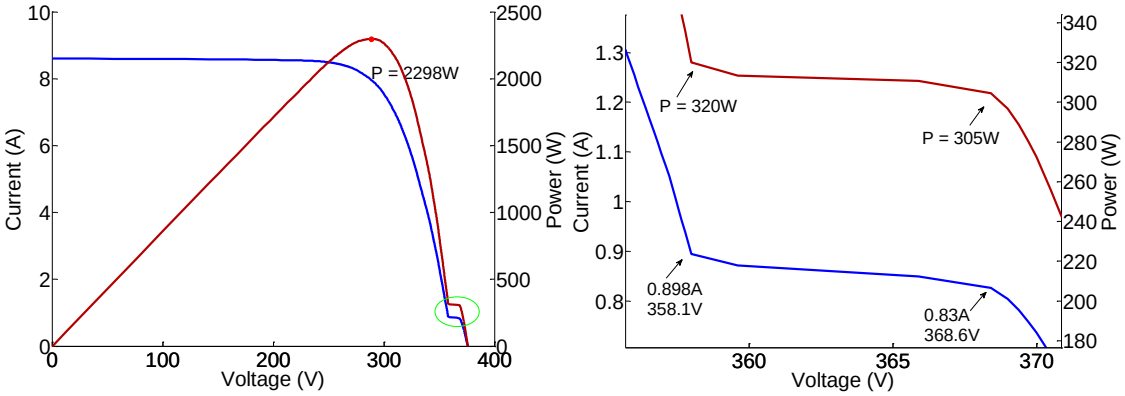

Figure 4.19: *I-V* and *P-V* curves of a PV generator with 10 modules in series with 90% shade over the 20 cells of one by-pass diode (left) and the zoom of the region enclosed by the circle (right).

The explanation of this effect has to do with the percentage difference of voltage and current between the possible local maximum (where the right-most arrows points at) and the point at which the diode starts to conduct (where the left-most arrows points at) or what has chosen to be called the "transition region". In this case the relative voltage loss (2.85%) is lower than the relative current gain (8.2%) being there a power gain as the working point moves left. In this case, there is no distinct local MPP and a P&O MPPT algorithm would pass through this region towards the absolute MPP.

By zooming-in into the transition region (Figure 4.20) of the case with only one module (Figure 4.18), we can see that the shape of the *I-V* curve in this region is very similar and that the current values at the possible local maximum and the point at which the diode starts to conduct are the same as the case for the ten module generator. However, now the relative voltage loss is higher (29.4%) and there is a power loss as the working point moves left. In this case a P&O MPPT algorithm will stay at the local MPP.

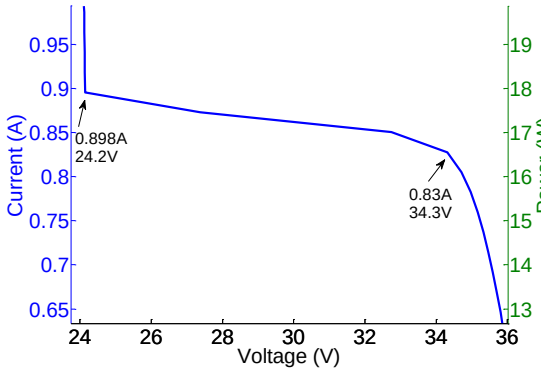

Figure 4.20: Zoom into the transition region of the *I-V* curve of one module (Figure 4.18). The shape of this curve is very similar to that of the transition region of the ten module system in Figure 4.19. The current values are practically identical and only the voltage values change.

Following this logic, we could think that if more sub-modules were shaded at the same time then a higher voltage drop would occur in the transition region, thus creating a local maximum. For example, Figure 4.21 shows the same example as Figure 4.19 but now shading all cells from six sub-modules. Now, a local maximum appears.

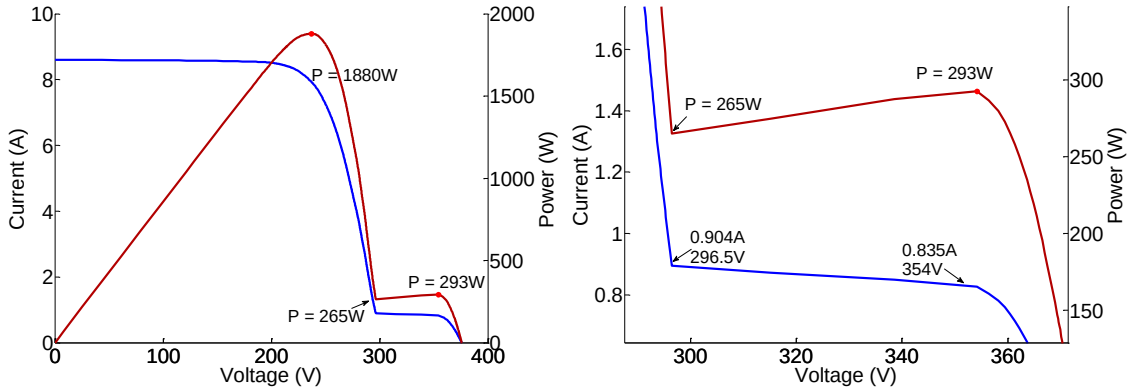

Figure 4.21: *I-V* and *P-V* curves of a 10 module PV generator with all cells from two modules (six sub-modules) shaded at 90% and a zoom of the transition region. In this case it can be seen how a distinct local maximum appears.

Following a similar logic, for lower shading percentages (higher currents) the relative current gain is lower and if it is lower than the relative voltage loss, then a local maximum appears. In addition, the voltages of the transition region are lower (higher relative voltage loss), since it is further away from V_{OC}, amplifying the possibility for a local maximum to appear. Figure 4.22 shows the same example as in Figure 4.19 but with only 40% shade. Although the absolute voltage loss and current gain is exactly the same as in the previous example (10V and 0.067A), relatively, this difference changes (2.94% voltage loss and 1.28% current gain), causing a local maximum.

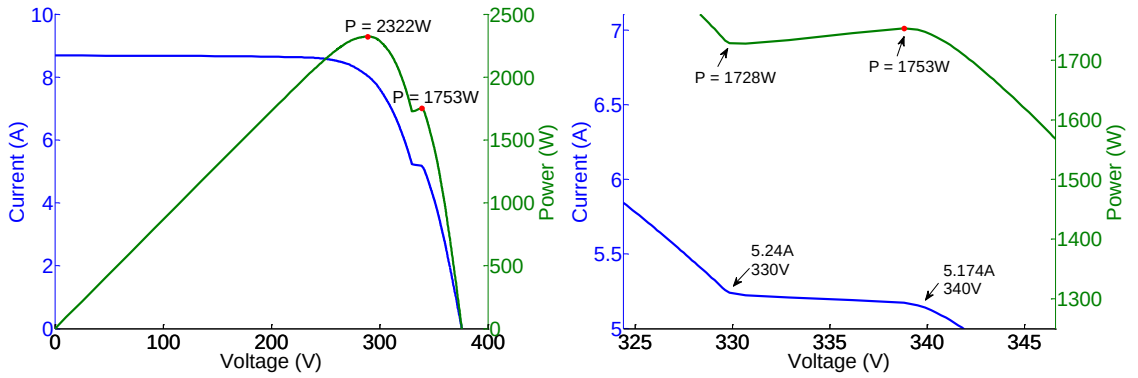

Figure 4.22: *I-V* and *P-V* curves of a 10 module PV generator with all cells from one sub-module shaded at 40% and a zoom of the transition region. In this case it can be seen how a distinct local maximum appears which differs from the example in Figure 4.19 in which the same cells were shaded at 90% and no local maximum appeared.

This effect is however lost if less cells from the same sub-module are shaded. Figure 4.23 shows the *I-V* and *P-V* curves of the same ten module generator of Figure 4.22 but now only one cell is shaded at 40%, both for a cell with V_b = -5V (left) and for a cell with V_b = -25V (right). It can be seen how this amount of shade has basically no effect over the generator's curve if the breakdown voltage is low, while having slightly more effect if it is high.

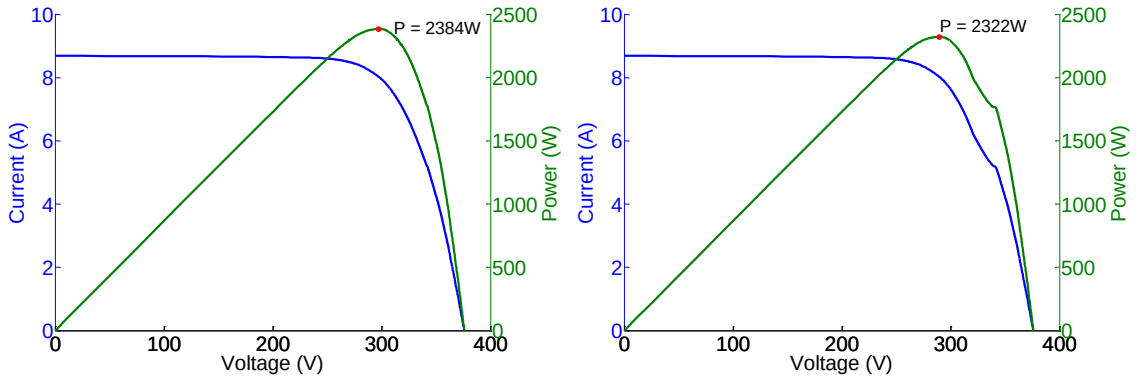

Figure 4.23: ***I-V*** **and** ***P-V*** **curves of a 10 module PV generator with only one cell from one sub-module shaded at 40% for a V_b=-5V (left) and a V_b=-25V (right). In this case, due to having less cells shaded, no local maxima appear. In the case for the cell with V_b=-5V (left), no changes are appreciated in the** ***I-V*** **curve.**

If the number of shaded cells is increased to ten, local maxima now appear, as is shown in the zoomed in *P-V* curves of Figure 4.24. However, there is a substantial difference between both curves; corresponding to shaded cells with V_b = -5V and V_b = -25V for the left and right curves respectively. The right curve is very similar to that of Figure 4.22 with the same voltage difference (10V) in the transition region and very similar power values (remember that the shaded cells of Figure 4.22 are of V_b = -5V). The left curve, however, has only a 3V voltage difference in the transition with a very small power difference. Although the power difference is not very important, the small voltage difference will pose no problem for the MPPT algorithm since its searching range is usually over this value (seen in section 4.5.2.3).

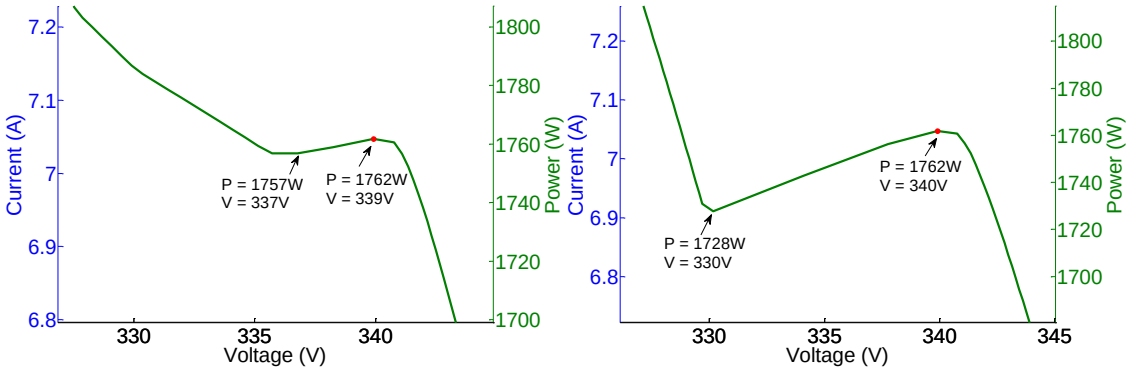

Figure 4.24: Zoom of the transition region of the *I-V* and *P-V* curves of a 10 module PV generator with ten cells from one sub-module shaded at 40% for a V_b=-5V (left) and a V_b=-25V (right). In this case, local maxima appear in both cases. However, in the case for the cell with V_b=-5V (left), the voltage difference between the local maximum and the transition point is of only 2V, lower than the voltage step of an MPPT algorithm, meaning that at some point the MPPT algorithm will pass the transition region towards the absolute MPP.

It would then seem logical that for lower irradiances (during the morning and afternoon when shading is more probable), because the current is lower, it is less possible for local maxima to appear. However, this is not the case as can be seen in Figure 4.25, where the same example as of Figure 4.22 (10 module generator with all cells from one sub-module under shade) is presented but with an irradiance of only 160W/m^2 instead of 1000W/m^2. With this irradiance, the current of the local maximum at 40% shade is the same as the current of the local maximum at 90% shade and 1000W/m^2 (the case of Figure 4.19). In this case, as opposed to the case of Figure 4.19 a local maximum does appear. The reason is that the current increase in the transition region is affected by the irradiance change. If in Figure 4.19 the current increase in the transition region is 68mA in Figure 4.25 it is of 11mA, being it reduced by a factor of 6.25 just like the irradiance. This shows that the reasons that cause local maxima to appear are independent from the irradiance level.

In the case of PV generators with parallel strings, although the power loss at the MPP due to the shadow is greater, the probability of local maxima appearing is less. If, for example, we change the example of Figure 4.22 to a generator with two parallel strings, that is, five modules in series in each string, and keeping the same shading (all cells from one sub-module shaded 40%) we obtain the curves shown in Figure 4.26. It can be seen how now there is only one MPP and that the power of this MPP is lower than the power of the absolute MPP of Figure 4.22.

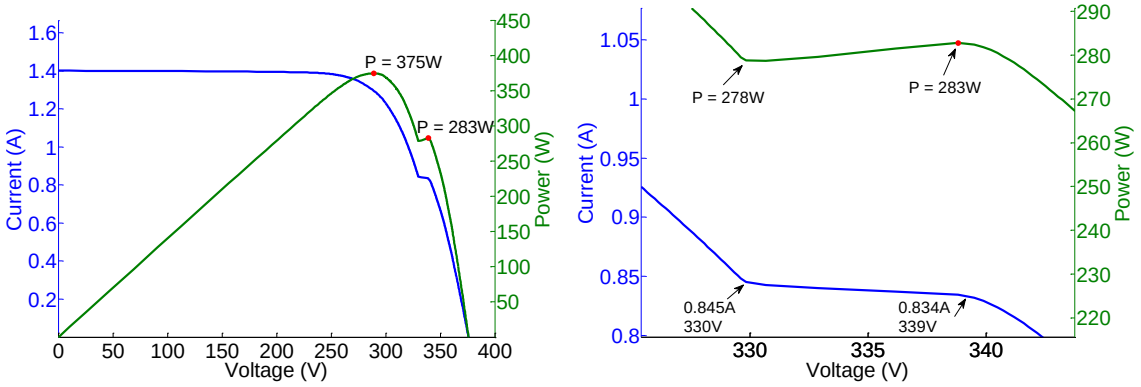

Figure 4.25: *I-V* and *P-V* curves of a 10 module PV generator at G=160W/m² with all cells from one sub-module shaded at 40% and a zoom of the transition region. The current at the local maximum is the same as the current at the local maximum from the example in Figure 4.19, however, now a local maximum appear and before it didn't. This shows that the reasons that cause local maxima to appear are independent from the irradiance level.

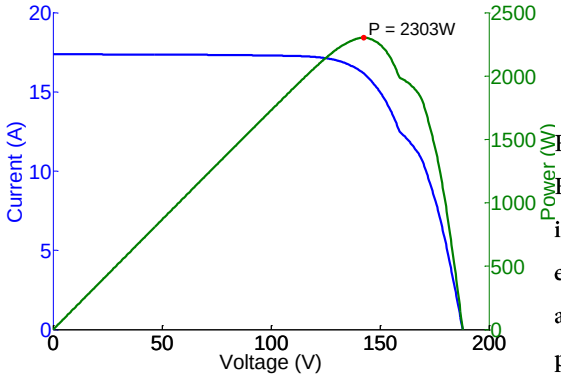

Figure 4.26: *I-V* and *P-V* curves of the same example of Figure 4.22, but now instead of having the 10 modules in series, there are two parallel strings of five modules each. It can be seen how now there is only one MPP and that the power of this MPP is lower than the power of the absolute MPP of Figure 4.22.

Probably the most important shading pattern to consider when thinking about the effects over the MPPT is when cells under the same by-pass diode are shaded by different percentages. As is seen in section 4.5.2.2, this is how shadows due to nearby objects affect the PV generator as they are coming in, which in turn is the crucial moment for the MPPT to track the absolute MPP. If, again, we take the example from Figure 4.22 and modify it so that now the 20 cells under the same by-pass diode are shaded by different percentages (groups of 5 cells each at 10%, 20%, 30% and 40%), the curves of Figure 4.27 are obtained. Now, contrary to the example were all 20 cells were shaded by 40%, no local maxima appear and the P&O MPPT algorithm would have no problem in tracking the absolute MPP. As the shadow progresses, it is less probable for local maxima to appear, as we have seen in the previous examples, so normally the P&O MPPT algorithm will find the absolute MPP in strings with many modules. More on irregular shading of cells under the same by-pass diode is seen in section 4.5.2.2.

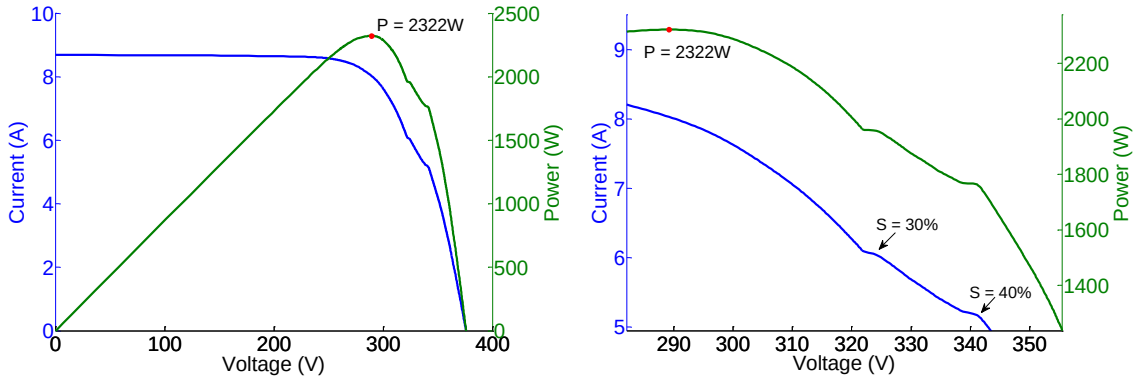

Figure 4.27: *I-V* and *P-V* curves of a 10 module PV generator with all 20 cells from one sub-module shaded in groups of five at 10%, 20%, 30% and 40% and a zoom of the transition region. Now, contrary to the example were all 20 cells were shaded by 40% (Figure 4.22), no local maxima appear.

This same amount of shading will however cause local maxima to appear in the individual shaded module as can be seen in Figure 4.28. Although in this case the maximum on the right side is the MPP, as the shadow progresses through the module this local maximum becomes smaller than the absolute maximum and the P&O algorithm starts tracking a non-optimum point. This, as was already pointed out earlier, shows that the *I*-V curves of individual modules are more likely to have local maxima than the *I*-V curves of whole generators. It is important to realize this, especially when working with DMPPT systems.

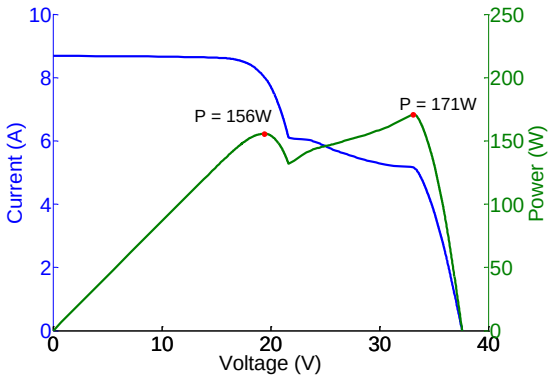

Figure 4.28: *I-V* and *P-V* curves of one module with all 20 cells from one sub-module shaded in groups of five at 10%, 20%, 30% and 40%. Now, contrary to the example of the ten module generator (Figure 4.27), a local maximum appears very clearly.

4.5.2.2 Nature of incoming shadows due to nearby objects

In order to fully understand the negative effects of shading on MPPT algorithms, it is first necessary to understand how shadows from nearby objects affect a PV generator. This focuses on the progressive shading of a PV generator and how its *I-V* curve, and the *I-V* curve of each module, change with time. For each example presented, the time

frame of analysis is chosen so that in each time step only a small change occurs in the *I-V* curve. In turn, this depends directly on the speed of the passing shadow, which in turn mainly depends on the distance that the object is from the generator.

All the calculations of the shadow over the generator and of the shaded *I-V* curve have been performed with a simulation program developed by the author of this PhD thesis, which is presented and validated in section 2.1.3 and section 5.3.1. In addition, for the sake of visualisation of the shadows, the examples presented have been modelled with Google SketchUp. It must be noted that the shaded percentage given by the simulation program developed and the shadow presented with Google SketchUp are in very good accordance, as shown in Figure 4.29 for the example of a chimney located west of the PV generator. The numbers presented represent the shading percentage of each cell of the two modules affected by the shadow of the chimney.

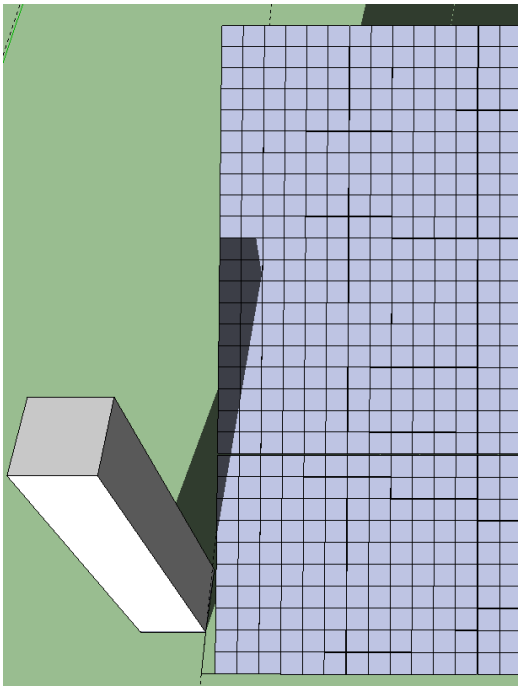

1.0	0.76	0.00	0.00	0.00	0.00
1.0	0.93	0.00	0.00	0.00	0.00
1.0	0.82	0.00	0.00	0.00	0.00
1.0	0.64	0.00	0.00	0.00	0.00
1.0	0.50	0.00	0.00	0.00	0.00
1.0	0.34	0.00	0.00	0.00	0.00
1.0	0.17	0.00	0.00	0.00	0.00
0.98	0.03	0.00	0.00	0.00	0.00
0.85	0.00	0.00	0.00	0.00	0.00
0.70	0.00	0.00	0.00	0.00	0.00
0.52	0.00	0.00	0.00	0.00	0.00
0.37	0.00	0.00	0.00	0.00	0.00
0.21	0.00	0.00	0.00	0.00	0.00
0.06	0.00	0.00	0.00	0.00	0.00
0.00	0.00	0.00	0.00	0.00	0.00
0.00	0.00	0.00	0.00	0.00	0.00
0.00	0.00	0.00	0.00	0.00	0.00
0.00	0.00	0.00	0.00	0.00	0.00
0.00	0.00	0.00	0.00	0.00	0.00
0.00	0.00	0.00	0.00	0.00	0.00

Figure 4.29: Google SketchUp picture of the shadow cast by a chimney on a PV generator compared with the shading matrix obtained with the developed simulation program for the same generator. The matrix shows the shading percentage obtained for each cell of the two modules affected by the shadow. It can be seen how there is very good agreement between the two.

The example presented, which is a real PV system on a rooftop in Germany (Figure 5.4) and is also used to model energy gains in section 5, consists of 15 PV modules in

series which are affected by the shadow of a nearby chimney at the east side of the generator. In these first examples the chimney has been changed to the west side to see the effects over the *I*-V curve of an incoming shadow on a non-shaded array. Later, in this same section, the chimney is placed on the east side to see the effects of a shadow at inverter start-up. This installation has been chosen as it can be considered as a typical rooftop installation affected by shadows and it has been slightly modified to include other possible examples. An V_b = -25V has been used for these simulations with this value it is more likely to by-pass shaded sub-modules, i.e. if no local maxima are present with V_b = -25V, no local maxima will be present with a lower V_b. On the other hand, if local maxima are present with V_b = -5V they will also be present with a higher V_b.

Figure 4.30 shows the progression of the shadow cast by the chimney over the previously described PV system, for minutes 2, 3, 6, 20, 40 and 90 after the shadow touches for the first the generator and for the 20th of January. At the same time, the corresponding *I-V* curve for each instant is also presented (at non-shaded conditions the MPP is at 448V). At minute 2 there are two MPPs in the *I-V* curve, being the absolute MPP the one of higher voltage and both points separated by 27V. The next minute, because the shaded percentage is now higher, the MPP is now the point of lower voltage (where the shaded sub-module is by-passed). However, because the MPPT algorithm was previously tracking the point of higher voltage, the working point of the generator (supposing a P&O algorithm), will be the lower power point. At the next time instant, minute six, this situation changes because now there are no local maxima in the *I-V* curve, due to the irregular shading pattern and other effects, like the large number of modules in series and the increases shade percentage, thoroughly explained in the previous section, and the working point will shift to the MPP at 437V. As another sub-module is shaded, a similar situation occurs due to this irregular shading and the large number of modules that make up the generator and there will be a moment, minute 20, where no local maxima are present and the MPPT algorithm will shift the working point towards the MPP, now at 427V. The same occurs when a third sub-module starts to get shaded, minute 40, and finally at minute 90 although there are three local maxima in the *I-V* curve, because the working point has been progressively shifted towards a lower voltage, the working point will be at the absolute MPP.

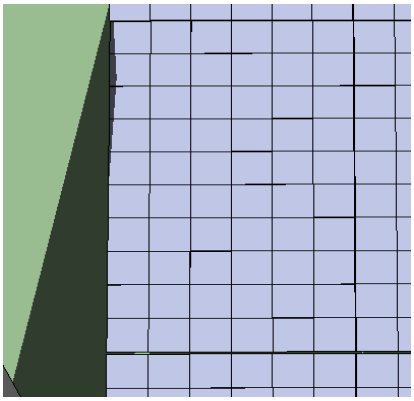

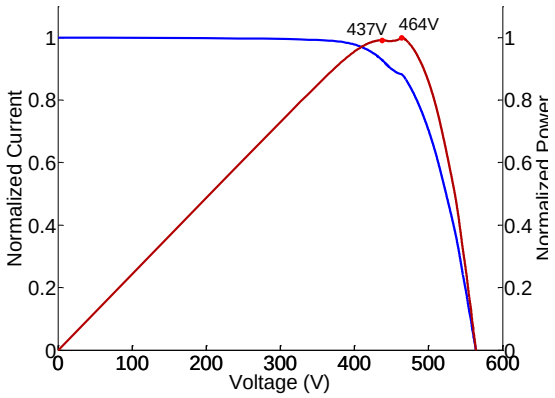
437V
464V
Normalized Current
Normalized Power
Voltage (V)

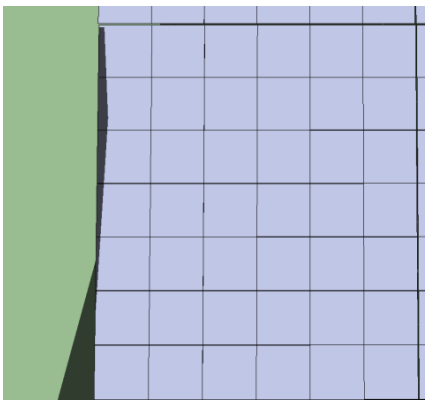

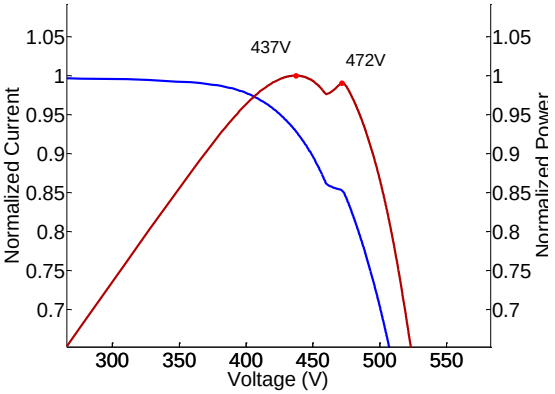
437V
472V
Normalized Current
Normalized Power
Voltage (V)

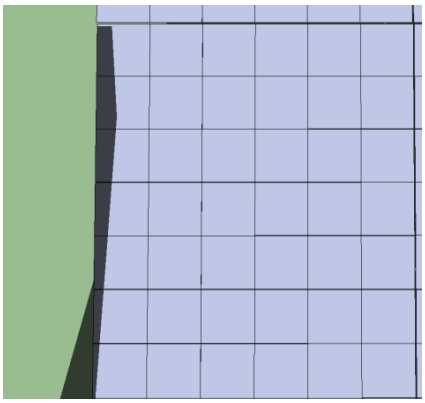

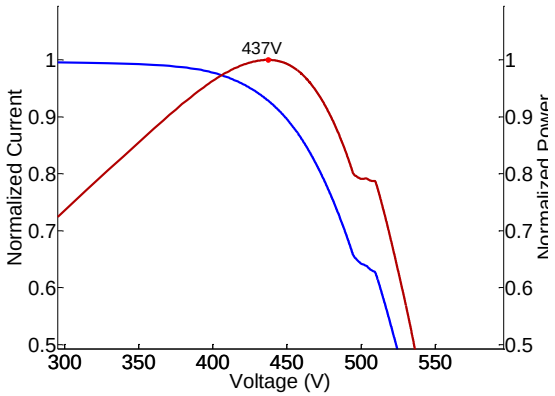
437V
Normalized Current
Normalized Power
Voltage (V)

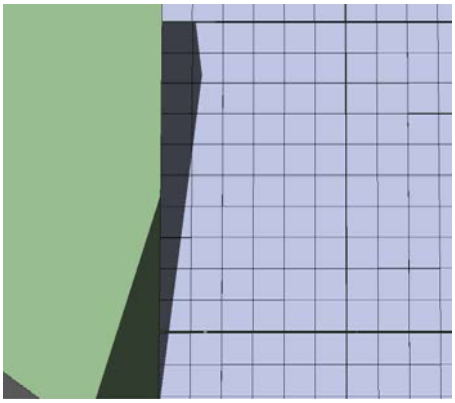

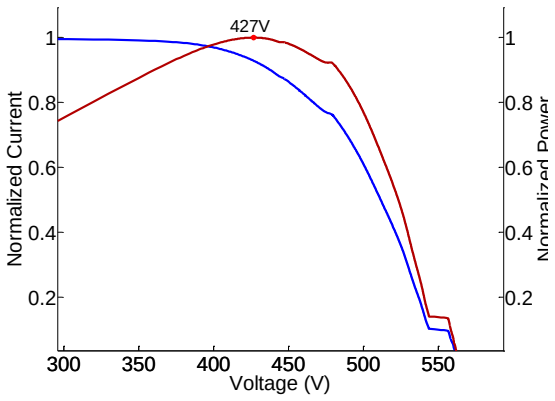
427V
Normalized Current
Normalized Power
Voltage (V)

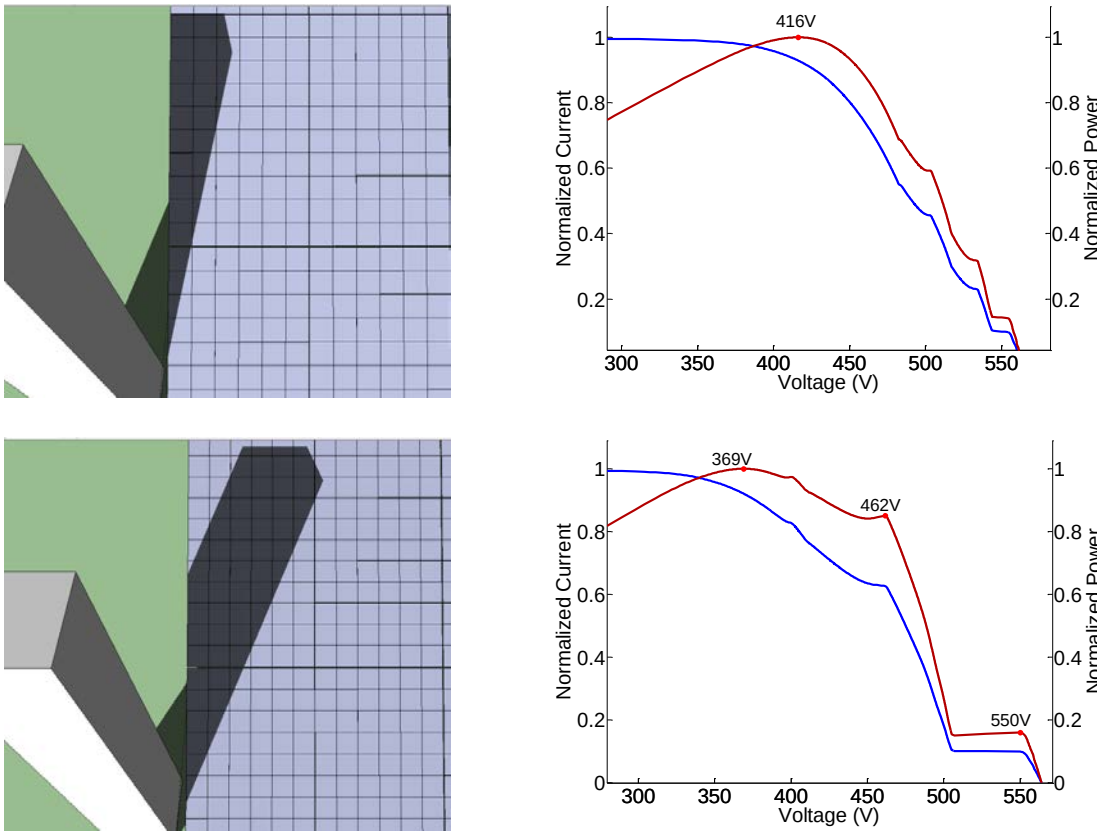

Figure 4.30: Pictures of the progression of a shadow from a nearby chimney over a PV generator and the corresponding *I-V* and *P*-V curve for each instant. The moments correspond to minutes 2, 3, 6, 20, 40, 90 of January 20th; considering minute 1 as the first minute in which shaded affects the generator.

This example is a clear case of a shadow that should have no negative effect over the MPPT of a central PV inverter; i.e. it will not get stuck in a local maximum. However, the situation changes completely when considering the effect over the MPPT of a power optimizer or micro-inverter. As has been previously seen, individual PV modules are more likely than generators to have local maxima in their *I*-V curve. Now considering only one of the shaded modules in the example of Figure 4.30, it can be seen in Figure 4.31 how distinct local maxima are present in the module's *I-V* curve throughout the whole shading sequence. This example is a case where a simple P&O MPPT algorithm can cause DMPPT systems to produce less energy than central MPPT systems during certain time periods (more on this is seen in section 4.5.2.4 and section 5).

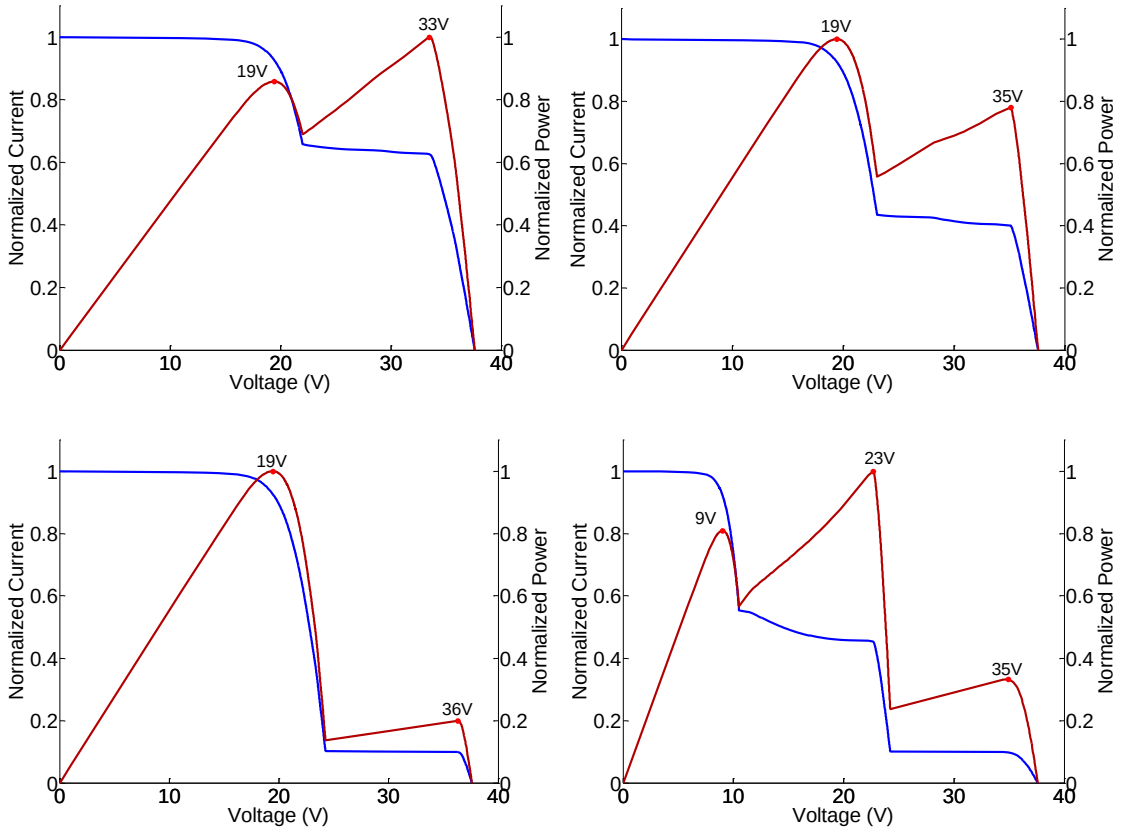

Figure 4.31: ***I-V*** **and** ***P-V*** **curves of the shaded module for minutes 3, 6, 20 and 40. It can be seen how in this case there are distinct local maxima at all time periods, causing a simple P&O algorithm of a DMPPT system to not work at the absolute MPP; while with the CMPPT it would not occur.**

This situation changes completely if the chimney were to be situated east of the PV generator. In this case, shown in Figure 4.32, because the PV generator "wakes up" under very shaded conditions, there is a distinct local maximum which could cause the string inverter's MPPT algorithm to not find the absolute MPP (this is actually what occurs in the tests performed which results are shown in 4.5.2.3.a), continuing this situation until the shadow is small enough that it does not create distinct local maxima. In this specific situation, for the equinox, this occurs during approximately five hours; from half an hour after sunrise until 11:15 solar time. In this case the CMPPT system would underperform in comparison with the DMPPT system (simulation results that confirm this are shown in section 5.4).

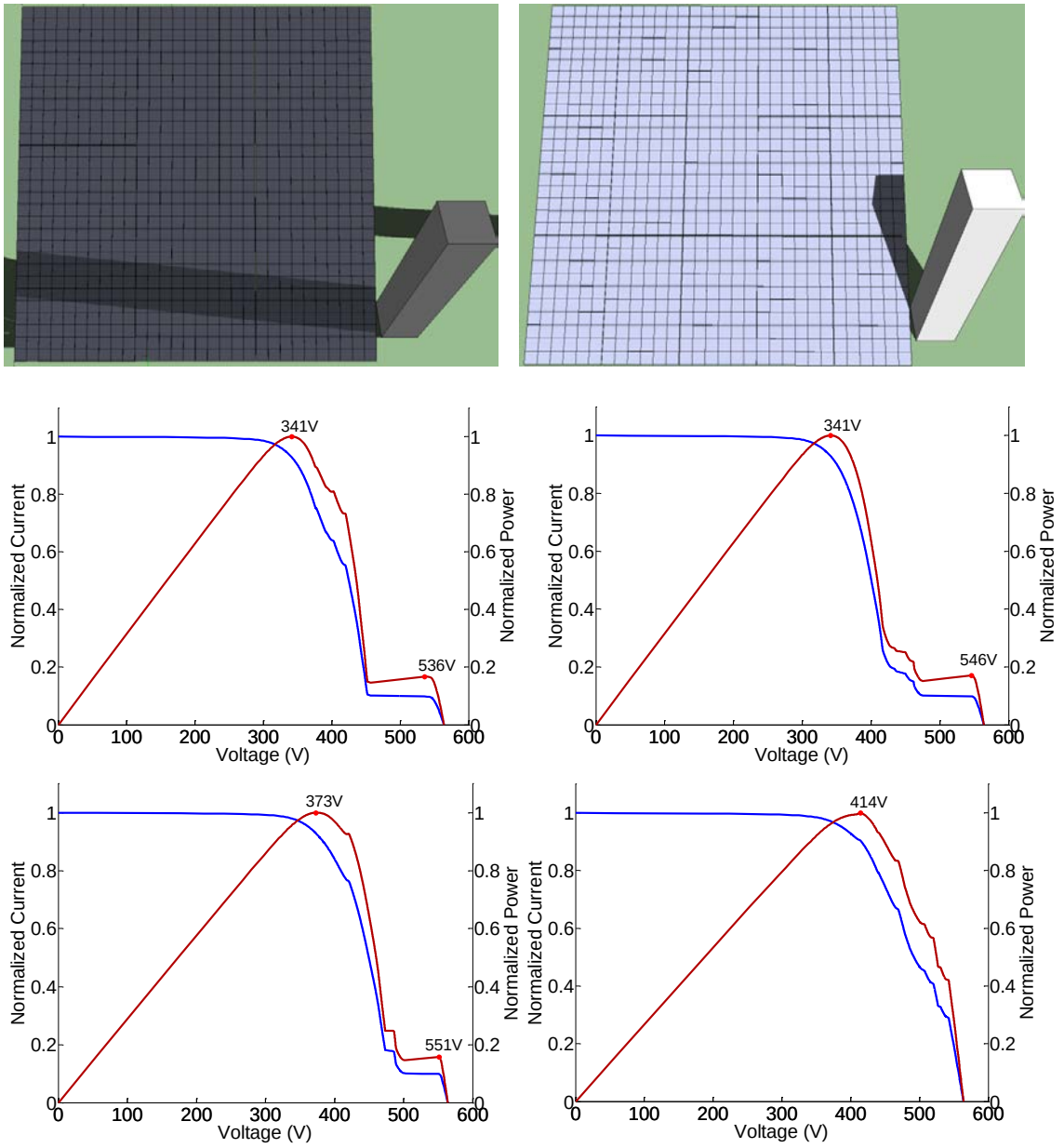

Figure 4.32: Pictures of the shadow cast by the chimney on the PV generator 30 minutes and 5.5 hours after sunrise and *I-V* and *P-V* curves of the generator 30 minutes, 2.5 hours, 4 hours and 5.5 hours after sunrise. It can be seen how there is a distinct local MPP from sunrise until 5.5 hours after sunrise, which could cause an inverter to operate away from the absolute MPP for almost half of the day.

Other specific shading situations in which very distinct local maxima can appear is the case of solar trackers. Because two axis trackers and azimuthal trackers are always pointing at the same azimuth angle (the sun's position), the nature of the incoming shadow is totally rectangular; shading many cells from different by-pass diodes at the same time, shading them by an equivalent amount and progressing through the generator from left to right in the afternoon and from right to left in the morning. This causes the *I-V* curves to have very distinct local maxima possibly causing the MPPT

algorithm to track a local maximum instead of the MPP. This specific effect on PV trackers has been documented in [García, Maruri et al., 2008] and an example of the rectangular shadow affecting PV trackers is shown in Figure 4.33, obtained from [Martinez, 2012].

Figure 4.33: Examples of the rectangular shadows cast by PV trackers. Such rectangular shadows cause very distinct local maxima causing P&O MPPT algorithms to not find the absolute MPP as has been shown in [García, Maruri et al., 2008].

4.5.2.3 Measurements with a solar array simulator

This section presents the results obtained from the measurements performed on inverters, power optimizers and micro-inverters and related with the capability of the MPPT algorithm of finding local maxima. All of the measurements were performed on modern equipment, all purchased after 2011. The different equipment used for the measurements are: SMA Sunny Boy 2000HF, Ingeteam Suncon Lite5, Fronius Symo, SolarEdge power optimizer, Tigo power optimizer and the Enphase micro-inverter. Table 4.3 lists the power conditioning equipment used during these tests and their MPPT voltage range.

Table 4.3: MPPT range of the different equipment that whose MPPT algorithm was put under test.

Equipment	Type	MPPT range (V)
Sunny Boy 2000HF	Inverter	175-560
Ingecon Sunlite 5	Inverter	160-450
Fronius Symo	Inverter	150-800

SolarEdge	Power optimizer	5-60
Tigo	Power optimizer	16-48
Enphase	Micro inverter	22(16)-36

As is shown in this section, most of the modern equipment tested is not able to find the absolute MPP once it gets stuck in a local maximum.

4.5.2.3.a Local Maxima at start-up

SMA SB 2000-HF, Ingeteam Ingecon Sunlite 5.0 and Fronius

As has already been discussed in section 4.5.2.2, shadows at start-up are likely to have the worst effect over the MPPT algorithm. This section presents the results of introducing *I-V* curves with different local maxima into different PV inverters at start-up and observing the operation of the MPPT algorithm.

For the tests with inverters, due to their high MPPT range in comparison to the SAS's voltage range, the maximum number of biased diodes is limited to two. If more diodes are by-passed then the MPP will lie outside the MPPT range. Therefore, the first *I-V* curve used corresponds to a PV generator with two biased diodes where both maxima are in the MPPT region of the inverters as shown in Figure 4.34-bottom-left. This curve is used for testing the SMA and Fronius inverters. For the Ingeteam inverter a very similar curve is used but with a lower voltage MPP (@169V).

From the figure it can be seen how there is an initial start-up time and once the inverter is started the MPP is found very quickly, having the local maximum absolutely no effect over the MPPT algorithm. This occurs because, normally, MPPT algorithms at start-up go directly to a region close to 0.8 of V_{OC} (191V and 196V for the SMA and Ingeteam inverters respectively), where the MPP is approximately located in a typical *I-V* curve, and then starts performing the P&O. In this case the point at which the power starts to increase after the first local maximum (we call this the transition point from now on) is at a higher voltage (211V), so at start-up the working point is located at a lower voltage than the transition point and once the algorithm starts the P&O search it is led towards the absolute MPP.

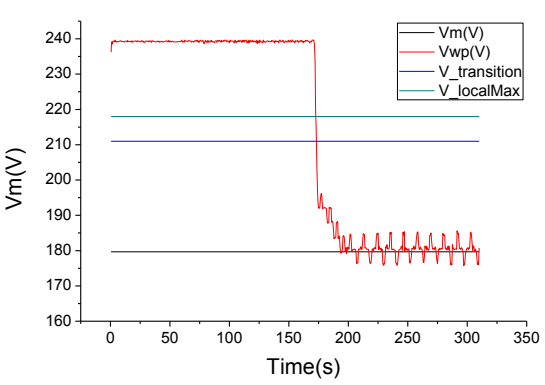

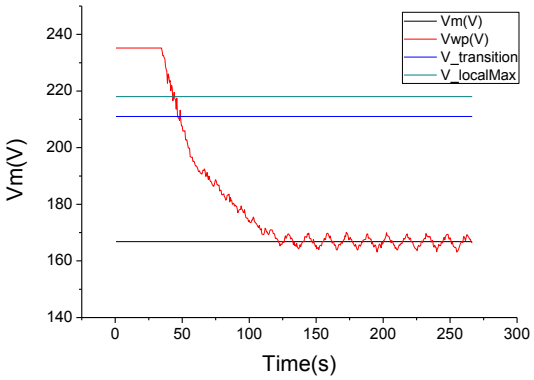

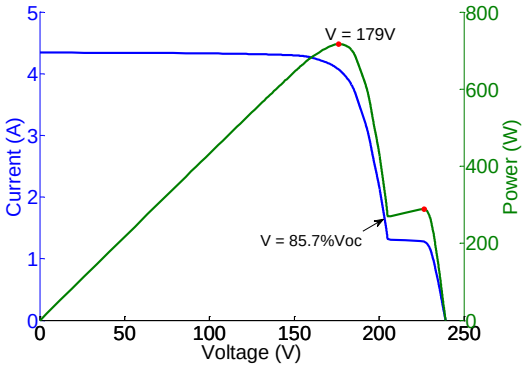

Figure 4.34: (left) *I-V* curve with a local maximum used as an input to the SB-2000HF inverter at start-up and (right) working voltage of the inverter, and local MPP voltage, the transition point's voltage and absolute MPP voltage of the *I-V* curve. It can be seen how in this case the local MPP has no negative effect over the MPPT algorithm.

If an *I-V* curve with four shaded sub-modules is used for the simulations, then this situation changes. Now the point at which the power starts to increase after the first local maximum is at 189V and the working point never reaches this voltage in none of the three inverters as shown in Figure 4.35, so the working point remains at the local MPP. It should also be noted that although the absolute MPP is outside the MPPT region (@146V) there are still higher power points up to the lower value of the MPPT range, at 175V, being them not found.

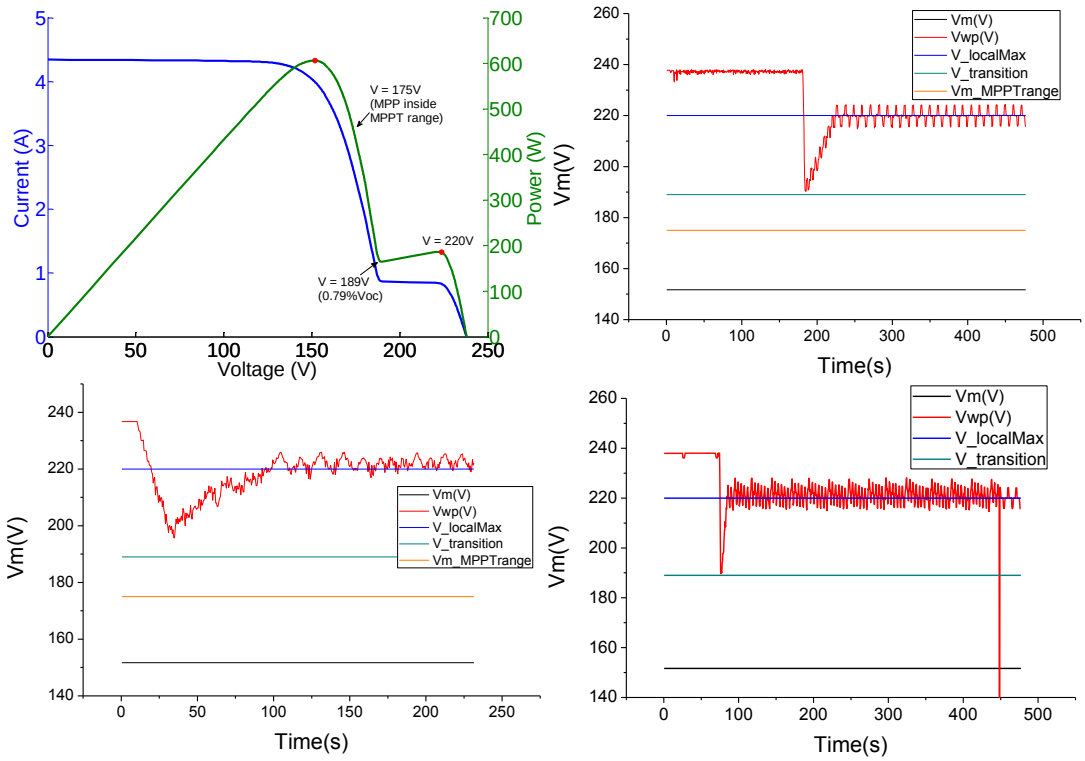

Figure 4.35: Results of the MPPT behaviour at start-up of the SMA SB2000HF (top-right), Ingeteam (bottom-left), and Fronius (bottom-right) inverters.

Enphase, SolarEdge and Tigo

Figure 4.36 shows the results from the MPPT test at start-up performed on the SolarEdge power box and on the Enphase micro-inverter as well as the *I-V* curve uses with the SAS. The *I-V* curve shows a clear local MPP at 34V and the absolute MPP at 20V. It can be seen how the SolarEdge power box does not find the absolute MPP at start-up. From its behavior it can be seen how the SolarEdge's MPPT algorithm performs a typical P&O method from the beginning. On the other hand, the Enphase micro-inverter sweeps the whole *I-V* curve at start-up and therefore finds the absolute MPP.

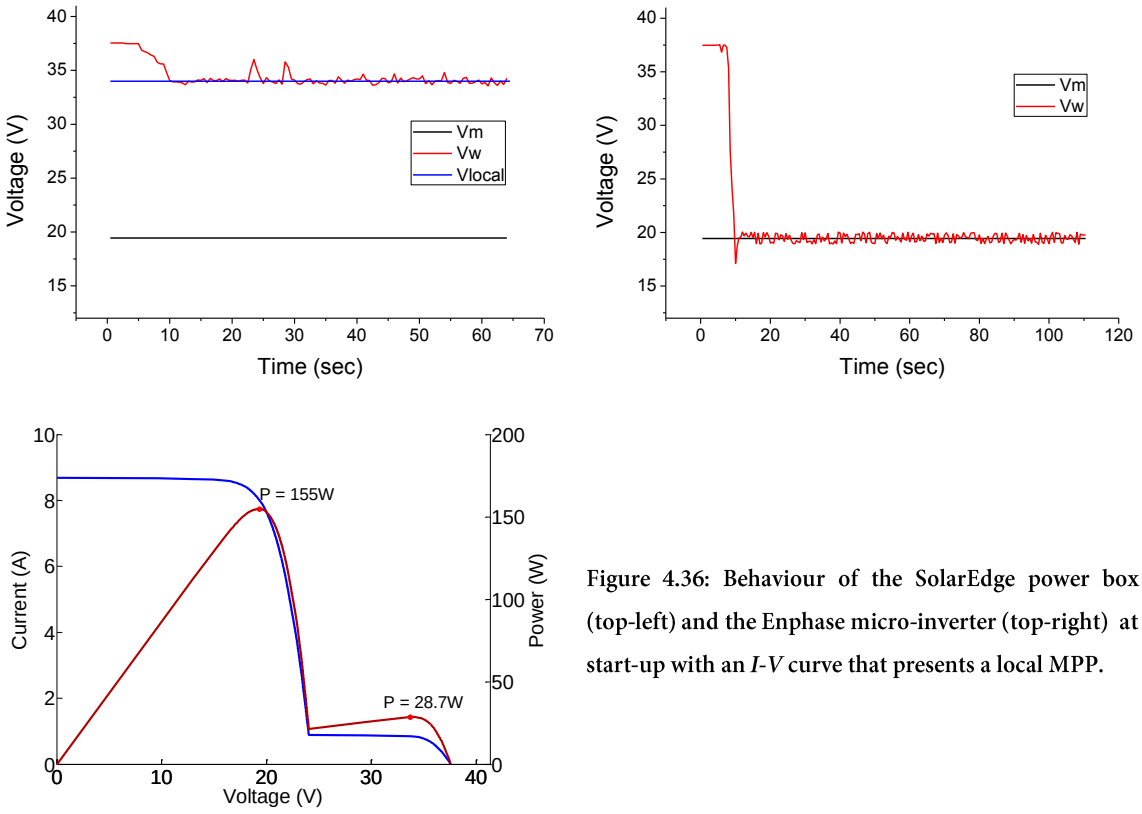

Figure 4.36: Behaviour of the SolarEdge power box (top-left) and the Enphase micro-inverter (top-right) at start-up with an *I-V* curve that presents a local MPP.

4.5.2.3.b Local Maxima during operation

Section 4.5.2.2 presents how shadows tend to progressively affect PV arrays and their *I-V* curves. The experiments performed with the SAS regarding local maxima try to resemble the situations presented in that section as close as possible. In that section, it is shown that it is uncommon for local maxima to appear in PV generators with a medium to large number of modules in series and that it takes a large amount of shade over many different cells from different sub-modules for distinct local maxima to appear, which occurs a long time after the shadow starts entering the generator.

However, it was also shown that there are certain situations where abrupt local maxima do appear and can cause the MPPT algorithm to not find the absolute MPP; like at inverter start-up or in the case of PV trackers. In addition, in PV systems with DMPPT it is a lot more probable for local maxima to appear and, therefore, for the MPPT algorithm to not work at the absolute MPP. For these reasons, two examples are simulated: one in which the incoming shadow creates small and non-abrupt local maxima and another in which the created local maxima are abrupt.

The first experiment here presented show how the MPPT algorithms of the different equipment respond to a set of curves which simulate a progressive shadow entering the generator. Because the idea is to the test the algorithm's capability of finding the absolute MPP in presence of local maxima, it is supposed that these shadows create distinct local maxima in both the generator's *I-V* curve and the modules' *I-V* curves.

The test procedure used is as follows:

1. Start up the specimen[24] with a normal *I-V* curve and wait until the working point stabilizes at the MPP. This time depends on each unit.

2. Progressively change the *I-V* curve for a new curve with a small shading percentage over all the cells of one or various sub-modules. This change should be small enough so that the new point of the *I-V* curve where the power starts to rise towards the absolute MPP does not enter the MPPT region of the previous curve. Otherwise this could cause the MPPT to artificially find the absolute MPP. This is also realistic, since in normal operation this change is infinitely small.

3. Continue introducing *I-V* curves with more shading until reaching 90%. Keep this last curve as the active curve for at least five minutes.

The first set of experiments was performed on three inverters: SMA, Ingeteam and Fronius. The SMA inverter was tested with and without the OptiTrac Global Peak, which must be activated, and is an additional function of the standard MPPT OptiTrac. It has been developed in order to find the absolute MPP in presence of local maxima. Because this new algorithm must search the whole *I*-V curve periodically, in unshaded condition it is less efficient than a standard P&O algorithm, although not much: SMA claims a 0.2% maximum loss in unshaded conditions [SMA, 2010]. In order to minimize these losses, SMA recommends varying the search period (which goes from 6 to 30min) in case of slowly incoming shadows.

In total 36 different *I-V* curves were used, each being left on the SAS for 25 seconds and where progressive shading was simulated over two sub-modules: each step

[24] Specimen refers to inverter, power optimizer or micro-inverter.

increments the shade on 2.5%. The curves used present very distinct local maxima, having the absolute MPP shift to the lower voltage region after the eighth curve; that is at 22.5% shade.

Figure 4.37 shows the results obtained for the three inverters with the set of curves previously described. In the figure, the working voltage, the MPP voltage and the voltage of the local maximum are represented. It can be seen how the MPPT correctly tracks the MPP until the MPP shifts to the lower voltage region. Once this occurs, the working point remains at the local maximum until the end of the experiment. During the experiment the working point has remained at a local maximum, different from the absolute MPP, for 12 minutes, accounting for an energy loss of 1.5 kWh or 33.2%. For the SMA inverter with OptiTrac it can be seen how the MPPT tracks the local maxima for about two minutes and then immediately shifts to the global MPP. The periods while the OptiTrac is at a local maximum correspond to when the difference in power between the local and global maximum is minimum; causing only 25Wh of total energy loss or 0.9%.

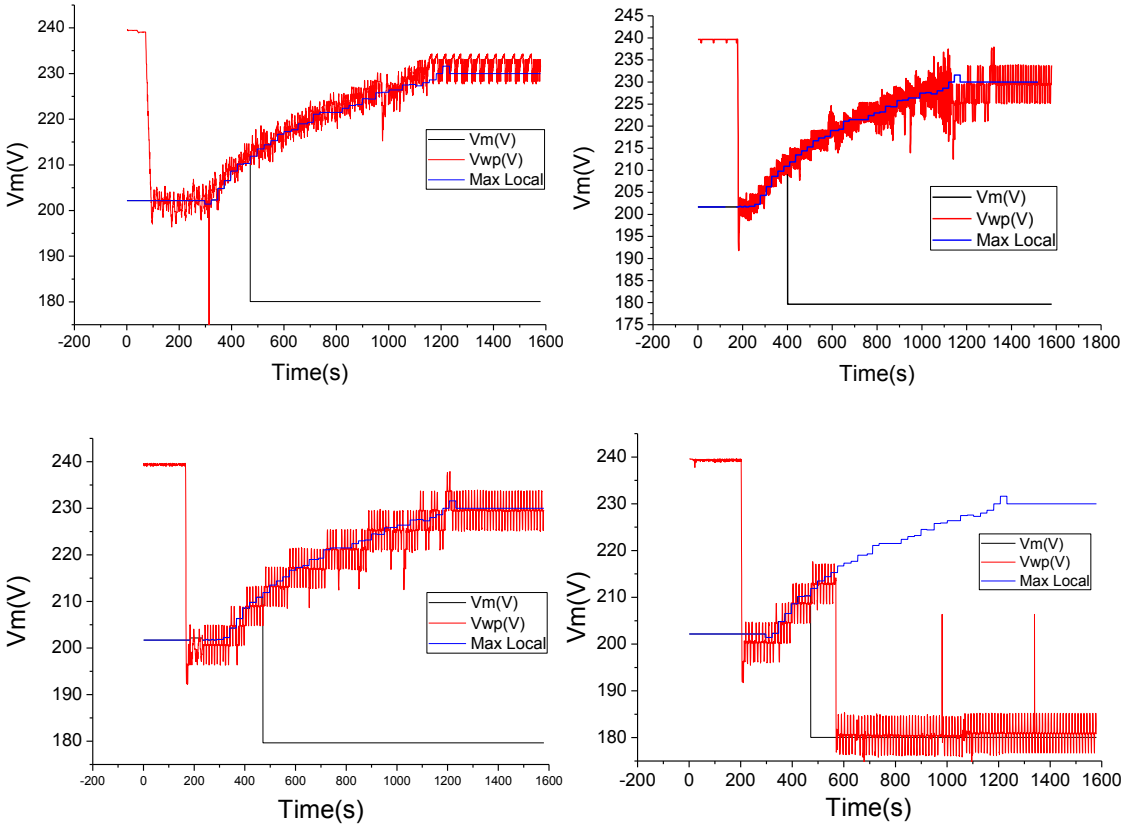

Figure 4.37: Ingeteam (top-left), Fronius (top-right), SMA without optitrac (bottom-left) and SMA with optitrac (bottom-right).

The second set of experiments was performed on DMPPT equipment: the Enphase microinverter and the SolarEdge and Tigo power optimizers. In this case the curves used to test the three products were the same with a total of 46 curves. The initial curve corresponds to a PV module with sixty cells in series (V_m = 30V) and three by-pass diodes (three sub-modules). The other 45 curves can be divided in three groups: shaded over the first, second and third sub-modules. Each of these fifteen curves increment the shaded percentage by 6%, from 0% to 90% over each sub-module. Figure 4.38 shows the working voltage, the voltage of the MPP and the voltage of the local maximum. It can be clearly seen that once the MPP shifts to a lower voltage the Enphase micro-inverter remains at the local maximum point, therefore not maximizing the energy output of the PV module. From the figure it can also be seen how once the input power to the micro-inverter drops below 30% of its rated power, the searching voltage range increases (around minute 8.5). This occurs because of an interesting feature that have the Enphase micro-inverters called "Burst Mode" [Enphase, 2012]. Because at low powers the DC/AC conversion efficiency drops, the "Burst Mode" holds the available energy during one or more AC cycles (50Hz or 60Hz) and adds it to the next cycle's energy, and then does the DC/AC conversion when it is more efficient. This way the conversion is done at a higher power, optimizing the conversion efficiency.

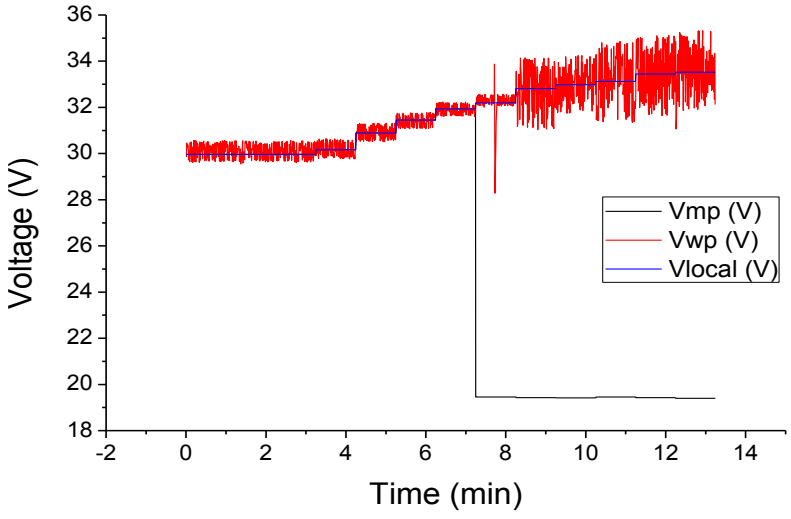

Figure 4.38: Response of the Enphase micro-inverter's MPPT algorithm to *I-V* curves with local maxima. Around minute seven the MPP shifts to a lower voltage (sub-module is by-passed) but it can be seen how the working point remains at the local maximum.

In Figure 4.39 the results of the test applied to the SolarEdge optimizer are presented, which are a curious case to discuss. Just like in the case with the Enphase micro-inverter, when the MPP shifts to a lower voltage, at around minute four, the MPPT algorithm of the SolarEdge optimizer keeps following the local MPP. However, at a certain moment,

close to minute six, the MPPT quickly jumps to the absolute MPP, at a lower voltage (equivalent to the loss of one sub-module since now one by-pass diode is in forward bias). The working point remains at the absolute MPP for some time but when the MPP again shifts to an even lower voltage (two sub-modules by-passed) around minute 9.5 the MPPT algorithm stays at the second local MPP. Again, after some time the working point jumps to the absolute MPP. A few minutes pass at the MPP of lowest voltage (two by-passed sub-modules) and the module is set at V_{oc}, around minute 15. From then on the module remains at V_{oc} with periodical voltage scans on the *I-V* curve.

From a first glance at the behavior of the SolarEdge MPPT algorithm it could be concluded that it is capable of finding the absolute MPP in presence of local maxima but that it needs some time; something like the OptiTrac. However, this is far from reality. If we take a look at the output voltage of the optimizer to which this module is connected Figure 4.39-right, we can see that at the same exact moment that the working point passes from the local MPP to the absolute MPP V_o reaches 5V; which is V_{o_min} for the SolarEdge optimizer. As has already been presented in section 3.3.2 and 4.2.2 and also shown in these results, a drop in V_o is caused by a drop in I_i. This causes that when V_{o_min} is reached the MPPT algorithm of the optimizer searches the *I-V* curve to see if a working point at a higher current is available. This occurs again the second time V_{o_min} is reached, at around minute 11, and the third time V_{o_min} is reached it does not occur because there are no points with higher currents since now all three sub-modules are shaded. From the results, it can also be seen how V_{o_min} is reached at a higher current the second time. This is because each time the working voltage is lower which, because *M(d)* is the same[25], causes a lower V_o for the same I_i. It should be noted that depending on the number of modules of the system and the working voltage of the modules, V_{o_min} might not be reached and thus the absolute MPP not found. Curiously, the limited output values of the optimizers, which is a limitation towards shadow mitigation, fixes another limitation, the non-possibility of the MPPT algorithm of finding the absolute MPP in presence of local maxima.

[25] Remember *M(d)* only depends on the current mismatch

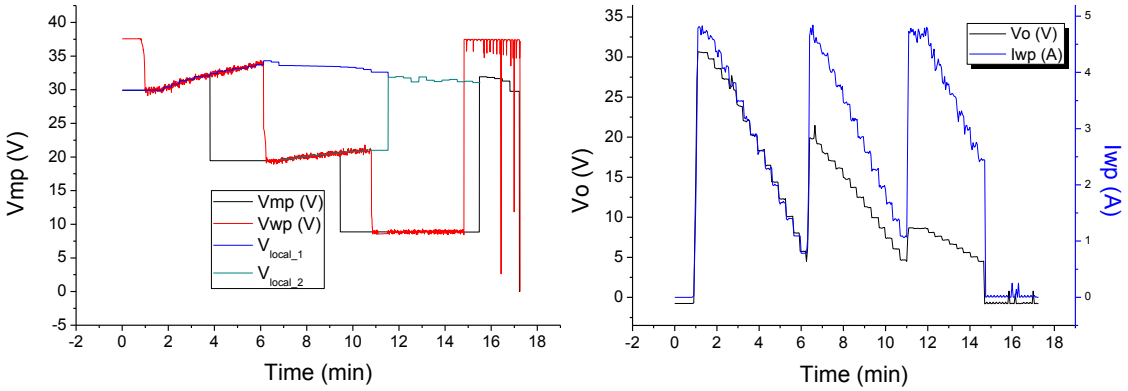

Figure 4.39: Response of the SolarEdge power optimizer's MPPT algorithm to *I-V* curves with local maxima. Around minute four the MPP shifts to a lower voltage (sub-module is by-passed) and the working point remains at the local maximum. However, at minute six, because V_{o_min} of the optimizer is reached, the working point shifts to the MPP, at a higher current. The same occurs when the second sub-module is shaded, and finally when the third sub-module is shaded, because there are no longer higher currents to shift to, the optimizer is by-passed, remaining the module at V_{OC}.

Finally, the Tigo power box was also put under test. The results are shown in Figure 4.40 were it can be seen that the behaviour is very erratic. In all the tests performed the Tigo power box has behaved differently, although always showing an erratic behaviour. This behaviour could be due to the fact that the MPPT algorithm of the Tigo system is centralised and each power box receives orders of at which point to operate from the central MMU. Tigo has also stated that their algorithm is predictive, that they need some time to adapt and that it is based on previous behaviour in similar situations. This could be the cause that when unnormal curves are inputed with a SAS the MPPT does not know what to do. Further tests should be performed to truly conclude on the efficacy of the Tigo's MPPT efficiency.

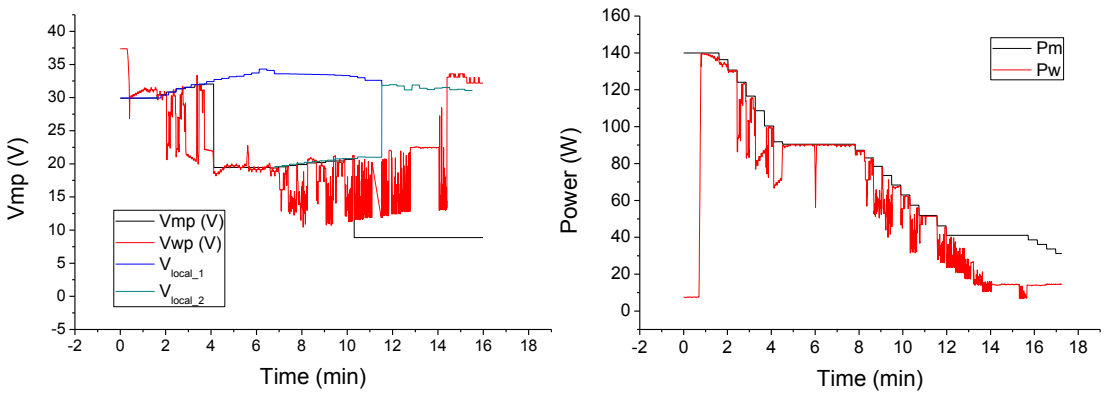

Figure 4.40: Results of the MPPT efficiency tests performed on the Tigo system.

4.5.2.4 Measurements in real PV systems

To further validate the results obtained with the SAS, experiments have been performed in two real PV systems. The first system is one of the generators of Magic Box, the solar home used a test bank at the IES's central facilities, and the second is a rooftop generator of the IES facilities in Vallecas, Madrid. Both generators are shown in Figure 4.41.

Figure 4.41: The PV generators used for the MPPT experiments. Left- the generator at IES-Vallecas and right- the MagicBox.

The two generators are composed of different types of modules, being the main difference the reverse characteristics of the cells of each module. While the generator of Magic Box has modules with cells of low breakdown voltages, the generator at Vallecas is composed of modules with cells of high breakdown voltages. This causes the *I-V* curves of the generator at Vallecas to have much more abrupt local maxima than those of the generator at Magic Box, which in many cases will not even have local maxima, as is the case of Figure 4.42 where one cell of a module of each generator is shaded at 50%. This effect will influence the MPPT efficiency under shaded conditions as we will see in the results here presented.

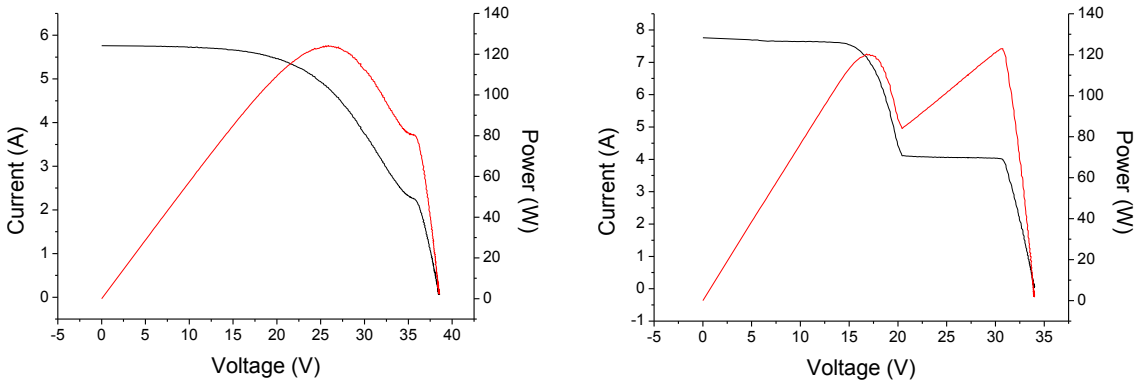

Figure 4.42: Measured *I-V* and *P-V* curves of a PV module with one cell shaded at 50% for the generators of Magic Box (left) and Vallecas (right).

The generator at Vallecas is made up of two parallel strings of twelve Siliken SLK 60 P6L PV modules of 245W, connected to an Ingeteam Ingecon SunLite 5 inverter (one of the models used in the experiments with the SAS). However, for simplicity, during these experiments only one string was used. In addition, in order to see the effects of shading when having more or less modules in series, the string was modified from twelve to eight modules in series.

4.5.2.4.a Measurements at Magic Box

The measurements performed at Magic Box are aimed at showing the different effects that shading has over DMPPT systems and CMPPT systems. As has been predicted in section 4.5.2.2, the use of DMPPT systems can be worse than CMPPT systems if simple P&O algorithms are used at the MPPT. The reason behind this is that certain shadows cause very distinct local maxima at module level but these local maxima disappear when the shaded module or modules are connected in series with other non-shaded modules. For this reason, the CMPPT system will work at the absolute MPP while the DMPPT system's working point can get "stuck" at a local maximum.

The experiment conducted consists on applying a progressive shade (from 0% shade to 100% shade) to various cells of one sub-module and measuring the working voltage of the power optimizer to which this module is connected. Immediately after, the power optimizers are disconnected and the modules are connected in series to a central inverter. The same shade is applied to the same module and now the working voltage of the whole system is measured.

The generator used is made up of twenty Isofoton I-110 PV modules connected in series to an SB 2000HF, one of the models used in the measurements with the SAS. When connected in the DMPPT system the modules are grouped in pairs, having two modules per power optimizer and totalling ten power optimizers. In this case it is the Solar Edge system that is used.

Before starting each system and measuring the working voltage, *I-V* curves at different shading percentages of the progressive shade applied were measured. These measurements allow comparing the working voltage to the MPP voltage and seeing if the inverter or power optimizer is working at the correct point. Figure 4.43 shows four

I-V curves at 25%, 50%, 75% and 100% of the progressive shade applied and the working voltage or input voltage to the power optimizer (V_i) during the experiment as well as the output voltage of the power optimizer (V_o).

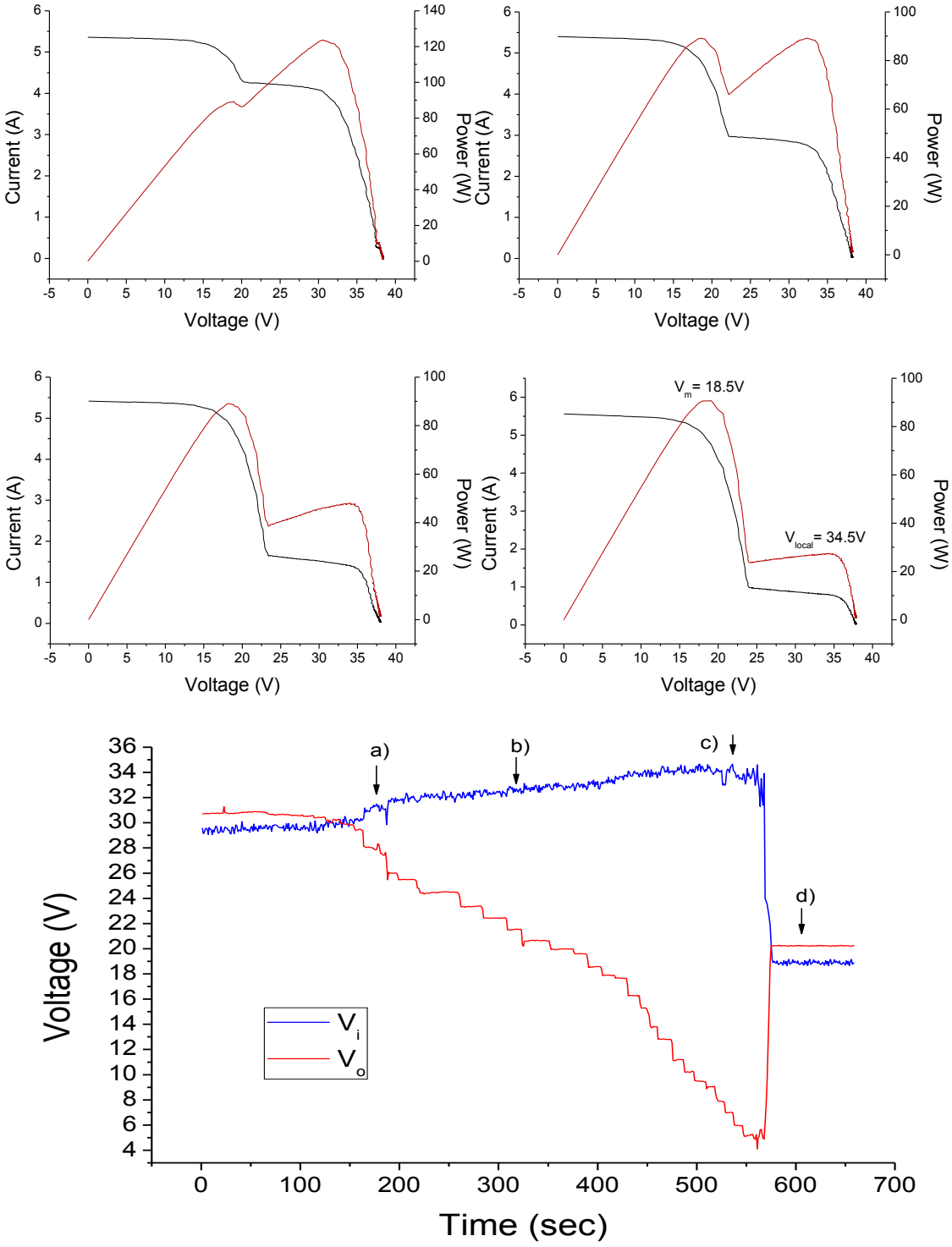

Figure 4.43: *I-V* and *P-V* curves at 25% (a), 50% (b), 75% (c) and 100% (d) of the progressive shade applied to one module and the input and output voltages of the power optimizer of the shaded module.

From the measured curves, we can see how the absolute MPP is the one of higher voltage (all cells reduce their current to match the shaded cells current) up until approximately 50% shade and from then on the absolute MPP is that of lower voltage (the by-pass diode is in forward bias). The curves also show how the MPP of higher voltage increases its voltage as the shade increases while the MPP of lower voltage keeps its voltage constant. The measured working voltage (V_i), which goes from 29V at no shade up to 34V, shows that the power optimizer is following the MPP of higher voltage up until almost the end of the measurement. This means that the MPPT is tracking the absolute MPP until approximately 50% shade (at 350 seconds) but from then on it fails to track the absolute MPP, remaining at the local MPP. Then, towards the end of the measurement, the working point drops in voltage to the absolute MPP. The point when this occurs coincides in time when the output voltage (V_o) of the power optimizer reaches its limit at approximately 5V. At this point, the power optimizer cannot keep on working and it automatically displaces the working point towards $I_{sc,}$ luckily finding the absolute MPP. It is important to emphasize that it is not the MPPT algorithm that finds the absolute MPP but that this occurs due to a limitation in V_o of the optimizers and the working current and voltage relations between all optimizers. If, for example, there are less optimizers in the system or there are more shaded modules it could occur that the V_o limit is never reached and the absolute MPP never found. This same effect has also been found in the experiments with the SAS presented in section 4.5.2.3.b.

Figure 4.44 shows the *I-V* and *P-V* curves of the twenty module generator for 12.5%, 25%, 50% and 100% of the progressive shadow applied over one sub-module and the working voltage of the inverter during the progressive shading. It can be seen how none of the curves present distinct local maxima that could obstruct the MPPT algorithm from finding the absolute MPP. The working voltage shows that there is a short period when the voltage is increasing, up to approximately 305V, but that it quickly descends to the absolute MPP at 280V. This short time when the voltage is increasing is from 0% shading up to around 10-15% shading where it is still more power beneficial to reduce the current of the non-shaded cells than to lose a whole sub-module.

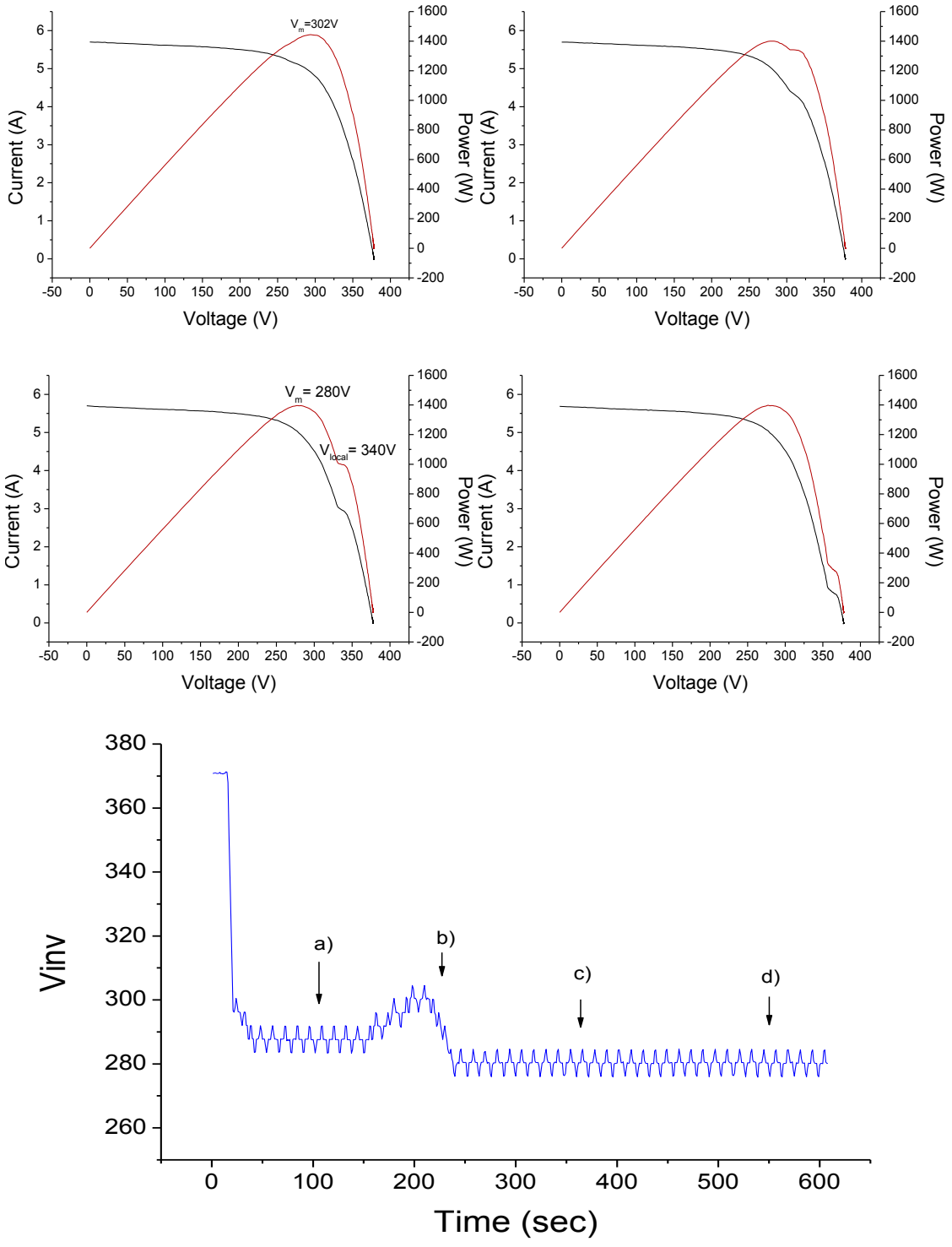

Figure 4.44: *I-V* and *P-V* curves at 12.5%, 25%, 50% and 100% of the progressive shade applied to one sub-module and the working voltage of the inverter.

From these measurements, where the same shade is applied to a module in a central MPPT and a DMPPT system, show how the difference between finding and not finding the absolute MPPT can be due only to the shape of the *I-V* curve that the MPPT

algorithm is seeing and that DMPPT systems are more prone to MPPT problems in presence of shading.

MPPT BEHAVIOR AT INVERTER START-UP UNDER SHADED CONDITIONS

As has been predicted in section 4.5.2.2 and measured with an SAS in section 4.5.2.3.a, large shadows over PV generators at invert start-up can cause a simple P&O MPPT algorithm to not work at the absolute MPP. In order to verify this, the same generator from MagixBox has been used during the morning hours were it is heavily affected by a nearby tree, as can be seen in Figure 4.41. During two consecutive days, with nearly identical irradiance, the power output has been measured with the generator connected to an SMA SB2000HF inverter, with and without the OptiTrac option, being the results shown in Figure 4.45.

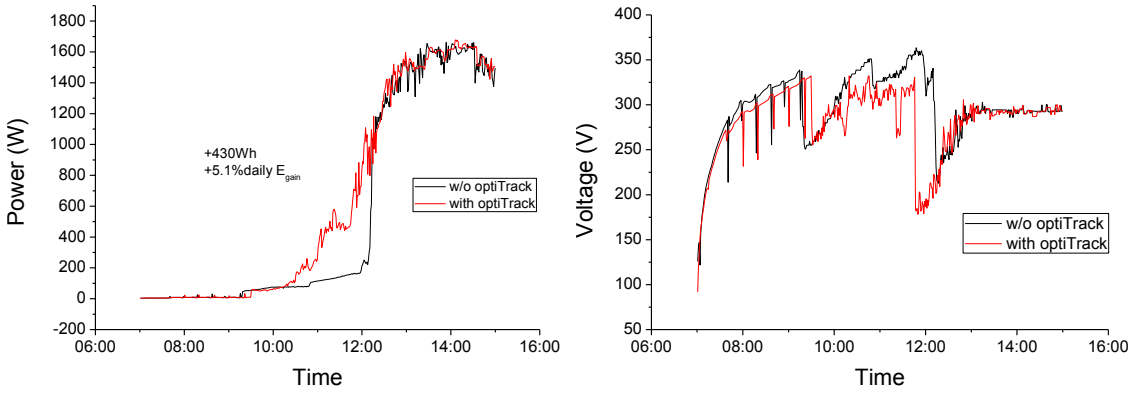

Figure 4.45: Production curves (left) of one of the MagicBox generators affected by morning shaded with an SB2000HF with and without the optiTrac option enabled and (right) working voltage in each of the two cases.

It can be clearly seen how the system with the OptiTrac option starts producing earlier than the system without OptiTrac. It can also be seen how the system without OptiTrac outputs an almost constant power until around 12:20 when it quickly rises from 200W to 1000W. This moments coincides with the quick voltage change that can be seen in Figure 4.45-right. The measurement also shows how the system without OptiTrac, during the time when its power is lower, is working at a higher voltage. This means that there are local maxima present and that the system without OptiTrac is stuck at a lower producing maximum point while the system with OptiTrac is working at the absolute MPP. When the shadows are no longer cast over the generator, or only in a small amount, both systems start to work at the same voltage and output the same power. The energy gain obtained in this shading situation with the OptiTrac option is of

430Wh, which accounts for an extra 5.1% of the total daily energy generation without OptiTrac.

4.5.2.4.b Measurements at IES-Vallecas

The measurements performed at Vallecas aim at verifying what the theory that the reverse characteristics of the shaded cells and the number of modules connected in series determine the shape of the *I*-V curve and therefore influence the operation of the MPPT to the point of determining whether the absolute MPP is found or not. As was already shown in Figure 4.42, the reverse characteristics of the modules at Vallecas cause more distinct local maxima to appear. For these experiments two different strings were used: one with eight and one with twelve Siliken SLK 60 P6L modules and different progressive shading was applied to a different number of cells from different sub-modules. The inverter used is the Ingeteam Ingecon SunLite 5 (MPPT range: 160V-450V), one of the models tested with the SAS in section 4.5.2.3.

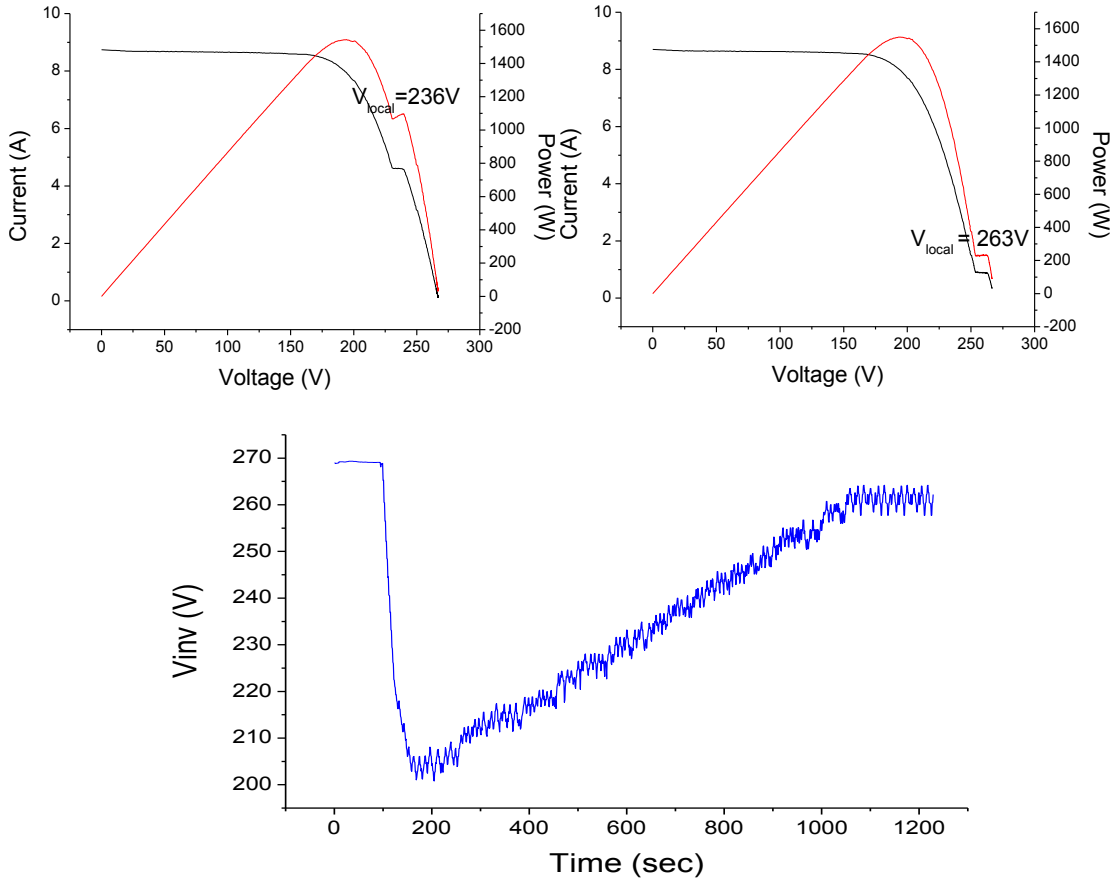

Figure 4.46: *I-V* and *P-V* curves of the eight module string with all ten cells from one sub-module shaded at 50% and 100% and the working voltage during the progressive shade applied (from 0% to 100%) to these ten cells,

Figure 4.46 shows the *I-V* and *P-V* curves of the eight module generator when ten cells of the same sub-module are shaded at 50% and 100% as well as the working voltage of the system during the progressive shade applied from 0% to 100%. This example is comparable to the experiment at Magic Box shown in Figure 4.44. The difference from both examples is that in this case the inverter's MPPT does not find the absolute MPP while with the modules of Magic Box the inverter does find the absolute MPP. This is basically due to the reverse characteristics of the cells of each module type, which in this case create more distinct local maxima in the *I-V* curve.

In the next experiment, the two lower cells of two modules (six sub-modules) were progressively shaded from 0% to 100%, simulating an incoming shadow from below, similar to the one produced from inter-row shading or from shading due to a tracker directly in front. Figure 4.47 shows the *I-V* and *P-V* curves at 0%, 25%, 50% and 100% shading over these two cells and the working voltage of the inverter during the progressive shading. From the results it is clear that in this case the inverter also fails to track the absolute MPP.

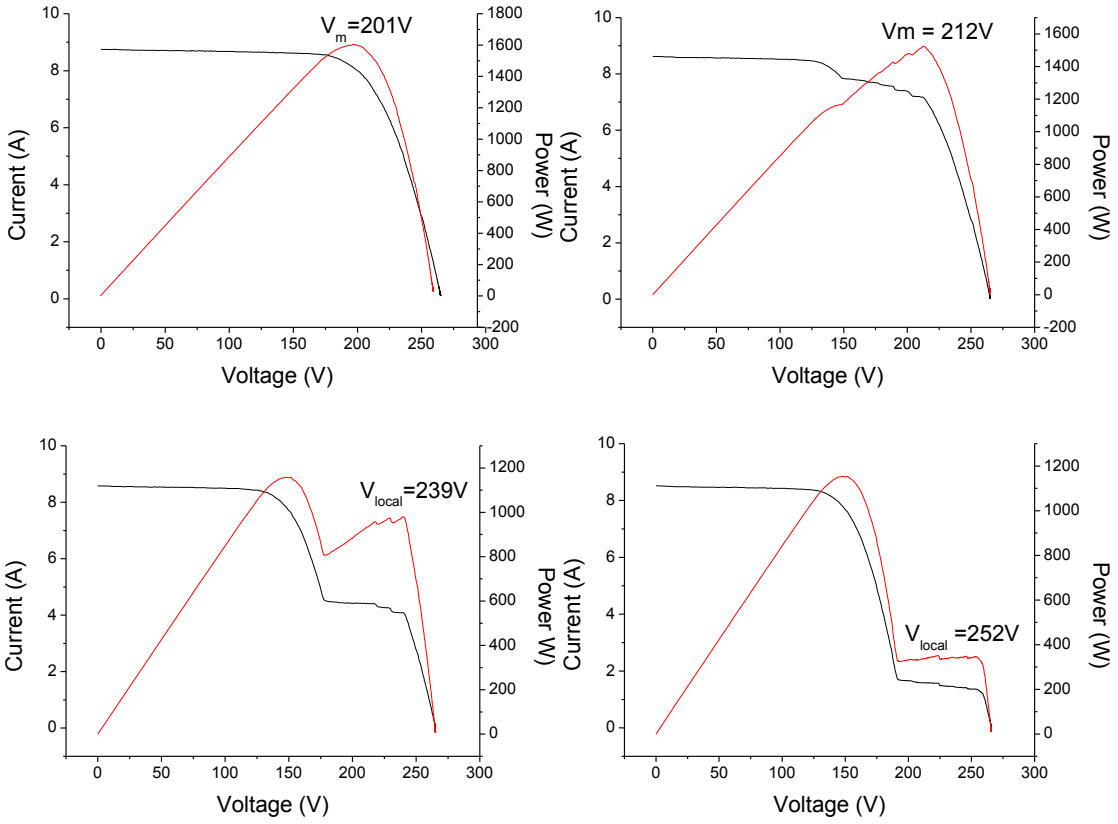

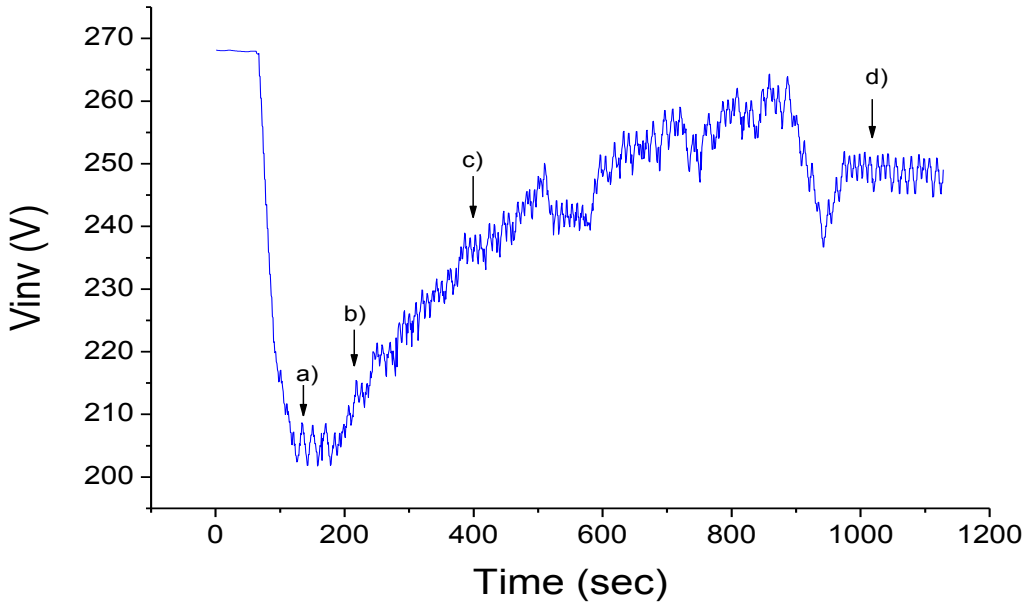

Figure 4.47: *I-V* and *P-V* curves at 0% (a), 25% (b), 50% (c) and 100% (d) shading over six sub-modules in an eight module generator and the working voltage of the inverter during the progressive shading. It can be seen how the inverter fails to track the absolute MPP remaining at a local maximum.

In order to analyse the influence of having more modules in series, the same shade as in the example of Figure 4.47 was applied to a generator of twelve modules connected in series. As was already presented in 4.5.2.2, systems with more modules in series are less prone to develop distinct local maxima for the same degree of shading. This is verified with these measurements and presented in Figure 4.48, where it can be clearly seen that in this case, for the same cell as in the previous example but with more modules connected in series, the inverter does finally track the MPP. Although it is true that this does not occur until almost the end of the measurement, it is very important that it does occur because once the MPPT is stuck at a local MPP it will not leave this point until the shadow exits the generator.

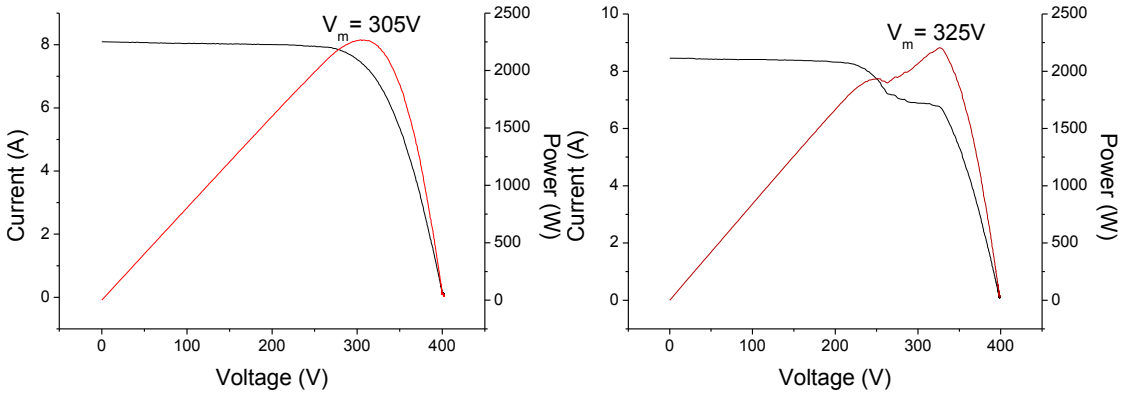

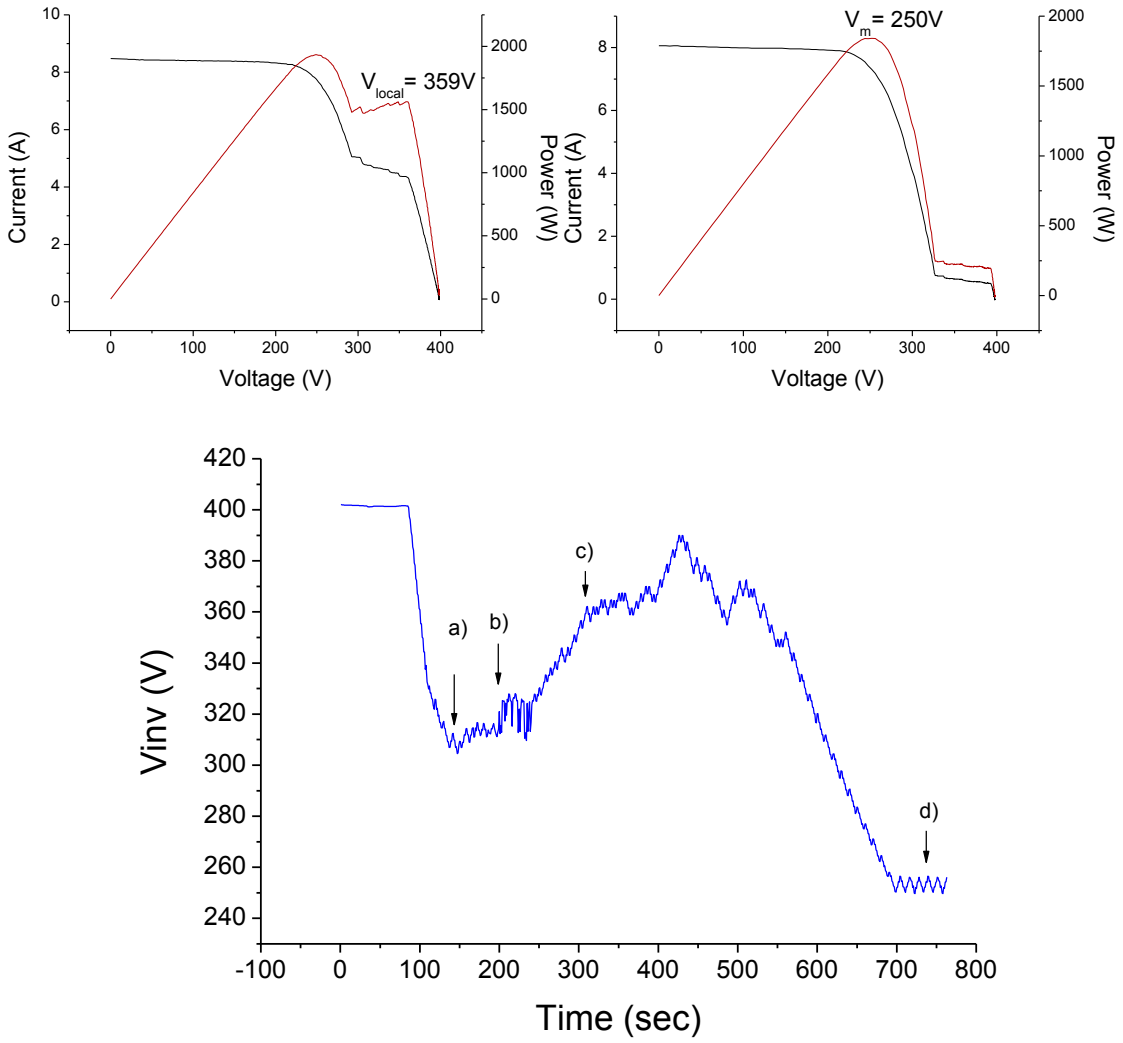

Figure 4.48: *I-V* and *P-V* curves at 0% (a), 25% (b), 50% (c) and 100% (d) shading over six sub-modules in a twelve module generator and the working voltage of the inverter during the progressive shading. It can be seen how in this case the inverter does find the absolute MPP.

Finally, one last example where shading is applied to three modules (nine sub-modules) of the twelve module generator shows that in this case (larger percentage of shaded sub-modules) the MPPT again fails to track the absolute MPP.

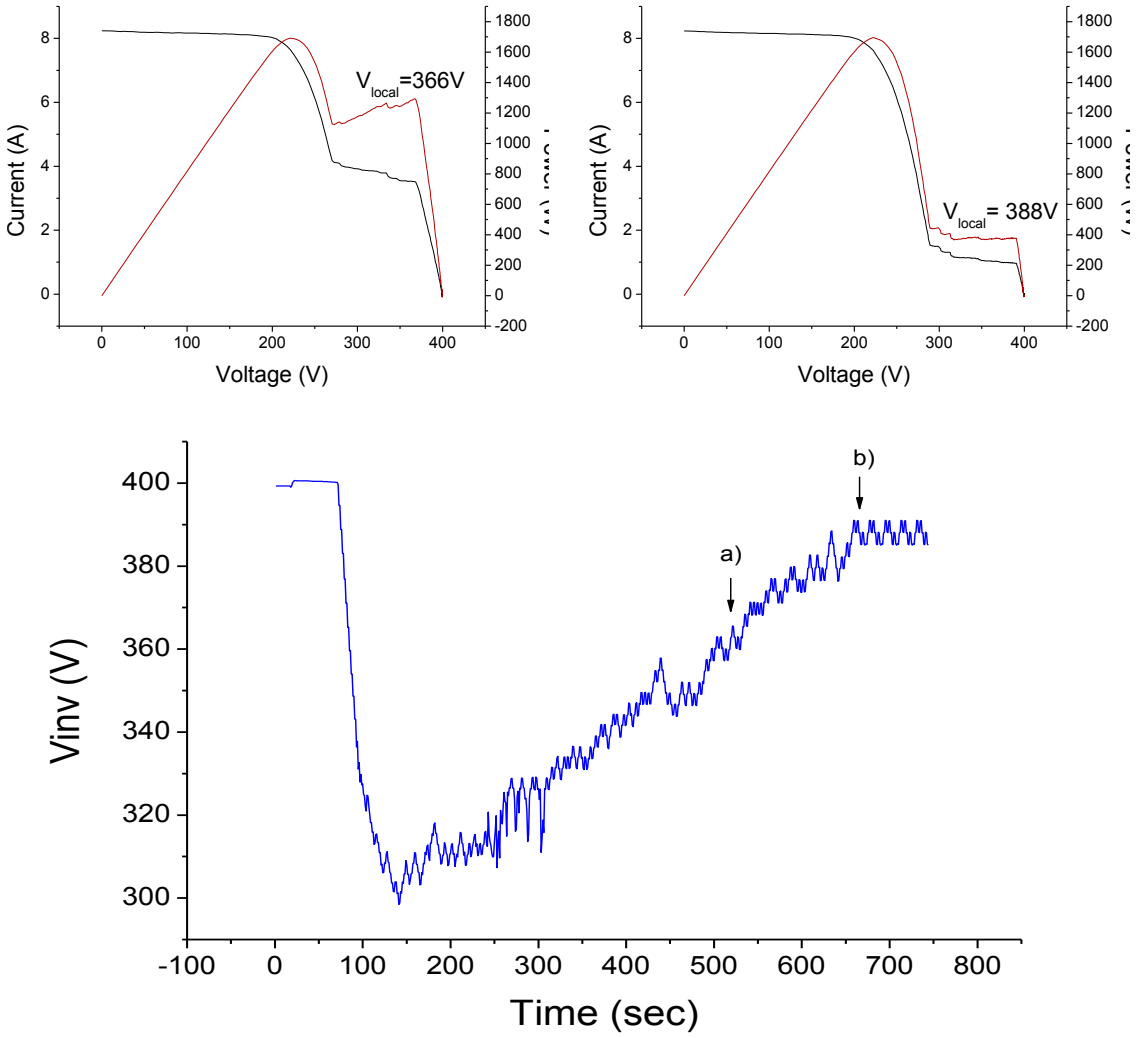

Figure 4.49: *I-V* and *P-V* curves at 50% (a) and 100% (b) shading over nine sub-modules in a twelve module generator and the working voltage of the inverter during the progressive shading. In this case, again the inverter fails to track the absolute MPP.

4.5.2.5 Conclusions on MPPT efficiency in presence of local maxima

Section 4.5.2 has analysed the effect on the MPPT of different equipment of local maxima appearing on *I-V* curves. More specifically the following points have been looked into:

- The effect of incoming shadows on the *I-V* curve of PV generators and individual modules.
- How do different MPPT algorithms react to *I-V* curves with distinct local maxima at start-up and during normal working. This has been studied with an SAS and in real PV systems.

With respect to the first point, the following conclusions have been drawn:

- Distinct local maxima are more probable to appear in generators with a lower number of modules in series. Therefore, MLPE are more susceptible to have MPPT inefficiencies in presence of local maxima and more emphasis in a good MPPT algorithm is necessary in MLPE.

- Incoming shadows tend to cause irregular shading over a PV array, causing each shaded cell to produce a different current and reducing the possibility of local maxima appearing during the incoming process. This allows the MPPT algorithm to shift to a lower voltage during the incoming process and when distinct local maxima are present (at the end of the incoming process) the working voltage is at the absolute MPP. Again, this is more probable to occur in PV generators than in individual modules.

- Shadows affecting the PV generator at start-up are probable to cause very distinct local maxima to appear on the *I-V* curve as, due to the low elevation of the sun, these shadows tend to cover a large part of the generator. In this case, inverters tend to not find the absolute MPP, remaining at a local maximum until the shadow exits the generator.

- Most of the MPPT algorithms that have been tested fail in finding the absolute MPP. What is even more disturbing is that all MLPE MPPT algorithms fail at finding the absolute MPP in presence of local maxima. One of the main aims of this technology is the mitigation of the power losses caused by shading and the fact that they fail in finding the absolute MPP in presence of local maxima is very contradictory.

4.5.3 Measurement protocol proposal for testing MPPT algorithms' capability of finding absolute MPPs in presence of local maxima

At present, the only international standard that focuses on measuring the MPPT efficiency of PV inverters is the European Standard EN 50530:2010 of title: *Overall efficiency of grid connected photovoltaic inverters* [CENELEC, 2010]. This standard

proposes the measurement of the static and dynamic MPPT efficiency of PV inverters. However, nothing related with *I*-V curves with local maxima is proposed. Previous measurements of different MPPT algorithms of commercial products have returned poor results (none so far can find the absolute MPP in presence of local maxima), which can cause large power losses in presence of shadows; added these to the losses due to lower irradiance caused by the shadow. For this reason, from the Instituto de Energía Solar we propose a testing protocol for testing the MPPT's capability of inverter's, micro-inverters and power optimizers to find the absolute MPP in *I-V* curves with local maxima. We are also studying the possibility of including this protocol, or a similar one, in the future IEC standard for testing the efficiency of PV inverters.

This protocol proposes two different experiments: at inverter start-up and during normal operation. Normally, during start-up, MPPT algorithms tend to either search the whole MPPT range or start directly at 80% of V_{OC}, sometimes allowing for the absolute MPP to be found in this case. During operation, whether the absolute MPP is found depends on the nature of the incoming shadow and the configuration of the PV array.

4.5.3.1 Testing at inverter start-up

The experiment at inverter start-up aims at reproducing a situation in which the PV array is shaded in the morning and when the inverter starts the *I-V* curve of the PV generator contains local maxima. From the experiments performed, we have seen three different possibilities: that the algorithm traces the whole *I-V* curve inside the MPPT range, that the algorithm jumps directly to a percentage of V_{OC}, in which in the three cases it has been around 80% of V_{OC} and then starts performing the P&O algorithm, or that the algorithm starts performing the P&O algorithm from the beginning. In the first case the absolute MPP will always be found. In the second case, whether the absolute MPP is found or not depends on where it is located with respect to the transition

point[26]. If it is located towards V_{OC} it will be found, otherwise it will not. Finally, in the third case, the absolute MPP will only be found if it is the point closest to V_{OC}.

For determining under which of these cases each algorithm falls into, the following is proposed. First, an *I-V* curve with three local MPPs should be used were the absolute MPP is closest to I_{SC}. This point should be located at most 5-10% from the minimum value of the MPPT range. One of the local MPPs should be located very close to V_{OC}, representing the most shaded sub-module; this point could be at around 90%-95% of V_{OC}. In turn, V_{OC} should be as close as possible to the maximum value of the MPPT range, i.e. 5% difference at most. A third MPP should be located between these two points and having the transition point between the point closest to V_{OC} and this point at a voltage higher that 85% of V_{OC}. Examples of the *I-V* and *P-V* curves that can be used for this test are shown in Figure 4.50.

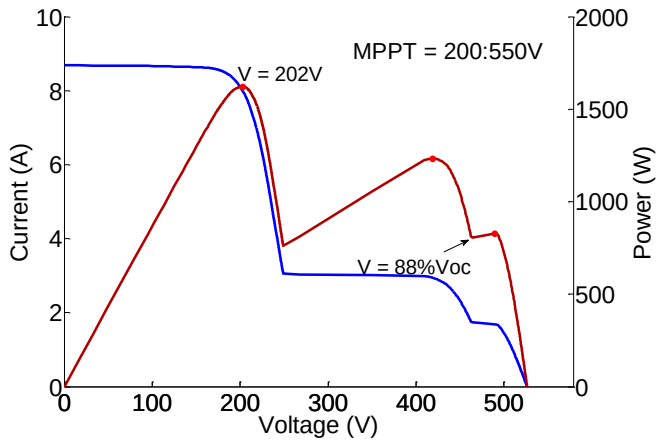

Figure 4.50: Examples of the *I-V* and *P-V* curves used for testing the capability of a device in finding the absolute MPP in presence of local MPPs.

If with this test the absolute MPP is found, the algorithm of this device will pass the test and be categorized as, *pass*: *full MPPT range immediately at start-up*. If the lowest power point is found, it will be categorized with a *fail*. If the middle point is found, a behaviour similar to that of the Ingeteam and SMA inverters shown in Figure 4.34 and Figure 4.35 is occurring. For this reason, a second test should be performed where the middle MPP is eliminated and the inverter is re-started with the new curve. The voltage, as a percentage of V_{OC}, at which the algorithm jumps to at inverter start-up should be

[26] The transition point is the point where the *P-V* curve changes from decreasing to increasing when coming from V_{OC} and which is shown as 85% of V_{OC} in Figure 4.39.

recorded and presented as a result. For example, the result for the SMA and Ingeteam inverters would be, *partial failure: 80% V_{OC}*.

If during the first test, the absolute MPP is not found, the curve should be left active until the working point stabilizes at one of the two MPP and from this moment the curve should be kept active for at least another 10 minutes. If during this time the absolute MPP is found, the test will be considered positive and the time taken to find the absolute MPP will be recorded, i.e, *pass: 6 minutes.*

4.5.3.2 Testing during normal operation

The experiments during normal operation aim at simulating the effect of a shadow entering the PV array at a time after start-up, i.e. at midday or during the afternoon. The input to the SAS should be a set of curves in which the first curve is a normal *I-V* curve (i.e. with no local maxima) and the following curves present gradual shading. Because as shading increases the voltage of the transition point also increases, the gradual shading of each curve should be kept small enough (in reality this is infinitesimally small) so that the increase of voltage of the transition region does not enter the MPPT voltage step of the working point, giving thus the possibility of passing the transition point in a non-realistic manner. This can also be obtained if the number of shaded sub-modules is large enough.

As has been seen in the measurements that are presented in section 4.5.2.3.b, there are some inverters that have the option of a periodic search of the *I-V* curve, thus finding the absolute MPP in presence of local maxima. However, even in this case there is a power loss because there is a period of time, before this periodic search in done, where the device is working at a local MPP (see Figure 4.37). The losses in this case depend on the time programmed for the periodic search. These losses will again occur as a new sub module starts to get shaded and a new absolute MPP appears. A shorter time will reduce these losses, although it will increase the losses of the static efficiency measurement defined in [CENELEC, 2010]. Ideally, a good algorithm would minimize the losses in both situations.

With the above said, this test aims at two things: verifying whether the absolute MPP when local maxima appear during operation is found and, in case that it is found, the efficiency of the algorithm. The test proposed is as follows:

- The first curve will be a normal *I-V* curve (i.e. with no local maxima) where V_{OC} is at least the maximum value of the MPPT range. This curve should be left active long enough so that the inverter finds the MPP and is stable.

- For inverters: once the working point is stable at the MPP, the shaded curves can be inputted. It will be considered that the shadow affects one module at a time; affecting all sub-modules of the module. For typical modules of 60 cells and three by-pass diodes, the transition region will be of 30V, larger than the voltage step of the MPPT algorithm, typically around ±7-8V. The decrease in irradiance over the shaded sub-modules will be done at 5% steps until an 85% irradiance decrease, for a total of 17 curves not including the non-shaded curve. Each curve will be kept on for one minute, which represents that it takes the shadow 17 minutes to completely cover one module. Once this point is reached, the next module (again with all three sub-modules being shaded) starts to have an irradiance decrease. This process is continued until the absolute MPP passes the minimum MPPT voltage.

- For MLPE: because now there is typically only three sub-modules under the same MPPT algorithm, it is proposed that in this case only one sub-module is shaded at a time. The same process will be done as in the previous case, but shading one sub-module at a time until the three sub-modules are shaded. Each curve will be left on for 30 seconds, as now the shadow only has to pass one sub-module.

Two results will be obtained from this test. First, a *pass* or *fail* will be given to each device considering whether or not the absolute MPP is found at some time during the test. In case that it is found, the percentage of energy lost in the process will be recorded and also given as a result.

4.6 HOT-SPOT MITIGATION IN PV ARRAYS WITH DMPPT

4.6.1 THEORETICAL ANALYSIS

This analysis supposes that the MPPT algorithm of the inverter, micro-inverter or power optimizer always finds the absolute MPP. As we have seen in the previous section this is not always true. However, we could say that it occurs most of the time in central MPPT systems, especially when only one or few cells are shaded, as would be the case here, and as the number of modules in series increases. In the case of DMPPT it is more probable that the absolute MPP is not found and this, despite the power loss, would actually benefit the hot-spot mitigation with DMPPT. So, in conclusion, we could say that what is presented here is a worst case benefit of hot-spot mitigation with DMPPT and the shading percentages for which DMPPT is hot-spot free could actually be higher, while those of central MPPT should not change in most situations.

4.6.1.1 Theory

When a solar cell is partially shaded, generally, two situations can occur:

a) the shaded cell works in reverse bias and matches the current of the non-shaded cells

b) the non-shaded cells reduce their current to match that of the shaded cell's.

Each of these possibilities creates a local MPP and the MPPT algorithm polarizes the array or module at the global MPP. In turn, this depends on the number of sub-modules for which the MPPT algorithm is applied and the amount of shade applied to the cell.

As an example we can consider a ten module PV generator with three by-pass diodes per module. If a cell is shaded by 20%, and the rest of the cells lower their current, a 20% power loss occurs in both a DMPPT system and a classic MPPT system. On the other hand, if the shaded cell is in reverse bias, and its negative voltage is enough to polarize the diode in forward bias, the power from a whole sub-module is lost. In a central MPPT system, the MPPT algorithm will detect a loss of approximately 1/30 (one sub-module out of 30) of the power and with DMPPT the algorithm detects a power loss of

approximately 1/3[27], since it is now at module level and there are three by-pass diodes. With DMPPT the algorithm will "choose" to reduce the current of the non-shaded cells while with central MPPT, the algorithm will "choose" to lose the power from a sub-module, meaning that the shaded cell will work in reverse bias with little shading in CMPPT but a larger shade is needed for this with DMPPT.

However, further considerations should be taken:

1) The shaded cell has some margin until it works in reverse bias: from I_M to I_{SC}, related to the shunt or parallel resistance, R_P.

2) If the non-shaded cells reduce their current they are also increasing their voltage, so the power lost is not exactly equal to the current reduction and it depends on the slope of the I-V curve from V_M to V_{OC}, which is related to the series resistance, R_S, of the cells.

3) The reverse characteristics of the shaded cell(s) will affect the power lost by the sub-module when the shaded cell(s) work(s) in reverse bias and, therefore, the decision of the MPPT algorithm.

In order to analyze all these effects a series of simulations have been performed with different PV modules and with cells of different reverse characteristics.

4.6.1.2 Simulations

These simulations have been performed with the real I-V curves of two different PV modules. Module-1 is made up of 60 mono-crystalline solar cells in series and three by-pass diodes and Module-2 of 72 poly-crystalline solar cells in series and four by-pass diodes. For each module type, ten modules are connected in series for the central MPPT simulations.

Both modules' I-V curves and their characteristic values are presented in Figure 4.51. Module-2 is the module that is used in the "in-field analysis" in section 4.6.2. From the curves it can be seen that Module-2 has a lower fill factor (FF), having both a lower R_p

[27] Note that in the global system the power loss is the same in both systems. 1/3 in one module out of ten is the same as 1/30.

and a higher R_s. These factors will influence the results of the simulations as seen further on in this same section.

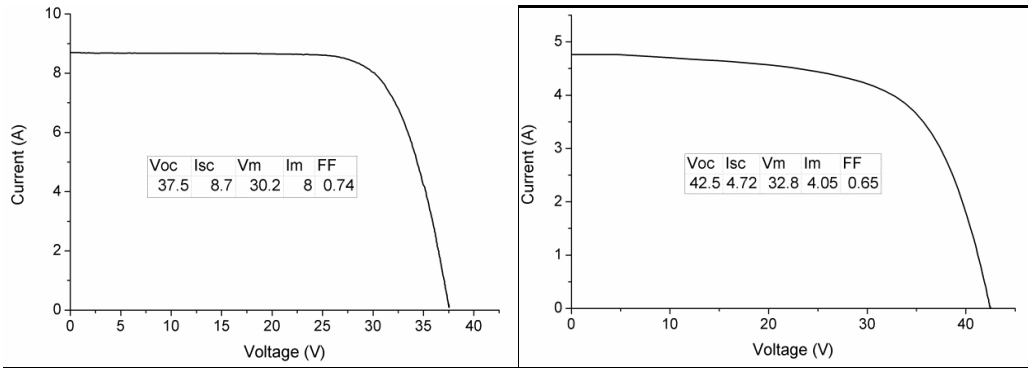

Figure 4.51: Real I-V curves of the modules used for the simulations and their main characteristics. Module-1 (left) and Module-2 (right).

The cell's reverse *I-V* curve has been modeled with equation (2.13), introduced and explained in section 2.1.3 and proposed in [Alonso-García and Ruíz, 2006]. The procedure for the simulations has also been explained in that section.

Large differences have been found in the reverse characteristics of solar cells in the same module [Alonso-García, Ruiz et al., 2006a]. These differences will affect the negative voltage at which each cell is biased and, therefore, the power lost by the system as well as whether the MPP is located at a point where the shaded cell is in reverse bias or not. For the two previous modules, the reverse characteristics of two cells have been obtained by shading these cells in different percentages, measuring the I-V curve of the module and then matching the simulated I-V curve with the measured one. This method was already presented and validated in [Solórzano-Moral, Masa-Bote et al., 2013b], using the same module as Module-1. The values obtained are: V_B = -27V and c =-0.0055 for "Module 1" and V_B = -6.5V and c =-0.005 for "Module 2". Both modules present clear differences in their I-V curves and in the reverse characteristics of their cells. Simulations have been carried out considering these differences and quite different results are obtained for each case.

For finding the shaded cell's working point, V_{m_c} and I_{m_c}, first the MPP of the module or generator (for DMPPT and central MPPT respectively) is obtained. We then consider that the current of the generator's MPP is the same as that of the shaded cell and we find the working voltage of the shaded cell. If this voltage is not negatively large enough to

forward bias the diode (as is the case with Module-2), this remains as the shaded cell's working point. If it is negatively large enough (Module-1), then the sub-module is isolated and considered to have a working voltage of -0.6V. Then, considering that the current through the shaded cell and the non-shaded cells under the same diode must be the same and that their voltages must add -0.6V, the working point of the shaded cell is obtained.

Figure 4.52 and Figure 4.53 show the working voltage of the shaded cell and its dissipated power as a function of the amount of shading for Module-1 and Module-2 respectively. It can be observed how there is an initial region where the shaded cell works in forward bias in both systems, region which depends on the difference between I_{SC} and I_M of each module; being it close to 12% for Module-1 and 17% for Module-2. In both cases, the MPP is found at a point where I_M is slightly reduced, expanding the range until the shaded cell works in reverse bias (note that the ratio between I_{SC} and I_M is ~8% and 14% respectively).

In both modules, after the initial region, 12% and 17% shade respectively, the cells in the central MPPT system start working in reverse bias and start to dissipate power. In the case of Module-1, the cell starts working in reverse-bias increasing its negative voltage and the dissipated power until it reaches a high enough negative voltage that places the diode in forward bias, at approximately -10.5V. At this point the diode limits the power dissipated by the shaded cell, accomplishing its function. Since the negative voltage at which the shaded cell is biased remains almost constant, due to the -0.6V imposed by the diode, as the shade increases, the working current decreases[28] and therefore the dissipated power also decreases, reaching a value of 0W at 100% shade.

[28] The lower current causes the non-shaded cells to slightly increase their voltage which in turn slightly increases the negative voltage of the shaded cell, from -10.5V to -12V approximately.

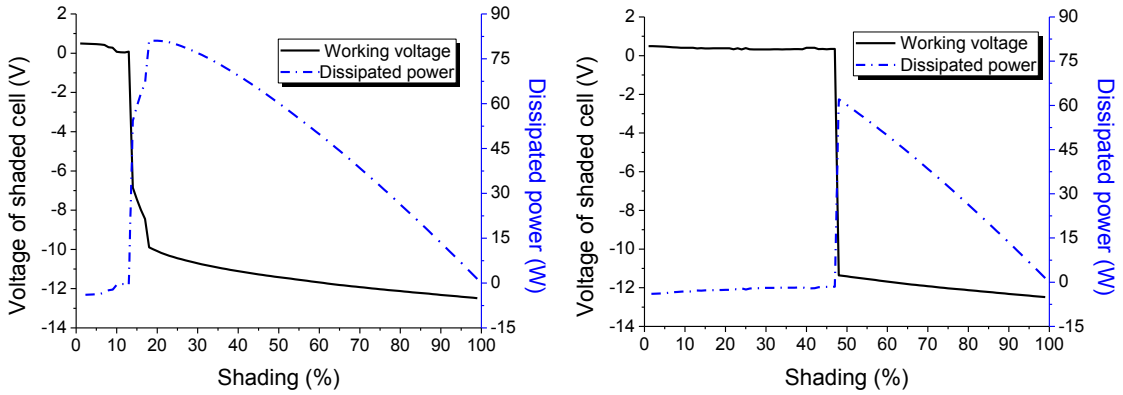

Figure 4.52: Comparison of the working voltage (solid line) and the power dissipated (dashed line) of the shaded cell in Module-1 in a ten module system for central MPPT (left) and DMPPT (right). With central MPPT the switch from forward to reverse bias is at 12% shade while with DMPPT it is at 48% shade.

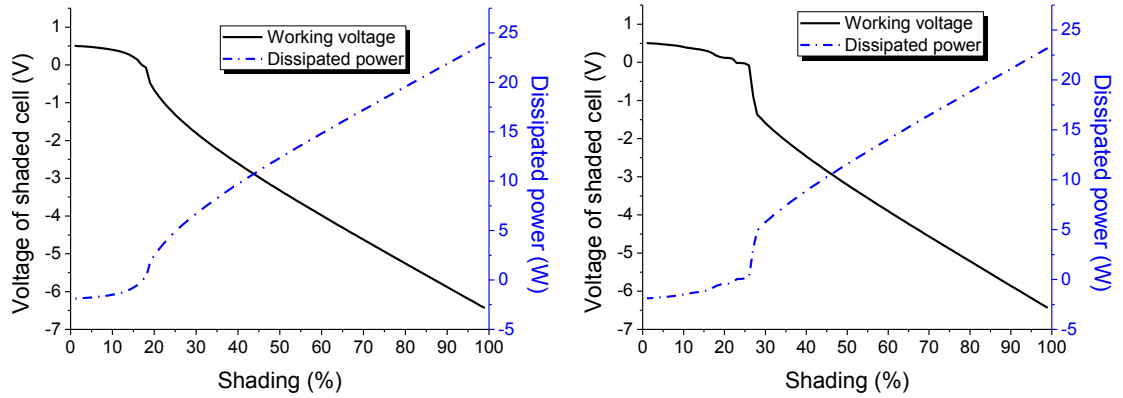

Figure 4.53: Comparison of the working voltage (solid line) and power dissipated (dashed line) of the shaded cell in Module-2 in a ten module system for central MPPT (left) and DMPPT (right). With central MPPT the switch from forward to reverse bias is at 17% shade while with DMPPT it is at 28% shade.

In the case of Module-2, since the maximum negative voltage of the shaded cell is not high enough to forward bias the diode, the dissipated power is always increasing and the working voltage always negatively increases until almost its maximum -6.5V (Figure 4.53).

In Module-1, from 12% to 48% the cell in the DMPPT system keeps on working in forward bias and does not dissipate any power, being, therefore, hot-spot risk free (Figure 4.52-right).

It should be noted that this range of shade is for which the cell in the CMPPT system dissipates the most power (see Figure 4.52), because the by-pass diode works progressively in reducing the dissipated power. So, in this case, not only does the system with DMPPT eliminate a shade range of possible hot-spots but it eliminates the worst

range. This occurs in modules with cells that have large breakdown voltages or high shunt resistances. From 48% onwards there is no difference in using central MPPT or DMPPT.

In Module-2, due to the difference in reverse characteristics of the shaded cell and to the larger number of by-pass diodes the range for which the shaded cell in the DMPPT system keeps on working in forward bias is much lower, from 17% to 28%. In addition, because the shaded cell's breakdown voltage is not high enough to polarize the by-pass diode in forward-bias, it never works in reducing the dissipated power, being it always incremental, as opposed to the previous case. Also, because the V_b of the shaded cell is lower, the maximum dissipated power is lower than the case for Module-1, although this isn't always synonymous to dissipating less heat as shown in [Alonso-García, Herrmann et al., 2003] and further experiments should be undertaken in this area.

Further simulations were conducted mixing the characteristics of both modules and adding new supposals, showing the results in Table 4.4. The table shows the percentage that a cell can be shaded before working in reverse bias for central MPPT and DMPPT systems. After these percentages of shade, the cell will work in reverse bias in both systems. It can be seen that in all cases the maximum shading that a cell can handle before working in reverse bias is higher in DMPPT systems. Having an shadow range where the shaded cell or cells do not work in reverse bias could solve hot-spot problems like those identified in [Lorenzo, Moretón et al., 2013].

Table 4.4: Maximum possible shade over one cell while it continues to work in forward bias.

	Maximum Shade	
	MPPT	DMPPT
Mod-1, Vb = -6.5V, diodes = 3	8%	19%
Mod-1, Vb = -27V, diodes = 2	12%	62%
Mod-1, Vb = -27V, diodes = 4	12%	40%
Mod-2, Vb = -27V, diodes = 4	20%	47%
Mod-2, Vb = -27V, diodes = 3	20%	55%
Mod-2, Vb = -6.5V, diodes = 3	17%	27%
Mod-2, Vb = -27V, diodes = 2	20%	66%

From the previous results and those shown in Table 4.4, it can be concluded that DMPPT is more beneficial against hot-spot problems in modules with a lower number of by-pass diodes and with a lower R_S as is the case with Module-1 (see Mod-1, Vb = -6.5V, diodes = 3 vs Mod-2, Vb = -6.5V, diodes = 3), as well as in cells with higher

breakdown voltages. A lower R_P means that more shade is needed for the cell to work in reverse bias, in both central MPPT and DMPPT.

This, however, does not necessarily mean that fewer diodes should be used in PV modules or that cells should be manufactured with lower FFs. The first point could be valid but it should be further investigated and the second point will cause a loss in efficiency which in some cases is worse than having a hot-spot. The second point could be valid when a very robust system is preferred over an efficient one.

4.6.2 IN FIELD ANALYSIS

The experimental verification has been conducted at the rooftop of the Institut National de l'Energie Solaire (INES) in Chambery, France, at midday and in the month of February 2013. The string used for the tests consists of ten PV modules of the same model as Module-2 used in the simulations. Two different experiments were carried out:

a) The string was connected to an inverter with a centralized MPPT and a solar cell in one of the ten modules shaded at different percentages. At each shading step, module voltage measurements and thermographic images were recorded.

b) The string was connected in a DMPPT system (each module to a power optimizer) and the same solar cell was shaded with the same pattern as before. Again, module voltage measurements and thermographic images were recorded.

During the experiments the shaded cell was monitored until it reached a stable temperature value, considered as the maximum value and I-V curves were recorded. During each shade step the cell was given enough time to cool down to the temperature of the non-shaded cell and the I-V curves were compared to those of the simulations with good agreement.

Table 4.5 shows the working voltage of the shaded module with central MPPT and DMPPT and the temperature difference between the shaded cell and the non-shaded cells. The results agree with what was exposed in the theory, showing that the shaded cell does not heat up more than the non-shaded cell until over 25% shading, that the non-shaded cells increase their voltage when shading is applied (the current is,

therefore, reduced) and also shows an approximate 5-5.5V drop in the module at 90% shade.

Table 4.5: Corrected working voltage of the shaded module and temperature difference between the shaded cell and the non-shaded cells, with central MPPT and DMPPT

	MPPT		DMPPT	
Shading (%)	V_{mod}	ΔT (°C)	V_{mod}	ΔT
0	32.5	0	32.5	0
10	33	2	33	0
20	31	18	33.5	1
25	30	18	35	1.9
40	29.4	19	29.7	2
50	28.3	20	28.5	19
75	28.1	20	28.2	20
90	27.1	19	27.5	20

For the DMPPT system there are shadows where a temperature difference is noticed although the shaded cell is not in reverse bias. However, it is a small difference, 1-2°C, which can be considered negligible. It could however be because the same amount of current is passing through a smaller area of cell than in the non-shaded cells. Although the dissipated power by the shaded cell increases as the shade increases, no significant increase in temperature difference was observed. For all shading percentages the temperature difference was practically the same. This could possibly be because of the low breakdown voltage of this cell in particular.

Figure 4.54 and Figure 4.55 show thermographic images for 25% and 50% shade with and without DMPPT. It can be seen that for 25% shade the cell in the DMPPT system is not hotter than the other cells while it is in the CMPPT system. However, with 50% shade, the cells in both systems are heated by practically the same amount. Although the temperatures are not very high, it should be noted that the measurements were taken in February in the French Alps and that these temperatures will be much higher in PV systems in southern Europe during the summer or other warm locations.

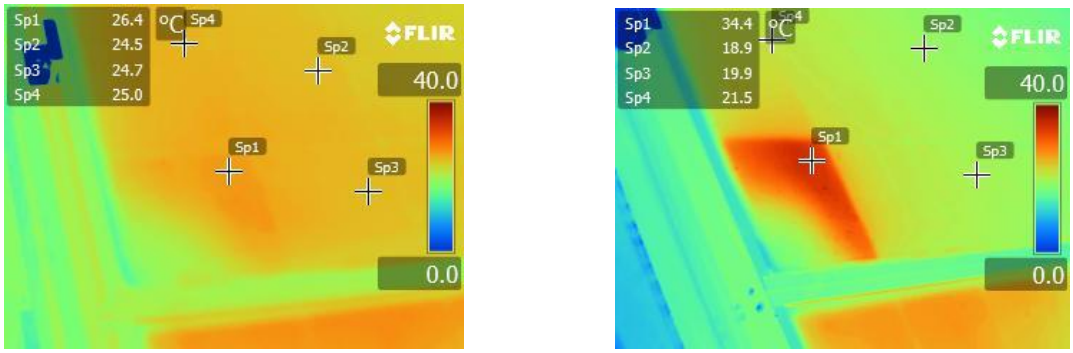

Figure 4.54: Thermographic images of shading over 25% of one cell for DMPPT (left) and central MPPT (right)

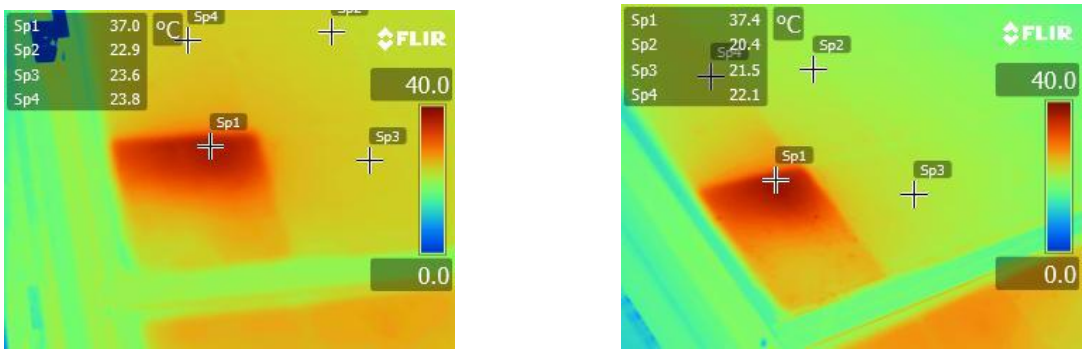

Figure 4.55: Thermographic images of shading over 50% of one cell for DMPPT (left) and central MPPT (right)

4.6.3 Conclusions

The effect of partial shading over one cell of a PV generator with central MPPT and DMPPT has been analyzed theoretically for modules with different characteristics and validated experimentally with one of the module types used for the simulations. The results show three different shading areas.

There is an initial area in which the shaded cell is not affected by hot-spots in either system. This depends on the difference between I_{SC} and I_M and, in turn, on the R_P.

A second area exists where central MPPT systems are affected by hot-spots and DMPPT systems are not. This area depends on the reverse characteristics of the shaded cell (mainly the breakdown voltage), the number of by-pass diodes and the R_S. This area is larger for modules with a lower number of by-pass diodes and with a lower R_S, as well as in cells with higher breakdown voltages. In one of the examples presented with real modules it ranges from 12% to 48%, meaning that cells of this module can handle up to 48% shade before working in reverse bias. And, in one of the simulations with supposed

modules it goes up to 66%. In addition, for shaded cells with high breakdown voltages, it is in this area of shade where the power that must be dissipated by the shaded cell in a central MPPT system is the highest, being it avoided in DMPPT systems.

Finally there is a third area where both systems are equally exposed to being affected by hot-spots and where the effect over the shaded cell is the same in both systems. In this area DMPPT has no benefit over central MPPT.

It has been shown that, in general, DMPPT systems are less prone to hot-spots, increasing the system's reliability and avoiding possible hot-spots in real PV systems like those pointed out by [Lorenzo, Moretón et al., 2013]. This is especially interesting for PV systems with little or difficult maintenance, like small rooftop PV systems (DMPPT's natural market).

5 ENERGY GAINS IN PV SYSTEMS WITH DMPPT

5.1 INTRODUCTION

Photovoltaic systems in the urban environment are more affected by shadows and dirt than ground mounted PV systems. These effects will cause losses due to less received radiation and will also cause losses due to mismatch between modules and an ineffective CMPPT. As has been presented throughout the thesis, the use of DMPPT at module level, whether power optimizers or micro-inverters, allows the independent MPPT of each module, solving part of the problems related to partial shadows, dirtiness or mismatching and making it possible to connect PV modules with different characteristics and tilt or orientation angles. The common denominator of the claims made by MLPE companies is the extra electricity produced by the use of their products, some claiming "extra power yields up to 30%" and others even claiming "up to 25% extra energy harvests".

In section 4.4 of this thesis and in other work [Orduz, Solórzano et al., 2011b; Podewils and Levitin, 2011; Sanz, Vidaurrazaga et al., 2011; Solórzano, Egido et al., 2010], various experimental tests have been presented that verify punctual power improvements due to different shading profiles. Various power improvement factors, normally around 10-15% but also up to 34%, can be observed as a function of the shade applied, the proportion of affected and non-affected modules, and also the interconnection of the modules.

To conclude whether the system is profitable or not further energetic and economic analysis must be carried out. The claim of up to 25% additional energy harvest is difficult to believe considering converter efficiency, non-static shading, shading at non-peak irradiance hours, etc, and more critical views [Rogalla, Burger et al., 2010] claim that with a 21% power increase, which is similar to the ones observed, only a 1% annual energy gain will be obtained.

All of these improvement factors depend greatly on the effect of shading on PV cells and the mismatch between them, which at the same time depends on their reverse characteristics. In other works, simulation models and experimental studies of the effects of shading on the I-V curve of a module have been conducted [Alonso-García, Ruiz et al., 2006a; Silvestre and Chouder, 2008], and these, combined with the analytical models and field results previously presented [Orduz, Solórzano et al., 2011b], have served as the base for a simulation model of the behaviour of PV generators with DMPPT converters.

This chapter presents a very detailed and precise simulation model for the estimation of possible energy improvements with the use of DMPPT techniques, as well as its verification, and simulation results of different PV generators with different shading patterns and module characteristics. At first, ideal energy gains are calculated, in which no differentiation is made between power optimizers and micro-inverters and which resulted in the following publication [Solórzano, Masa et al., 2011].

In a second part, the efficiency of the MLPE and inverters is introduced as well as the restriction due to limited conversion limits (section 3.5) of power optimizers and the inefficiency of MPPT algorithms in presence of local maxima (section 4.5.2). With the introductions of these parameters, new and more realistic energy gains were calculated as well as the losses due to each of these factors.

A third part presents the results obtained from experiments with a real PV system.

Finally a brief discussion of the economic viability of these systems is presented.

5.2 DESCRIPTION OF THE SIMULATION MODEL

The different tests that have been performed on DMPPT techniques in [Orduz, Solórzano et al., 2011b; Podewils and Levitin, 2011; Solórzano, Egido et al., 2010] have all been performed with real products and under real conditions. In [Orduz, Solórzano et al., 2011b] and [Solórzano, Egido et al., 2010] the devices were tested under real sun conditions and the whole generator, while under the same shade and practically at the same irradiance and temperature, was quickly switched from DMPPT to MPPT and the power improvement was recorded. In [Podewils and Levitin, 2011], thanks to the use of a large sun simulator, the tests were conducted in the laboratory and two generators were used, one with power optimizers and one without. However, these techniques are only suitable for measuring punctual power improvements and not for energy improvements over an extended period of time with varying irradiation and sun position.

In order to perform energy improvement tests under real conditions, two exact generators[29] under the exact same shading pattern and exposed to the same irradiance and temperature have to be under test for at least one year to consider all of the sun's positions and different irradiance and temperature conditions. Even if the exposed requirements are met, needing one year for each shading pattern makes this process not practical. In addition, these tests will be limited to weather patterns of only one location.

With the above exposed, it seems reasonable that a suitable model for simulating energy gains with DMPPT should be developed. For a detailed and precise analysis this model should consider, at least, the following points:

- The sun's relative position for a whole year with respect to the location (mainly latitude) of the generator
- Direct and diffuse components of the solar radiation every time period
- The shading profile on each module down to the cell level.

[29] Same number of modules and same interconnection; if there is a power difference this could be corrected.

- The distinct I-V curve of each module of the generator.
- The reverse characteristics of the I-V curve: these, when a cell is shaded, influence the I-V curve of the whole module and, therefore, that of the whole generator.

5.2.1 SOLAR RADIATION MODEL

The radiation data for Madrid used for this model comes from a weather station installed on the roof of the Instituto de Energía Solar (IES) building at Madrid, Spain: located at 40.5ºN and 3.7ºW. For this model, one minute interval values of direct horizontal radiation, *B(0)*, diffuse horizontal radiation, *D(0)*, and air temperature, T_a, are used. These values are averaged according to the time interval of the simulation.

These data are then converted to the tilt and orientation angles of the generator, with basic trigonometry for the beam radiation [Muneer, 2004] through equation (5.1).

$$B(\alpha,\beta) = \frac{B(0)\cdot \max(0, cos\theta_s)}{cos\theta_{zs}} \tag{5.1}$$

Where $cos\theta_S$ is the incidence angle of the sun's rays over the surface and $cos\theta_{ZS}$ is the zenith angle.

The calculation of the diffuse component over the PV generator is calculated using the Perez model for the diffuse radiation [Perez, Seals et al., 1987]. The governing expression in Perez's model is given in equation (5.2). The terms in brackets represent radiation, in the following order: from the background, from the circumsolar region, and from the horizon. k_3 and k_4 represent the contributions of the circumsolar and horizon regions to diffuse irradiation. *a* and *c* are, respectively, the values of the solid angle of the circumsolar region as seen from a surface with slope β and from a horizontal surface.

$$D_t(\propto,\beta) = D_t(0)\left[(1-k_3)\frac{(1+cos\beta)}{2} + k_3\frac{a}{c} + k_4 sin\beta\right] \tag{5.2}$$

With the exception of snowy grounds or vertically placed modules, the contribution of the reflected component is very small. For this model, the reflected component has not been considered.

The global radiation over the PV generator's surface is obtained with the sum of the two components as is equation (5.3).

$$G(\propto,\beta) = B(\propto,\beta) + D(\propto,\beta) \tag{5.3}$$

Shadows will affect each of these components in a different way, which is explained in the following section.

5.2.2 SHADING PROFILE MODEL

The shading profile module aims to characterize the shadows that affect each individual cell of the PV generator.

First of all, the obstacles surrounding the PV generator must be characterized. For every obstacle, the position of its relevant points relative to one point of the surface of the PV generator is used. The obstacle profile is a two dimensional function which describes the location of obstacles in the sky dome; a point in the sky dome is assigned the value of 1 if an obstacle is present or a value of 0 if the point is free of obstacles. The sky dome is defined in terms of azimuth, ranging from -180º to 180º, and elevation, from 0 to 90º. The obstacle profile contains all the information necessary to evaluate shadows and, therefore, estimate effective irradiation for the location at which it has been defined. The obstacle profile, defined in equation (5.4) , can be obtained from this collection of points.

$$OP(\psi,\gamma) = \begin{cases} 1; (\psi,\gamma) \ni obstacle \\ 0; otherwise \end{cases}; \psi = [-180,180], \gamma = [0,90] \tag{5.4}$$

In Figure 5.1 a representation of how the shadow profile is calculated for a whole PV generator and the shadow profiles obtained for two different points of the generator, G1 and G2, are shown. The generator is the same as the one that is simulated in section 5.4. It can be seen how the shadow profile is completely different for both points and if, for example, only the shadow profile from G1 were to be used the results would be that

there aren't any shadows on the generator along the whole year. From this comparison, the necessity of obtaining a shadow profile for various points of the generator is evident.

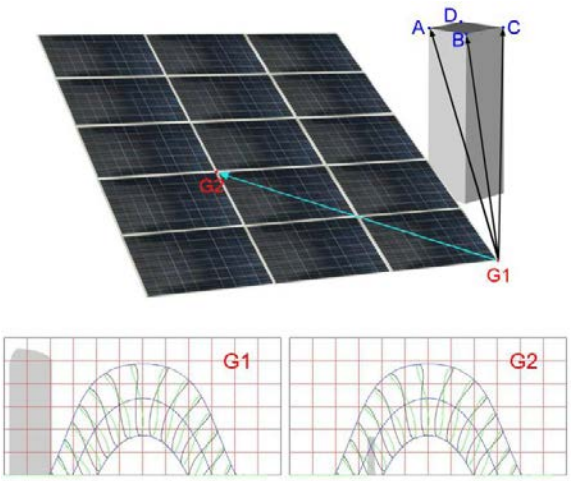

Figure 5.1: Representation of how the shadow profile is obtained and the two shadow profiles obtained for each point G1 and G2. From the comparison of both shadow profiles, the necessity of obtaining a shadow profile for various points of the generator is evident.

First, the location of the top points of the obstacle with respect to the south-eastern most corner of the generator is measured. In case the obstacle where to not be touching the ground, like in the case of a corbel, the bottom points of the obstacle should also be measured.

Since an obstacle profile is only valid for one point in the generator, it is necessary to obtain obstacle profiles for various points on the PV generator surface. As explained in section 5.3.1, a rectangular grid is defined over the generator's surface and a shadow profile for each point in the grid is calculated by translating the points in Table 5.1, which correspond to the coordinates of the object in the south-eastern most corner.

Table 5.1: The values obtained from the characterisation of the obstacles in Figure 5.1.

A(x,y,z)	B(x,y,z)	C(x,y,z)	D(x,y,z)
-0.1, -0.82, 2.76	-0.1, -0.32, 2.76	-0.6, -0.32, 2.76	-0.6, -0.82, 2.76

In this case, the chimney never affects G1 while it does affect G2 during certain time periods of the year. It can also be seen how the relative size of the obstacle decreases very quickly in a short distance. This indicates the importance of simulating the shadow profile down to the cell level, because in just a few cells the amount of shade can vary in a large amount.

Once the obstacle profile is calculated for every point of the PV generator, it is possible to calculate the radiation that reaches each point. We consider that points on

the generator that are blocked by the obstacle do not receive any direct radiation (beam + circumsolar). This is directly given by the obstacle profile calculated at each point of the PV generator.

For the diffuse radiation, its associated loss factor is the fraction of the sky dome "seen" by the generator which is blocked by the obstacle. For example, a PV façade with an infinitely high and long wall on one of its sides loses 50% of the diffuse radiation that it "sees" (note that being a façade, it already loses 50% of the sky dome).

5.2.3 *I-V* CURVE MODELLING

It is well known that shadows over PV modules affect their *I-V* curves and that this effect is conditioned by the reverse characteristics of the shaded solar cells as was seen in section 2.1.3 and also presented by various authors [Alonso-García, Ruiz et al., 2006b; Bishop, 1988; Silvestre and Chouder, 2008]. Despite this, most simulation software does not take the analysis of shadows to the level of the solar cell [Woyte, Nijs et al., 2003]. For this simulation tool it has been decided to model the *I-V* curve of each individual cell in the system. This is especially important for simulating energy gains with DMPPT as the largest power gains are obtained when a small percentage of a sub-module is shaded, as shown in section 3.4. Other models [Deline, Dobos et al., 2013; Martínez-Moreno, Muñoz et al., 2010; Masa-Bote and Caamaño-Martín, 2014] consider that when a shadow is cast over a sub-module this sub-module is by-passed, which is totally valid for large CMPPT systems. However, due to the nature of power gains with DMPPT this would not be valid for the simulations here proposed.

The *I-V* curve model used for these simulations and its validation has already been presented in section 2.1.3.1.

5.2.4 SHADING LOSSES AND ENERGY GAIN ESTIMATION

Combining the three models described above, an I-V curve for each module and for each time period in the simulations is obtained.

First of all, the extrapolated I-V curves and the shaded I-V curves are used to simulate the extrapolated generator and the shaded generator by simply adding together the I-V curves in the same way as the cell's I-V curves were added.

The comparison of the MPP of the shaded generator's I-V curve and the MPP of the extrapolated generator's I-V curve results in the shading losses.

The energy gain by the use of DMPPT techniques is obtained by adding the MPP of each module's shaded I-V curves for each time period. Comparing this sum with the sum of the MPPs for each time period of the shaded generator, results in the power gain with the use of DMPPT. It must be noted that this energy gain also takes into account any mismatch in the original I-V curves, so even if there is no shading present some energy gain could be obtained.

5.3 VALIDATION OF THE MODEL

This section presents a series of tests that have been conducted in order to validate the model and to show its precision. It is focused on validating the shading profile model and the I-V curve simulation model related to the shading model. The validation of the *I-V* curve simulation model by itself is already presented in section 2.1.3.2.

All the experimental tests were done at the roof of the Instituto de Energía Solar in Madrid in days close to the winter solstice and between 10:00 and 14:00 solar time. The equipment used was: a PV module, a photographic camera, a computer, an oscilloscope and an I-V curve tracer.

The PV module used consists of 60 cells in series, in 6 columns, and three by-pass diodes. Every two columns are protected by one by-pass diode. Pictures are shown in Figure 5.2.

5.3.1 SHADING PROFILE MODEL

The procedure used for validating the shading profile model consists in projecting shadows over a module from different obstacles, taking a photograph of the shade at a

certain time of the day and comparing this photograph with the shading profile obtained from the model.

All the shadows applied to the PV modules were cast by nearby rectangular objects. The exact dimensions and the distance to the modules of the obstacles were measured and a shading profile for each minute of the day was obtained. For all the shadows measured, the simulated shading profile was in very good agreement with the real shadow cast by the object.

Two differences were observed between the simulation and the real shadow. These were: a small displacement in time and an error due to the discrete nature of the simulated shading profile.

The small displacement in time has no worse effect than not matching the irradiance and temperature of the exact moment with the exact shading profile. Being the difference less than five minutes, this effect can be considered negligible.

Due to the finite number of points defined in the shading profile (equation (5.4)) an error, analogous to the quantification error of any digital machine, is inevitable. For the simulations presented in this paper different resolutions have been used. In this section shading profiles with a 4x4 resolution[30] per cell are presented and the borders of the shadow are smoothed, as explained in section 5.2.2, in order to minimize the error. Therefore, in these simulations, the maximum error is ±12.5% of shade in each cell.

This, at first glance, can seem like an enormous error to consider the simulations as valid. However, we must understand that this is an instantaneous error and it is far from the overall error; and various simulations back it up. There are mainly two reasons for this. The first one is that the error in a cell is mainly only traduced to an error in the I-V curve when it occurs in the most shaded cell in a diode zone; since it is this cell that limits the current through the series. Once a cell is shaded 100% in one diode zone, the error committed in the shading of the other cells has very little influence on the I-V curve.

[30] In total for a module of 6x10 cells and a 4x4 resolution per cell, 960 points are modeled.

And, secondly, since the shadows cast by static objects sweep the whole generator from left to right, there will be times when the error is positive and others when it is negative, compensating itself and reducing the final error.

Figure 5.2 shows two pictures of two shaded modules, their shadow profile (in red) and the percentage of shaded cell estimated with border smoothing. Looking at the picture on the right, we can see that we are underestimating the maximum shade on the fifth column, being the real shadow close to 20% in the bottom cell, and overestimating the maximum shade on the fourth column. On the picture of the left, there is an underestimation of the maximum shaded cell on the third column. The effects of this are presented in the following section.

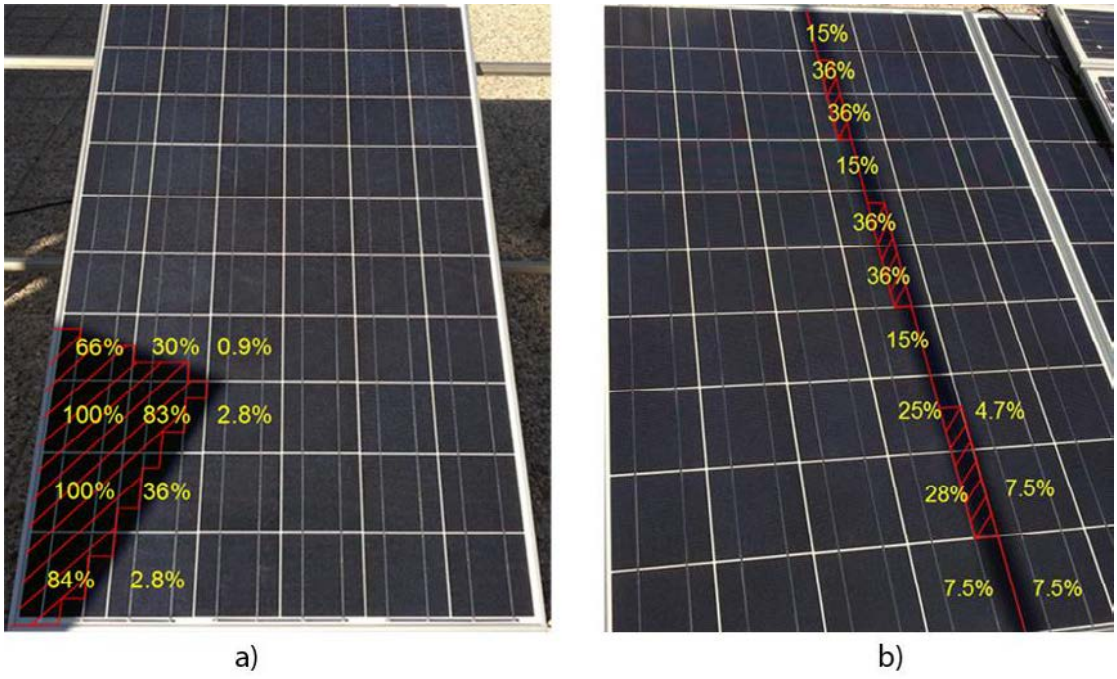

Figure 5.2: Shows two pictures of shaded modules with different shading patterns (one resulting from a medium or large sized object, i.e. chimney or building and the other from a small sized object, i.e. pole or antenna), their shadow profile obtained (in red), and the shading percentage obtained for each cell with the described procedure.

5.3.2 *I-V* CURVE VALIDATION

The validation of the *I-V* curve model has been presented in section 2.1.3. In that section the shading over each cell was inputted manually by the user. Now, for the model presented in this chapter, the shading over each cell is automatically inputted with the

shading profile model described in section 5.2.2. The objective of what is here presented is to validate that the *I-V* curves obtained with this procedure are also accurate.

Figure 5.3 shows the measured and simulated I-V curves of the shading profiles in of Figure 5.2. In these curves the errors from the I-V curve simulation and the shading profile simulation are both present, being the most important error due to the shading profile quantification. Each figure compares the measured I-V curve with two simulated curves: one with a 4x4 resolution in each cell and one with an 8x8 resolution in each cell. It can be seen how in both cases the 8x8 resolution results in a better simulation, being it especially important in the case of the shadow from the pole were the shadow does not cover entire cells.

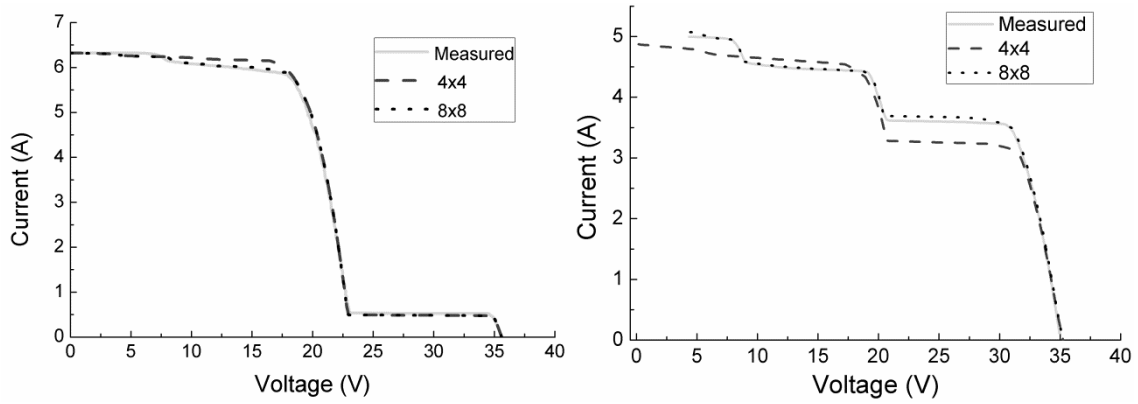

Figure 5.3: Shows the measured and simulated *I-V* curves from Figure 5.2 for a 4x4 and 8x8 resolution per cell.

It must be understood that the punctual shade presented of the solid object of Figure 5.2(a) is very rare. The tiny bit of shade on the third column, and second by-pass diode area is what makes it very difficult to simulate correctly. On the other hand, the thin object will always cast shadows which are difficult to simulate without a high resolution. More on this will be presented in the following section.

5.4 PERFORMED SIMULATIONS

Now that the model is validated, it can be used to simulate the energy gain obtained with the use of DMPPT in different situations. All of the following simulations are yearly, considering the sun's relative position and the different irradiance and ambient temperature at every time period. The process is as follows:

1. Extrapolate to the conditions of each time period [IEC, 2009].
2. Calculate the I-V curve of one cell and assume that all the cells in the module have the same I-V curve.
3. Simply divide the current by the number of cells in parallel and the voltage by the number of cells in series.
4. Calculate the cell's I-V curve in the second quadrant.
5. Use equation (2.13) with the adjusted parameters.
6. For each cell, multiply the current of each point of the I-V curve by its shading factor.
7. Add all the cells together to form the module.
    - For the cells in series: add the voltage of each cell for a given current.
    - For the cells in parallel: add the current of each cell for a given voltage.
8. Add all the modules together to form the generator.
    - For the modules in series: add the voltage of each module for a given current.
    - For the modules in parallel: add the current of each module for a given voltage.

When considering energy gains, two different concepts are usually taken into consideration: one is the percentage of recovered energy, E_R. That is, of all the energy lost how much is recovered. And the other is the improvement in energy, E_I, with respect to the centralized MPPT system; how much better is the DMPPT system than the MPPT system. They are both presented in equations (5.5) and (5.6).

$$E_I = \frac{E_{DMMPT} - E_{MPPT}}{E_{MPPT}} \tag{5.5}$$

$$E_R = \frac{E_{DMPPT} - E_{MPPT}}{E_{MAX} - E_{MPPT}} \tag{5.6}$$

Where E_{DMPPT} represents the generated energy with DMPPT, E_{MPPT} represents the energy generated with a centralized MPPT and E_{MAX} represents the maximum possible

extracted energy; that is the sum of the energy generated by each individual module considering there are no shadows.

It can be observed that E_R has a maximum value of 100%; all the lost energy is recovered and $E_{DMPPT} = E_{MAX}$. This would happen, for example, in the case of mismatch between modules when no shading is present.

On the other hand, E_I does not have a maximum limit; it can have values over 100%, although it is not normally the case.

The recovered energy tends to have a much higher value and commercial firms tend to use both values, sometimes focusing more on E_R; probably for marketing purposes. However, it must be understood that the real important value is E_I, and if this value is low there will be no interest in using DMPPT even if E_R is 100%.

5.4.1 IDEAL ENERGY GAIN SIMULATIONS

At first, simulations of ideal energy gains have been performed. These consider the power conversion efficiency of both the CMPPT and DMPPT systems to be equal, that the MPPT always finds the MPP and that there are no limitations due to the output limits of power optimizers. These simulations here presented are similar to those presented in [Solórzano-Moral, Masa-Bote et al., 2013a] but with some improvements. The irradiance threshold has been lowered to 50W/m^2, the number of simulated points for the *I-V* curves of the modules and the generator has been increased to 1024 and the effect of the irradiance on the voltage of the *I-V* curve has been added. This returns slightly different results, being the ones here presented more realistic. Just like in the previous publication, the effect of the mismatch of electrical characteristics is not considered.

In a second phase, the same simulations have been performed but including the efficiency of both the MLPE and inverters, the effects of the MPPT algorithms of each model (which have been analysed in section 4.5) and the limitations due to the output limits of power optimizers (section 3.5). The objective of these simulations is to present a more realistic model and more importantly to allow analysing the losses of each cause individually.

5.4.1.1 Single-family household

The first system that has been simulated is shown in Figure 5.4. It corresponds to a 34º tilted and south facing house roof with a chimney which shades part of the modules. This system was chosen as it already incorporates power optimizers to mitigate the losses and was used as a case study by SolarEdge [SolarEdge, 2010], the installer, to publicize the possible energy gains obtained with their system in presence of shadows; in this case the shadow cast by the chimney. The energy gains were calculated with PVSyst, a well-known simulation software. For calculating energy gains with DMPPT, PVSyst states that "the near shadings should be considered "Linear", i.e. without string partition" as is both stated in the case study and in the PVSyst files [PVSyst, 2014]. What this translates to is that while for CMPPT the effect of by-pass diodes is being considered, i.e. one shaded cell of a sub-module causes the loss of the sub-module, with DMPPT only the shaded fraction is being considered as lost, i.e. one shaded cell only causes a loss of 1/60 of the module (instead of 1/3)[31]. The analysis done this way leads to an energy gain of 12.5% (the losses in CMPPT cause a "loss of 13.4% of their potential energy while the real loss caused by the shaded area is merely 1.5%). As we will see further on in this section, the real gain is far from this 12.5%. The case study is included in Appendix B to serve as a reference.

The generator is composed of two series connected strings of 15 modules, each connected to a 3.3kW inverter. For the simulation only one string has been simulated, which corresponds to the series connection of the five bottom rows of the modules to the left of the chimney; the other one is less affected by shadows.

Figure 5.4: Image of the PV system used for the simulations of the single-family household. The real installation is divided into two strings with two different inverters. For the simulations only the string composed of the 15 modules in the three most-left columns and five lower rows were considered.

[31] For sixty cell modules with three by-pass diodes.

The chimney has been modelled as a rectangular cube with a 50x50cm base and a 2 meter height on its shorter side. It is separated 10 cm from the string and its top left corner coincides with the top right corner of the bottom row of modules.

Various annual simulations with different parameters have been performed: the resolution of the shadow profile has been varied, radiation data from Madrid has been used, and different shading profiles (and shading losses) for each location have been calculated; taking into account the relative position of the sun in both locations.

Table 5.2 shows the results obtained in each simulation for different resolutions with a 15 minute time step. In addition the same simulations were performed while changing the obstacle to model an antenna. Everything was kept the same except for the size of the base which was changed to 5x5cm[32]. The results obtained are shown in Table 5.3.

The simulations show that the possible energy gains for the PV system shaded by the chimney are not very large, around 2.3%, and much smaller than the 12.5% obtained with the simulation software PVSyst (Appendix B). Because the model here presented is much more precise than the one used by PVSyst, it seems logical to consider these energy gains as more realistic. A quick and easy calculation also leans the results towards the ones obtained with this model. Let's consider that three modules are completely shaded at all times and that there is a D/G ratio of 15%. Let's also consider that the non-shaded modules are always working at a V_M = 30V, that there are three by-pass diodes per module and that the bias voltage of the diode is -0.7V. In this situation the power gain would be constant and could be calculated as in equation (5.7), where the first term represents the power gain by adding three modules at 15% power to the twelve already working and the second term represents the power gain obtained by eliminating the negative voltage of the nine diodes in the CMPPT system.

$$\frac{12 + 3 * 0.15}{12} + \frac{30 * 12}{30 * 12 - 0.7 * 9} = 5.53\% \qquad (5.7)$$

Even in this situation, which is exaggerated with respect to the real shading cast by the chimney as shading occurs during less than half of the day and most of it during low energy periods, the gain is only of 5.53%. If we consider this situation during only half of

[32] The size of one cell of the modules is of 16x16cm so the antenna never shadows a whole cell.

the periods, the gain is of 2.26%, almost identical to that obtained with the yearly simulations.

Table 5.2: Annual simulation results with different parameters for the system of Figure 5.4, the single-family household.

Resolution	Max possible Energy	Energy lost without DMPPT	Max Gain	E_R	E_I
1x1		559 kWh (8.69%)	46.6%	34.0%	3.24%
2x2		534 kWh (8.30%)	42.0%	26.9%	2.44%
4x4	6.43 MWh	531 kWh (8.26%)	41.9%	25.0%	2.26%
8x8		539 kWh (8.38%)	42.0%	25.4%	2.33%
16x16		541 kWh (8.41%)	42.0%	25.3%	2.32%

Table 5.3: Simulation results changing the chimney for an antenna for the system of Figure 5.4, the single-family household.

Resolution	Max possible Energy	Energy lost without DMPPT	Max Gain	E_R	E_I
1x1		179 kWh (2.78%)	13.9%	71.9%	2.06%
2x2		234 kWh (3.64%)	19.1%	74.8%	2.82%
4x4	6.43 MWh	281 kWh (4.37%)	24.2%	71.9%	3.28%
8x8		310 kWh (4.82%)	30.0%	66.8%	3.38%
16x16		317 kWh (4.93%)	33.2%	63.3%	3.29%
32x32		320 kWh (4.98%)	32.4%	61.5%	3.23%

From the previous two tables we can observe the importance of considering the amount of shade on individual cells for simulating energy gains with DMPPT. When simulating large objects, a 2x2 resolution is probably more than enough. However, in objects like antennas at least a 4x4 resolution should be used.

For large objects, the difference between the energy lost with a 1x1 resolution and a 16x16 resolution is around 3%. With respect to the energy gain values, these become very stable starting at a 4x4 resolution, while there being a difference of almost 30% with the value obtained for a 1x1 resolution. This brings to our attention that although a model that does not consider the amount of shade on individual cells, like in [Deline,

Dobos et al., 2013; Martínez-Moreno, Muñoz et al., 2010; Masa-Bote and Caamaño-Martín, 2014], can be accurate in determining shading losses, it is not enough for estimating energy gains with DMPPT. It is even more evident in the case of thin objects like antennas.

We can also see that although the antenna is responsible for less energy losses, due to the high energy recovered, E_R, the final energy improvement, E_I, is higher and, therefore, also the interest in using DMPPT. This coincides with the results obtained in [Solórzano, Egido et al., 2010] and [Orduz, Solórzano et al., 2011b] which show that higher power gains are obtained for shadows that do not cover entire cells. It is also in accordance with what is exposed in section 3.4.1.2 of this thesis which shows that the highest power gains are obtained when the shadow does not cover entire cells.

The large difference between the maximum instantaneous gain and the total yearly gain should also be observed. This corroborates the hypothesis formulated in [Orduz, Solórzano et al., 2011b] and [Rogalla, Burger et al., 2010] which stated that although large instantaneous power gains are possible the overall yearly gain would be much lower, due to various factors like the stationary nature of the objects (shade during only one part of the day) and the different position of the sun throughout the year (higher means less shade). Both maximum gains occur close to the winter solstice, 21st of October and 13th of December for the chimney and antenna respectively, and in the first period of the day as is expected due to the lower elevation of the sun and longer shadows.

Another of the hypothesis formulated in previous work is that DMPPT will have less effect in locations or periods of a higher percentage of diffuse radiation. This could be true as when there is a large percentage of diffuse radiation, shadow have a lower effect. However, the D/G ratio also increases and as it has been previously seen this can produce higher power gains. In order to verify this, the two previous systems were simulated with radiation data from Stuttgart for both location (the same percentage of diffuse radiation and different sun position throughout the year). The yearly radiation data used for Madrid summed up to 1720kWh (results of Table 5.2 and Table 5.3) with a 29% of diffuse radiation on a horizontal plane, while that of Stuttgart summed up to 1250kWh with a 45% of diffuse radiation. The results are shown in Table 5.4.

Table 5.4: Simulation results for radiation data of Stuttgart, Germany, considering the obstacle being in Madrid and for a 4x4 resolution.

Obstacle	Max possible Energy	Energy lost without DMPPT	Max Gain	E_R	E_I
Antenna	4.71MWh	250 kWh (5.31%)	30%	60.8%	3.04%
Chimney	4.71MWh	450 kWh (9.54%)	20.7%	32.3%	2.68%

From this last simulation we can observe that in the case of large objects close to the PV generator, like the chimney, the diffuse fraction is also very important, obtaining a little more energy gain when the percentage of diffuse radiation has increased (compare the last result of Table 5.4 with the 4x4 resolution result of Table 5.2) . This is due to the fact that the modules close to the chimney are losing a large part of their diffuse radiation during all hours, which creates a constant mismatch in the PV generator and, therefore, a constant energy gain. The D/G ratio is also important, since with the large object there will be many time periods in which many modules are completely shaded and which are producing power only with diffuse radiation. Because this component is higher in Stuttgart, slightly higher energy gains are obtained.

This is, however, not true for thin objects, like the antenna. For the case of the antenna, less energy gain is obtained in Stuttgart as compared to Madrid, because the antenna has very little effect over the diffuse radiation available over the generator.

5.4.1.2 Building in an urban environment

In addition to the previous system, a PV installation in a more complex and more urban environment has been simulated. It is a 5kW PV system right in the centre of Madrid, Spain, belonging to the Institute for Research in Technology of the Universidad Pontificia de Comillas (IIT-UPC). The installation faces 18º west and the modules are tilted on a 29º angle. The 40 modules are grouped into five strings, of eight modules each, connected in parallel. The electrical diagram and a picture of the installation with the four obstacles that cast shade over the modules can be seen in Figure 5.5. The five strings are modules 1-8, 9-16, 17-24, 25-32 and 33-40, respectively.

The modules of the installation are the ATERSA A120 model, of the following characteristics: P_M = 120W, V_M = 16.9V, V_{OC} = 21V, I_M = 7.1A and I_{SC} = 7.7A. Since it

was not possible to stop the system from working and measure all the module's I-V curves, the exponential model of equation (5.8) was used to simulate the I-V curve of one module. All of the modules were assumed to have the same I-V curve, so no mismatch was considered.

$$V(I) = \frac{\frac{V_{OC} \cdot ln\left[2-\left(\frac{I}{I_{SC}}\right)^{R_P}\right]}{\ln(2)} - R_S(I - I_{SC})}{1 + \frac{R_S \cdot I_{SC}}{V_{OC}}} \tag{5.8}$$

Because of the limited space available on their rooftop, their PV installation is heavily affected by shadows of nearby objects. The main shading objects are: a building, an antenna, a wall and a metal structure; all shown in Figure 5.5 and numbered 1 to 4. In this case, a one year simulation with only the Madrid weather data and a 4x4 resolution in each cell was performed. The results obtained are shown in Table 5.5.

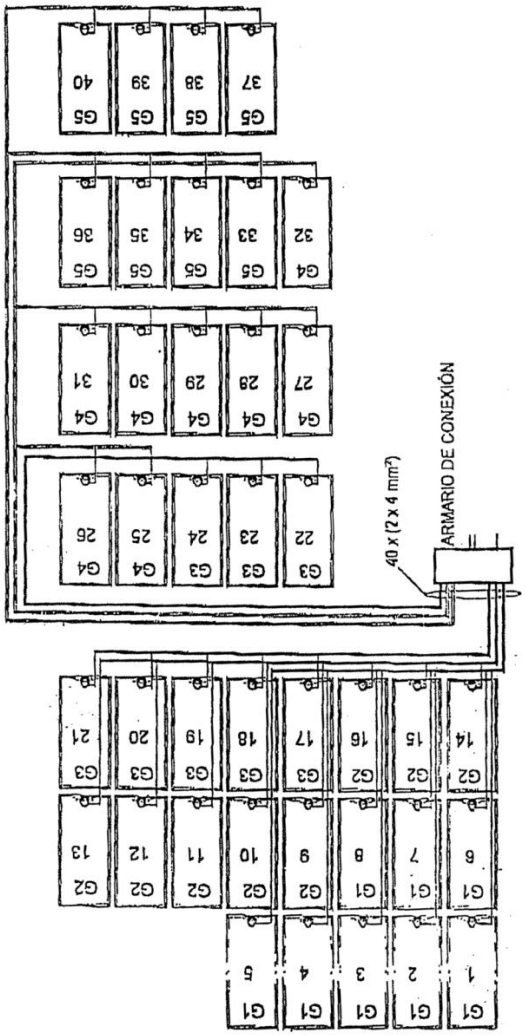

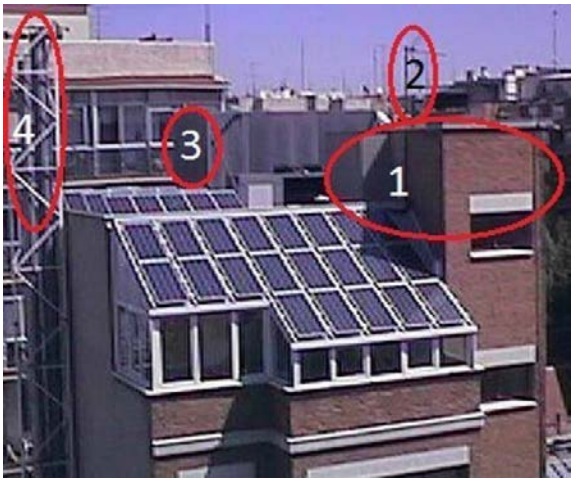

Figure 5.5: Electrical diagram and picture, with the nearby obstacles highlighted, of the PV installation of ICAII used for the energy gain simulations.

Table 5.5: Simulation results obtained for the urban PV system

Max possible Energy	Energy lost without DMPPT	Max Gain	E_R	E_I
8.31 MWh	3.09MWh (37.2%)	200%	28.3%	16.8%

With the idea of showing how the energy improvement varies along the year, Figure 5.6 shows the energy improvement during two different clear days, winter (left) and summer (right), and the on-plane irradiation, for the ICAII installation. It can be seen that during the winter days there is an improvement throughout the whole day, meaning that shade affects the system throughout the whole day, due to the sun being in a lower position. During the summer days, due to the sun's higher position, the installation is free of shades in mid-day and there is no energy improvement during those periods. The x-axis represents solar time and it is observed that the on-plane irradiance is a bit displaced from solar noon due to the installation facing 18º west.

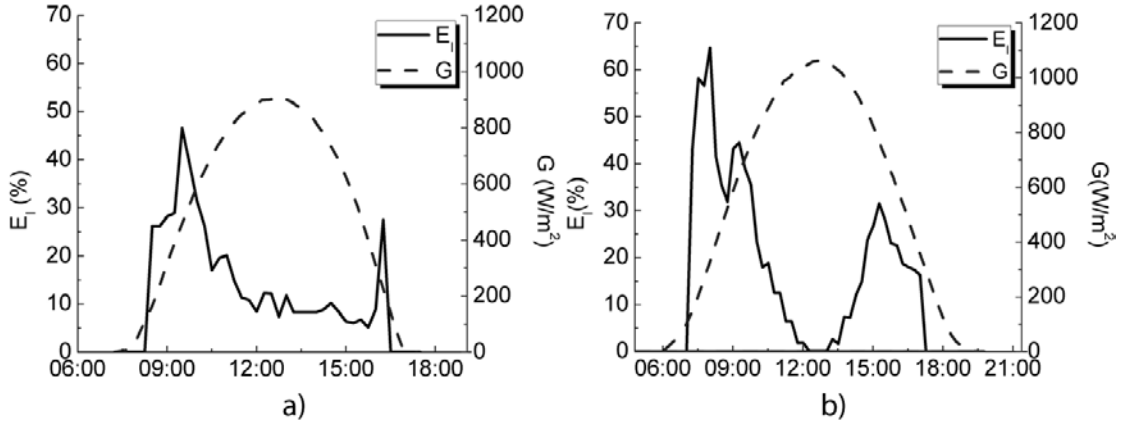

Figure 5.6: Shows the energy improvement during a clear winter day (left) and a summer day (right).

5.4.1.2.c New simulations with the modification of the installations topology

Although this installation is an example of poor design (40% of energy is lost due to shadows) it also seems to be an example of an installation where DMPPT can really have a high impact on the energy generated. It is also an example of the high energy gains that can be obtained in PV systems with parallel strings. However, this PV system is old and is connected to an inverter with an Atersa 4120 inverter with a maximum input voltage of 120V. With a more modern inverter the whole system could be connected as one string or even two strings each to one MPPT tracker. The results obtained with

these two configurations are shown in Table 5.6, being the energy produced with DMPPT the same in all cases (6.09MWh). The results reinforce the idea that parallel strings are more prone to losses due to shading due to possible voltage mismatches and shows that a large improvement can be obtained with the use of string inverters with independent MPPTs.

Table 5.6: Simulation results for the PV system of ICAII-UPC for one string with all modules connected in series and with two parallel strings each to an independent MPPT and with MLPE in each module

Configuration	Max possible Energy	Energy lost without DMPPT	E_R	E_I
One string	8.31 MWh	2.90MWh (34.9%)	23.4%	12.5%
Two string to one MPPT		3.1MWh (37.3%)	28.3%	16.8%
Two strings to independent MPPTs		2.88MWh (34.7%)	23%	12.2%

Going another step forward, we could consider that the current modules of the installation, of only 120W, would not be adequate for today's MLPE, made for approximately 250W modules. If the installation were to be equipped with MLPE, two modules in series would be connected to each device. New simulations were performed considering DMPPT per each two modules; the results being presented in Table 5.7.

Table 5.7 : Simulation results for the PV system of ICAII-UPC for one string with all modules connected in series and with two parallel strings each to an independent MPPT and with MLPE for each two modules

Configuration	Max possible Energy	Energy lost without DMPPT	E_R	E_I
Five strings to one MPPT	8.31 MWh	3.35 MWh (40%)	29.2%	19.8%
Two strings-One MPPT		3.24 MWh (39%)	26.8%	17.1%
One string		2.90MWh (34.9%)	18.1%	9.67%
Two strings independent MPPTs		2.88MWh (34.7%)	17.6%	9.36%

It is clear that now the energy gains are less because the MPPT is being done over a larger number of sub-modules; the energy lost with CMPPT is the same but the energy produced with DMPPT is less (now only 5.94MWh). The fact that DMPPT is more beneficial as it is performed over a lesser number of sub-modules has also been shown in [Olalla, Deline et al., 2014], where simulation were performed supposing one MPPT per sub-module, showing larger improvements than with module level MPPT.

5.4.2 ENERGY GAINS WITH COMMERCIAL MLPE

This section presents the results for the simulations of the same PV systems as in section 5.4.1, the single-family household and the building in an urban environment, but now considering that a real inverter and real MLPE are in place. With this, the effects of the MPPT range, the inefficiency of the MPPT algorithm and the limitation of the output parameters of power optimizers are considered and the losses due to each of these effects are studied. In the following lines, a brief description of how each effect has been considered is presented:

- MPPT range: if the MPP is out of the MPPT range, it has been considered that the working point is the highest power value inside the MPPT range.
- Local MPP: For the case in which it is supposed that local maxima are not found the behavior of each algorithm, studied in section 4.5.2.3, has been programmed. For each device it is as follows:
    - Central inverter: at start-up it jumps directly to 0.8*Voc and then starts performing a typical P&O algorithm with a voltage step of 7V.
    - Enphase: at start-up it finds the absolute MPP and then starts performing a typical P&O algorithm. Voltage step of 1V, and an MPPT range of 16:48V
    - SolarEdge & Tigo: they perform a typical P&O algorithm starting from Voc at start-up. Voltage step of 1V, and an MPPT range of 16:48V for Tigo and 5:60V for SolarEdge.

- Output limits for Tigo and SolarEdge: the equations of section 3.3 as well as the behavior studied in 4.2 have been used, with a variable V_{inv} for Tigo and a V_{inv} = 330V for SolarEdge.
    - The Tigo optimizer has been modelled as a buck converter with an I_{o_max} of 9.5A and V_{o_min} of 0V. V_{o_max} is 48V but because it is a buck converter it will most of the time be limited by V_W as modules with a V_M = 30V have been used.
    - The SolarEdge optimizer has been modelled as a buck-boost converter with an I_{o_max} of 15A V_{o_min} of 5V and V_{o_max} of 60V. Basically if V_{o_min} is reached the optimizer searches the curve for a higher current point and if it is not found the optimizer is by-passed, outputting -0.7V. This behavior will actually cause the MPP to be found in some cases. If V_{o_max} is passed the optimizer searches the curve for a lower voltage point which does not cause V_{o_max} to be reached.

All simulations are performed with a 15 minute time step and for an 8x8 resolution per cell.

5.4.2.1 Single-family household

Two sets of simulations were conducted: ones it was supposed that the MPPT algorithm perfectly tracks the absolute MPP and another in which the behavior of real MPPT algorithms (seen in section 4.5.2) is considered. For the CMPPT system, an MPPT range of 175-550V has been used. This range has been chosen in order to not cause losses due to the MPPT range of the inverter as this would be the case in a proper system design, as there is a wide range of inverters to choose from. For the case of MLPE this is more limited and the MPPT range of some of them could cause losses when local maxima are present. It has been chosen to not include the efficiency because depending on which inverter is chosen it can vary 3-4% percentage points. In any case the efficiency of MLPE is comparable to the efficiency of a central inverter system, even greater in some cases. For example, the weighted efficiency of the enphase microinverter is of 96% and that of a Fronius IG Plus 3700 is of 95%. The weighted efficiency of the SolarEdge power box is

of 98.5% which when multiplied by the weighted efficiency of the SolarEdge inverter (97.5%) returns a 96% global efficiency.

First of all, simulations are performed considering that the MPPT algorithm of both the central inverter and the MLPE perfectly tracks the MPP. The possible losses due to the limited MPPT range of the MLPE and the inverter are however considered. Table 5.8 shows the results obtained for these simulations. The E_i indicated for the central inverter is the gain obtained considering the MLPE being ideal. In this case, because there are no losses in the inverter's MPPT the gain is the same as the one presented in Table 5.2. The idea of these simulations is to evaluate the losses due to the output limits of the power optimizers and the limited MPPT range of the Tigo and Enphase devices. From the results it can be seen how for this system, these losses are very low; less than 0.5%. Curiously, the losses due to the output limits of the SolarEdge system are comparable to the losses due to the limited MPPT range of Tigo and Enphase. All of these losses are added to the losses obtained by the shadows and because no losses are added to the CMPPT system, the real energy gains are lower.

Table 5.8: Simulation results for the single-family household considering the real commercial equipment being in place and considering that the absolute MPP is always found.

	Maximum possible generation	Output limit Losses	MPPT Losses		E_I (%)
			Range	Local maxima	
Central inverter	6430 kWh	N/A	0	0	**2.32%**
SolarEdge		**18.4 kWh (0.29%)**	0	0	**2.01%**
Tigo		0	**19.8kWh (0.3%)**	0	**1.98%**
Enphase		N/A	**19.8kWh (0.3%)**	0	**1.99%**

In a second step, the inefficiency of the MPPT algorithm in finding the absolute MPP in presence of local maxima has been simulated and the results are presented in Table 5.9. For this case, it can be seen how the energy losses greatly increase for the CMPPT system. The reason for this is that at inverter start-up the generator is shaded by the chimney and the *I-V* curve has many MPPs. Because of the inability of the inverter in finding the absolute MPP at inverter start-up, as seen in section 4.5.2, the CMPPT is

working at a local MPP during a large part of the day. Although this also occurs in the MLPE, the effect is much less because many modules are totally shaded at start-up and there are no local maxima. This can be seen by comparing the losses of Enphase and Tigo. The Enphase algorithm was programmed to find the absolute MPP at start-up while the Tigo was not, and the losses are practically the same. Even in the case when there are local maxima, because each module is independent close to the end of the shaded period the losses are only in the shaded modules, while in the case of the CMPPT system, until the end of the shaded period, even if only two modules are shaded, the power loss can be very large if working at a local MPP.

The case of SolarEdge is curious. As was already seen in section 4.5.2.3.b, when V_{o_min} is reached by the SolarEdge optimizer it searches the *I-V* curve for a higher current point and it causes it to unintentionally move away from a local maximum to the absolute MPP. This is also reflected in these simulations, as the losses due to the inefficiency of the MPPT algorithm are lower for SolarEdge than for Tigo and Enphase.

Table 5.9: Simulation results for the single-family household considering the real commercial equipment being in place and considering the real behaviour of the MPPT algorithm of each device.

	Maximum possible generation	Output limit Losses	MPPT Losses		E_l (%)
			Range	Local maxima	
Central inverter	6430 kWh	N/A	0	**581kWh (9.2%)**	**12.13%**
SolarEdge		9.9 kWh (0.15%)	0	24.5kWh	**12.86%**
Tigo		0	19.8kWh (0.3%)	55.6 kWh	**12.1%**
Enphase		N/A	19.8kWh (0.3%)	53.1 kWh	**12.2%**

A final simulation exercise was performed, where the chimney was moved to a symmetric location at the west side of the roof. Because the system is facing south, the shadow profile is totally symmetric, affecting the same number of modules in the same way. The only difference is that now the shadow starts entering the generator while the inverters and MLPE are already working. As was already predicted in section 4.5.2.2 and experimentally verified in section 4.5.2.4.a, due to the nature of incoming shadows on PV systems it is rare that distinct local maxima are formed at the beginning of the

shaded period, allowing a simple P&O MPPT algorithm to shift the working point to a lower voltage during the incoming shadow, therefore avoiding getting trapped at a local MPP. Because of the importance of precisely simulating the *I-V* curve during the incoming shadow, the simulation step was lowered to one minute.

From the results presented in Table 5.10 it can be seen how the losses due to the P&O MPPT algorithm on the CMPPT are now almost an order of magnitude lower than in the previous case. This is in agreement with what was predicted in section 4.5.2.2 and with some more results presented in the following section. Because now the losses in the CMPPT system are lower the possible energy gains obtained with DMPPT are also much lower. Again, the output limits of the SolarEdge optimizer have a positive effect on its MPPT algorithm, resulting in the best performing device.

Table 5.10: Simulation results for the single-family household considering the real commercial equipment being in place and considering the real behaviour of the MPPT algorithm of each device but having moved the chimney to the west side of the roof. This way the shadow enters the generator while the inverters are already working.

	Maximum possible generation	Output limit Losses	MPPT Losses		E_l (%)
			Range	Local maxima	
Central inverter	6430 kWh	N/A	0	82.8 kWh (1.29%)	**1.58%**
SolarEdge		15.8 kWh (0.2%)	0	20.0kWh	**2.39%**
Tigo		0	20.9kWh (0.3%)	62.3 kWh	**1.57%**
Enphase		N/A	20.9kWh (0.3%)	62.3 kWh	**1.57%**

5.4.3 OTHER SIMULATIONS

As an external consulting service for a spanish engineering company, the model for simulating energy gains with DMPPT was applied to a PV installation in the center of Madrid. The curiosity of this installation is that PV system is installed on the façade of a round building and, therefore, the building itself, depending on the time of day, cast a

shadow over some of the modules, while the others are fully illuminated. The results of this study are shown in Appendix C.

5.5 ENERGY GAINS IN REAL PV SYSTEMS

Although in the literature there exist various references of power gain measurements [Neuenstein and Podewils, 2009; Orduz, Solórzano et al., 2011a; Podewils and Levitin, 2011; Sanz, Vidaurrazaga et al., 2011; Solórzano, Egido et al., 2010] there are not many that deal with energy gains. This is mainly because a very long time is needed for each shading pattern in order to consider all of the sun's positions and the differences in irradiance during the year.

[Deline, Meydbray et al., 2012] have devised a method in which they measure power gains for certain conditions and then they apply a weight to each condition in order to calculate the annual gain. The results obtained are promising, showing 4%, 8% and 12.6% annual gains for a light, moderate and heavy shading situation, respectively; each of these considering a 7%, 19% and 25% irradiance loss. When compared to the simulation results obtained in the previous sections, these energy gains seem a bit high.

The reason could be the method applied, in which a 37% transmittance fabric was used to simulate the shadows. With the use of a 37% transmittance fabric (simulation of a D/G ratio of 37%) the amount of irradiance reaching the shaded modules is quite high. As shown in section 3.4.1.2.b a higher D/G will normally return higher energy gains. Although it does depend on the number of shaded modules, Figure 3.19 shows that a D/G ratio of 37% is quite optimum for all the percentage of shaded modules. However, from the analysis of the D/G ratio shown in

Appendix A, the reality is that most of the yearly irradiance occurs for D/G ratios below 15% or above 90%; which, as shown in Figure 3.19. Even if the average D/G ratio for a location is 37%, the results from using 37% as the D/G ratio and using all the D/G ratios for each time period would be quite different, because at high and low D/G ratios the power gains are lower than at middle D/G ratios.

In another publication by the same author [Hanson, Deline et al., 2014] in which a PV system affected by real shadows was measured for nine months with and without MLPE, only a 5.8% energy gain was observed for a system with an estimated 20% shading loss as determined from an on-site shading survey. This energy gain does seem more reasonable and within what is expected with the use of DMPPT.

This section presents the results from a series of measurements done on a real PV system (MagicBox: seeFigure 4.2) affected by shading and aimed on observing real energy gains.

5.5.1 Method used for estimating energy gains on a real PV system

Ideally, for estimating energy gains with the use of DMPPT, two identical PV systems[33] would be placed sided by side and the same exact shadow, or shadows, would be applied to both of them. One of the systems would be equipped with MLPE and the other with a central or string inverter. By measuring the production of each system, the most realistic energy gains would be obtained. This is a recommendation that is made from the experience gained throughout the various measurements performed during the years in which this thesis has taken place. Using this method would allow comparing energy gains in clear days, days of passing clouds, covered days, and moments with different D/G ratios. If the power at STC of each generator is corrected, the only uncertainty could come from the energy gains obtained due to module mismatch. However, as was seen in section 3.4.2, this should be very small.

[33] Identical in number of modules, type of modules and interconnection of the modules. The *I-V* curve of each generator should be measured and if there is a power difference between the two, it should be corrected in the data analysis.

For the experiments performed, there has not been access to two identical PV generators in which the shadows can be chosen by the user. Therefore a different method has been devised. The method consists of using the same PV generator and changing from CMPPT to DMPPT in consecutive clear days. This way the shadow profile over the generator is practically identical, only needing to account for the difference in irradiance and cell temperature. Because only ambient temperature was measured, equation (2.9) which uses the NOCT is used to obtain T_C. Then with equation (5.9) the power produced one day is corrected with respect to the G and T_C of the second day; while the power produced the second day is not corrected. This, of course, could be done the other way around, correcting day two and leaving day one as it is.

$$P_1 = P_1 \cdot \frac{G_2}{G_1} \cdot [1 + \gamma \cdot (T_{c1} - T_{c2})] \tag{5.9}$$

where γ is the relative power temperature coefficient, estimated at 0.4%/ºC.

Finally, by integrating the power produced during each time instant, the energy produced each day is obtained and by applying equation (5.5), the energy gain is obtained.

5.5.2 Results of the energy gain measurements in Magic Box

The experiments have been performed during three consecutive days, from the 21st of July to the 23rd of July, on a ten module string located on the rooftop of MagicBox. The string is affected by morning shade from a tree, by a shadow in the afternoon from a chimney and by evening shadows from trees. During the three consecutive days the ten module string has been used with an SB2000 inverter with OptiTrac enabled, with a SolarEdge system and with a SB2000 inverter without the OptiTrac option, respectively. The instantaneous DC power has been measured for each of the three systems in one minute intervals, supposing the power constant during the rest of the minute.

The energy lost due to the shadows with the CMPPT system (with OptiTrac enabled) has been estimated in order to categorize the installation with respect to the losses due to shading. A 26.8% energy loss has been obtained, categorizing the installation into a heavy shaded system. In order to do this, the sixty power values obtained during an

unshaded hour at midday are extrapolated to STC conditions and they are averaged, obtaining the value of $P_M^\star$ = 1821W±1.6%. With this value, the expected power in unshaded conditions for each time period is estimated by applying equation (5.10).

$$P = P^* \cdot \frac{G}{1000} \cdot \left(1 + 0.004 \cdot (25 - T_c)\right) \tag{5.10}$$

In addition, the incidence angle is calculated for each time period and the direct irradiance component is multiplied by the transfer function of the acceptance angle for typical mono-crystalline PV modules; shown in Figure 5.7. It should be noted that the difference in energy lost obtained by applying and not applying the acceptance angle transfer function is from 28.1% to 26.8%.

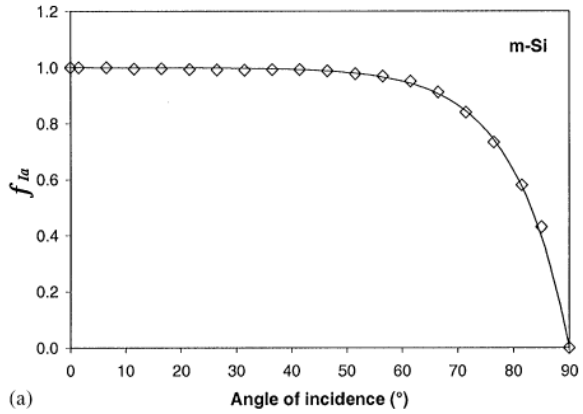

Figure 5.7: Transfer function of the acceptance angle for typical mono-crystalline PV modules.

For each time interval, the power has been corrected in irradiance and temperature as described in the previous section and the corrected powers have been used to calculate the energy production with each system, as well as the estimated production in unshaded conditions. The results are presented in Table 5.11.

Table 5.11: Results for the energy gain measurements performed at MagicBox

	Production (kWh)	Energy lost (kWh)	E_i
Unshaded	11.5	N/A	N/A
SolarEdge	8.81	2.69 (23.4%)	4.63% / 10.96%
SB2000 (OptiTrac)	8.42	3.08 (26.8%)	6.05%
SB2000 (No OptiTrac)	7.94	3.56 (31%)	N/A

The results show that the SolarEdge system performs better than both of the CMPPT systems, resulting in a 4.63% and 11% energy gain with respect to the inverter with and without OptiTrac. The OptiTrac algorithm performs 6% better than the non-OptiTrac inverter, highlighting the necessity for an MPPT algorithm that can find local maxima for PV systems affected by shading. The SolarEdge system only performs a 4.6% better than the OptiTrac inverter, which is not a huge energy gain for a PV system with such a high degree of shading.

For more information we can look at the production curve of each system, shown in Figure 5.8. During the morning hours, were the installation is heavily affected by the shadow of a nearby tree, it can be seen how it is the central inverters that start producing earlier. When we looked into the data of the working point of each optimizer, the working voltage of all optimizers was high and the currents were low, which could mean that they were working at a local MPP, as this has been shown to be a problem at start-up for the SolarEdge optimizers (4.5.2.3.a). However, at around 11:30 the SolarEdge system is already producing more than both of the CMPPT systems. Also at around 11:30 it can be seen how the OptiTrac inverter starts producing more than the non-OptiTrac inverter but less than the SolarEdge System. This same pattern goes on until around 13:00, when the system starts to be free of shadows and the three systems produce the same. It can be seen how at this time, the non-OptiTrac inverter has an abrupt power change, meaning that it has at this points changed from a local MPP to the absolute MPP. The working voltage of both inverters in a similar situation can be seen in Figure 4.45.

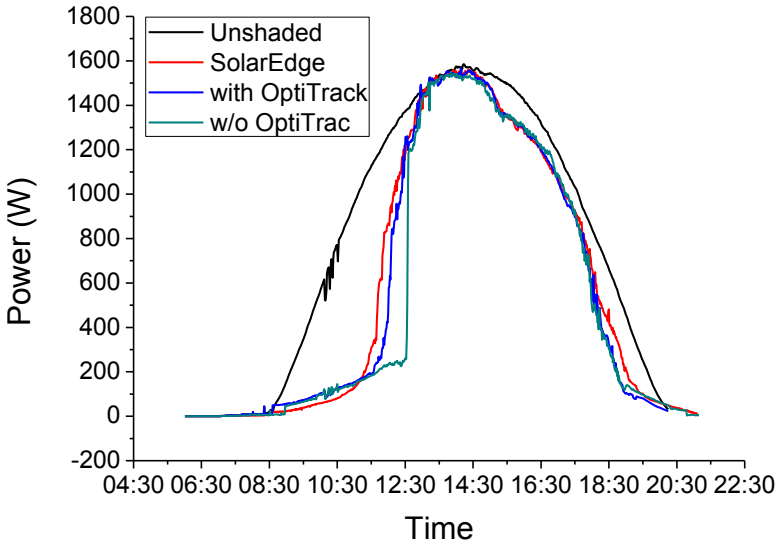

Figure 5.8: Production curves for the estimated unshaded system, the SolarEdge system and the SB2000 with and without OptiTrac, all connected to a ten module generator heavily affected by shadows.

The shadow from the chimney starts affecting the system at around 15:00 and is the only shadow affecting the system until around 18:00. During this period there is no appreciable energy gain, with all the systems producing a similar power. At around 18:00, when the shadow from nearby trees is cast over the system, a power gain is appreciated with SolarEdge. It can also be seen how the central inverter systems are producing the same amount, even though local maxima are present. This again reinforces what was exposed in section 4.5.2.2 about the nature of incoming shadows.

5.6 Some considerations on the economic viability of DMPPT PV systems

Evaluating the economics of a system technology is not an easy task which depends on many variables and also in having real prices and field experience. This section does not pretend to present a very detailed economic analysis but more to provide the reader with a general perspective of the economic benefits of using MLPE in PV systems. Because the market share of these systems is growing steadily year after year, even exceeding 50% of the U.S. residential market share in 2013 [Grana and Shiao, 2014], it would seem that they provide some benefit to the installer; despite their higher cost in comparison to a central inverter.

However, it is not only the hardware costs that should be considered but the whole installation cost. A report by the National Renewable Energy Laboratory (NREL)

[Friedman, Ardani et al., 2013], which surveyed 55 residential PV installers, representing 4,260 residential installations and approximately 27MW of residential capacity installed during the first half of 2012, presents the non-hardware balance-of-system costs—often referred to as "soft" costs—for U.S. residential and commercial PV systems. They concluded that soft costs accounted for 64% of the total residential system price, 57% of the small (less than 250 kW) commercial system price, and 52% of the large (250kW or larger) commercial system price. The detailed breakdown of the different costs is presented in Figure 5.9.

While the total hardware were 1.90$/W (1.03$/W for the modules, 0.43$/W for the inverter and 0.44$/W for installation material), the soft costs added 3.32$/W, where the installation labor accounted for 0.55$/. In 2014, the hardware costs have dropped even more, while the soft costs have remained more stable. Some soft costs could even increase with time, like the installation labor cost if salaries increase.

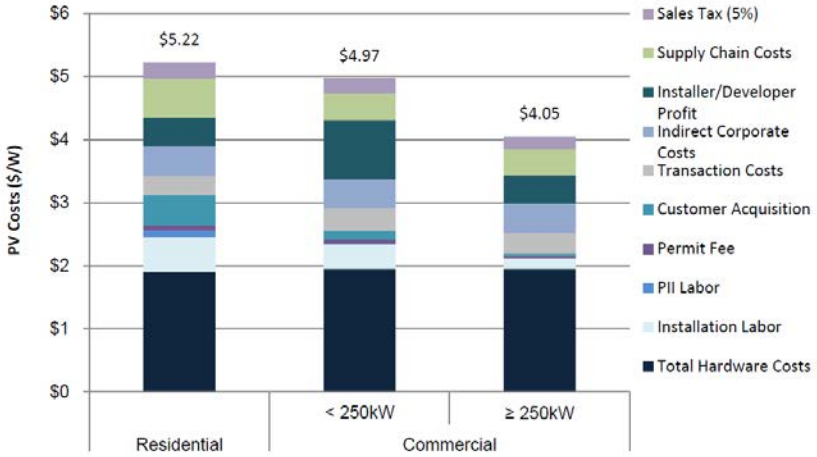

Figure 5.9: Detailed breakdown of the costs to install a PV system in the U.S. in the year 2012. [Friedman, Ardani et al., 2013]

There is an interesting webpage, [EnergyTrend, 2014], which shows the price for PV modules and inverters resulting from a periodical survey of manufacturers. In it, for the 16th of July 2014, the average module price is of 0.58$/W with a maximum of 0.9$/W while the same prices for the inverter is of 0.182$/W and 0.25$/W. Although the module price does not vary greatly for systems over 5kW, the inverter price does. For example, the GTM report, [Grana and Shiao, 2014], estimates the cost for a residential inverter at 0.34$/W. This same report estimates the cost for power optimizers and microinverters at an average price of 0.60$/W. It is evident that the use of MLPE increases the hardware costs, by about 0.3$/W. However, MLPE has the potential of reducing the installation time (estimated at 10% of total cost) and slightly increasing the production. The O&M

costs can also be reduced as there is module level monitoring making automatic fault diagnosis procedures possible, as shown in chapter 6.

Figure 5.10 presents an interesting chart, taken from the GTM report, in which the cost of a microinverter is presented as well as the savings obtained with their use. When adding up all the savings, it is concluded that a microinverter system is 0.12$/W cheaper than a CMPPT system. However, some of these numbers are questionable. This is the only quantitative analysis on cost of MLPE that has been found and it has served as a reference for the analysis here presented.

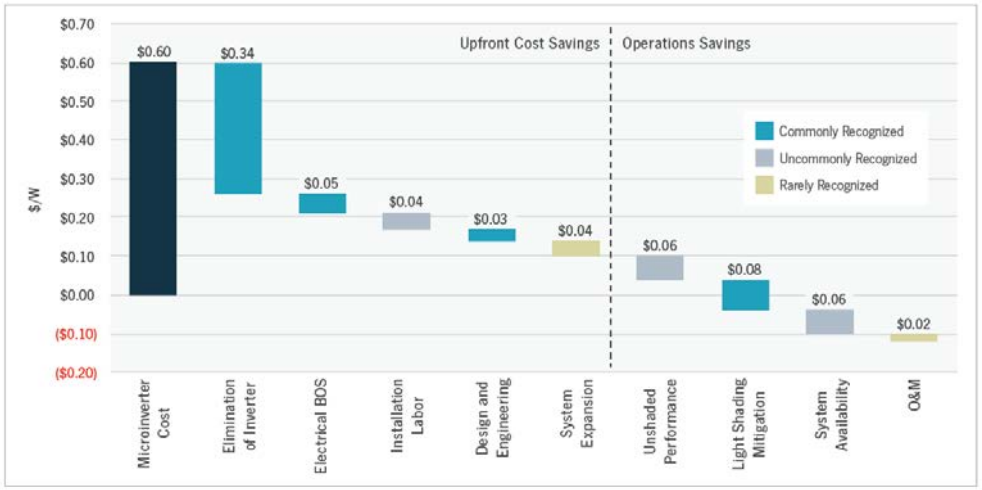

Figure 5.10: Residential microinverter system and operation saving, 2014. [Grana and Shiao, 2014]

For example, as we have seen in section 3.4.2, there is not much room for improvement due to mismatch of electrical characteristics and as we have seen throughout the thesis, the efficiency of both MLPE and central inverters is very similar. In the most optimistic case a 0.01$/W is considered. Also the savings claimed for light shading conditions are quite overestimated. From what we have seen in previous sections of this same chapter, energy gains for light shaded condition, i.e. the chimney or antenna, are around 2-3%. Even for heavily shaded systems, like the one at ICAII, energy gains over 10% are not guaranteed, especially if the system is correctly designed. If we consider that this energy increase can be obtained by installing a larger system and considering a module plus inverter cost of 1.2$/W (0.9+0.3), a savings of 0.03$/W to 0.12 $/W is obtained for a 2.5% and 10% energy gain respectively.

The system expansion refers to being able to add more modules to the roof because with DMPPT shaded areas can also be used. This allows installing a larger system and

lowering the final cost per Watt. However, these areas will still be underperforming with DMPPT and it is unclear that adding modules to them will actually produce savings. The 0.04$/W seems like a very optimistic saving for shadows although it could be realistic for roof with different tilt and orientation angles.

Something similar can be said about system availability. It is commonly said that because there are many microinverters if one fails the others are still producing, opposite to a CMPPT system. From when the system falls until it is repaired there is an amount of potential energy that is lost and this is accounted as 0.06$/W in the report. Again if we consider a 1.2$/W for the module and inverter cost, this 0.06$/W corresponds to a 5% energy lost, or 5% system downtime (18 days per year), which is very pessimistic and, therefore, gives a very optimistic saving. System availability can also refer to an improved inventory management. Because residential installers can encounter systems that can range from a few kW to 20 kW it would require having many different inverters at the warehouse – with MLPE inventory management is easier, particularly for smaller, lower-volume installers.

On the other hand, there are some predictions that seem a bit pessimistic, for example, the savings in installation time. From the NREL report these are around 0.55$/W. Saving 0.04$/W translates to only reducing the installation time in 7%. For example, for the case of AC modules the installation time can be reduced by half when compared to module add on microinverters, as can be seen in the following experiment [SolarBridge, 2014]. On the other hand, it is difficult to image large time saving in the installation of power optimizers as the same wiring and DC protections must be installed as in the case with a central inverter. Interesting savings could also appear in the design and engineering phase as it is drastically reduced with the use of microinverters and power optimizers, especially for roofs with shadows or different tilt and orientation angles. Another report, [Woodlawn, 2012], estimates these savings at 0.07$/W.

Finally, the O&M could report more savings than those predicted by GTM Research. If an automatic failure and diagnosis system like the one presented in chapter 6 is implemented, it could be the user the one that takes care of the O&M. In the case of underperforming modules, the user can be alerted of which is the actual problem and be

guided on how to solve it without needing to call the installation company. This will also be quicker resulting in less energy lost. An optimistic estimate could be of 0.05$/W.

With the above discussion two plots, similar to that of Figure 5.10, have been produced. One is the pessimistic case and the other the optimistic. The results can be seen in Figure 5.11 and Figure 5.12 . In both cases a 0.60$/W is considered for the MLPE system. The pessimistic case considers a 2.5% energy gain (light shading) and no gain in unshaded conditions, a 0.25$/W cost for the central inverter, 0.05$/W saving in electrical BOS (cabling, protections, etc.), a 0.04$/W saving in installation labour, a 0.03$/W saving in design and engineering, a 0.03$/W for inventory savings and a 0.02$/W in O&M. For the optimistic case a 10% energy gain is considered due to shading (heavy shaded installation) and a 0.7% energy gain in unshaded conditions, a 0.35$/W inverter cost, a 0.25$/W in installation costs, a 0.03$/W savings in design and engineering, a 0.03$/W for inventory savings and a 0.05$/W in O&M.

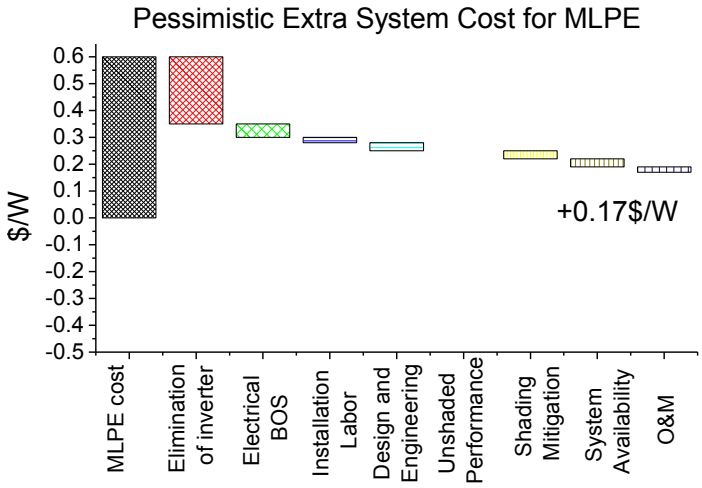

Figure 5.11: Pessimistic extra system cost for a PV system with MLPE. In this case MLPE would not be economically beneficial.

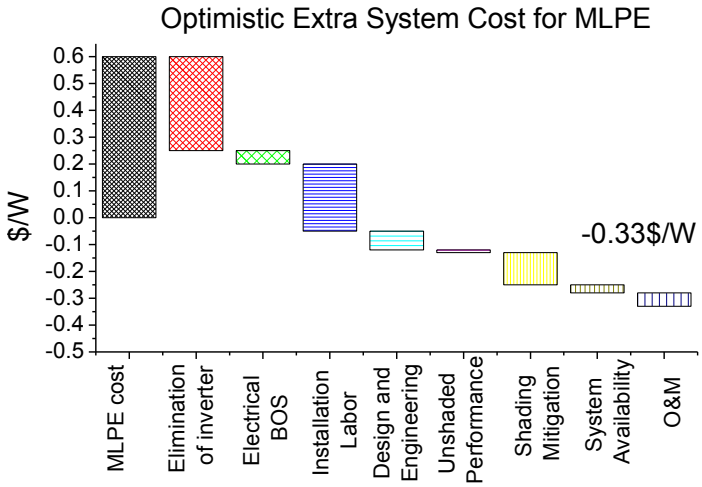

Figure 5.12: Optimistic extra system cost for a PV system with MLPE. In this case MLPE could prove very beneficial.

Other factors for specific installations can also incline the balance towards MLPE. For example, the 2.2MW installation with Tigo optimizers shown in Figure 1.4 was done due to the irregular orography of the terrain, probably being the costs of flattening the terrain higher than the extra cost of installing MLPE. Also the peculiar installation shown in Appendix C is ideal for MLPE. Although these are atypical installation, as BIPV increases more of these will be seen and MLPE could find its market niche.

5.7 CONCLUSIONS

A model for simulating energy gains with DMPPT has been presented and validated. Various simulations have been performed and it is has become clear that simulating at the cell level is important in order to obtain accurate results. It has been confirmed that although large power gains can be obtained, these will not translate to a large annual energy gain due to various factors like the stationary nature of the objects, the different position of the sun throughout the year and, in some cases, the fraction of diffuse radiation. Improvements between 2.5-3.5% are obtained for simple objects like chimneys or antennas and higher improvements of up to 12% are obtained for a heavily shaded installation with four different shading objects.

It has also been observed that large objects close to the generator can reduce the amount of diffuse radiation of the nearby modules creating a constant mismatch in climates with a large fraction of diffuse radiation and a larger energy improvement. A larger D/G ratio also causes higher energy improvements.

The performed simulations also show that there are cases where DMPPT can be very beneficial for the installation, like the urban installation presented in this paper. However, this also requires that the efficiencies of the DMPPT equipment match, or are as close as possible to, the efficiency of a centralized system. This point is rapidly improving and there are already power optimizers with an average efficiency of 98.5% and maximum values over 99% [Neuenstein and Podewils, 2011].

Other improvements with respect to central MPPT topologies like, an advanced monitoring system, the possibility for system designers of combining different tilt and

orientation angles and higher security in the case of fire, should also be considered when deciding whether or not to install DMPPT products.

6 AUTOMATIC FAULT DIAGNOSIS IN PV SYSTEMS WITH DMPPT

6.1 INTRODUCTION

Production systems should be monitored in order to control the correct functioning of the system: control its production and detect any possible faults. In the case of photovoltaic (PV) systems there are international standards that guide the user to the correct implementation [IEC, 1998] and the historic monitored data has been used to develop guides and benchmarks for PV system performance [IEA, 2000].

Different possibilities exist for data analysis. Some do it yearly [IEA, 2004], analysing the performance of the PV system over a significant time period of operation and comparing it with similar systems. This shows that a system is performing poorly but it has the disadvantage that it cannot be used to explain the causes of this underperformance. Others [Chouder and Silvestre, 2010; Drews, de Keizer et al., 2007; Firth, Lomas et al., 2010; Oozeki, Izawa et al., 2003] use high-resolution monitoring (minutely to hourly intervals) to analyse the performance of the system. With this higher resolution a fault diagnosis procedure can be executed.

A common denominator of monitoring and fault diagnosis systems is that they use irradiance and temperature sensors to compare the PV systems production at standard test conditions (STC). Most systems use local sensors [Chouder and Silvestre, 2010;

Firth, Lomas et al., 2010; Oozeki, Izawa et al., 2003] and some use satellite observations [Drews, de Keizer et al., 2007], this last one being less accurate in hourly values. The use of either local sensors or satellite data implies an added cost to the PV installation, which can be a significant percentage of the total installation cost in small systems of 1-10 kWp. In addition, the system owner, sometimes uneducated energy wise, is responsible for its maintenance, unless a higher price is paid to hire a maintenance company.

Another point in which all previous monitoring systems coincide is that they analyse data from the whole PV generator or, at most, each PV string, limiting the range of possible faults diagnosed. In addition, most of them only analyse the power production ignoring the voltage and current. These systems can detect the general fault like: constant energy losses, total blackout, short time energy losses [Drews, de Keizer et al., 2007] and the best can also detect shading [Firth, Lomas et al., 2010]. However, they cannot detect the exact cause.

With the introduction of distributed maximum power point tracking (DMPPT) systems—power optimizers and micro-inverters—a new level of PV system monitoring, where the exact system fault and power lost is determined, is possible. These distributed topologies where initially designed to reduce the losses caused by shadows and mismatch in central maximum power point tracking (MPPT) PV systems. Since these systems require the monitoring of the modules' operating voltage and current (for the MPPT algorithm), the use of voltage and current sensors for each module is at no extra cost. It is only necessary to add a communication module and make use of a PLC signal to obtain the data of all the modules' working points. Most commercial firms offering these products already incorporate this type of monitoring system, however, they are limited to only detecting a lower power production in the exact module.

The monitoring and fault diagnosis system here presented improves the range of diagnosed faults in previous monitoring systems and reduces its cost by eliminating the need for irradiance and temperature sensors. Apart from general faults like in the previous systems, this tool can detect: fixed object shading and location of the object, localized dirt, possible hot-spots, module degradation, excessive DC cable losses and

generalized dirt, this last one only with the addition of an irradiance sensor or irradiance data. In this section only the new fault diagnosis is described.

The rest of the chapter presents the different PV system faults that this procedure aims at diagnosing, our experimental system and the main functioning principles of the diagnosing procedure. Although the work has been verified with power optimizers, the design is also valid for micro-inverters since both of these architectures find the MPP of each module, which is what is used to analyse the failures.

6.2 PV SYSTEM FAULTS

6.2.1 FIXED OBJECT SHADING

Shadows cast by fixed objects on PV generators—such as buildings, tress or antennas—are very common in the urban environment. These should be avoided in the design of the installation, however, this is sometimes not possible and other times they could even appear during the life of the system. In humid and densely vegetated areas it is very common that overgrown trees or plants cast shade over the PV system, Figure 6.1, and in urban areas new buildings, antennas or other obstacles can appear. Their detection is important to solve the problem if possible and avoid further energy losses. The effects on the PV generator values and how they are detected is discussed in section 6.4.

Figure 6.1: Overgrown vegetation in a PV plant causing shading and power losses.

6.2.2 Generalized dirt

The accumulation of dust on the surface of a photovoltaic module decreases the radiation that reaches the solar cell and, thus, it's generated power. Depending on the climate of each region and the type of dust accumulated these losses will be higher or lower, ranging from 2-4% annual loss, reaching up to 20% after long periods without rain and 40% after a dust storm [Kalogirou, Agathokleous et al., 2013; Massi Pavan, Mellit et al., 2011; Zorrilla-Casanova, Piliougine et al., 2012].

Normally when a module is affected by generalized dirt all modules will be similarly affected so our comparison procedure does not work in this case. It will, however, work if some modules are dirtier than other, i.e. an area of the generator receives more rain, or is less affected by dirt. For correctly detecting generalized dirt in the whole generator it is recommended to compare the power output with a clean irradiance sensor or with satellite measurements.

A reduction in incoming radiation causes a reduction in the output current of the module, so in the case of only having a certain amount of modules affected by generalized dirt, they can be detected by a drop in output current and normal voltage.

6.2.3 Localized or irregular dirt

Localized dirt in PV generators refers to obstacles that cover only small parts of a PV module, normally covering less than one whole cell. This could be produced by bird droppings, fallen leaves, dirt building up on the lower edges, pollution and even lichens (Figure 6.2). In dry climates these problems can be magnified due to the low frequency of rains, reducing the possibilities of the dirt being washed away. If dirt is not cleaned regularly and allowed to dry it can reach a state where it is not washed away even after a day of heavy rain, as is the case of the bird dropping in Figure 6.2, which has caused a hot-spot in the module.

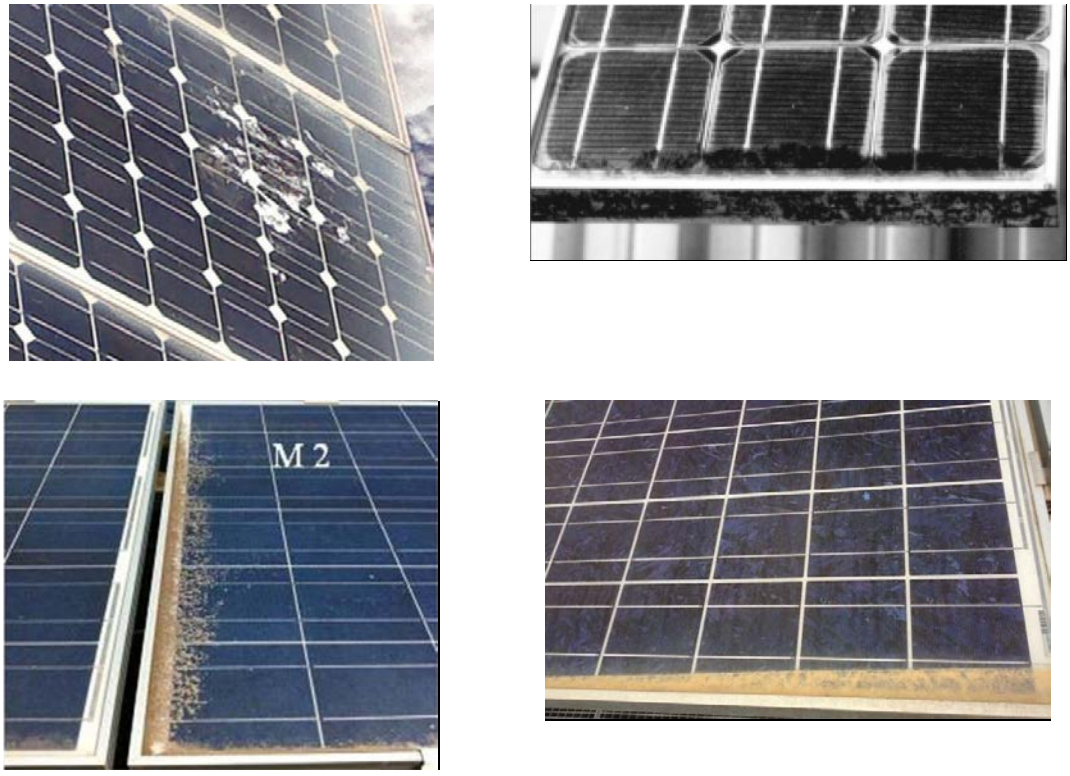

Figure 6.2: Different causes of localized dirt in PV systems: a) bird droppings, b) lichens [Haeberlin and Graf, 1998], c) [Lorenzo, Moretón et al., 2013] and d) irregular dirt patches.

6.2.4 HOT-SPOTS

Hot-spots are a well-known phenomenon in PV arrays, described as early as 1969 [Blake and Hanson, 1969] and still present in PV arrays [Lorenzo, Moretón et al., 2013; Muñoz, Lorenzo et al., 2008; Sánchez-Friera, Piliougine et al., 2011]. They occur when a cell, or group of cells, operates at reverse-bias, dissipating power instead of producing it. When this occurs, the cell operates at abnormally high temperatures and it can cause irreparable damage to the cell. Therefore, their detection before damage occurs is very important.

The reason why a cell operates in reverse-bias is because it is not capable of generating the same current as the rest of the cells serially connected and this can occur due to various reasons: cell degradation, shadows, localized dirt, etc. In order to match the current of the normally operating cells, the affected cell works in the second quadrant of its I-V curve as can be seen in Figure 6.3.

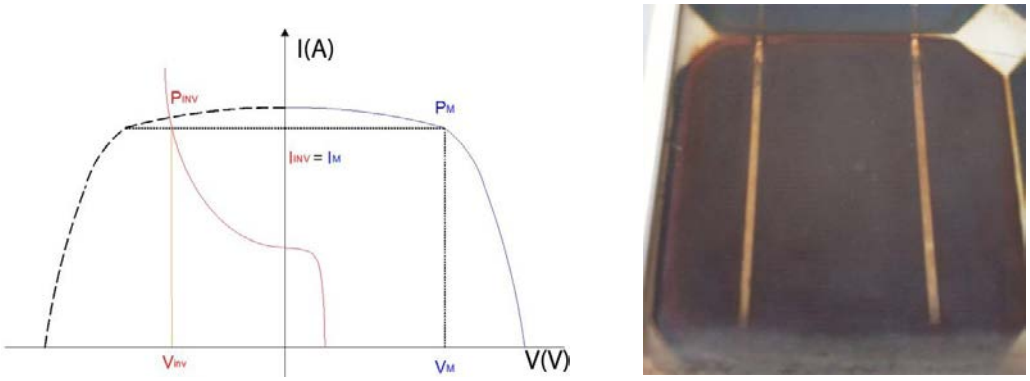

Figure 6.3: Example of the working point of a shaded cell in a series connection of various cells (left) and its effects (right).

Normally, to detect a hot-spot it is necessary to perform an infrared inspection of the PV plant, with the consequent time expenditure and large difficulty in BIPV. However, since we know that when a cell, or group of cells, is in reverse-bias the voltage of the whole module is reduced, we can automatically detect, or at least have the suspicion, that a hot-spot is occurring when a module operates at a lower power and lower voltage than the rest.

6.2.5 MODULE DEGRADATION

It is well known that PV modules degrade over time, normally following a linear average annual degradation between 0.35%-1.5% [Reis, Coleman et al., 2002]. An initial degradation, of about 3-5% [Sánchez-Friera, Piliougine et al., 2011], is also present in PV modules during the first hours of installation and the IEC 61215, "Crystalline silicon photovoltaic (PV) modules – design qualification and type approval" [IEC, 2005] requires that PV modules must be above 95% of the nominal power after the first 60kWh/m^2 of solar radiation.

Regarding the long time degradation, most PV manufactures offer a warranty. Some offer a power warranty at different periods, e.g. 95% at 5 years, 90% at 12 years, 85% at 18 years and 80% at 25 years, and others offer a linear power warranty, e.g. no more than -0.7% per year.

Different studies [Parretta, Bombace et al., 2005; Sánchez-Friera, Piliougine et al., 2011; Skoczek, Sample et al., 2009] show that module degradation can be different for the same type of modules and that many times this degradation is below the warranty

threshold but many other times it is over the threshold. From the power analysis of a whole PV plant it is difficult to know if the power losses are due to module degradation and it could even occur that the power loss is above the threshold but some modules are performing below the warranty levels.

6.2.6 DC CABLE LOSSES

Normally, if an installation is well designed, DC cable losses should be lower than 2% and not rise over time. However, this isn't always the case and the cables can degrade over time, mainly due to corrosion or overheating, and therefore increasing their resistance. In cases where the inverter is far away from the PV generator, the voltage drop due to the cable resistance can be quite significant.

With the use of DMPPT the voltage output of each power optimizer and the voltage input at the inverter can both be measured and recorded automatically. By adding all voltage outputs and comparing it to the inverter's input, the voltage drop can be easily calculated and can set off alarms when it is too high.

This diagnosis will only work with power optimizers and not with micro-inverters since the output of the module and the inverter are at the same location.

6.3 EXPERIMENTAL SET-UP AND MEASUREMENT SYSTEM

The experiments to verify the developed system have been carried out in two different PV generators. Both generators form part of the MagicBox, a solar house presented in the Solar Decathlon 2005 and now installed at the Instituto de Energía Solar, in Madrid, for research purposes. In addition, two different power optimizers were used for the experiments, one is a prototype built by Tecnalia (a participant of the project) for the INTEGRA PV national Spanish project and the other is the commercial optimizer SolarEdge.

Both generators are made up of Isofoton I-110/12 PV, with a V_M of 17.4V and I_M of 6.32A. In order to better match the voltage range of the power optimizers the modules

were grouped in serially connected pairs each connected to a power optimizer, making a total of seven module pairs for the PV generator with the prototype optimizers and eight module pairs for the generator with SolarEdge[34]. A picture of "MagicBox" can be seen in Figure 4.2. The tool has proven to work well in both systems.

Although the SolarEdge monitoring portal provides data of the voltage and current values every 15 minutes, for the purpose of having more frequent and reliable data another measuring system has been built. In this system every module's working voltage and working current points were measured every minute with an Agilent 34970A data-logger; in total measuring 30 different values in both generators. The voltage was measured directly by the datalogger and the current was measured by incorporating a shunt resistance in series at the input of each power optimizer and measuring the voltage drop at the shunt resistance. The datalogger has 0.004%dcV measuring accuracy and the shunt resistances are calibrated at less than 1%. This data was stored in a computer and afterwards it was processed by our failure diagnosis tool.

6.4 FUNCTIONING PRINCIPLES AND EXPERIMENTAL VERIFICATION

This automatic failure diagnosis tool has been purposely developed for small and medium sized PV systems with MLPE. It can be installed locally, being the owner of the system the one who gets the failure alarms, or remotely if it is a local service provider who is in charge of the maintenance. It can prove especially time saving for a local maintenance company who is in charge of various installations around a city or an area.

The purpose of the routine is the detection of the exact underperforming modules, the diagnosis of why they are underperforming and its consequences. With DMPPT, the first point is easily achieved and most companies that offer DMPPT products already offer this solution. Even some of the consequences, like the amount of power lost, can be estimated by an easy interpretation of the data. It is, however, the second point, the

[34] Only seven prototypes were available and the SolarEdge system requires at least eight optimizers to be connected. This difference in module numbers does not affect the results.

diagnosis, which requires a more in depth analysis of the data and it is what this procedure aims at providing.

This tool does not use irradiance or temperature sensors and is based on the comparison of the power produced by the different modules. In this tool, the most producing module(s) at each time period is considered as the irradiance and temperature sensor and all other modules are compared to it, to see if they are underperforming in any way and why.

6.4.1 DATA STORAGE AND INITIAL CONFIGURATION

The only data that is stored are the values of each module's working point, supposing these to be the module's maximum power point, V_M and I_M, from which the maximum power, P_M, of each module is easily obtained. This assumes that the MPPT algorithm works correctly. If this does not occur, as can be the case, in some diagnosis false results could be returned, although it is not very problematic as can be seen from the results presented in this chapter and the nature of incoming shadows (section 4.5.2.2) and the effect of hot-spots on the voltage (section 4.6.2)

For the DC cable losses' estimation, the output voltage of each power optimizer and the working voltage of the inverter must also be stored.

In order to take into account the PV modules' initial power tolerance, there is an initial configuration which corrects all the modules' MPP parameters with respect to their flash report, obtaining the corrected MPP parameters, $V_{M,C}$, $I_{M,C}$ and $P_{M,C}$. For example a 200W module in catalogue that only gives 195W in the flash report will have its power multiplied by 1.026; same for I_M and V_M respectively. These values can also be determined on a clear day without any failures during the first weeks of the installation if no flash-curves are available. Figure 6.4 shows the normalized power of all the modules of the system with respect to the maximum producing module of each time period, before and after the initial power correction. The initial correction values will be stored for their use in the diagnosis algorithms, except for the module degradation diagnosis which uses the real values and not the corrected ones.

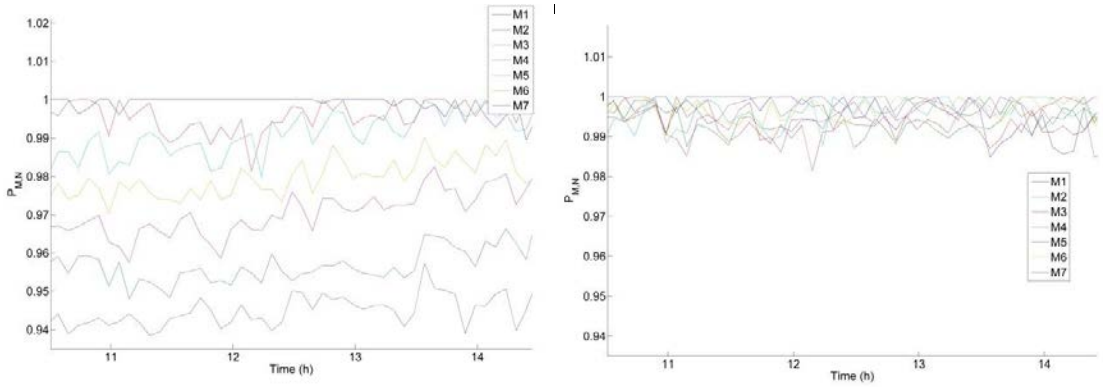

Figure 6.4: Normalized power of each module in the system with respect to the maximum producing module of each time period, before (left) and after (right) the correction.

Table 6.1 shows all the parameters used in the failure diagnosis procedure, their description and how they are obtained.

Table 6.1: Description of the parameters used in the failure diagnosis procedure and how they are obtained.

Parameter	Description	Origin
V_M, I_M and P_M	Working MPP voltage, current and power values of each module	Original measured data. P_M is obtained by multiplying V_M*I_M
$V_{M,C}$, $I_{M,C}$ and $P_{M,C}$	Working MPP values corrected with respect to the initial real values and their rated valued.	Obtained by correcting the measured values with respect to the flash-curve (FC) values and the rated values (RV). i.e. $P_{M,C} = P_M$*RV/FC.
$P_{M,N}$	Normalized maximum power (values between 0 and 1). Used to determine a module's failure in each time period. Also used to diagnose continuous and temporal failures and the type of object for temporal failures.	Obtained by dividing each module's $P_{M,C}$ by the maximum producing module's P_{MAX} for each time period.
P_{MAX}	Power of the maximum producing module for each time period.	Obtained for each time period by finding the maximum value of all modules' $P_{M,C}$.
$V_{average}$ and $I_{average}$	Average $V_{M,C}$ and $I_{M,C}$ of all modules for each time period. Used to diagnose hot-spots, small localized dirt, module degradation and generalized dirt on one module.	Obtained for each time period by averaging all the values of $V_{M,C}$ and $I_{M,C}$.

6.4.2 CLEAR DAY PROCEDURE

From the experiments carried out it has been found that an analysis during a cloudy day, or partially cloudy day, does not return accurate results. For this reason, the diagnosis procedure is only executed during clear days. Figure 6.5 shows the normalized

power of the seven modules for two consecutive days, a cloudy day and a clear day. It is observed that no reliable information can be extracted from the cloudy day but it can from the clear day.

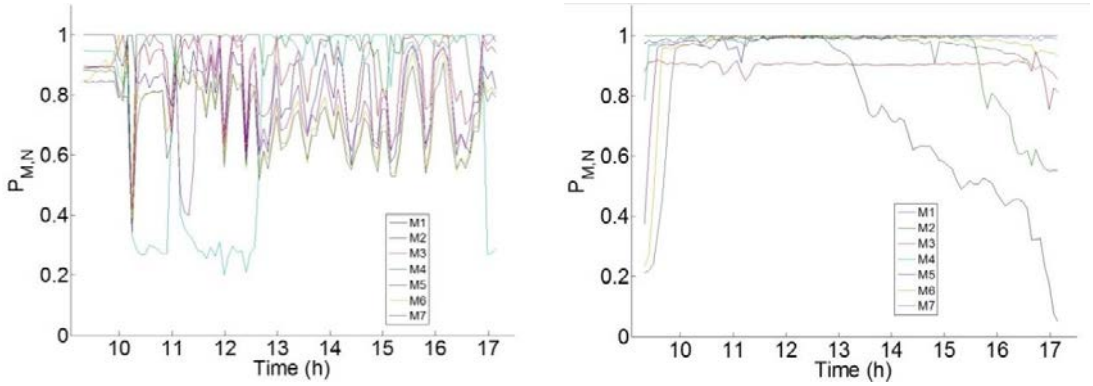

Figure 6.5: Normalized power of the modules in the system for two consecutive days: a cloudy day (left) and a clear day (right).

First, the data is analysed to see whether the day is clear or not. When an irradiance sensor completely free of shadows is available, this procedure is very straight forward to implement. By a simple analysis of the irradiance curve it can be determined whether the day is a clear day or not. During a clear day the irradiance follows a very characteristic bell-type curve, always increasing until it reaches its maximum at midday and then always decreasing until the night arrives; resembling that of Figure 6.6-b.

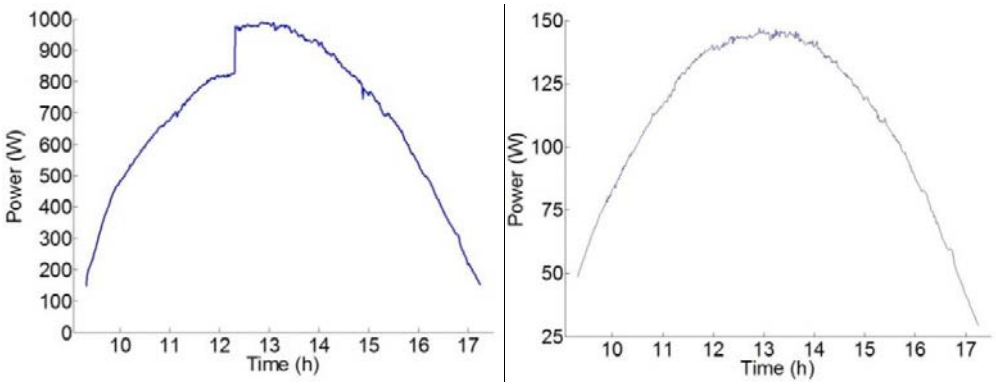

Figure 6.6: Production curve of the whole seven module system during a clear day (a) and of the maximum producing module for each time period (b)

When no irradiance sensor is present, the solution could be to observe the production curve of the PV system. This works well in systems free of shadows, however, when shadows or other failures are present, the production curve will not

resemble the irradiance curve of a clear day, as shown in Figure 6.6 (left). In this case two modules have heavy shade during the morning hours

The method proposed in our procedure is to analyse the curve produced by the maximum producing module at each time period. This curve, unless all modules are failing at the same time, will be very similar to the irradiance curve of a clear day, as shown in Figure 6.6 (right). For obtaining the curve, five modules were used at different times of the day, each contributing in 27%, 14%, 37%, 15% and 6.9%. Each of these five modules is the maximum producing module during the percentage of day indicated.

6.4.3 Detection procedure and energy loss estimation

In order to detect module failures, the corrected power of each module is normalized with respect to the maximum power at each time instant, obtaining the normalized maximum power, $P_{M,N}$, of each module. At each time period, all non-failing modules will have a $P_{M,\,N}$ equal to one, or very close to, and the rest will have a different $P_{M,\,N}$ depending on their failure.

In order to allow a bit of uncertainty in the data, a threshold is chosen for when to report a failure. For this system, a time period is defined as failing when its $P_{M,N}$ is lower than 0.96. In addition, in order to give some margin for errors, modules have only been classified as failing modules when they have errors during at least 5% of the time periods being analysed. Both of the values can be, and should be, modified depending on each system's precision and further field experiences. For our experiments they have worked well enough.

The failure detection algorithm described previously can be seen graphically in Figure 6.7. For the modules that have been found to contain a failure, the diagnosis algorithms are run.

The energy losses caused by each module's failure can be determined, showing the severity of each failure. This way, the user can be alerted of which failures are more important to solve. For obtaining the energy losses, each module's power is compared with the most producing module at each time period. By adding the power losses during each failure's period the total energy losses are obtained.

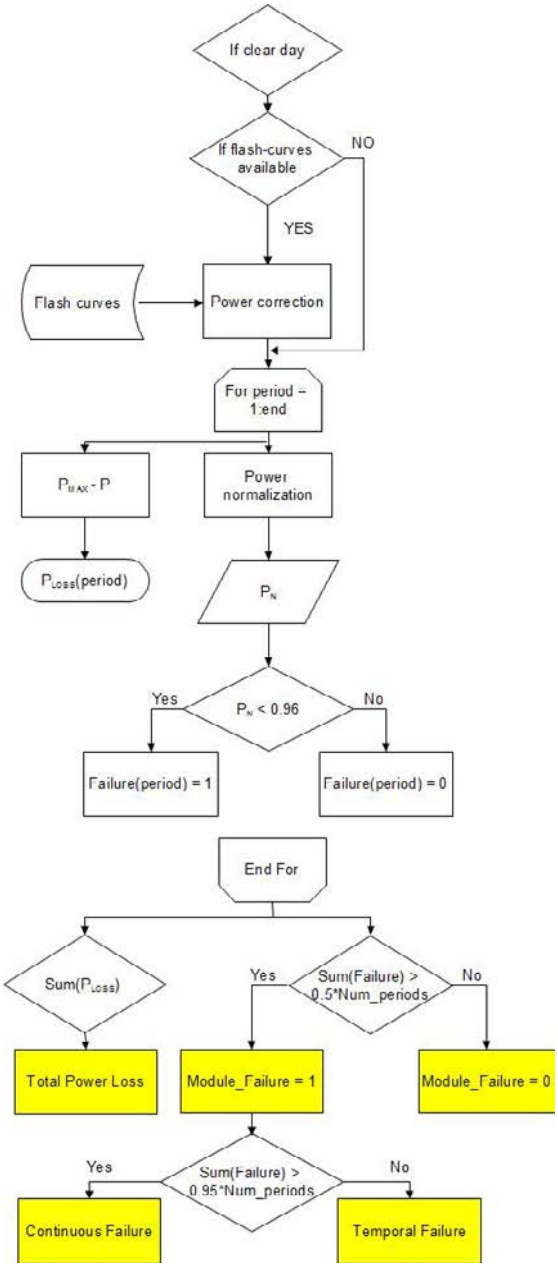

Figure 6.7: Failure detection algorithm

6.4.4 DIAGNOSIS PROCEDURE

For all modules which are found to contain a failure during each day, the diagnosis procedures are run to determine which failure affects each module. The first analysis that is performed is to find out whether the failure is a temporal failure, normally caused by fixed object shading, or a continuous failure, localized dirt, degradation or total module failure. All failures will be categorized under temporal failure or continuous failure; if the number of periods with a failure is over 95% of all periods, the module will

be considered to have a continuous failure, otherwise it will be considered to have a temporal failure.

6.4.4.1 Temporal failures and fixed object shading

Temporal failures can cause total power losses or only partial power loss failures. Total temporal failures can be caused by maintenance work or objects placed on top of modules, for example. The exact cause is difficult to determine and the diagnosis is left at that: total temporal failure. These will not be caused by shades of far-away objects because even when modules are totally shaded by far-away objects they are still receiving diffuse radiation.

Partial temporal failures will be mainly caused by the shadows cast by fixed objects. The nature of the power loss caused by fixed object shading is a progressive loss of power until a minimum value is reached and a subsequent increase of power until normal values. Figure 6.8 shows the effect of fixed object shading over the different modules of the system. This effect on the power is caused by the shade slowly moving through the module, firstly covering a very small fraction and slowly covering more and more. The same occurs, but on the opposite direction (power wise), when the shade is leaving the module.

Going a little further it can be noticed that the time that each module is shaded and the time it takes for the adjacent module to be affected by the same shadow, as well as the amount of power lost, is different for each object. In the same figure, three different shading patterns can be observed. These are caused by: a faraway building, a not so faraway tree and a very close by antenna. The analysis of consecutive days affected by the same shadows returns the same results. However, as the sun's relative position changes this pattern also changes and some failures do not occur. This can be seen comparing Figure 6.8 and Figure 6.5 (right). These two figures are of the same generator but on different days, the 15ht of December and the 5th of February respectively. In Figure 6.5 the effect of the shadow due to the tree is no longer present because of the higher position of the sun.

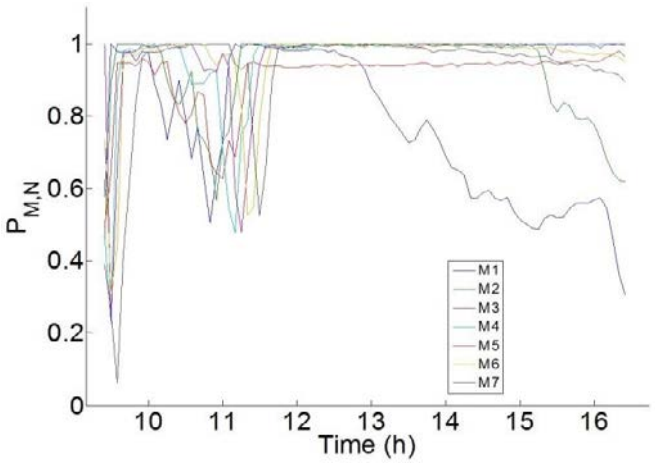

Figure 6.8: Effect of different shading objects over each module of a PV generator the 15th of December

The first object, a building about 30 meters away, causes a large power loss in the module during a short period of time. It causes a large power loss because, being the building a large solid obstacle, it covers all the cells losing more than 90% of its power; being the 10% left the diffuse radiation. On the other hand, this power loss only occurs during a short period of time because the farther away the object is the faster the shadow casted by object moves along the PV generator.

The second object, a tree fifteen meters away from the generator, causes a smaller power loss during a larger period of time; from 10:15 to 11:45. Since these experiments have taken place during the winter months, the trees are leafless and their shadow doesn't cover entire cells. Therefore, the power loss is less than that caused by the building's shadow. In addition, since the tree is closer to the generator than the building, the time that the shadow affects each module is larger.

The last fixed object whose shadow affects the generator is a very close by antenna. Even though the total effect of the shadow cannot be appreciated because the day ends, it can observed that the duration of the shadow's effect over each module is much longer than in the more far-away objects. It also occurs that, due to width of the antenna being less than a cell's width, there is not a total power loss in each module, just like in the tree.

By knowing the width of the modules and the time when each module is affected by shadows, the location of the object which causes each shadow can be determined. Figure 6.9 shows a schematic of the shadow trace over a PV generator and the angles involved. ψ_S, azimuth angle of the sun when the shadow starts to affect the first module and $\Delta\psi_S$,

change in the azimuth angle from when the shadow affects the first module to when it starts to affect the second module (or any chosen module), can be obtained by applying the equations of the sun's position and knowing the day of the year, the latitude, the width of the modules and the time when the shadow affects the first module and when it affects the second module (or any chosen module).

$$cos\psi_s = (sin\gamma_s \cdot sin\emptyset - sin\delta)/(cos\gamma_s \cdot cos\emptyset) \tag{6.1}$$

Where δ is the sun's declination for the day, ϕ is the latitude and $\sin(\gamma_s)$ is equation (6.2) in which w is the solar angle.

$$\sin(\gamma_s) = \sin(\delta)\cdot\sin(\emptyset) + \cos(\delta)\cdot\cos(\emptyset)\cdot\cos(w) \tag{6.2}$$

In order to obtain the distances, the triangle which represents the shadows at the first and second module is divided into two rectangular triangles. First, the height, h, of these triangles is obtained by equation (6.3).

$$h = w'\cdot\cos(\psi_s) \tag{6.3}$$

where w' is the width of the module, or chosen modules, and d' is obtained with equation (6.4).

$$d' = h/(\sin(\Delta\psi_s)) \tag{6.4}$$

Finally d is obtained with equation (6.5).

$$d = d'\cdot\cos(|\psi_s| - \Delta\psi_s) \tag{6.5}$$

It can be considered that the object is at a distance from the generator between d and d'. This method has been applied to the effects of the tree shown in the previous figure. For a better precision, the time lapse has been considered between the lowest point in the power curve of the first and last modules, obtaining that the tree is at a distance, d', of 17 meters and at an angle of 46º east. In comparison with the real object, the angle matches exactly and the distance is off by two meters; being the real distance 15 meters. This is due to the inaccuracy of the time lapse between the shade affecting the first module and the last module; which has been found to be 43.5 minutes. A difference of only four minutes will give the exact value of 15 meters. This method should, therefore,

only be considered as an estimate but good enough to decide if an object is close-by or far-away and it should be applied by the most far-away modules to have a better estimate.

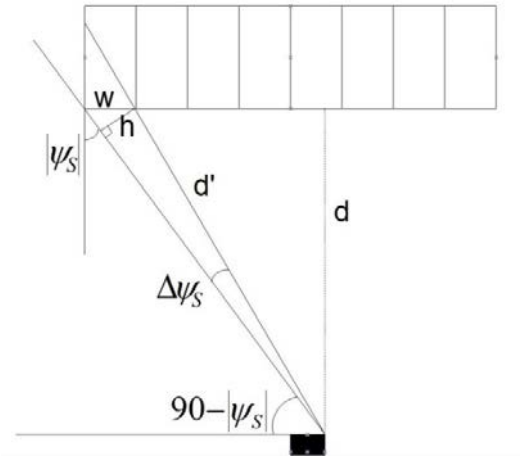

Figure 6.9: Schematic of an objects shadow over a PV generator and the angle and distances involved

From this analysis, the nature of the effect each shadow has over the PV generator's power has been analysed and the procedure aims at diagnosing at least four different fixed objects: close-by large object, close-by small object, far-away large object and far-away small object. Figure 6.10 shows the algorithm for temporal failures.

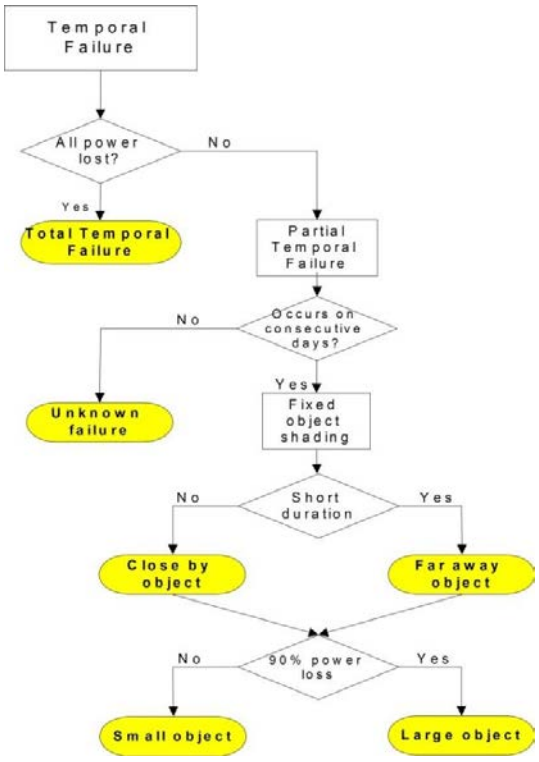

Figure 6.10: Temporal failure diagnosis algorithm

6.4.4.2 Continuous failures

Continuous failures are detected because the failing module is working at a lower power than the rest of the modules during the whole day. Under the continuous failure category the procedure can diagnose different failures depending on their power loss and their voltage and current values. The different diagnosed failures are:

- Total continuous failure
- Partial continuous failures
    - Hot-spot
    - Module degradation
    - Localized dirt

The total continuous failure is diagnosed when the analysed module does not produce any energy during the whole day. For diagnosing the rest of the failures, a deeper analysis that also considers voltage and current values must be undertaken.

The continuous failure algorithm is shown in Figure 6.11.

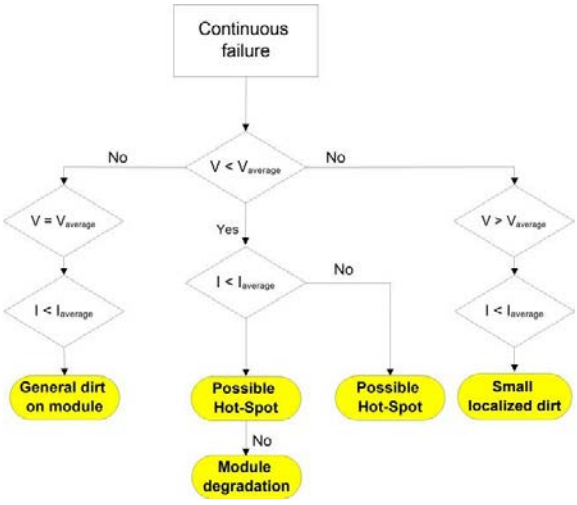

Figure 6.11: Continuous failure algorithm

6.4.4.2.a Small localized dirt

In this procedure small localized dirt is considered as that which is small enough that it does not cause the affected cell to work in reverse-bias (in DMPPT systems). Whether

this occurs or not depends on: the size of the dirt spot and the reverse characteristics of the shaded cells. When there is small localized dirt on a PV module the current of the module will be diminished in a proportion equal to the amount of shade on the cell and the voltage of the module will increase a little bit, due to the displacement of the working point towards V_{OC}. An example of this can be seen in Figure 6.12 where module number 3 has one cell shaded at about 25%. Since the modules have two strings of cells in parallel, the percentage of current lost is only about 12.5%. A small voltage increase is also observed with respect to the average of all modules.

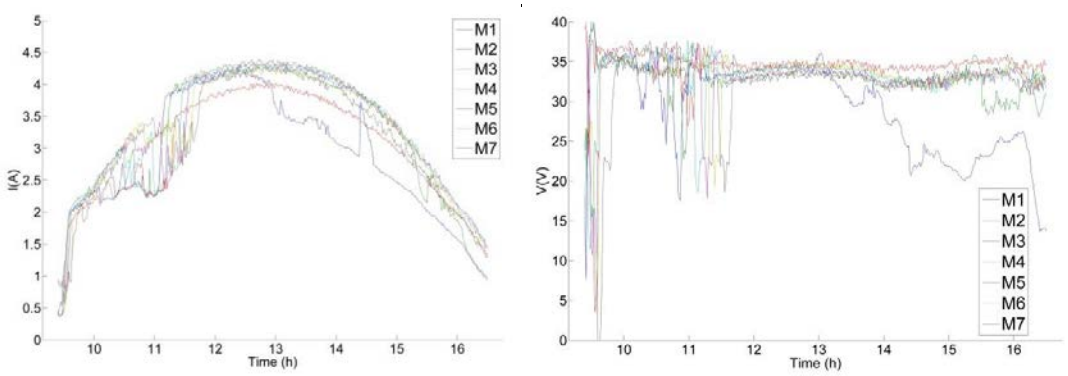

Figure 6.12: Current and voltage measurements of generator 1, where module 3 is partially shaded, simulating small localized dirt.

A thermographic picture of the shaded cell was taken at midday, Figure 6.13 (left), to show that the temperature increase in these situations is very small.

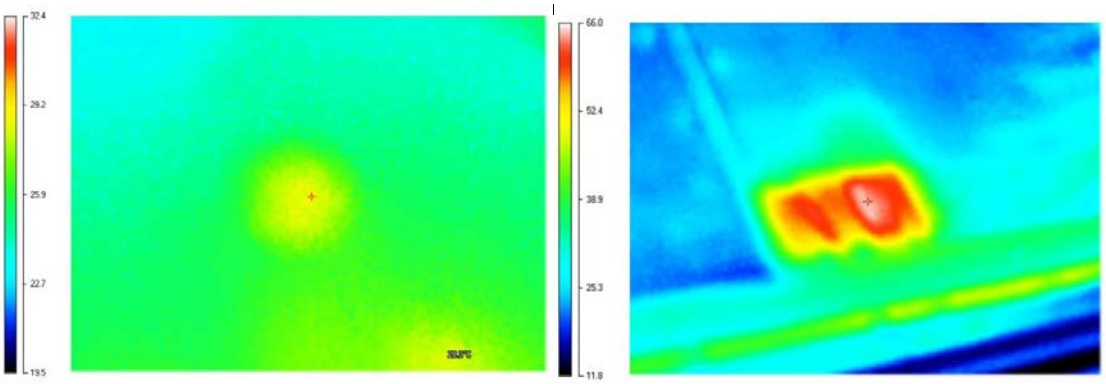

Figure 6.13: Thermographic image of a cell affected by small localized dirt (left) and by large localized dirt (right), this last one producing a hot-spot

6.4.4.2.b Hot-spots

As it was already introduced in section 6.2.4, hot-spots are a serious problem in PV systems and they should be quickly identified. In section 6.2.4 it was also explained how hot-spots can be identified when a voltage drop in the module is detected. In this sub-section an example of a hot-spots and its effect on the module's voltage and current is presented.

The experiment consisted in shading two electrically parallel cells of a module by 50%; both protected by the same by-pass diode. The result after half an hour of exposure with the system connected to the inverter is a 40ºC above normal working temperature hot-spot. This experiment was carried out in winter and under 800W/m^2 irradiance and the shaded cells reached 65ºC, as shown in Figure 6.13 (right). In hot summer middays with normal cell temperature close to 70ºC this hot-spot could easily reach values over 100ºC, resulting in irreparable damage.

Figure 6.14 shows the effect that this shading has on the voltage and current of the module (module 2, green lines).

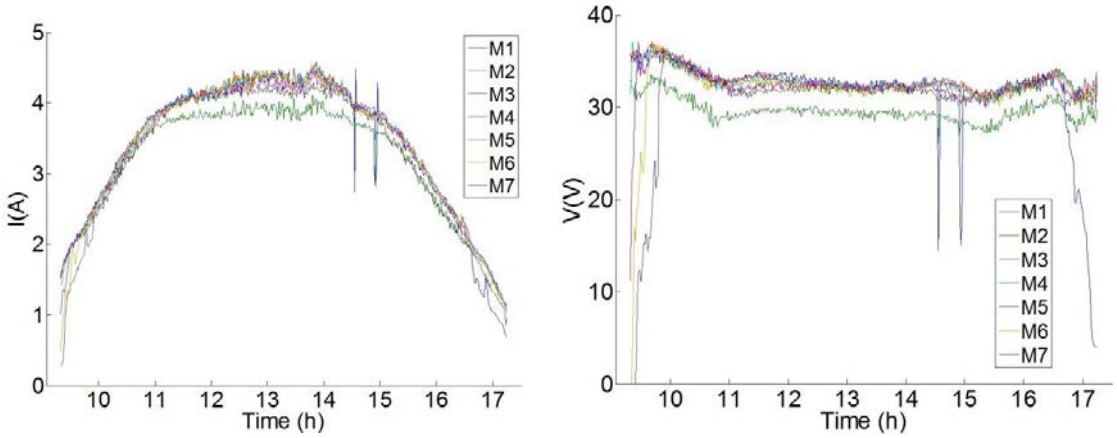

Figure 6.14: Current and voltage of the seven modules during a whole day. Module 2 is affected by a hot-spot

It is also known that the shape of a cell's *I-V* curve in reverse bias can be significantly different from cell to cell [Alonso-García, Ruiz et al., 2006a]. Depending on the cell's breakdown voltage, shunt resistance and the amount that it is shaded, it will cause the diode to work in forward bias or not. If the diode is in forward bias the current remains at its normal value and the voltage decreases in an amount proportional to the number of diodes in the module. If not, a reduction in both current and voltage is observed,

being the reduction in voltage less than if the diode is in forward bias. In both cases a reduction in voltage is observed and this is the information with which this tool detects hot-spots. Other works also relate a reduction in voltage to a hot-spot [Lorenzo, Moretón et al., 2013].

6.5 Conclusions

In this chapter the different possible faults that can occur in PV systems as well as real cases have been presented. Their effect on P_M, V_M and I_M of individual modules with DMPPT has been analyzed and has been used to create a failure diagnosis procedure which has been experimentally verified. The experiments conducted have shown that the tool works very well and returns consistent results during clear days. It has been shown that the results during cloudy days are not representative.

This procedure does not need the use of irradiance or temperature sensors as all other monitoring and failure detection procedures that have been found in the literature do. This is a great advantage for small PV systems in which calibrated irradiance and temperature sensors will increase the total price in a significant percentage.

This procedure can diagnose a large scope of failures including: fixed object shading with an estimate of distance to the object, small localized dirt, possible hot-spots, module degradation, generalized dirt and cable losses. In addition, an estimation of the energy losses caused by each failure can be obtained and it can be used to alert the user of the severity of each failure and the priority to solve it. This makes it a much more advanced procedure than any other previously presented in the literature making it ideal for system owners with no technical background or maintenance companies with many systems distributed over a large area, saving them much time and money.

7 CONCLUSIONS AND FUTURE LINES OF RESEARCH

This work is a contribution to PV systems with distributed maximum power point tracking (DMPPT), also known as module level power electronics (MLPE), a system topology characterized by performing the MPPT at module level, instead of the more traditional topologies which perform MPPT for a larger number of modules. The two DMPPT technologies available at the moment are known as microinverters and power optimizers and they provide certain advantages over string and central MPPT systems like: higher energy production in mismatch situations, monitoring of each individual module, system design flexibility (particularly for building integration) and higher system safety. DMPPT is not limited to urban environments although it is its natural market, since in large ground-mounted PV plants the extra cost is difficult to justify. This final chapter presents the main conclusions obtained throughout the thesis as well as the main contributions made by the author.

7.1 CONCLUSIONS

Since 2010 the MLPE market has not stopped growing and gaining market share and the predictions are that the tendency continuous this way, especially in distributed generation PV systems. In 2013 MLPE accounted for a 4% of the total inverter market and in 2012 54% of the residential PV systems installed in the United States were done

with MLPE. These numbers justify that theoretical and experimental studies on DMPPT are performed and keep on being performed in the future in order to fully understand the technology. Despite the large growth in market share of these products the number of publications on this topic is still very small.

Because one of the key objectives of DMPPT implementation in PV systems is the mitigation of the losses produced by shading, a profound study on the effects of shading in PV systems has been performed. For this task an advanced tool has been developed that permits simulating *I-V* curves for different shading situations.

- This tool allows choosing the radiation that each cell in the system receives as well as its parameters in reverse bias (like the breakdown voltage), the Diffuse/Global solar radiation ratio, the number and type of modules and the system configuration.

- The tool has been validated with experimental measurements and the results are in very good agreement with the simulations.

With the use of this tool as well as with measurements in PV prototype installations a study on the effects of shading has been conducted and presented. It has been shown that there is a large number of shading patterns possible and the effects that they have over the generator's or module's *I-V* curve depend on many factors like: the number of shaded cells and number of shaded sub-modules, the breakdown voltage of the shaded cells, the configuration of the system in terms of the number of parallel strings and the total number of modules.

- In parallel strings, if the shadow does not affect both strings equally the losses will be much higher than in serially connected strings due to voltage mismatch.

- In shaded situations, the breakdown voltage of the shaded cells directly affects the shape of the *I-V* curve being it responsible for activating or not activating the by-pass diode. As more cells are shaded the effect of the breakdown voltage diminishes and even disappears.

A profound study of the functioning of PV systems with power optimizers has been presented. The mathematical equations that govern their functioning have been derived, showing that the use of DC/DC converters in PV strings (power optimizers) creates some non-trivial constraints due to their limited output parameters.

- These equations show that not all mismatch situations can be solved with power optimizers and that opposite to what some manufacturers are doing, a variable input inverter voltage should be used for maximizing the situations of mismatch that can be solved.
- Graphical examples of the resulting *I-V* and *P-V* curves of PV systems with power optimizers have been presented which also verify the limitations of power optimizers in solving all mismatch situations.
- With these equations, some simulations in power optimization for different system topologies and shading patterns have been performed showing in an initial step that a large power gain is not to be expected with DMPPT.

In a next step power gain measurements with the use of DMPPT in real PV systems have been conducted with the following conclusions

- Power gains up to 20% have been recorded.
- The power gains are higher as the number of shaded sub-modules in the string increases.
- For the same number of shaded sub-modules, higher power gains are obtained for shadows that cover less than 50% of the cells, than for shadows that completely cover the cells of the same sub-module.
- It has also been shown that the possible energy gain in unshaded situations due to the mismatch of the electrical characteristics is very small. For example, for one of the tested modules, for a 5% current mismatch only a 1% power gain is obtained.

- In these measurements it has become evident that when the MPPT does not find the global MPP in a central MPPT system, the power gains obtained with DMPPT are much higher than normal.

The last conclusion obtained from the power gain measurements has motivated a study on the MPPT efficiency of inverters and MLPE in presence of local maxima. It has been found that many of the algorithms implemented in modern equipment are not able to find the absolute MPP in presence of local maxima. What is even more disturbing is that none of the algorithms of MLPE, although they are designed for mitigating the shading losses in PV arrays, finds the absolute MPP in presence of local maxima. The findings on MPPT efficiency in presence of local maxima and the fact that no international standard has a test protocol to test the ability of inverters or MLPE in these situations, have motivated the proposal of a testing protocol for verifying the ability of MPPT algorithms in finding the global MPP.

A new benefit of DMPPT that has never before been mentioned has been discovered, which deals with the beneficial effects of using DMPPT for hot-spot mitigation.

- It has been found that systems with DMPPT are less prone to be affected by hot-spots caused by localized dirt because since the perform the MPPT at module level it is more probable that the shaded cells keep on working in forward bias and the non-shaded cells reduce their current to match that of the shaded cells.

- The percentage of shade until which this occurs depends on the module type, especially the number of by-pass diodes, and it is close to 50%; meaning that for shadows covering less than 50% of a cell there is no hot-spot risk.

- It has also been found that when the cell works in reverse bias, the dissipated power by the shaded cell is higher the lower the percentage of shade, meaning that the use of DMPPT eliminates the hot-spot risk for the worst case situation.

- This can prove especially interesting for increasing the reliability of PV systems, especially those with low maintenance like small roof-top PV systems.

From the performed shading analysis and the power gain measurements it has become clear that there is an infinite number of possible shading situations making it impossible to create a general methodology for determining the energy gains obtained with DMPPT. This has motivated the development of a model for simulating energy gains that has been experimentally verified.

- With the geometry of a nearby obstacle and considering the equations of the relative movement of the sun, this model creates a grid of shaded points in a PV generator that goes down to the cell level. Up to 64 points in each cell are modelled allowing the simulation of the exact *I-V* curve of a PV generator in any instant of the year.

- With these curves and the restraints of MLPE, also presented in the thesis, the energy gains obtained for different obstacles have been simulated, as well as the losses associated to each concept.

It has been found that the final energy gains are much lower that the instantaneous power gains and that the high percentages advertised by MLPE companies, i.e.:

- For a roof top system affected by the shadow of a chimney (9% energy loss), the yearly energy gain obtained is approximately 2.5%.

- A more heavily shaded installation (40% energy loss) has also been simulated obtaining higher yearly energy gains up to 18%. However, this is an old installation with five strings in parallel, which greatly increases the losses. Only by reconfiguring the installation to two strings with independent MPPTs (common in many modern inverters) the losses are reduced to 34.5% and the possible energy gain with DMPPT is now only of 10.4%, considering MLPE for each module. Because the modules are of only 120W the more realistic situation would be to have MLPE for each two modules, reducing the possible energy gain to 7.3%.

A short economic analysis has also been presented, highlighting other benefits than energy gains, like reduced O&M and installation costs that could make this technology viable. Because in small rooftop installations manual labor is a very large percentage of the total installation price (up to 50%) and because DMPPT systems can reduce

installation time, especially microinverters, in an optimistic scenario DMPPT systems could end up in a lower final price per kWh.

Another interesting option of MLPE is that the working values of each module are monitored. This permits knowing which exact module is under-producing reducing the maintenance costs in a case of failure. However, even more interesting is the failure diagnosis possibilities that this provides if a look into the voltage and current values of each module is taken.

- A failure diagnosis tool has been developed and experimentally verified.
- The tool can diagnose the following failures: fixed object shading and location of the object causing the shade, localized dirt, possible hot-spots, module degradation, excessive DC cable losses and generalized dirt.
- With the exception of generalized dirt, the failure diagnosis tool does not require the use of irradiance or temperature sensors, reducing the cost of the system, especially interesting in small installations and this can a large percentage of the total installation price.

7.2 FUTURE LINES OF RESEARCH

Although the results obtained in this thesis are not very optimistic towards the possible energy gains obtained with DMPPT, other benefits of this technology have been pointed out and in general they can be a good option for small rooftop PV systems. Because of their recent introduction into the market there are still points to be solved related to MLPE. The following lines of research have been identified related to these products:

- Improve the MPPT algorithms of MLPE so that the global MPP is always found in the shortest time possible, increasing the energy yield.
- Experimental evaluation of the energy gains obtained with DMPPT in situations of partial shading from nearby obstacles, in days of passing clouds and in non-shaded situations. For this task the ideal setup would be to have to identical PV strings affected by the same shadows, one with DMPPT and one with a central

inverter. The energy produced by each system should be monitored and compared to assess the benefits of DMPPT in different situations.

- More specifically to the work developed in this thesis, the model for simulating energy gains should be more deeply experimentally verified.
- Reliability experiments of MLPE should be undertaken, both in the laboratory and in a field setup. Electronic equipment reliability is known to be dependent of working at high temperature and because MLPE will work behind PV modules, easily reaching temperatures of over 70ºC, they could fail prematurely forcing their replacement and increasing the cost of the installation.

APPENDIX A

ANALYSIS OF THE D/G RATIO IN MADRID AND SANTANDER

This appendix presents an analysis of the D/G ratio for Madrid and Santander, Spain. Madrid represents a location with a low annual diffuse component, of only 8.1%. Main data of Madrid and Santander can be seen in Table 7.1.

Table 7.1: Data of interest of Madrid and Santander for the D/G ratio analysis.

	Latitude	Altitude (MASL)	Annual G(0) (kWh/m^2)	Annual D/G ratio
Madrid	40º25'08" N	655	1720	8.1%
Santander	43'28'00"N	15	1220	47.8%

The data for Madrid has been obtained from a meteorological station located on the rooftop of the Instituto de Energía Solar. The meteorological station records minutely data of global and diffuse horizontal irradiance. The global irradiance values are recorded with a normal pyronometer while the diffuse irradiance values are recorded with a pyronometer that has a black ball which rotates on two axes and is permanently blocking the direct irradiance. The accuracy of this data is considered very high. The data for Santander has been obtained from the Agencia Estatal de Meteorología (AEMET), also with the same equipment as the data for Madrid.

In a first step, the data has been analysed yearly and the number of periods for each D/G ratio (calculated on steps of 0.005, from 0 to 1) has been recorded. In a second step, the D/G ratio has been grouped as a function of the irradiance. That is, the amount of annual irradiance for each D/G ratio step has been added together. The data has also

been processed and extrapolated to an optimum tilt (34º). Figure 7.1 and Figure 7.2 show the results obtained. Various conclusions can be obtained:

- Most of the D/G ratios are concentrated below 20% and above 90%.
- If the analysis is done based on irradiance, the weight of low D/G ratios is higher.
- On a tilted plane the weight of high D/G ratios decreases and most of the irradiance occurs for D/G ratios between 7-15%.

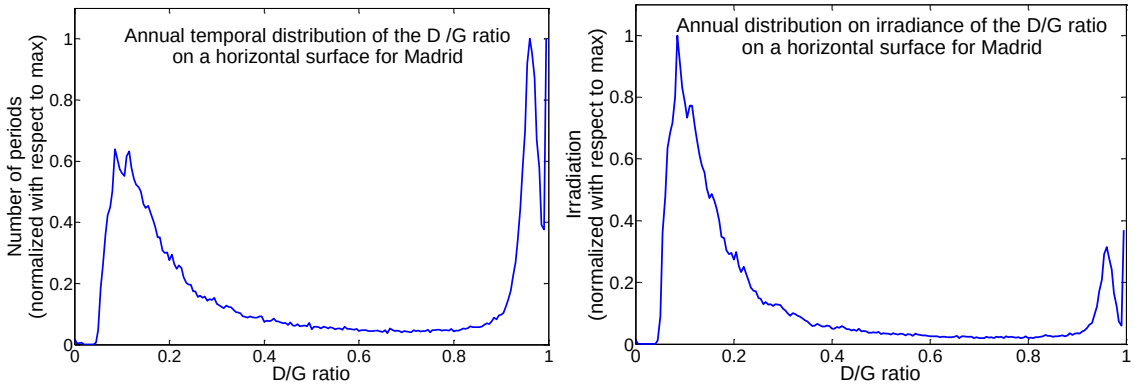

Figure 7.1: (left) Temporal distribution function for the D/G ratio on a horizontal surface for Madrid, and (right) the same distribution but weighted on irradiance.

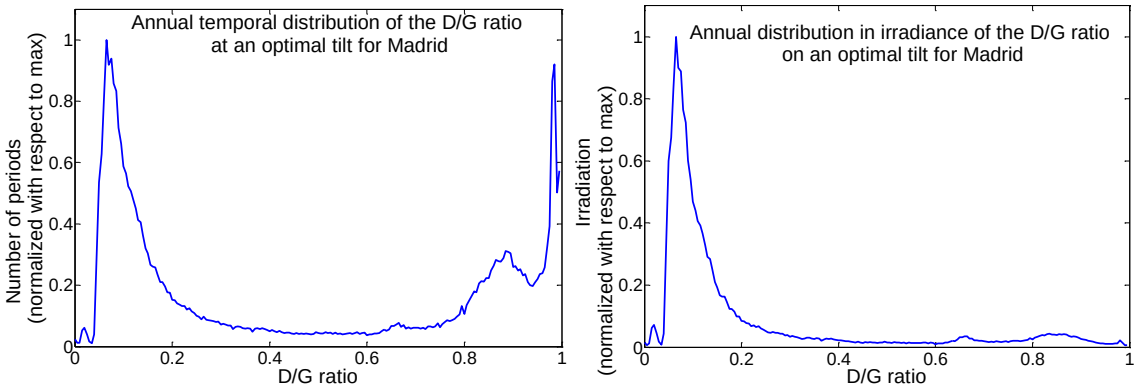

Figure 7.2: (left) Temporal distribution function for the D/G ratio on a 34º surface facing south for Madrid, and (right) the same distribution but weighted on irradiance.

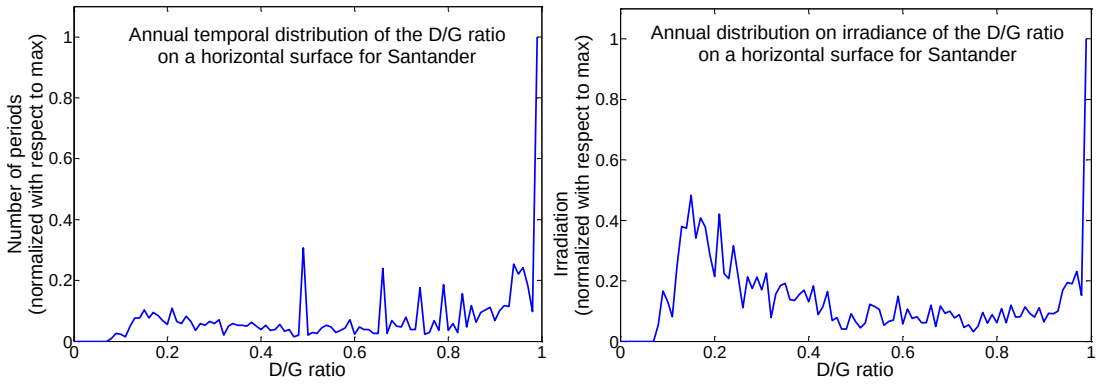

Figure 7.3: (left) Temporal distribution function for the D/G ratio on a horizontal surface for Santander, and (right) the same distribution but weighted on irradiance.

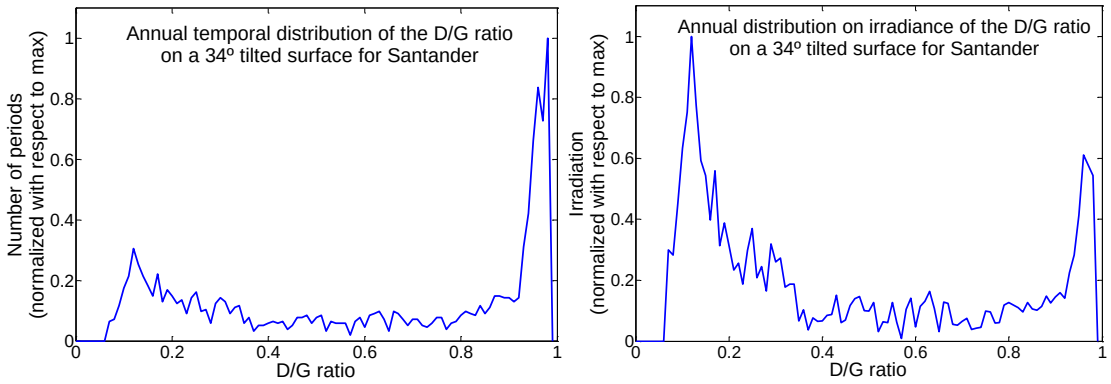

Figure 7.4: (left) Temporal distribution function for the D/G ratio on a 34º surface facing south for Santander, and (right) the same distribution but weighted on irradiance.

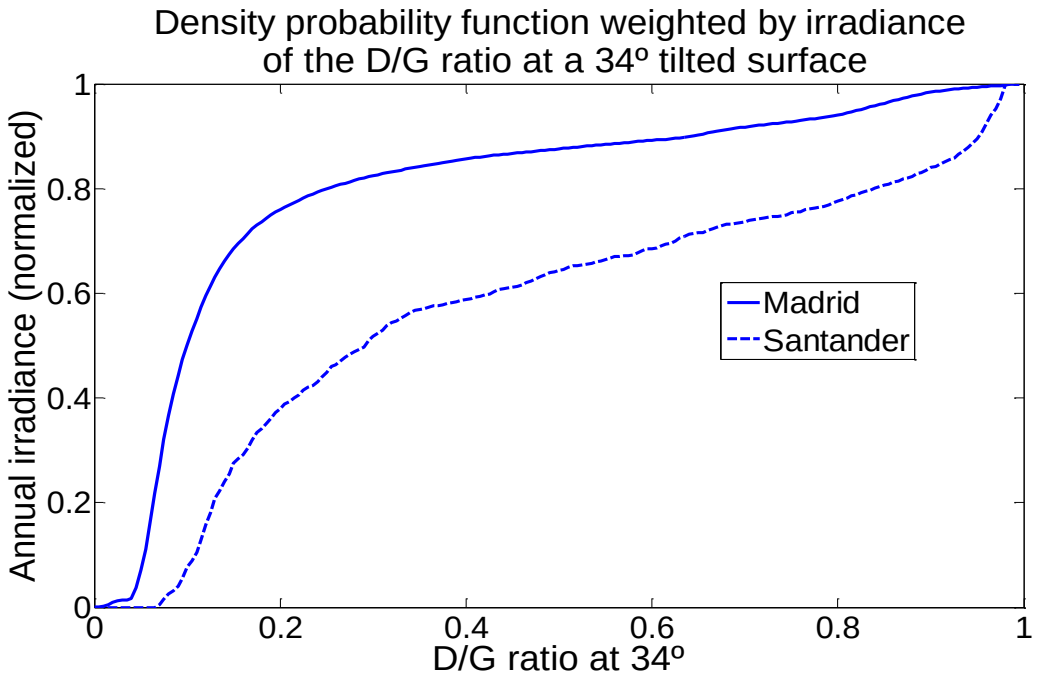

Figure 7.5: Probability density function of the D/G ratio weighted on irradiance and on a 34º tilted surface for Madrid and Santander.

APPENDIX B

SOLAR EDGE CASE STUDY

CASE STUDY

The Way to Energy Gain

Aidlingen, GERMANY

OVERVIEW

Highlighted Features:
Chimney shading

Installer: SL Solarlösungen GmbH

Installation Date: December 2010

Location: Aidlingen, Germany

Installed capacity: 6.75 KWp

Average Irradiance:
1,180 kWh/m²/year

Modules: Solaria S6P 225

String Layout: 2 inverters, 1 string per inverter with 15 modules

The photo shows how the SolarEdge system allowed Mr. Schneider to install modules close to the chimney without risking disproportional energy losses.

How much energy really gets lost from partial shading? Installer Bernhard Schneider was called to install a PV system on the roof of a family home in Aidlingen. Besides a small chimney in the middle, the roof was generally suitable for a 6.75kW installation. *"The chimney was a major reason why I recommended that Mr. and Mrs. Gerstner use SolarEdge power optimizers. The chimney could cast a shadow on some of the modules. A small shadow is enough to cause energy losses which are much greater than the actual shaded area would imply"*, says Mr. Schneider.

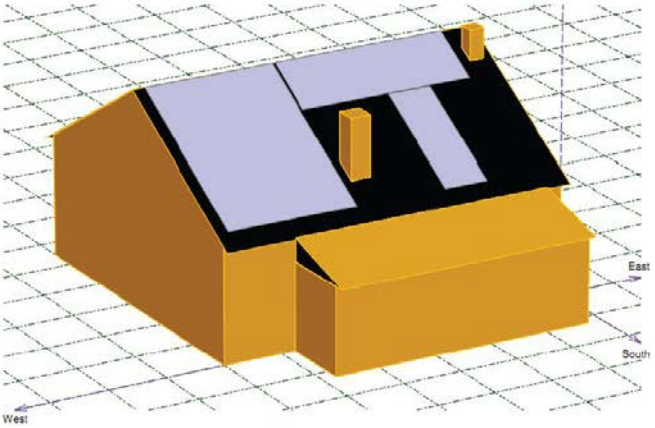

The picture shows the PVsyst model of the house with 6.75kWp and 30 x 225W modules and the chimney in the middle.

It is a well-known fact that modules interfere negatively with each other in a serial connection; while the modules' peak operating points are diverse, traditional inverters use a 'one-size-fits-all' approach to harvest their energy. Partial shading, or uneven exposure to sunlight, diversifies the modules even further as some can produce more than others now. All modules obviously produce less energy

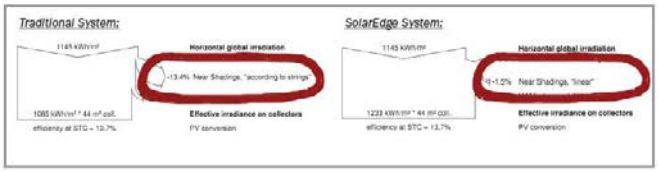

The result summary of the PVsyst simulation shows the improved ability of the SolarEdge system to mitigate losses caused by partial shading (only 1.5% loss) compared to 13.4% loss by the traditional system.

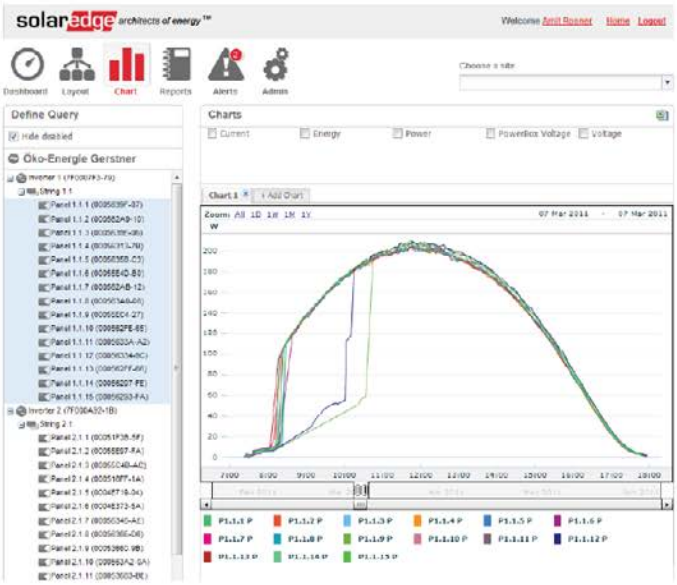

This screenshot from the SolarEdge monitoring portal shows the performance of each module in a chart. The chart proves that modules 9 and 12 are shaded in the morning between 8-10 o'clock.

when they are shaded, but in a serial connection shaded modules bring down the output of all other modules connected to them in a string. Hence, the question is: how great is the energy loss really?

This screenshot from the monitoring portal of the installation shows two modules in an alerted state as they are being partially shaded by the chimney.

In order to examine the impact of partially shaded modules on the overall energy production, we use this 6.75kW installation as an example. The SolarEdge monitoring portal, which offers insight into each module's performance, reveals the following: module 9 and module 12 in string 1 (marked in the server as 1.1.9 and 1.1.12, respectively) are shaded in the morning hours between 8:00 - 10:00.

In order to quantify the impact of shaded modules 9 and 12 on the energy production of the system, we employed PVsyst (a simulation software developed for installers by the University of Geneva) to create a model of our 6.75kW installation. We then simulated its energy output, once using a traditional 'one size-fits-all'-inverter and once using SolarEdge power optimizers with individual maximum power point trackers for each module.

With maximum power point tracking per module, the shading losses calculated by PVsyst are proportional to the shaded area and constitute 1.5% of the potential output. The overall system perfomance ratio is 80.7%. The traditional inverter however, loses 13.4% of the potential output because of the two shaded modules. The overall system perfomance ratio is 71.8%. The power optimizers managed to harvest 12.4% more energy in the first year of operation alone. This percentage is likely to grow over the 20 year typical lifetime of an installation as the disparity between the modules grows with their exposure to changing weather conditions.

Quick fact:
Aidlingen is situated in the state Baden-Württemberg. The town is famous for its surrounding nature and for being the home of Germany's first female fighter jet pilot, Ulrike Flender.

Summary: This case shows that a small chimney which casts a shadow on two modules in the morning, combined with normal module mismatch, unnecessarily causes the home owners to lose 13.4% of their potential energy while the real loss caused by the shaded area is merely 1.5%. The truth is that few installations in residential neighborhoods are completely free from shading elements. Therefore, next time when planning a PV installation, keep this study in mind.

"We are very happy with Mr. Schneider's recommendation to use power optimizers. Our chimney proved no obstacle for the SolarEdge system and the results simply speak for themselves."

Mr. and Mrs Gerstner
System Owners

www.SolarEdge.com info@solaredge.com

2/2

solaredge
architects of energy

APPENDIX C

TORRE TITANIA

C.1 Introducción

C.1.1 El problema

El problema analizado y presentado en este informe trata sobre las pérdidas en el sistema fotovoltaico de la Torre Titania debido a las sombras del propio edificio y, más concretamente, con las posibles ganancias energéticas con el uso de sistemas con seguimiento distribuido del punto de máxima potencia (DMPPT).

La particularidad de esta instalación (Figura C.1) es que está instalada sobre la fachada del edificio, el cual es circular y es por ello que cada módulo tiene una orientación acimutal diferente. Debido a la inclinación de los módulos, 2º sobre la horizontal, la diferencia de radiación captada por los módulos, debido a la diferente orientación de cada uno, es despreciable. Sin embargo, no es despreciable la sombra arrojada por el propio edificio en los diferentes módulos a lo largo del día.

Para minimizar este problema hubiera sido suficiente conectar en serie los módulos de cada planta con la misma orientación. Sin embargo, esto suponía pasar cables de planta en planta, lo cual no era posible. Se optó entonces por conectar los módulos de cada planta en serie. Esta conexión implica que, debido a las sombras producidas por el propio edificio, los módulos en una misma serie trabajan en distintas condiciones de iluminación y, por tanto, su punto de máxima potencia (MPP) es diferente. Si la diferencia en el MPP es en corriente y como los módulos están conectados en serie, se producen unas pérdidas por *mismatch* ya que la corriente en una conexión en serie es siempre la misma y, por tanto, no todos los módulos podrán estar trabajando en su MPP.

Desde el año 2009 existen en el mercado fotovoltaico equipos que llevan a cabo el seguimiento del punto de máxima potencia (MPPT) a nivel de módulo, eliminando así las pérdidas por *mismatch* que pueden ocurrir en sistemas con un MPPT centralizado. Actualmente existen dos tipos de sistemas DMPPT: microinversores y optimizadores de potencia. Es objeto del estudio realizado y presentado en este informe estimar las pérdidas en la instalación fotovoltaica y la posible ganancia con el uso de sistemas DMPPT.

Figura C.1: Imagen de la Torre Titania con sus 22 líneas horizontales de 18 módulos cada una.

C.1.2 La instalación fotovoltaica

La instalación fotovoltaica de la Torre Titania se divide en 22 pisos con 18 módulos de 160 W_p cada piso, creando 22 *strings* de 2.88 kW_p que hacen un total de 63.36kW_p [Rosell, 2012]. Cada módulo tiene 42 células (6x7) conectadas en serie y dos diodos de paso[35] cubriendo 21 células cada uno. Los módulos son vidrio-vidrio y están hechos a medida para la forma del edificio. Debido a que el edificio es de forma circular, los módulos se han fabricado con forma trapezoidal para que encajen unos con otros (C.2). Aun así, la forma de las células y el espacio que ocupan es rectangular.

[35] Esto es una suposición ya que no existe el dato.

Los módulos están todos inclinados 2º respecto a la horizontal (β=2º) y cada uno tiene una orientación diferente debido a la estructura circular del edificio. En concreto están orientados desde -17.6º hasta 107.2º en pasos de 7.35º.

Figura C.2: Los módulos utilizados en la instalación fotovoltaica de la Torre Titania. Se puede observar como los módulos son más anchos en la parte alejada del edificio, permitiendo que encajen entre si.

En cada piso, los 18 módulos están conectados en serie a un inversor Sunny Boy 2500HF.

C.2 Simulaciones y resultados

C.2.1 Los obstáculos

La instalación fotovoltaica de la Torre Titania está afectada por sombras de varios obstáculos (C.3). El primero es el propio edificio, que al ser circular arroja sombras sobre distintos módulos en función de la hora del día. En términos generales, los módulos mirando al oeste están sombreados por la mañana y aquellos mirando al este están sombreados por la tarde.

La segunda sombra que afecta al generador es un muro que está al sureste de la torre. El muro está a la misma altura que el sexto piso de módulos. Aunque si miramos la C.1, se puede observar que por encima de ese muro existe otro muro que no viene en los planos y que llega casi hasta la fila 19 de módulos. Además, existe un tercer obstáculo al

noroeste del generador muy parecido al muro que está al sureste. Sin embargo, por su posición este muro no arroja muchas sombras sobre el generador, haciéndolo solo en los días más cercanos al solsticio de verano.Para las simulaciones se ha supuesto que todos los *strings* por encima del quinto piso no están afectados por la sombra de ningún muro, estando solo afectados por la sombra del propio edificio. Respecto a la posible sombra arrojada entre filas superiores de módulos sobre las filas inferiores, ésta es inexistente incluso en el solsticio de verano ya que la separación entre pisos es suficientemente grande (cuatro metros).

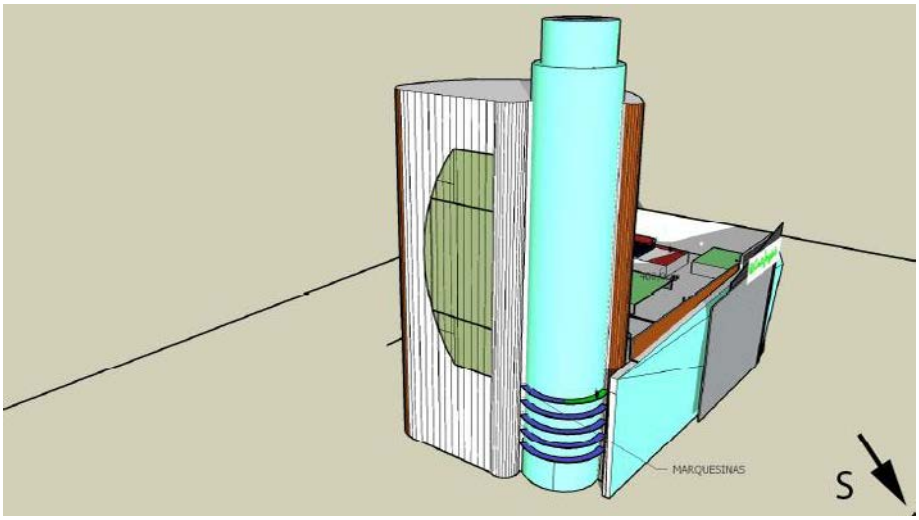

Figura C.3: Dibujo en autocad de la Torre Titania con los cinco generadores fotovoltaicos inferiores

C.2.2 Las simulaciones

Se han llevado a cabo una serie de simulaciones teniendo en cuenta distintos factores que afectan al funcionamiento del generador fotovoltaico. Éstos se detallan a continuación:

- Obstaculos: Se han simulado seis *strings* diferentes. Los cinco más bajos de la torre, afectados por los dos obstáculos, el edificio y el muro, y uno cualquiera de los 17 *strings* superiores que solo están afectados por el propio edificio.

- Ganancias energéticas en curvas *I-V*: esta es la ganancia ideal si no hay pérdidas debido a los equipos de acondicionamiento de potencia (DMPPT e inversor central). Se compara el MPP de la curva *I*-V del generador con la suma de MPPs de las curvas *I*-V de cada módulo. Se ha seguido el mismo procedimiento que en [Solórzano, Masa et al., 2013].

- Simulaciones con equipos reales: tiene en cuenta las características de equipos reales en el mercado. En este caso solo se ha simulado con SolarEdge ya que no se ha encontrado ningún micro-inversor que tenga un rango MPPT por debajo de 22V, mientras que los módulos tienen una tensión máxima, V_M, igual a 20V. Se ha decidido simular como si se pusiese un optimizador de potencia por cada dos módulos, para adaptar mejor la tensión y potencia de los módulos a los optimizadores SolarEdge.

- Pérdidas debido a los equipos de acondicionamiento de potencia: se han introducido los rangos de tensión de búsqueda del MPPT de cada equipo y añadido las pérdidas causadas por estar el MPP fuera del rango. Se han utilizado características de equipos reales

- Diodos de paso: ya que se desconoce el número de diodos de paso en cada módulo, se ha llevado a cabo una primera simulación con dos y tres diodos. Debido a que los resultados obtenidos son prácticamente iguales, se han llevado a cabo el resto de simulaciones suponiendo dos diodos por módulo; es decir, un diodo cada 21 células.

- Pérdidas debido a no encontrar máximos locales: investigaciones propias del grupo GEDIRCI así como de otros autores [García, Maruri et al., 2008; Sanchis, López et al., 2007] han puesto de manifiesto que muchos algoritmos MPPT no logran encontrar los máximos locales en curvas *I-V* con sombras. Se ha simulado también este supuesto. Es importante mencionar que no está muy claro cómo responden los inversores centrales a este tipo de fallos y que depende mucho del paso en tensión que tenga el algoritmo MPPT. Los resultados de este caso puede ser que no sean del todo fiables y se está trabajando en mejorar esta parte de la simulación.

- Para todos los casos anteriores se han calculado las pérdidas debido a las sombras que inciden sobre el generador.

Aunque las simulaciones se han llevado a cabo para una serie de supuestos casos posibles la producción ideal en DC es la misma para todos los sistemas:

- Producción ideal en caso de no tener sombras: **4.43 MWh**

La producción ideal solo tiene en cuenta las pérdidas debido a temperatura e irradiancia en la tensión del sistema, las cuales son las mismas para todas las simulaciones.

Desde la tabla C.1 a la tabla C.7 se muestran los resultados obtenidos para las simulaciones descritas anteriormente. De la tabla C.1 a la tabla C.5 se muestran los resultados para las cinco filas inferiores, afectadas por ambos obstáculos, la tabla C.6 muestra los resultados para los cinco *strings* inferiores y la tabla C.7 muestra los resultados para una de las filas superiores, solo afectada por el edificio.

En las tablas se muestra la producción en DC para cada supuesto con DMPPT y con MPPT central. Las pérdidas totales se refieren a aquellas que ocurren con inversor central y, por tanto, su suma con la producción con MPPT central resulta en la producción máxima posible o producción ideal: 4.43MWh. En el caso de la tabla C.6 la producción ideal es 22.15MWh, cinco veces la de un *string*.

La energía recuperada se refiere al porcentaje de energía perdida que se recupera con DMPPT y se calcula según la ecuación c.1.

$$E_R = \frac{E_{DMPPT} - E_{MPPT}}{E_{MAX} - E_{MPPT}} \qquad \textbf{c.1}$$

Mientras que la ganancia energética se refiere a cuanta energía más se produce con DMPPT. Este es el valor a considerar a la hora de decidir si se instala DMPPT o no. La ganancia energética se calcula según la ecuación c.2.

$$E_I = \frac{E_{DMMPT} - E_{MPPT}}{E_{MPPT}} \qquad \textbf{c.2}$$

El caso ideal se refiere a un equipo DMPPT por cada módulo y sin pérdidas debido al MPPT de los equipos. Es, por tanto, la comparación entre la suma de los MPP de las curvas *I-V* individuales de cada módulo con el MPP de la curva del generador (18 módulos en serie). En este caso las pérdidas son solo debido al sombreamiento.

En los casos “SolarEdge.Sí” y “SolarEdge.No” se tienen en cuenta las características de los equipos de acondicionamiento de potencia y si el MPPT encuentra o no máximos locales. En este caso las pérdidas son las pérdidas del caso ideal más aquellas debido a los límites del MPPT. Además, hay que tener en cuenta que en este caso al tener dos

módulos en serie por cada equipo DMPPT, la optimización no es tan buena y hay otras pérdidas no reflejadas en las tablas.

Tabla C.1: Resultados de la simulación para el string del primer piso

	Producción (MWh)		**Pérdidas totales (MWh)**	**Pérdidas MPPT SE (kWh)**		**Pérdidas MPPT SB (kWh)**		**Energía recuperada**	**Ganancia**
	DMPPT	MPPT central		Rango	Max local	Rango	Max local		
Ideal	2.38	1.98	2.44 (55.2%)	0	0	0	0	16.3%	**20.1%**
SolarEdge Local Sí	2.32	1.93	2.50 (56.4%)	0.02	0	52.4	0	15.4%	**19.9%**
SolarEdge Local No	2.21	1.67	2.76 (62.4%)	0	109	0	319	20.1%	**33.2%**

Tabla C.2: Resultados de la simulación para el *string* del segundo piso

	Producción (MWh)		**Pérdidas totales (MWh)**	**Pérdidas MPPT SE (kWh)**		**Pérdidas MPPT SB (kWh)**		**Energía recuperada**	**Ganancia**
	DMPPT	MPPT central		Rango	Max local	Rango	Max local		
Ideal	2.46	2.04	2.39 (53.9%)	0	0	0	0	17.8%	**20.8%**
SolarEdge Local Sí	2.39	1.99	2.44 (55.1%)	0.02	0	52.1	0	16.7%	**20.5%**
SolarEdge Local No	2.30	1.68	2.75 (62.1%)	0.06	95.0	0	360	22.6%	**36.9%**

Tabla C.3: Resultados de la simulación para el *string* del tercer piso

	Producción (MWh)		**Pérdidas totales (MWh)**	**Pérdidas MPPT SE (kWh)**		**Pérdidas MPPT SB (kWh)**		**Energía recuperada**	**Ganancia**
	DMPPT	MPPT central		Rango	Max local	Rango	Max local		
Ideal	2.58	2.13	2.30 (52%)	0	0	0	0	19.7%	**21.3%**
SolarEdge Local Sí	2.51	2.08	2.35 (53.1%)	0.02	0	50.9	0	18.4%	**20.8%**

SolarEdge Local No	2.42	1.71	2.72 (61.4%)	0.06	91.8	0	416	26.0%	**41.2%**

Tabla C.4: Resultados de la simulación para el *string* del cuarto piso

	Producción (MWh)		**Pérdidas totales (MWh)**	**Pérdidas MPPT SE (kWh)**		**Pérdidas MPPT SB (kWh)**		**Energía recuperada**	**Ganancia**
	DMPPT	MPPT central		Rango	Max local	Rango	Max local		
Ideal	2.76	2.27	2.16 (48.7%)	0	0	0	0	22.5%	**21.4%**
SolarEdge Local Sí	2.68	2.21	2.21 (50%)	0.01	0	56.9	0	21.2%	**21.2%**
SolarEdge Local No	2.60	1.79	2.64 (59.7%)	0.01	86.3	0	486	30.7%	**45.5%**

Tabla C.5: Resultados de la simulación para el string del quinto piso

	Producción (MWh)		**Pérdidas totales (MWh)**	**Pérdidas MPPT SE (kWh)**		**Pérdidas MPPT SB (kWh)**		**Energía recuperada**	**Ganancia**
	DMPPT	MPPT central		Rango	Max local	Rango	Max local		
Ideal	3.06	2.63	1.80 (40.6%)	0	0	0	0	23.9%	**16.4%**
SolarEdge Local Sí	3.0	2.56	1.87 (42.1%)	0.02	0	67.6	0	23.3%	**17.0%**
SolarEdge Local No	2.90	2.05	2.37 (53.6%)	-0.01	92.5	0	574	35.8%	**41.4%**

Tabla C.6: Resultados de la simulación para los cinco *strings* afectados por el muro. La producción y las pérdidas es la suma de los cinco *strings* individuales. En este caso la producción ideal es 22.15MWh.

	Producción (MWh)		**Pérdidas totales (MWh)**	**Pérdidas MPPT SE (kWh)**		**Pérdidas MPPT SB (kWh)**		**Energía recuperada**	**Ganancia**
	DMPPT	MPPT central		Rango	Max local	Rango	Max local		
Ideal	13.24	11.05	11.09 (50.1%)	0	0	0	0	19.7%	**19.8%**
SolarEdge Local Sí	12.9	10.77	11.37 (51.3%)	0.1	0	280	0	18.7%	**19.9%**

SolarEdge Local No	12.43	8.9	13.24 (59.8%)	0.12	475	0	2155	26.7%	**33.2%**

Tabla C.7: Resultados de la simulación para el *string* de un piso solo afectado por la sombra del edificio

	Producción (MWh)		**Pérdidas totales (MWh)**	**Pérdidas MPPT SE (kWh)**		**Pérdidas MPPT SB (kWh)**		**Energía recuperada**	**Ganancia**
	DMPPT	MPPT central		Rango	Max local	Rango	Max local		
Ideal	3.62	3.42	1.01 (22.8%)	0	0	0	0	20.1%	**5.91%**
SolarEdge Local Sí	3.60	3.33	1.10 (24.7%)	0.03	0	89.3	0	24.6%	**8.1%**
SolarEdge Local No	3.53	2.71	1.73 (39.0%)	0	67.9	0	720	48.2%	**30.8%**

C.3 Conclusiones

De los resultados obtenidos de las simulaciones se pueden sacar conclusiones sobre dos líneas generales: pérdidas por sombreamiento y posibles ganancias con el uso de DMPPT

Respecto a las pérdidas por sombreamiento es conveniente tener en cuenta el valor obtenido en el diseño de la instalación con el programa PVSyst. En el diseño con el PVSyst solo se tuvieron en cuenta las pérdidas debido al propio edificio, con lo que los resultados del PVSyst se pueden comparar con los de la tabla C.7. Además, en la simulación del PVSyst el módulo más al este se ha orientado al sur, mientras que en los diseños de autocad este módulo está orientado a 17.8º este.

Según los resultados de simulación del PVSyst, existen unas pérdidas debido al sombreado de 19.7%. Este valor es comparable con el 22.8% obtenido en las simulaciones realizadas por el grupo GEDIRCI. Debido a que el PVSyst solo tiene en cuenta las pérdidas de radiación debido a las sombras y no tiene en cuenta los efectos eléctricos que una menor radiación sobre un módulo puede ocasionar sobre el resto de módulos, las pérdidas reales tienden a ser mayores, como muestran las simulaciones del grupo GEDIRCI, siendo de un 22.8% para los *strings* que solo están sombreados por el propio edificio.

Además, si se tienen en cuenta otros efectos como que el MPP esté fuera del rango de búsqueda MPPT del inversor o que el inversor no encuentre máximos locales, estas pérdidas aumentan aún más, llegando hasta el 39% en caso de no encontrar máximos locales. Como ya se ha mencionado en el informe, esto es un problema real en inversores comerciales y se debería de tener en cuenta. En este caso el hecho de no encontrar máximos locales implica unas pérdidas anuales de casi el 17%.

Para los *strings* que también están afectados por la sombra del muro, las pérdidas aumentan considerablemente. Esto se debe a que el muro está situado al sur del edificio tapando casi completamente una gran parte del generador durante la primera mitad del día. Por ello se obtienen unas pérdidas superiores al 50% para el conjunto de los cinco *strings*, siendo del 52% o del 60% en el caso de encontrar o no máximos locales.

Respecto al uso de equipos DMPPT para paliar estas pérdidas, se ha visto que la única posibilidad lógica es el uso de los equipos SolarEdge. Los equipos Tigo no cumplen los márgenes de tensión para conectar dos módulos en serie y conectando solo uno estarían muy sobredimensionados. En el caso de equipos micro-inversores el rango MPPT no baja de 22V lo que ocasionaría unas pérdidas por MPPT fuera de rango.

Con el uso de optimizadores SolarEdge, conectando dos módulos en serie a cada optimizador, las pérdidas se reducen en todos los casos simulados, obteniendo ganancias muy interesantes. Para los *strings* afectados por el muro inferior se obtienen ganancias entre el 16% y el 45% dependiendo del *string* y de si se encuentran máximos locales o no. El no encontrar máximos locales es más perjudicial cuando se tiene un inversor central y por eso aumenta la ganancia obtenida en estos casos. En el caso de los *strings* solo afectados por la sombra del edificio la ganancia es solo del 8.1% suponiendo que se encuentran máximos locales y del 31% en el supuesto de no encontrarlos.

En líneas generales, las pérdidas debido al sombreamiento en los generadores de la Torre Titania son mucho mayores que la norma reduciendo gravemente la rentabilidad de la instalación. En este caso concreto el uso de equipos DMPPT puede paliar considerablemente estas pérdidas, aumentando la producción de la instalación y, por tanto, su rentabilidad.

PUBLICATIONS

Publications in international journals

- **Solórzano J.** and Egido M.A., *Hot-spot mitigation in PV arrays with distributed MPPT (DMPPT).* Solar Energy, 2014. **101**(0): p. 131-137.

- Matallanas E., **Solórzano J.**, Castillo-Cagigal M., Navarro I. et al., Electrical energy balance contest in Solar Decathlon Europe 2012. Energy and Buildings, 2014(0).

- Navarro I., Gutiérrez Á., Montero C., Rodríguez-Ubiñas E., Matallanas E., Castillo-Cagigal M., Porteros M., **Solórzano J.**, Caamaño-Martín E., Egido M.A., Páez J.M., and Vega S., *Experiences and methodology in a multidisciplinar energy and architecture competition: Solar Decathlon Europe 2012.* Energy and Buildings, 2014(0).

- **Solórzano J.** and Egido M.A., *Automatic fault diagnosis in PV systems with distributed MPPT.* Energy Conversion and Management, 2013. **76**(0): p. 925-934.

- **Solórzano J.**, Masa D., Egido M.A., and Caamaño E., *A model for the simulation of energy gains when using distributed MPPT (DMPPT) in PV arrays.* Progress in Photovoltaics: Research and Applications, 2011. **N/A**.

- Orduz R., **Solórzano J.**, Egido M.Á., and Román E., Analytical study and evaluation results of power optimizers for distributed power conditioning in photovoltaic arrays. Progress in Photovoltaics: Research and Applications, 2011b. 21(3): p. 359-373.

Contributions to international conferences and seminars

- Egido M.A., **Solorzano J.**, and Fernandez M. *Towards energy sustainability in ecolodges for Latin America: A case in the Bolivian amazon.* in PV Hybrids and mini-grids. 2014. Bad Hersfeld, Germany

- **Solorzano J.** and Egido M.A. *Simulation of AC, DC and AC-DC coupled hybrid mini-grids: In search of the most efficient system.* in 6th European conference PV-Hybrid and Mini-Grids. 2012. Chambery, France

- **Solorzano J.** and Egido M.A. *Herramientas para el diseño y la simulación de sistemas híbridos.* in Seminario ELECORURAL: miniredes y sistemas híbridos con energía renovables en la electrificación rural. Sao Paulo, Brasil, 25 y 26 de mayo de 2011.

- **Solórzano J.**, Egido M.A., and Orduz R. *Power optimisation in PV generators using MPPT modules.* in 25th European Photovoltaic Solar Energy Conference. 2010. Valencia, Spain 4595-4600

REFERENCES

[Alonso-García, Herrmann et al., 2003].Alonso-García M.C., Herrmann W., Böhmer W., and Proisy B., *Thermal and electrical effects caused by outdoor hot-spot testing in associations of photovoltaic cells.* Progress in Photovoltaics: Research and Applications, 2003. **11**(5): p. 293-307. doi: 10.1002/pip.490.

[Alonso-García and Ruíz, 2006].Alonso-García M.C. and Ruíz J.M., *Analysis and modelling the reverse characteristic of photovoltaic cells.* Solar Energy Materials and Solar Cells, 2006. **90**(7–8): p. 1105-1120. doi: 10.1016/j.solmat.2005.06.006.

[Alonso-García, Ruiz et al., 2006a].Alonso-García M.C., Ruiz J.M., and Chenlo F., *Experimental study of mismatch and shading effects in the I–V characteristic of a photovoltaic module.* Solar Energy Materials and Solar Cells, 2006a. **90**(3): p. 329-340. doi: 10.1016/j.solmat.2005.04.022.

[Alonso-García, Ruiz et al., 2006b].Alonso-García M.C., Ruiz J.M., and Herrmann W., *Computer simulation of shading effects in photovoltaic arrays.* Renewable Energy, 2006b. **31**(12): p. 1986-1993. doi: 10.1016/j.renene.2005.09.030.

[Alonso, Ibaez et al., 2009].Alonso R., Ibaez P., Martinez V., Roman E., and Sanz A. *An innovative perturb, observe and check algorithm for partially shaded PV systems*. in *Power Electronics and Applications, 2009. EPE '09. 13th European Conference on*. 2009 1-8.

[Alonso, Roman et al., 2012].Alonso R., Roman E., Sanz A., Santos V.E.M., and Ibanez P., *Analysis of Inverter-Voltage Influence on Distributed MPPT Architecture Performance.* Industrial Electronics, IEEE Transactions on, 2012. **59**(10): p. 3900-3907. doi: 10.1109/tie.2012.2189532.

[Beetz, 2012].Beetz B., *PV microinverters and power optimizers set for significant growth* in PV magazine, September 2012,

[Bishop, 1988].Bishop J.W., *Computer simulation of the effects of electrical mismatches in photovoltaic cell interconnection circuits.* Solar Cells, 1988. **25**(1): p. 73-89. doi: 10.1016/0379-6787(88)90059-2.

[Blake and Hanson, 1969].Blake F. and Hanson K., *The hot-spot failure mode for solar arrays*, in *4th Intersociety Energy Conversion Engineering Conference*. 1969: Washington D.C. ISBN.

[CENELEC, 2010].CENELEC, *Overall efficiency of grid connected photovoltaic inverters*, in *EN 50530:2010*. 2010. ISBN.

[Chao, Dean et al., 2009].Chao Z., Dean Z., Jinjing W., and Guichang C. *A modified MPPT method with variable perturbation step for photovoltaic system*. in *Power*

Electronics and Motion Control Conference, 2009. IPEMC '09. IEEE 6th International. 2009 2096-2099.

[Chouder and Silvestre, 2010].Chouder A. and Silvestre S., *Automatic supervision and fault detection of PV systems based on power losses analysis.* Energy Conversion and Management, 2010. **51**(10): p. 1929-1937.

[Damm, Heinemann et al., 1995].Damm W., Heinemann D., and Pukrop D., *Power losses in PV arrays due to variations in the I-V characteristichs of PV modules*, 1995, Energiemeteorologie, University of Oldenburg, http://www.uni-oldenburg.de/fileadmin/user_upload/physik/ag/ehf/enmet/publications/solar/conference/1995/Power_Losses_in_PV_Arrays_Due_To_Variations_in_the_I_V_Characteristics_of_PV_Modules.pdf (date accessed 03-04-2014).

[Deline, Dobos et al., 2013].Deline C., Dobos A., Janzou S., Meydbray J., and Donovan M., *A simplified model of uniform shading in large photovoltaic arrays.* Solar Energy, 2013. **96**(0): p. 274-282. doi: http://dx.doi.org/10.1016/j.solener.2013.07.008.

[Deline, Meydbray et al., 2012].Deline C., Meydbray J., Donovan M., and Forrest J., *Photovoltaic Shading Testbed for Module-Level Power Electronics*, NREL-Technical Report/TP-5200-54876, May 2012.

[Drews, de Keizer et al., 2007].Drews A., de Keizer A.C., Beyer H.G., Lorenz E., Betcke J., van Sark W.G.J.H.M., Heydenreich W., Wiemken E., Stettler S., Toggweiler P., Bofinger S., Schneider M., Heilscher G., and Heinemann D., *Monitoring and remote failure detection of grid-connected PV systems based on satellite observations.* Solar Energy, 2007. **81**(4): p. 548-564. doi: 10.1016/j.solener.2006.06.019.

[Dunselman, Weiden et al., 1994].Dunselman C.P.M., Weiden T.C.J.v.d., Haan S.W.H.d., Heide F.t., and Zoligen R.J.C.v., *Feasibility and development of PV modules with integrated inverter: AC-modules*, in *12th European Photovoltaic Solar Energy Conference*. 1994: Amsterdam, Netherlands. ISBN.

[Eclareon, 2013].Eclareon, *PV grid parity monitor: residential sector 2nd issue*. 2013. ISBN.

[EnergyTrend, 2014].EnergyTrend. *PV Energy trend*. 2014 17-7-2014]; Available from: http://pv.energytrend.com/pricequotes.html.

[Enphase, 2012].Enphase, *"Burst-Mode" Makes Enphase Micro-inverter Systems the Smarter Choice*, 2012, http://enphase.com/downloads/WhitePaper_BurstMode.pdf (date accessed 23-04-2014).

[EPIA, 2012].EPIA, *Connecting the sun: solar photovoltaics on the road to large-scale grid integration*, European Photovoltaic Industry Association-Technical Report/1, September 2012.

[Erickson, 2001].Erickson R.W., *Fundamentals of Power Electronics (Second Edition)*. 2001, New York: Springer.

[Esram and Chapman, 2007].Esram T. and Chapman P.L., *Comparison of Photovoltaic Array Maximum Power Point Tracking Techniques.* Energy Conversion, IEEE Transactions on, 2007. **22**(2): p. 439-449. doi: 10.1109/tec.2006.874230.

[Femia, Lisi et al., 2008].Femia N., Lisi G., Petrone G., Spagnuolo G., and Vitelli M., *Distributed Maximum Power Point Tracking of Photovoltaic Arrays: Novel*

Approach and System Analysis. Industrial Electronics, IEEE Transactions on, 2008. **55**(7): p. 2610-2621. doi: 10.1109/tie.2008.924035.

[Femia, Petrone et al., 2013].Femia N., Petrone G., Spagnuolo G., and Vitelli M., *Power electronics and control techniques for maximum energy harvesting in photovoltaic systems*. 2013, Boca Raton, Florida: CRC Press. 978-1-4665-0691-6.

[Firth, Lomas et al., 2010].Firth S.K., Lomas K.J., and Rees S.J., *A simple model of PV system performance and its use in fault detection.* Solar Energy, 2010. **84**(4): p. 624-635. doi: DOI: 10.1016/j.solener.2009.08.004.

[Friedman, Ardani et al., 2013].Friedman B., Ardani K., Feldman D., Citron R., Margolis R., and Zuboy J., *Benchmarking Non-Harware Balance-of-System (Soft) Costs for U.S. Photovoltaic Systems, Using a Bottom-Up Approach and Installer Survey - Second Edition*, NREL-Technical October 2013.

[García, Maruri et al., 2008].García M., Maruri J.M., Marroyo L., Lorenzo E., and Pérez M., *Partial shadowing, MPPT performance and inverter configurations: observations at tracking PV plants.* Progress in Photovoltaics: Research and Applications, 2008. **16**(6): p. 529-536. doi: 10.1002/pip.833.

[Grana and Shiao, 2014].Grana P. and Shiao M., *The microinverter an DC optimizer landscape: 2014*, GTM Research-Technical

[Gross, Marttin et al., 1997].Gross M.A., Marttin S.O., and Pearsall N.M., *Estimation of output enhancement of a partially shaded BIPV array by the use of AC modules*, in *26th IEEE Photovoltaic Specialists Conference*. 1997: Anaheim, CA, USA. ISBN.

[Haeberlin and Graf, 1998].Haeberlin H. and Graf J.D., *Gradual Reduction of PV Generator Yield due to Pollution*, in *2nd World Conference on Photovoltaic Solar Energy Conversion*. 1998: Vienna, Austria. ISBN.

[Hanson, Deline et al., 2014].Hanson A., Deline C., MacAlpine S., Stauth J., and Sullivan C. *Partial-Shading Assessment of Photovoltaic Installations via Module-Level Monitoring*. in *40th IEEE Photovoltaic Specialists Conference*. 2014. Colorado, USA

[Hempel, Kleinkauf et al., 1992].Hempel H., Kleinkauf W., and Krengel U., *PV-module with integrated power conditioning unit.*, in *11th European Photovoltaic Solar Energy Conference*. 1992: Montreaux, Switzerland. ISBN.

[Herrmann, 2005].Herrmann W., *Analyses of array losses caused by electrical mismatch of PV modules*, in *20th European Photovoltaic Solar Energy Conference and Exhibition*. 2005: Barcelona, Spain. ISBN.

[Hohm and Ropp, 2003].Hohm D.P. and Ropp M.E., *Comparative study of maximum power point tracking algorithms.* Progress in Photovoltaics: Research and Applications, 2003. **11**(1): p. 47-62. doi: 10.1002/pip.459.

[IEA, 2000].IEA, *Analysis of photovoltaic systems*, International Energy Agency-Technical

[IEA, 2004].IEA, *Country reports on PV system performance*, International Energy Agency-Technical

[IEC, 1998].IEC, *Photovoltaic system performace monitoring - Guidelines for measurement, data exchange and analysis*, in *IEC 61724*. 1998, International Electrotechnical Commitee: Geneva, Switzerland. ISBN.

[IEC, 2005].IEC, *Crystalline Silicon Terrestrial Photovoltaic (PV) Modules. Design Qualification and Type Approval*, in *IEC 61215*. 2005: IEC Central Office, Geneva, Switzerland. ISBN.

[IEC, 2006].IEC, *Photovoltaic devices-Measurement of photovoltaic current-voltage characteristics*, in *60904-1*. 2006, International Electrotechnical Commission: Geneve, Switzerland. ISBN.

[IEC, 2009].IEC, *Photovoltaic devices - Procedures for temperature and irradiance corrections to measured I-V characteristics*, in *IEC 60891*. 2009, International Electrotechnical Commission: Geneve, Switzerland. ISBN.

[IEC, 2011].IEC, *Photovoltaic devices-Determination of the equivalent cell temperature of photovoltaic devices by the open-circuit voltage method*, in *IEC-60904-5*. 2011, International Electrotechnical Commission: Geneve, Switzerland. ISBN.

[IMS, 2013].IMS, *The world market for PV microinverters and power optimizers*, IMS Research-Technical

[Kalogirou, Agathokleous et al., 2013].Kalogirou S.A., Agathokleous R., and Panayiotou G., *On-site PV characterization and the effect of soiling on their performance.* Energy, 2013. **51**(0): p. 439-446. doi: http://dx.doi.org/10.1016/j.energy.2012.12.018.

[Katz, 2009].Katz D., *Micro-Inverters and AC modules*, 2009, AEE Solar

[Kern and Kern, 2000].Kern E. and Kern G., *Cost Reduction and Manufacture of the SunSine AC Module*, NREL-Technical

[Kleinkauf, Sachau et al., 1992].Kleinkauf W., Sachau J., and Hempel H., *Developments in inverters for photovoltaic systems*, in *11th E.C. Photovoltaic Solar Energy Conference*. 1992: Montreux, Switzerland. ISBN.

[Knaupp, Schekulin et al., 1996].Knaupp W., Schekulin D., Volgtlander I., Bleil A., and Binder C., *Operation of a 10kW PV façade with 100W AC photovoltaic modules*, in *25th PVSC*. 1996: Washington D.C., USA. ISBN.

[Lorenzo, Moretón et al., 2013].Lorenzo E., Moretón R., and Luque I., *Dust effects on PV array performance: in-field observations with non-uniform patterns.* Progress in Photovoltaics: Research and Applications, 2013: p. n/a-n/a. doi: 10.1002/pip.2348.

[Luque and Hegedus, 2002].Luque A. and Hegedus S., *Handbook of Photovoltaic Science and Engineering*, ed. Wiley. 2002, West Sussex, England.

[MacAlpine, Deline et al., 2012].MacAlpine S., Deline C., Erickson R., and Brandemuehl M. *Module mismatch loss and recoverable power in unshaded PV installations*. in *Photovoltaic Specialists Conference (PVSC), 2012 38th IEEE*. 2012 001388-001392.

[Martín and Ruiz, 1999].Martín N. and Ruiz J.M., *A new method for the spectral characterisation of PV modules.* Progress in Photovoltaics: Research and Applications, 1999. **7**(4): p. 299-310. doi: 10.1002/(sici)1099-159x(199907/08)7:4<299::aid-pip260>3.0.co;2-0.

[Martínez-Moreno, Muñoz et al., 2010].Martínez-Moreno F., Muñoz J., and Lorenzo E., *Experimental model to estimate shading losses on PV arrays.* Solar Energy Materials and Solar Cells, 2010. **94**(12): p. 2298-2303. doi: 10.1016/j.solmat.2010.07.029.

[Martinez, 2012].Martinez F. *Caracterización y modelado de grandes centrales fotovoltaicas. PhD Thesis. Instittuto de Energía Solar. Universidad Politécnica de Madrid. Madrid, Spain,*

[Masa-Bote and Caamaño-Martín, 2014].Masa-Bote D. and Caamaño-Martín E., *Methodology for estimating building integrated photovoltaics electricity production under shadowing conditions and case study.* Renewable and Sustainable Energy Reviews, 2014. **31**(0): p. 492-500. doi: http://dx.doi.org/10.1016/j.rser.2013.12.019.

[Massi Pavan, Mellit et al., 2011].Massi Pavan A., Mellit A., and De Pieri D., *The effect of soiling on energy production for large-scale photovoltaic plants.* Solar Energy, 2011. **85**(5): p. 1128-1136. doi: http://dx.doi.org/10.1016/j.solener.2011.03.006.

[Massi Pavan, Mellit et al., 2014].Massi Pavan A., Mellit A., De Pieri D., and Lughi V., *A study on the mismatch effect due to the use of different photovoltaic modules classes in large-scale solar parks.* Progress in Photovoltaics: Research and Applications, 2014. **22**(3): p. 332-345. doi: 10.1002/pip.2266.

[Meyer and Ernest van Dyk, 2005].Meyer E.L. and Ernest van Dyk E. *The effect of reduced shunt resistance and shading on photovoltaic module performance*. in *Photovoltaic Specialists Conference, 2005. Conference Record of the Thirty-first IEEE*. 2005 1331-1334.

[Meza, 2013].Meza E., *Global microinverter market to quadruple by 2017* in PV magazine, August 2013,

[Muneer, 2004].Muneer T., *Solar radiation and daylight models*. 2004: Elsevier Butterworth-Heinemann. 0 7506 5974 2.

[Munoz, Alonso-García et al., 2011].Munoz M.A., Alonso-García M.C., Vela N., and Chenlo F., *Early degradation of silicon PV modules and guaranty conditions.* Solar Energy, 2011. **85**(9): p. 2264-2274. doi: http://dx.doi.org/10.1016/j.solener.2011.06.011.

[Muñoz, Lorenzo et al., 2008].Muñoz J., Lorenzo E., Martínez-Moreno F., Marroyo L., and García M., *An investigation into hot-spots in two large grid-connected PV plants.* Progress in Photovoltaics: Research and Applications, 2008. **16**(8): p. 693-701. doi: 10.1002/pip.844.

[Nann and Emery, 1992].Nann S. and Emery K., *Spectral effects on PV-device rating.* Solar Energy Materials and Solar Cells, 1992. **27**(3): p. 189-216. doi: http://dx.doi.org/10.1016/0927-0248(92)90083-2.

[Ndiaye, Charki et al., 2013].Ndiaye A., Charki A., Kobi A., Kébé C.M.F., Ndiaye P.A., and Sambou V., *Degradations of silicon photovoltaic modules: A literature review.* Solar Energy, 2013. **96**(0): p. 140-151. doi: http://dx.doi.org/10.1016/j.solener.2013.07.005.

[Neidlein, 2013].Neidlein H.-C., *PV power optimizer shipments to reach 4GW by 2016* in PV magazine, February 2013,

[Neuenstein and Podewils, 2009].Neuenstein H. and Podewils C., *Magic Powers?* in Photon International, September 2009, p. 172-180

[Neuenstein and Podewils, 2011].Neuenstein H. and Podewils C., *Convincing performance* in Photon International, October 2011, p. 216-221

[Olalla, Deline et al., 2014].Olalla C., Deline C., and Maksimovic D., *Performance of Mismatched PV Systems With Submodule Integrated Converters.* Photovoltaics, IEEE Journal of, 2014. **4**(1): p. 396-404. doi: 10.1109/jphotov.2013.2281878.

[Oldenkamp and Jong, 1998a].Oldenkamp H. and Jong I.d., *AC modules: past, present and future*, in *Workshop Installing the solar solution*. 1998a: Hatfield, UK. ISBN.

[Oldenkamp and Jong, 1998b].Oldenkamp H. and Jong I.d., *Next generation of AC-module inverters*, in *2nd World Conference and Exhibition on Photovoltaic Energy Conversion*. 1998b: Vienna, Austria. ISBN.

[Oozeki, Izawa et al., 2003].Oozeki T., Izawa T., Otani K., and Kurokawa K., *An evaluation method of PV systems.* Solar Energy Materials and Solar Cells, 2003. **75**(3–4): p. 687-695. doi: 10.1016/s0927-0248(02)00143-5.

[Orduz, 2009].Orduz R. *Contribución a los sistemas de control de potencia micro-distribuida en edificios fotovoltaicos. PhD Thesis. Instituto de Energía Solar. Universidad Politécnica de Madrid. Madrid, Spain, September 2009.*

[Orduz and Egido, 2006].Orduz R. and Egido M.A., *Evaluation test results of a new distributed MPPT converter*, in *22nd European PV Solar Energy Conference and Exhibition*. 2006: Milan, Italy. ISBN.

[Orduz, Solórzano et al., 2011a].Orduz R., Solórzano J., Egido M.Á., and Román E., *Analytical study and evaluation results of power optimizers for distributed power conditioning in photovoltaic arrays.* Progress in Photovoltaics: Research and Applications, 2011a. **21**(3): p. 359-373. doi: 10.1002/pip.1188.

[Orduz, Solórzano et al., 2011b].Orduz R., Solórzano J., Egido M.Á., and Román E., *Analytical study and evaluation results of power optimizers for distributed power conditioning in photovoltaic arrays.* Progress in Photovoltaics: Research and Applications, 2011b: p. n/a-n/a. doi: 10.1002/pip.1188.

[Oreski and Wallner, 2005].Oreski G. and Wallner G.M., *Aging mechanisms of polymeric films for PV encapsulation.* Solar Energy, 2005. **79**(6): p. 612-617. doi: http://dx.doi.org/10.1016/j.solener.2005.02.008.

[Oreski and Wallner, 2009].Oreski G. and Wallner G.M., *Evaluation of the aging behavior of ethylene copolymer films for solar applications under accelerated weathering conditions.* Solar Energy, 2009. **83**(7): p. 1040-1047. doi: http://dx.doi.org/10.1016/j.solener.2009.01.009.

[Parkinson, 2013].Parkinson G., *Deutsche sees "sustainable" global solar market in 2014* in Reneweconomy,

[Parretta, Bombace et al., 2005].Parretta A., Bombace M., Graditi G., and Schioppo R., *Optical degradation of long-term, field-aged c-Si photovoltaic modules.* Solar Energy Materials and Solar Cells, 2005. **86**(3): p. 349-364. doi: 10.1016/j.solmat.2004.08.006.

[Patel and Agarwal, 2008].Patel H. and Agarwal V., *Maximum Power Point Tracking Scheme for PV Systems Operating Under Partially Shaded Conditions.* Industrial Electronics, IEEE Transactions on, 2008. **55**(4): p. 1689-1698. doi: 10.1109/tie.2008.917118.

[Perez, Seals et al., 1987].Perez R., Seals R., Ineichen P., Stewart R., and Menicucci D., *A new simplified version of the perez diffuse irradiance model for tilted surfaces.* Solar Energy, 1987. **39**(3): p. 221-231. doi: 10.1016/s0038-092x(87)80031-2.

[Podewils, 2009].Podewils C., *Power booster* in Photon International, August 2009, p. 122-129

[Podewils, 2011].Podewils C., *Ready to work magic?* in Photon International, October 2011, p. 204-215

[Podewils and Levitin, 2011].Podewils C. and Levitin M., *Hidden powers* in Photon International, February 2011, p. 136-147

[PVSyst, 2014].PVSyst, *SolarEdge Architecture*, 2014, http://files.pvsyst.com/help/index.html?solaredge_architecture.htm (date accessed 12-july-2014).

[Reis, Coleman et al., 2002].Reis A., Coleman N., Marshall M., Lehman P., and Chamberlain C. *Comparison of PV module performance before and after 11-years of field exposure*. in *29th IEEE Photovoltaics Specialists Conference*. 2002. New Orleans, Lousiana 1432-1435.

[Reza Reisi, Hassan Moradi et al., 2013].Reza Reisi A., Hassan Moradi M., and Jamasb S., *Classification and comparison of maximum power point tracking techniques for photovoltaic system: A review.* Renewable and Sustainable Energy Reviews, 2013. **19**(0): p. 433-443. doi: http://dx.doi.org/10.1016/j.rser.2012.11.052.

[Rogalla, Burger et al., 2010].Rogalla S., Burger B., Goeldi B., and Schdmidt H. *Light and shadow--When is MPP-tracking at the module level worthwile?* in *25th European Photovoltaic Solar Energy Conference*. 2010 3932-3936.

[Roman, 2006].Roman E. *Viabilidad de Sistemas Fotovoltaicos con Múltiples Seguidores del Punto de Máxima Potencia. PhD Thesis. Universidad del País Vasco. Bilbao, October 2006.*

[Roman, Alonso et al., 2006].Roman E., Alonso R., Ibanez P., Elorduizapatarietxe S., and Goitia D., *Intelligent PV Module for Grid-Connected PV Systems.* Industrial Electronics, IEEE Transactions on, 2006. **53**(4): p. 1066-1073. doi: 10.1109/tie.2006.878327.

[Ropp, Cale et al., 2011].Ropp M., Cale J., Mills-Price M., Scharf M., and Hummel S.G. *A test protocol to enable comparative evaluation of maximum power point trackers under both static and dynamic irradiance*. in *Photovoltaic Specialists Conference (PVSC), 2011 37th IEEE*. 2011 003734-003737.

[Rosell, 2012].Rosell A.D., *Resurgir de la cenizas* in Photon España, p. 78-84

[Sánchez-Friera, Piliougine et al., 2011].Sánchez-Friera P., Piliougine M., Peláez J., Carretero J., and Sidrach de Cardona M., *Analysis of degradation mechanisms of crystalline silicon PV modules after 12 years of operation in Southern Europe.* Progress in Photovoltaics: Research and Applications, 2011. **19**(6): p. 658-666. doi: 10.1002/pip.1083.

[Sanchis, López et al., 2007].Sanchis P., López J., Ursúa A., Gubía E., and Marroyo L., *On the testing, characterization, and evaluation of PV inverters and dynamic MPPT performance under real varying operating conditions.* Progress in Photovoltaics: Research and Applications, 2007. **15**(6): p. 541-556. doi: 10.1002/pip.763.

[Sanz, Vidaurrazaga et al., 2011].Sanz A., Vidaurrazaga I., Pereda A., Alonso R., Roman E., and Martinez V. *Centralized vs distributed (power optimizer) PV system architecture field test results under mismatched operating conditions*. in *Photovoltaic Specialists Conference (PVSC), 2011 37th IEEE*. 2011 002435-002440.

[Sanz, 2010].Sanz D. *Maximum Power Point Tracking Algorithms for Photovoltaics Applications. Faculty of electronics, communication and automation. Aalto University.*

[Sera, Kerekes et al., 2006].Sera D., Kerekes T., Teodorescu R., and Blaabjerg F. *Improved MPPT Algorithms for Rapidly Changing Environmental Conditions*. in *Power Electronics and Motion Control Conference, 2006. EPE-PEMC 2006. 12th International*. 2006 1614-1619.

[Shah, Booream-Phelps et al., 2014].Shah V., Booream-Phelps J., and Min S., *2014 Outlook: Let the Second Gold Rush Begin*, Deutsche Bank-Technical Report/1, January 2014.

[Shiao, 2013].Shiao M., *The global PV inverter landscape 2013: technologies, markets and survivors*, GTM Research-Technical

[Silvestre, Boronat et al., 2009].Silvestre S., Boronat A., and Chouder A., *Study of bypass diodes configuration on PV modules.* Applied Energy, 2009. **86**(9): p. 1632-1640. doi: http://dx.doi.org/10.1016/j.apenergy.2009.01.020.

[Silvestre and Chouder, 2008].Silvestre S. and Chouder A., *Effects of shadowing on photovoltaic module performance.* Progress in Photovoltaics: Research and Applications, 2008. **16**(2): p. 141-149. doi: 10.1002/pip.780.

[Skoczek, Sample et al., 2009].Skoczek A., Sample T., and Dunlop E.D., *The results of performance measurements of field-aged crystalline silicon photovoltaic modules.* Progress in Photovoltaics: Research and Applications, 2009. **17**(4): p. 227-240. doi: 10.1002/pip.874.

[SMA, 2010].SMA, *Shade Management: efficient operation of partially shaded PV plants with OptiTrac Global Peak*,

[SolarBridge, 2014].SolarBridge. *Installing AC Solar Modules: Time Lapse Comparison (HD)*. 2014 17-07-2014]; Available from: https://www.youtube.com/watch?v=wB8RbrlORaE.

[SolarEdge, 2010].SolarEdge, *Case Study: The way to energy gain*, 2010, http://www.solaredge.com/files/pdfs/solaredge-Case-Study-Aidlingen-Germany.pdf (date accessed 12-july-2014).

[Solórzano-Moral, Masa-Bote et al., 2013a].Solórzano-Moral J., Masa-Bote D., Egido-Aguilera M.A., and Caamaño-Martín E., *A model for the simulation of energy gains when using distributed maximum power point tracking (DMPPT) in photovoltaic arrays.* Progress in Photovoltaics: Research and Applications, 2013a. doi: 10.1002/pip.2413.

[Solórzano-Moral, Masa-Bote et al., 2013b].Solórzano-Moral J., Masa-Bote D., Egido-Aguilera M.A., and Caamaño-Martín E., *A model for the simulation of energy gains when using distributed maximum power point tracking (DMPPT) in photovoltaic arrays.* Progress in Photovoltaics: Research and Applications, 2013b: p. n/a-n/a. doi: 10.1002/pip.2413.

[Solórzano, Egido et al., 2010].Solórzano J., Egido M.A., and Orduz R. *Power optimisation in PV generators using MPPT modules*. in *25th European Photovoltaic Solar Energy Conference*. 2010. Valencia, Spain 4595-4600.

[Solórzano, Masa et al., 2011].Solórzano J., Masa D., Egido M.A., and Caamaño E., *A model for the simulation of energy gains when using distributed MPPT (DMPPT) in PV arrays.* Progress in Photovoltaics: Research and Applications, 2011. **N/A**.

[Solórzano, Masa et al., 2013].Solórzano J., Masa D., Egido M.A., and Caamaño E., *A model for the simulation of energy gains when using distributed MPPT (DMPPT) in PV arrays.* Progress in Photovoltaics: Research and Applications, 2013. **N/A**.

[Strong, 1999].Strong S., *The Development of Standardized, Low-Cost, AC PV Systems*, NREL-Technical

[Taheri, Salam et al., 2010].Taheri H., Salam Z., Ishaque K., and Syafaruddin. *A novel Maximum Power Point tracking control of photovoltaic system under partial and rapidly fluctuating shadow conditions using Differential Evolution*. in *Industrial Electronics & Applications (ISIEA), 2010 IEEE Symposium on*.82-87.

[TamizhMani, 2010].TamizhMani G., *Testing the reliability and safety of photovoltaic modules: Failure rates and temperature effects*, TÜV Rheinland-Technical

[Vitelli, 2012].Vitelli M., *On the necessity of joint adoption of both Distributed Maximum Power Point Tracking and Central Maximum Power Point Tracking in PV systems.* Progress in Photovoltaics: Research and Applications, 2012: p. n/a-n/a. doi: 10.1002/pip.2256.

[Walker and Sernia, 2004].Walker G.R. and Sernia P.C., *Cascaded DC-DC converter connection of photovoltaic modules.* Power Electronics, IEEE Transactions on, 2004. **19**(4): p. 1130-1139.

[Wesoff, 2013a].Wesoff E., *Enphase dominates the PV microinverter channel: where's the competition?* in GreentechSolar, July 2013,

[Wesoff, 2013b].Wesoff E., *World-Record 2-Megawatt Microinverter Solar Installation* in Greentech Media, August 2013,

[Woodlawn, 2012].Woodlawn, *Solar Installation Effectiveness*, Woodlawn Associates-Technical September 2012.

[Woyte, Nijs et al., 2003].Woyte A., Nijs J., and Belmans R., *Partial shadowing of photovoltaic arrays with different system configurations: literature review and field test results.* Solar Energy, 2003. **74**(3): p. 217-233. doi: 10.1016/s0038-092x(03)00155-5.

[Young-Hyok, Doo-Yong et al., 2011].Young-Hyok J., Doo-Yong J., Jun-Gu K., Jae-Hyung K., Tae-Won L., and Chung-Yuen W., *A Real Maximum Power Point Tracking Method for Mismatching Compensation in PV Array Under Partially Shaded Conditions.* Power Electronics, IEEE Transactions on, 2011. **26**(4): p. 1001-1009. doi: 10.1109/tpel.2010.2089537.

[Zorrilla-Casanova, Piliougine et al., 2012].Zorrilla-Casanova J., Piliougine M., Carretero J., Bernaola-Galván P., Carpena P., Mora-López L., and Sidrach-de-Cardona M., *Losses produced by soiling in the incoming radiation to photovoltaic modules.* Progress in Photovoltaics: Research and Applications, 2012: p. n/a-n/a. doi: 10.1002/pip.1258.